THE USE OF PAPER PROCESSING RESIDUES IN THE DEVELOPMENT OF CERAMICS WITH IMPROVED THERMAL INSULATION PROPERTIES

A Thesis Submitted to
the Graduate School of Engineering and Sciences of
İzmir Institute of Technology
in Partial Fulfillment of the Requirements for the Degree of

DOCTOR OF PHILOSOPHY

in Mechanical Engineering

by
Mücahit SÜTÇÜ

June 2010
İZMİR

We approve the thesis of **Mücahit SÜTÇÜ**

Prof. Dr. Sedat AKKURT
Supervisor

Prof. Dr. Metin TANOĞLU
Committee Member

Assoc. Prof. Dr. Sait Cemil SOFUOĞLU
Committee Member

Prof. Dr. Mustafa GÜDEN
Committee Member

Prof. Dr. İ. Akın ALTUN
Committee Member

03 June 2010

Prof. Dr. Metin TANOĞLU
Head of the Department of Mechanical Engineering

Assoc. Prof. Dr. Talat YALÇIN
Dean of the Graduate School of Engineering and Sciences

ACKNOWLEDGEMENTS

I would like to thank my advisor, Prof. Dr. Sedat Akkurt, for his constant support throughout dissertation. His friendly manners and continuous guidance are greatly appreciated. I am grateful to the other committee members.

I would like to thank to the workers of IZTECH Materials Research Center (IYTE-MAM) for their helps in the analysis of XRF, XRD and SEM. I am grateful to IZTECH Geothermal Energy Research and Application Center (IYTE-JEOMER) for assisting me in performing thermal conductivity measurements. Special thanks go to specialists Deniz Şimşek and Filiz Özmıhçı for their helps in dilatometric and thermal analysis.

Also, I would like to thank to Levent Kağıt Sanayii A.Ş., Yüksel Tuğla Kiremit Sanayii A.Ş., Eczacıbaşı Esan and Kalemaden for providing of raw materials. We acknowledge the financial support of İYTE BAP project number 2009İYTE07 and TUBITAK TEYDEP project number 7080919, Turkey.

I would like to appreciate deeply my room-mates Uğur Türkan, Emre Yalamaç and Sinan Yüksel for the moments that we shared together.

I would like to thank my mother, my father and my brothers for their constant encouragement and support.

Finally, I would like to express my special thanks to my wife Sümeyra and my daughter Şerife Rüveyde for their constant encouragement, support and patience during this graduate work.

ABSTRACT

THE USE OF PAPER PROCESSING RESIDUES IN THE DEVELOPMENT OF CERAMICS WITH IMPROVED THERMAL INSULATION PROPERTIES

Recycled paper processing residues, those are industrial wastes, are utilized in the manufacture of porous and lightweight ceramics with improved thermal insulation properties for structural brick and refractory firebrick applications. These residues that contained micro-sized calcium carbonate (<5 μm) and cellulose fibers (<20 μm of diameter), were successfully used as an additive to earthenware brick to create porous structure during firing. A solid porous brick and a vertically perforated porous brick had 0.4 W/mK and 0.158 W/mK of thermal conductivity, respectively. This means substantial potential energy savings in houses and other buildings. When the paper residue was added in extreme amounts to the brick clay, it was found that anorthite ($CaO{\cdot}Al_2O_3{\cdot}2SiO_2$) formed in the brick at the high-end of the firing temperatures of 1000-1100°C. This inspired the second part of the thesis which dealt with the production of porous, lower density insulating firebrick. Addition of the paper residue in excessive amounts up to 30% into the clay systems and firing at higher temperatures (1100–1400°C) formed a crystalline anorthite phase. Highly porous anorthite lightweight ceramics from the mixtures with up to 30% sawdust addition (used as additional pore-former) was successfully produced. Thermal conductivities of the samples decreased from 0.25 W/mK (1.12 g/cm^3) to 0.13 W/mK (0.64 g/cm^3) with increasing sawdust addition. Samples were stable at high temperatures up to 1100°C, and their cold strength was sufficiently high. Two separate porous lightweight ceramics were developed for insulation in buildings to reduce heat losses, and for insulation in high temperature applications.

ÖZET

ISIL YALITIM ÖZELLİKLERİ İYİLEŞTİRİLMİŞ SERAMİKLERİN GELİŞTİRİLMESİNDE KAĞIT ÜRETİM ATIKLARININ KULLANILMASI

Endüstriyel bir atık olan geri dönüşüm kağıt üretimi atıkları, yapı tuğlası ve refrakter ateş tuğlası uygulamaları için, ısıl yalıtım özellikleri iyileştirilmiş gözenekli ve ağırlıkça hafif seramiklerin üretilmesinde kullanılmıştır. Mikro-boyutlu kalsiyum karbonat (<5 μm) ve selüloz lifleri (<20 μm çaplı) içeren bu atıklar yapı tuğlasında pişme esnasında gözenekli bir yapı oluşturmak için katkı maddesi olarak başarılı bir şekilde kullanılmıştır. Atık katkısıyla gözenekli olan dolu (deliksiz) tuğla ve düşey delikli tuğla örnekler sırasıyla 0.4 W/mK ve 0.158 W/mK'lik ısıl iletkenliğe sahiptir. Bu değer, evlerde ve diğer binalarda önemli enerji tasarrufu anlamına gelmektedir. Kağıt atığı tuğla kiline yüksek miktarda ilave edildiğinde, 1000–1100°C'lik pişirme sıcaklıklarında tuğla bünyesinde anortit ($CaO{\cdot}Al_2O_3{\cdot}2SiO_2$) fazı oluşmuştur. Bu oluşum, gözenekli ve düşük yoğunluklu yalıtım ateş tuğlasının üretilmesiyle ilgili olan tezin ikinci kısmı için bir esinlenme olmuştur. Ağırlıkça %30'a kadar yüksek miktarlarda kağıt atığının farklı kil sistemlerine ilave edilmesiyle hazırlanan karışımların yüksek sıcaklıklarda (1100–1400°C) pişirilmesiyle kristal anortit fazı oluşmuştur. Ağırlıkça %30'a kadar talaş ilavesiyle hazırlanan karışımlardan oldukça yüksek gözenekli ve ağırlıkça hafif anortit seramikleri başarıyla üretilmiştir. Örneklerin ısıl iletkenlikleri talaş ilavesinin artmasıyla 0.25 W/mK (1.12 g/cm^3)'den 0.13 W/mK (0.64 g/cm^3)'e düşmüştür. Üretilen örnekler 1100°C'ye kadar yüksek sıcaklıklarda kararlıdır ve oda sıcaklığındaki eğme dayanımları yeterince yüksektir. Bu tez kapsamında, hem binalarda ısı kayıplarını düşürmek ve ısı yalıtımı sağlamak için ve hem de yüksek sıcaklık uygulamalarında ısı yalıtımı sağlamak için gözenekli ve ağırlıkça hafif iki farklı türde seramikler geliştirilmiştir.

TABLE OF CONTENTS

LIST OF FIGURES

LIST OF TABLES

CHAPTER 1

INTRODUCTION

1.1. Background

Paper production inevitably produces large amounts of residue containing cellulose fiber along with calcite and clay. This residue contains about 65% water and is generally dumped on land disposal sites in Izmir which are about 35 km away. Hence, their transportation means the transportation of water which is not feasible at all. Paper producers are seeking ways to eliminate this residue in an environmentally friendly way. Brick producers use large amounts of natural clayey raw materials for production of clay based ceramics with wide compositional variations. Therefore, these products can tolerate compositional fluctuations due to changes in the raw materials. Brick and roof tile industry is, hence, capable of incorporating high proportions of waste without significantly losing their product quality (Dondi 1997, Segadaes 2006). In same cases the product is even better after waste addition (Uslu 2004). Energy efficiency of buildings is nowadays increasingly gaining attention for concerns about saving energy. Construction industry uses large amounts of brick in houses, schools, industrial constructions. These brick, if improved by proper processing, can have significantly lower thermal conductivity which means lower heat loss through the walls of houses. When paper residues are used in brick as an additive, cellulose will burn and leave micrometer scale pores behind which help reduce thermal conductivity of the brick. The brick is also lighter if made more porous. For this reason, the use of wastes containing pore-forming agents is favorable to produce porous ceramics (Dondi 1997, Kornmann 2007, Stefanov 2003). In addition, if the paper residue is used in excessive amounts up to 20-30% and fired at higher temperatures, a new phase of anorthite ($CaO \cdot Al_2O_3 \cdot 2SiO_2$) forms. This phase is known to be refractory, which is resistant to high temperatures. When anorthite is produced in a porous form, its thermal conductivity at room temperature can be reduced down to 0.11 W/mK. Porous anorthite ceramics are commercially produced and used as insulating firebrick (IFB) refractories using gypsum as the major raw material (Brosnan 2004, Pirogov, et al. 1972, Thermal

Ceramics 2009). The use of gypsum and subsequent thermal treatment to synthesize anorthite appears not to be environmentally the perfect method for IFB production. An alternative method as described above is proposed in this thesis by incorporating paper residues into clay. Details of this proposed technique are given in detail in this thesis.

1.2. Objectives

This thesis focuses on the utilization of recycled paper processing residues in manufacture of porous and lightweight ceramics such as structural clay insulating bricks as a building material, and also anorthite based insulating firebricks as a refractory material for thermal insulation applications.

1.3. Dissertation Outline

In Chapter 2, a literature review is given of the subjects covered in the thesis.

In Chapter 3, the recycled paper processing residues obtained from a paper producer were characterized to determine their chemical, mineralogical, physical and thermal properties using different analysis methods.

In Chapter 4, incorporation of industrial paper production residues into a ceramic product and as a result, production of porous and light-weight bricks with reduced thermal conductivity and acceptable compressive strength is accomplished. Paper processing residues were used as an additive to an earthenware brick to produce the pores. Chemical, physical, mineral and thermal properties of the raw materials were performed. Mixtures containing brick raw materials and the paper waste were prepared at different proportions (up to 30% by weight). The granulated powder mixtures were compressed in a hydraulic press, and the green bodies were dried before firing at 1000–1100°C. The dilatometric behaviors, drying and firing shrinkages of the fired bricks were investigated as well as their loss on ignition, bulk density, apparent porosity and water absorption. Their mechanical and thermal conductivity measurements were performed. In addition, mineralogical and microstructural properties of the fired bricks were investigated.

In Chapter 5, production of porous anorthite ceramics from mixtures of paper processing residues and three different clays are investigated. Suitability of three

different clays such as enriched clay, commercial clay and fireclay for manufacturing of anorthite based lightweight refractory bricks was studied. Porous character to the ceramic was provided by addition of paper processing residues. Anorthite ($CaO \cdot Al_2O_3 \cdot 2SiO_2$) formation for all clay types was investigated depending on the calcite to clay ratio and firing temperatures.

In Chapter 6, the production of porous and lightweight anorthite based insulating firebricks from the mixtures of different types of clay (K244 clay and fireclay) and recycled paper processing waste with pore-making sawdust addition was investigated. Addition of sawdust into the mixtures will provide to form the additional pores at result of firing. Physical properties of the products such as density, porosity, thermal conductivity, shrinkage and modulus of rupture were performed.

It was concluded that the recycled paper processing wastes could be used as a suitable alternative raw material source for production of porous thermal insulation ceramics. Porous and lightweight ceramics with different compositions were successfully produced for use in both industrial and building heat insulation applications.

CHAPTER 2

LITERATURE REVIEW

2.1. Industrial Waste Materials – Utilization and Recycling of Industrial Wastes in Production of Ceramic Materials

Today, increasing global industrial activities brings about the important environmental problems. Specifically, significant amounts of waste materials are generated from different industrial sources. Wastes are regarded as having zero value by the producers, and are intended to be dumped in landfills. However, increasing amounts of waste materials need wide landfills for their disposal, which is difficult to maintain. For this reason, the utilization or recycling of industrial wastes has been recognized worldwide not only as an economic opportunity but also for solving environmental problems. The recycling waste materials can be used in energy intensive industries such as iron-steel, aluminum, glass and paper (Rawlings, et al. 2006). When they consume or reuse in these industrial sectors, they can especially find wide application areas in the ceramic industry for production of building materials. Clay based ceramic bodies are generally heterogeneous since they consist of raw materials with a very wide compositional ranges. Therefore, these ceramic bodies can tolerate compositional changes due to the presence of different types of wastes, even in high percentages (Dondi 1997, Pereira 2006, Rawlings, et al. 2006). The ceramic industry is particularly capable of incorporating of various wastes. Moreover, at high firing temperatures, incorporation of the wastes into ceramic body is attractive when dealing with the immobilization of hazardous wastes (Bingham and Hand 2006, Marra and Jantzen 2004).

There has been considerable research on the use of different types of wastes for making various constructional materials such as tiles, bricks, glass and cement (Ahmadi and Al-Khaja 2001, Alleman 1983, Alleman and Berman 1984, Aloisi, et al. 2004, Dasgupta and Das 2002, Demir 2008, Demir, et al. 2005, Dondi 1997, Ducman 2007, Goroyias 2004, Köhler 2002, Kurama and Ozel 2009, Montero, et al. 2009, Rawlings, et al. 2006, Sarkar and Das 2003, Toya, et al. 2007, Toya, et al. 2006). Silicate based wastes such as coal and fly ash, slag from steel production, hydrometallurgical mud,

and different types of industrial sludge are proper materials for using in the ceramic and cement industries due to their chemical and mineralogical contents. Utilization and applications of these wastes (especially fly ash) have been intensively studied and research is still ongoing for further use (Rawlings, et al. 2006).

Recently, utilization and recycling of wastes from pulp and paper industry have gained very importance due to their organic and inorganic content (Ahmadi and Al-Khaja 2001, Boni, et al. 2004, Brosnan 2003, Confederation of European Paper Industries 2004, Dasgupta and Das 2002, Demir, et al. 2005, García, et al. 2008, Goroyias 2004, Liaw, et al. 1998, Sutcu and Akkurt 2009, Sutcu and Akkurt 2010). Pulp and paper processing wastes could be used as a new source of raw material due to their inorganic substances such as calcium carbonate, kaolin and talc, or as pore-forming agents due to their organic substances such as cellulose fiber in the production of ceramic materials. They are very suitable materials for production of clay based porous ceramics. They provide good physical and thermal properties such as high porosity, low density and low thermal conductivity to the products. The ceramics produced with incorporation of these wastes can find various applications such as building bricks and refractory bricks for thermal insulation.

2.2. Pulp and Paper Processing Residues

Different processes in the pulp and paper industry result in the formation of different residues or sludge. Pulp and paper processing residues consist of water treatment rejects separated from the paper processing. They generate mainly from three sources: (1) pulping, (2) de-inking operations and (3) wastewater treatments (Monte, et al. 2009).

(1) Pulping residues as called primary sludge come from the production of natural wood fiber, where the coarse particles are removed from waste water. Their fiber concentration is high and the sludge can be easily dewatered.

(2) De-inking sludge occurs by removing of paper additives and inks. This residue includes fibers and high concentrations of inorganic minerals.

(3) Wastewater treatment plant residues originate from secondary systems, which typically is a biological process. Paper residues are composed of the solids removed from process water.

The amount and chemical composition of residues depend on the paper manufacturing process, raw materials used and the wastewater treatments applied. Generally, pulp and paper processing residues or sludge are a combination of water, ink, wood and cellulose fibers, different synthetic organic components and fillers and pigments such as kaolin, talc and calcium carbonate, separated from the recovered paper feedstock. The organic components of the residues are hemicellulose, cellulose, and lignin. During firing, these components are decomposed at different temperature ranges; hemicellulose, cellulose, and lignin are decomposed at 150–300°C, 275–300°C, and 250–500°C, respectively (Kalita 2009).

Paper grades show variations according to the proportion of organic and inorganic substances in their content. Therefore, inorganic components usually exist in printing paper and board production, whereas in the packaging paper industry, sludge of a more organic character is typical (Cernec, et al. 2005). The compositions of paper residues vary widely throughout the industry depend on the raw materials used and the type of operations carried out at paper mill.

The different types of residues at important amount are produced as a result of pulp and paper processing, which have generally a moisture content of 40–60%. The main types of solid waste generated in pulp and paper mills are rejects, green liquor sludge, dregs and lime mud, wastewater treatment sludge, and chemical flocculation sludge from pulp mills; and rejects, de-inking sludge, primary sludge, and secondary or biological sludge from paper mills (Monte, et al. 2009). Sludge generation rates vary widely among mills. For instance, in 2005, as the total waste generated through paper production was about 11% of the total paper production, the waste generated through recycled paper production was about 16% of the total paper production (Confederation of European Paper Industries 2006).

Some portion of the paper residues generated can be reused again in processes, but the un-reusable portion of residues can be disposed in a safe and environmental way. However, the difficult physical form of these residues causes to problems in waste handling and disposal. These residues need to a wide landfill site for their disposal. Therefore, in some European countries such as Germany, Spain and The Netherlands, the residues cannot be disposed at landfill areas. In addition, some researches for the management or new uses of pulp and paper industry wastes have been continued due to their current legislations and increased taxes (Monte, et al. 2009). Recently, the amount of residues disposed in landfills has constantly decreased in European countries. The

reuse of the residues in other industries and applications has constantly increased since 2000 as shown in Figure 2.1 (Confederation of European Paper Industries 2004).

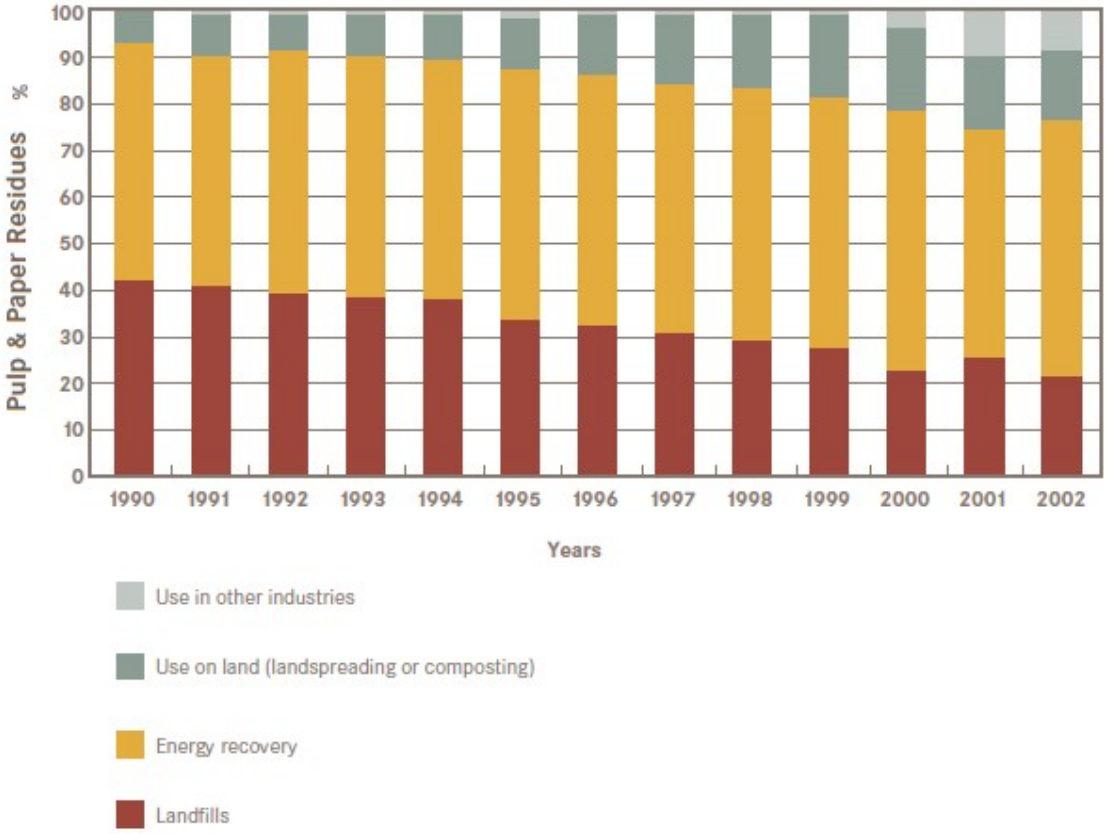

Figure 2.1. Applications of the pulp and paper production residues.
(Source: Confederation of European Paper Industries 2004)

2.2.1. Utilization and Recycling of Paper Processing Residues in Different Applications

The majority of the paper residues originate from wood that is a natural resource. Their composition is composed of calcium carbonate, aluminum and magnesium silicates as well as cellulose and they are not in the group of hazardous wastes (Confederation of European Paper Industries 2004, Monte, et al. 2009). Therefore, these residues are used as a secondary raw material source in various industries. For instance, pulp and paper residues have been used as a soil conditioner due to their organic matters in agricultural applications (WRAP 2007). Use of these residues for various purposes as landfill cover due to their low permeability, and as acidity controlling substance and liming agent due to the high calcium carbonate

content (Boni, et al. 2004), and in the synthesis of calcium aluminum silicates with multifunctional sorption ability are also reported (Jha, et al. 2006).

In addition, pulp and paper residues have been successfully used as the fuel source in cement kilns; these residues based on wood are ideal for co-combustion in heat or power generated plants (Ahmadi and Al-Khaja 2001, CEMBUREAU-The European Cement Association 1997, Murray 2008).

Pulp and paper residues have been proposed to manufacture of an environmentally favorable material with incorporating into ceramic bodies (Dasgupta and Das 2002, Demir, et al. 2005, Dondi 1997, Ducman 2007, Liaw, et al. 1998). Paper residue ashes are used as a raw material in cement, brick and tile manufacturing to produce construction materials (Ahmadi and Al-Khaja 2001, Cernec, et al. 2005, Demir, et al. 2005). Use of these residues for various purposes as pozzolanic addition in cement manufacturing (García, et al. 2008), glass-ceramics (Toya, et al. 2006), light-weight, porous and high strength composite materials consisting of the mullite, cordierite and cristobalite phases (Dasgupta and Das 2002) and as an organic pore-forming agent in bricks (Demir, et al. 2005) are also reported. In the brick production, the addition of paper residues of 5–15% into brick clay mixture improves both the final product and the process (Cernec, et al. 2005, Demir, et al. 2005). Since their fiber content increase the porosity of the product, and also improve the flexibility of the brick body and make them more resistant to cracking during drying. Finally, they enable the production of lightweight bricks. Also, the recycling of paper processing residues into useful construction products such as softboard, hybrid MDF, cement bonded sludge board, tile, low density cement blocks and hardboard, is feasible (Goroyias 2004).

There have been some important advantages of utilization of paper processing residues on the properties of ceramics (Dondi 1997, Stefanov 2003).

(1) The most important advantage is the formation of porosity. During firing of the ceramics with added paper residues, the organic portion of paper residues is burned, and the carbonates are decomposed, leaving pores in the fired bodies. Since their fiber content increases the porosity of the product, and they enable the production of lightweight ceramics.
(2) In addition, their calcium carbonate content has a porosity enhancing effect and creates microporosity at high temperatures.
(3) Also, during drying of formed ceramics with paper residues, the paper residues improve the flexibility and strength of the ceramic body due to their fiber

content and make them more resistant to cracking. In addition, paper residues reduce the shrinkage. Unfired ceramic articles can be easily handled.

(4) They can be also provide an economically advantage because of their energy contribution.

There are also drawbacks of adding the paper residues to clay mixtures (Dondi 1997, Stefanov 2003):

(1) Plasticity of clay mixture reduces with adding of the residues.

(2) In some cases, there are some difficulties during the dosage and extrusion due to the fibrous parts contained in the residues.

(3) Strength of fired ceramic bodies decreases due to their high porosity.

2.3. Clay Minerals

There is a huge literature on clay minerals and presentation of the subject is far beyond the scope of this thesis. But four main clay raw materials are of interest in this thesis:

(1) Clayey earth used for brick production: This clay material has high plasticity, is abundantly available in tonnage quantities, and is widely used as the major raw material in construction brick and roof tile industry.

(2) Enriched clay obtained from an analytical grade chemical manufacturer: This clay is of relatively higher purity because it is enriched by mineral processing techniques to increase the relative proportion of clay.

(3) Industrial grade clay used by floor and wall tile producers: This clay is produced and sold by industrial mining company for use as raw material in industrial floor tile or wall tile manufacturers.

(4) Chamotte which is a thermally treated clay: Fireclay, or chamotte, is a higher purity type of clay that is heated to high temperatures to make it thermally more stable. This refractory product contains much less alkali to avoid low melting phases.

In general, clay minerals are hydrated aluminosilicates and are often found together with large amount of silica. Clay minerals have platy habit and offer high plasticity when in contact with water. The broken surface charges on clay minerals provide this character to clay. Man has long ago discovered the plasticity of clayey earth

and used it to produce a variety of objects. Clay is usually transported from its location of origin by weathering and is deposited in lakes or rivers. For this reason they are largely associated with quartz and organics. Although there is more quartz than clay minerals in most raw clay materials significant plasticity is retained by clay. Below is given an explanation of thermal changes occurring in clay upon heating. Further information about these clay raw materials used in this thesis are given in the following chapters.

2.4. Reactions Occurring During Firing of Clays

During firing of the clays, a lot of complex chemical and physical reactions take place in the clay body. These reactions lead to modifications in porosity, structure, density, dimensions, and mechanical properties of the brick (Meyers 2003). A summary of thermal transformations in a clay body is given in Table 2.1.

Up to about 200°C, the residual water (hygroscopic water adsorbed) is given off during drying. Form 200 to 450°C organic substances are eliminated by the oxidizing reaction. The combined water in the clay is driven off at about 500°C (dehydroxylation) and metakaolinite with amourphous structure forms (Meyers 2003).

$$(\sim 500°C): Al_2O_3 \cdot 2SiO_2 \cdot 2H_2O \rightarrow Al_2O_3 \cdot 2SiO_2 \text{ (metakaolinite)} + 2H_2O \quad (2.1)$$

At 573°C, the crystallographic phase of quartz changes. The room temperature form of quartz (α-quartz) changes to the high temperature form (β-quartz). This process involves a slight change in separation of silicon and oxygen atoms while maintaining the same spatial arrangement and a volume increase occurs (Norton 1952).

Above 1000°C, the mullite crystals are formed. Above 1200°C, quartz transformation to cristobalite is observed. The presence of impurities reduces the transformation temperatures of mullite and cristobalite (Lee, et al. 2008).

$$\sim 925°C: 2(Al_2O_3 \cdot 2SiO_2) \text{ (metakaolinite)} \rightarrow 2Al_2O_3 \cdot 3SiO_2 \text{ (spinel)} + SiO_2 \quad (2.2)$$

$$\sim 1100°C: 2Al_2O_3 \cdot 3SiO_2 \rightarrow 2(Al_2O_3 \cdot SiO_2) \text{ (1:1 mullite)} + SiO_2 \text{ (cristobalite)} \quad (2.3)$$

$$> 1200°C: 3(Al_2O_3 \cdot SiO_2) \rightarrow 3Al_2O_3 \cdot 2SiO_2 \text{ (3:2 mullite)} + SiO_2 \text{ (cristobalite)} \quad (2.4)$$

Table 2.1. Reactions during firing the clays.
(Source: Kornmann 2007)

Temperature	Kaolinite	Illite	Montmorillonite	Chlorite
130°C	Loss of adsorbed water			
150–250°C			Loss of hydration water	
400–550°C		Loss of combined water		
470°C	Loss of combined water, formation of metakaolinite			
700–850°C			Possible spinel formation	Loss of combined water of the brucite layer and micaceous system
900–1000°C		Possible spinel formation		
970–1300°C	Mullite formation			
1050–1200°C		Sintering, crystallization of mullite, fusion		Formation of a vitreous phase
1350–1700°C	Sintering, fusion			

If there is calcium carbonate in the clays, above 700°C, calcium carbonate decomposes into calcium oxide, and releases carbon dioxide. Then, the calcium silicates (wollostanite, $CaO \cdot SiO_2$) together with calcium aluminosilicates such as anorthite ($CaO \cdot Al_2O_3 \cdot 2SiO_2$) and gehlenite ($2CaO \cdot Al_2O_3 \cdot SiO_2$) are formed in small amounts. The gehlenite phase is crystallized from the reaction of metakaolinite and calcium oxide. Then, the formation of anorthite from gehlenite takes place. While the formation of gehlenite begins to occur at lower temperatures (around 800°C) and the anorthite begins to form at relatively higher temperatures (around 900–950°C) (Cultrone, et al. 2001, Traore, et al. 2003).

$$Al_2O_3 \cdot 2SiO_2 + 3CaO \rightarrow 2CaO \cdot Al_2O_3 \cdot SiO_2 \text{ (gehlenite)} + CaO \cdot SiO_2 \quad (2.5)$$

$$2CaO \cdot Al_2O_3 \cdot SiO_2 + 3SiO_2 + Al_2O_3 \rightarrow 2(CaO \cdot Al_2O_3 \cdot 2SiO_2) \text{ (anorthite)} \quad (2.6)$$

2.4.1. $CaO–Al_2O_3–SiO_2$ System

The phases that form from mixtures of paper residues and clays are shown within the $CaO–Al_2O_3–SiO_2$ ternary phase equilibrium diagram (Figure 2.2). The labeled areas show the liquidus surfaces of various solids. The thin curves represent the equal temperature lines while the thicker lines show lower melting compositions such as binary or ternary eutectics.

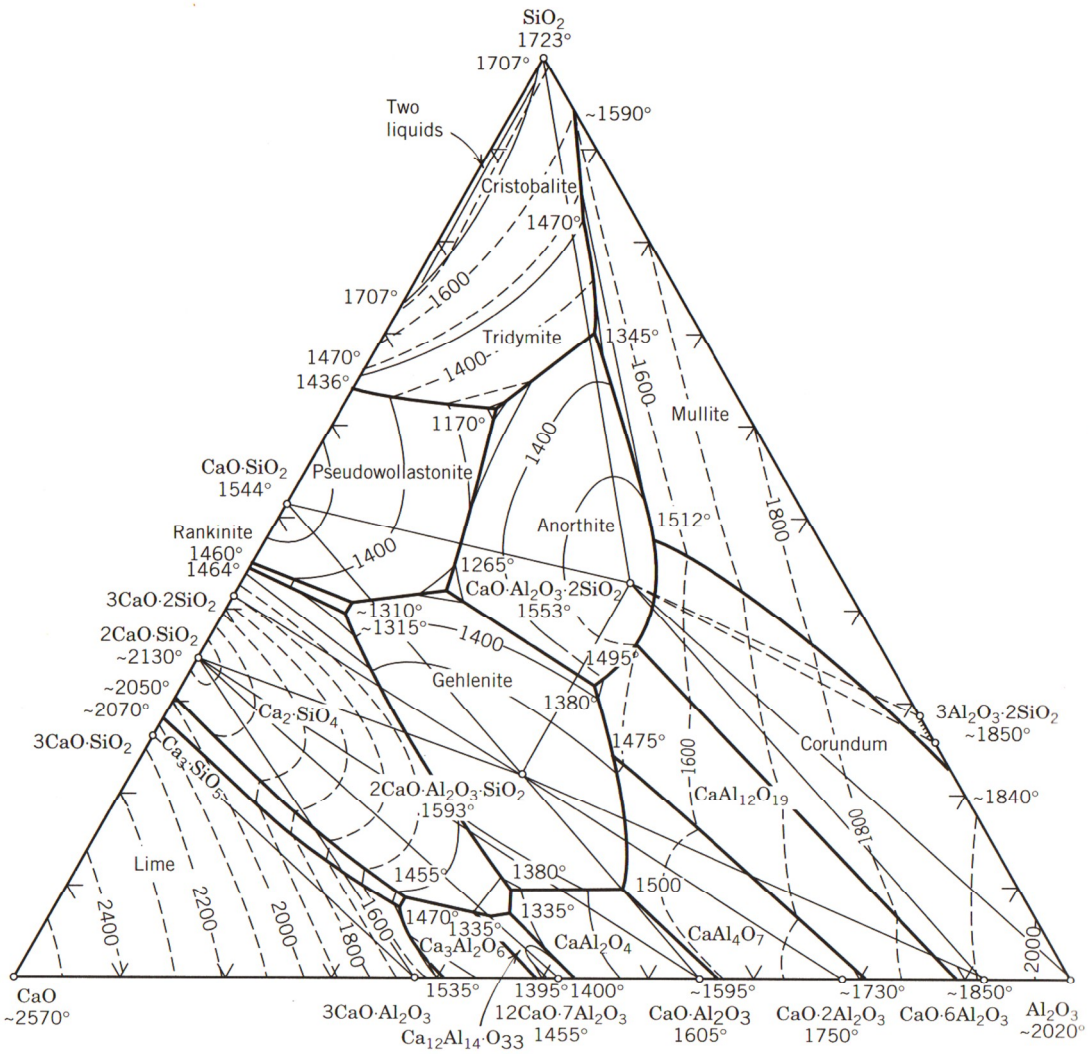

Figure 2.2. $CaO–Al_2O_3–SiO_2$ phase diagram.
(Source: Levin 1975)

In this thesis, during firing of the mixtures containing paper residue and clay, the reaction between calcium oxide (CaO) from paper residues and aluminosilicates (Al_2O_3

and SiO_2) from clays results in the formation of anorthite ($CaO{\cdot}Al_2O_3{\cdot}2SiO_2$) phase. The regions in the diagram contained ternary crystalline phases such as anorthite and gehlenite, as well as binary phases such as mullite and wollostanite. The residue addition into clay system shifts slightly towards the CaO corner. Ca is known to act as a fluxing agent in the alumina-silica system. Therefore, the compositions containing higher concentrations of CaO will be melting at temperatures of 1550°C. In this thesis, addition of paper residues containing CaO up to 30% into different clay systems will move the composition mostly along the anorthite phase region. According to CaO–Al_2O_3–SiO_2 equilibrium phase diagram, pure anorthite exhibits a melting point of 1553°C (Levin 1975).

2.5. Pore Forming Additives

The use of pore-forming agents is one of the frequently used methods to produce porous ceramics. During firing of the ceramics, these pore-forming additives are burned, leaving voids in the ceramics. There are two types of additive that increase porosity:

(1) Additions of compounds that are already porous and inert such as perlite, vermiculite, diatomite, porous glass, aluminum hydroxide etc. Some of these additives can lead to expansion during firing.

(2) Additions of organic compounds that compose, then burn and finally give off CO_2. Main additives are sawdust, paper, expanded polystyrene, organic wastes from papermaking, tanning and waste treatment plants, waste from foundry moulds, coal powder, coal ash and fly ash, etc.

2.6. Thermal Insulating Ceramics

In this thesis, two separate thermal insulating ceramics such as earthenware clay bricks for building applications, and also refractory insulating firebricks for high temperature applications, were studied.

2.6.1. Clay Bricks

Brick clays are composed of clay minerals and non-clay substances along with accessory minerals like carbonaceous matter and water. In industrial processing, the manufacturing of clay bricks is made up of several stages such as extraction of the raw materials, preparation of the clay body, shaping of the products, drying, firing, and treatments after firing. Manufacturing process of earthenware clay bricks and tiles is shown in Figure 2.3.

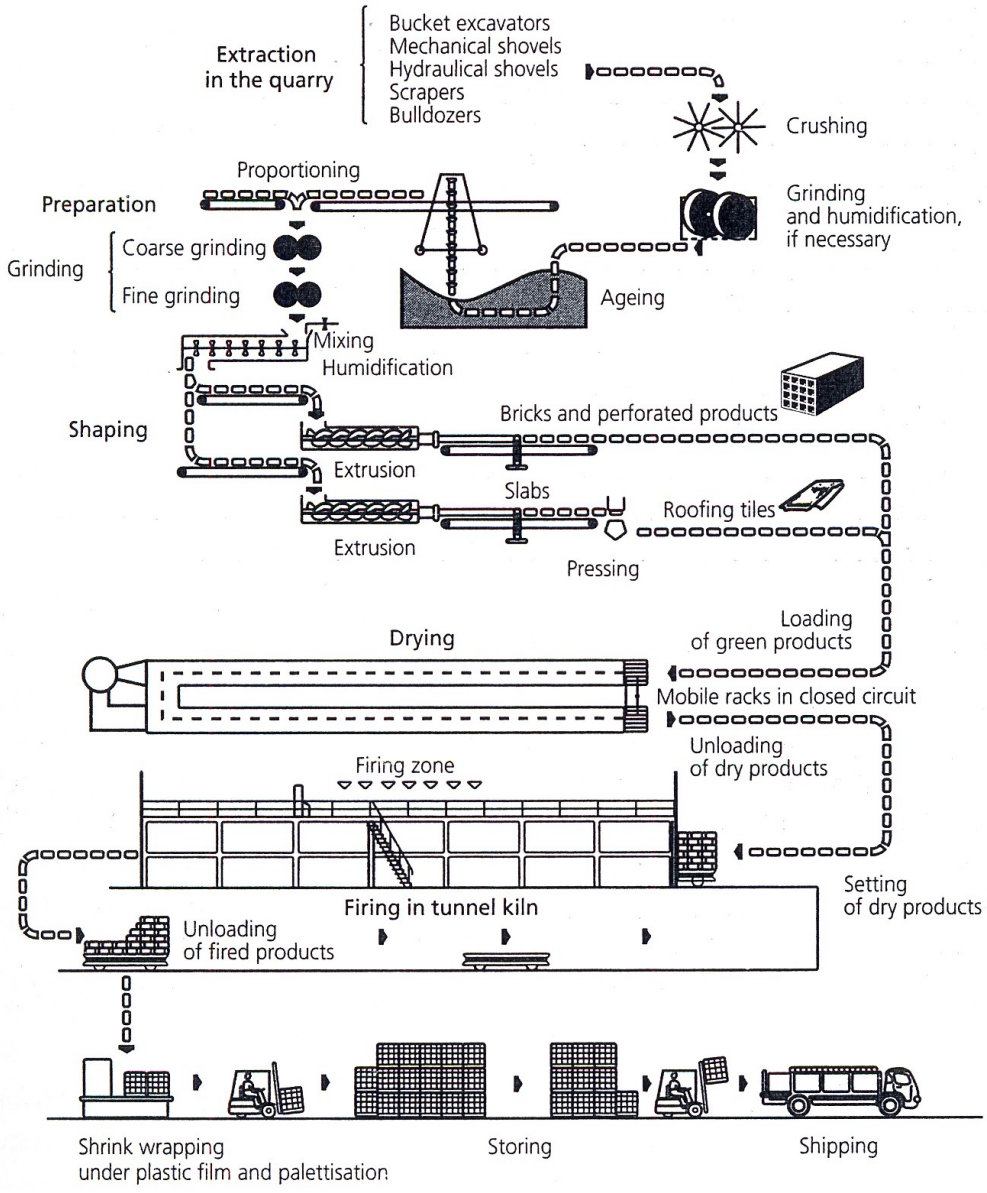

Figure 2.3. Manufacturing process of clay bricks.
(Source: Kornmann 2007)

Clay raw materials mined in open pits are transported to plant storage areas. Raw materials are blended to provide more uniform raw material mixtures. No grinding is done in earthenware industry. The raw material is used as is. The industry largely relies on experience of workers. No compositional control of the feed material is done. The preparation of clay raw material covers the stages such as removing stones and other impurities (roots, scraps); breaking up of the clay to obtain desired particle size; homogeneous blending of various additives; homogenizing and humidifying to obtain the correct plasticity. Water content is controlled and the moisture contents of material going on the shaping process range from 15 to 30% depending on the clay bodies. The shaping method used depends on the type of raw material and in particular water content and type of brick required. Shaping of bricks is usually made with these methods: (1) stiff-mud or extrusion process, (2) soft-mud process, and (3) dry-pressing (or semi-dry pressing) process (Kornmann 2007, The Brick Industry Association 2006).

(1) In stiff-mud or extrusion process, water in the range of 15–20% is mixed into the clay in a pug mill to provide plasticity. The clay mixture goes through a de-airing chamber to remove air bubbles, and the clay increased workability and plasticity gains the strength. The plastic clay is extruded through a die to produce a forming green brick.

(2) In soft-mud process, clay is mixed with 20–30% water and then formed into brick in molds. This process is suitable for clays containing too much water. Bricks are produced by machine or by hand.

(3) Dry pressing process is particularly suited to clays of very low plasticity. Clays are mixed with addition of water up to 10%, and then pressed into steel molds under a pressure from 3 to 10 MPa in hydraulic presses.

Before the firing process, shaped green bricks are dried in dryer chambers at temperatures ranging from 38 to 200°C using waste heat from the cooling zone of the kilns. The drying time varies between 24 to 48 h. In all cases, heat and humidity must be carefully controlled to avoid cracking of the bricks.

The most common type of kiln used for firing brick is the tunnel kiln. This kiln ranged up to 150 m in length includes a preheating zone, a firing zone and a cooling zone. The firing zone is maintained at a maximum temperature of about 1090°C. Kiln fuel may be natural gas, coal, and sawdust. Bricks are fired between 10 and 40 h depending on kiln type and other variables (The Brick Industry Association 2006).

The clay brick and tiles products are typically used in the constructional applications. These products are generally classic solid bricks that have a rectangular

shape, bricks with vertical perforations and roof tiles depending on the application purposes. The perforations in the bricks improve drying and firing, and reduce the quantities of raw materials required; they also increase the thermal insulation levels of the bricks (Kornmann 2007).

2.6.2. Refractory Insulating Firebricks

Refractories are defined as ceramic materials which are resistant to high temperatures. The property requirements of refractories vary significantly according to the application areas. For instance, while processes that demand resistance to gaseous or liquid corrosion need low porosity, high physical strength and abrasion resistance, process conditions that demand low thermal conductivity may need completely different refractories (Leigh 1982).

Insulating firebricks constitute one of the refractory groups which are the most frequently used for heat insulation in industrial applications today. They are the products with a total porosity of at least 45% and an application temperature of at least 800°C (Carniglia and Barna 1992, Norton 1949). They are composed of more or less refractory skeleton having a large proportion of pores. Insulating firebricks are porous and lightweight refractories having much lower thermal conductivity and heat capacity than other refractories. They are suitable materials for refractory lining of industrial furnaces with the aim of reducing heat losses. They are classified according to the bulk density and maximum service temperature by the ASTM standard (ASTM C155-97 2002). For example, the ASTM 20 and 23 groups with high CaO content represent the anorthite ($CaO \cdot Al_2O_3 \cdot 2SiO_2$) based insulating firebricks with maximum temperature limits of 1093°C (2000°F) and 1260°C (2300°F), respectively (Brosnan 2004, Leigh 1982). Also, lightweight refractory bricks have been classified according to their chemical structures as aluminium silicate lightweight refractory bricks, silica lightweight refractory bricks, zircon lightweight refractory bricks and corundum lightweight bricks (Harbison-Walker Refractories 2005). Moreover, they are made of diatomite (more than 70% SiO_2), perlite (high silica mineral), expanded vermiculite (hydrated magnesium-potassium aluminosilicate), calcium silicate, fireclay, kaolin, quartz, bubble alumina and other materials (Harbison-Walker Refractories 2005, Yurkov and Aksel'rod 2005). Insulating firebricks are manufactured by several methods

depending on the density desired. The most common method is to add to the brick mix a combustible material such as sawdust, or fine coke which burns out during the firing. Another method is to include in the brick mix, the materials of low bulk density such as diatomite or expanded forms of perlite, clay, vermiculite, or alumina minerals. In some cases, foaming agents are used to achieve the desired pore structure (Harbison-Walker Refractories 2005). While the safe operating temperatures in the materials based on diatomite, perlite and vermiculite vary between 800 and 1000°C, those based on chamotte, quartz and corundum are as high as 1300°C according to their densities (Harbison-Walker Refractories 2005, Yurkov and Aksel'rod 2005).

Insulating firebricks have high porosity between 45 and 90%. Their maximum pore diameters are smaller than 1 mm. High porosity causes low thermal conductivity and mechanical strength. Besides, they are susceptible to gas and corrosion attacks (Brosnan 2004, Carniglia and Barna 1992, Norton 1949). The thermal conductivity not only depends on their total porosity, but also their pore size and shape, chemical and mineralogical composition. The materials which have the well-developed interparticle contacts and relatively large pores of few millimeters exhibit the higher thermal conductivity (Yurkov and Aksel'rod 2005). Figure 2.4 shows the thermal conductivities of different materials. Porous firebricks show good thermal insulation property because the heat transfer mechanism in these materials is mainly by radiation across the voids, which is an inefficient process at low temperatures (Kingery, et al. 1976).

The porosity is normally formed by adding combustible material to the raw material mixture or via lightweight grog or additives that create porosity by a foaming action. Since it is impossible to build closed cell structures into high void volume ceramics, these materials are all open cell structures. They function by providing stagnant or “dead” gas space (Carniglia and Barna 1992). Pore forming agents such as sawdust, foam polystyrene, fine coke, binders and organic foams, or granular materials such as hollow micro-spheres and bubble alumina are commonly used to obtain decreased density or to create porosity in the bricks (Dergaputskaya, et al. 1980, Horie 1981, Koronthalyova 2007, Kryuchkov, et al. 1999, Pirogov, et al. 1970, Suvorov and Skurikhin 2003, Yurkov and Aksel'rod 2005). During firing, the sawdust burns out, and leaves a large fraction of interconnected pores within the fired body. Foaming agents such as foam polystyrene, organic foams or naphthalene and polymer additives such as special soaps, saponins, gelatin, albumin, phenol formaldehyde resin and polyvinyl

acetate powder can be used to accomplish high porosity into the refractory slip (Horie 1981, Kryuchkov, et al. 1999).

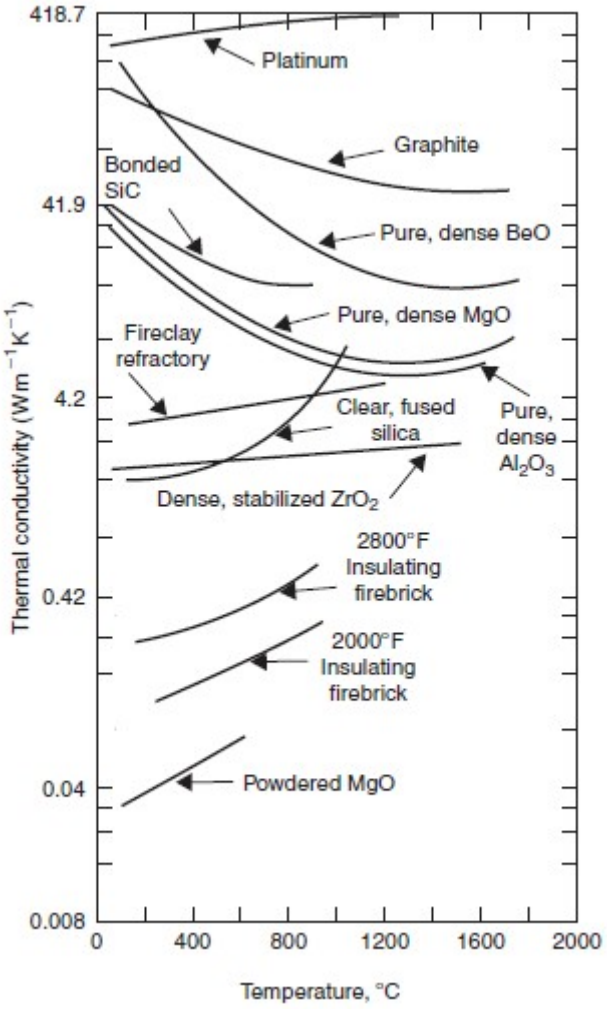

Figure 2.4. Thermal conductivities of different materials.
(Source: Kingery, et al. 1976)

Insulating firebricks are formed by slip-casting to the moulds lined with filter paper, extrusion for plastic mixes, and hydraulic or mechanical pressing for semi-dry and dry mixes. Also, bricks which are complicated in shape are produced by hand forming, vibration or moulding processes. The shaped bricks are dried and fired in chamber furnaces or tunnel kilns under carefully controlled conditions. The firing temperatures correspond to the classification temperatures of the bricks. The final sizing of many brick is accomplished by cutting or grinding (Harbison-Walker Refractories 2005).

Insulating firebricks are used most extensively as backup material for brick of

higher refractoriness and higher thermal conductivity, for the vessel to save energy and obtain acceptable furnace shell temperatures. Also, they may be used as the working linings of furnaces, when they are not subjected to erosion by molten metal or slag, or to abrasion and corrosion. Particularly, they find widely application fields in backup insulation of carbon baking furnaces, aluminum electrolytic cells and blast furnace stove linings, in carbonizing furnace linings, in forge furnace linings and in heat transfer linings, and also in laboratory type electrical kilns (Harbison-Walker Refractories 2005, Thermal Ceramics 2009). Their primary function is usually conservation of energy. Their refractory structure would minimize the heat storage during the periodic heating and cooling cycles of batch type furnaces. For instance, for the lining of aluminum electrolysis cells, heat insulating materials based on diatomite, vermiculite, perlite, calcium silicate, chamotte and anorthite products are preferred for sustaining long-term mechanical loading without deformation at temperatures as high as 900°C (Yurkov, 2005). Insulating firebricks may be preferred instead of castable or fiber products for construction and repair.

The expectations from heat insulating firebricks are low thermal conductivity and low bulk density. They must be capable of withstanding high temperatures of the applications. In addition, they must display low shrinkage and low deformations during their production. Their permanent linear change must be below 2% after exposing to test temperature of 24 hours (Carniglia and Barna 1992, Leigh 1982).

2.7. Heat Transfer Through Porous Structures and Thermal Conductivity Measurements

Heat transfer is the transition of thermal energy from a higher temperature situation to a lower temperature one. The heat transfer behavior of porous materials can be described as follows. Heat is transferred in the materials by means of convection, radiation and conduction (Bejan and Kraus 2003). Thermal conductivity is the property of material that plays a key role in heat transfer calculations of the construction or high temperature materials with aim of heat insulation (Abraitis, et al. 1999, Bhattacharjee and Krishnamoorthy 2004, Zivcova 2009). It is defined as the amount of heat flow under the unit temperature gradient for a unit area that includes some or all of the heat transfer mechanisms, therefore it is term as the effective thermal conductivity (Bejan and Kraus 2003). Thermal conductivity depends on the structure of ceramics, its density

or porosity, and the temperature. It is very sensitive to all defects (porosity, inclusions, and crystalline interfaces) that scatter the thermal flow (Kingery, et al. 1976, Kornmann 2007).

There are two types of conduction heat transfer: steady-state conduction (for local temperature distribution) or transient conduction (for time-dependent temperature distribution) (Bejan and Kraus 2003). For steady-state measurements, heat flow through solid in one dimensional form is governed by Fourier's first law:

$$q = -kA\frac{dT}{dx} \tag{2.7}$$

Where q is the heat flow (W), k is the thermal conductivity (W/mK), A is the cross-sectional area for heat flow, dT/dx is the temperature gradient. The steady-state measurement techniques are based on determining a thermal gradient over a known thickness of a sample to control the heat flow from one side to the other. One dimensional heat flow approach is frequently employed.

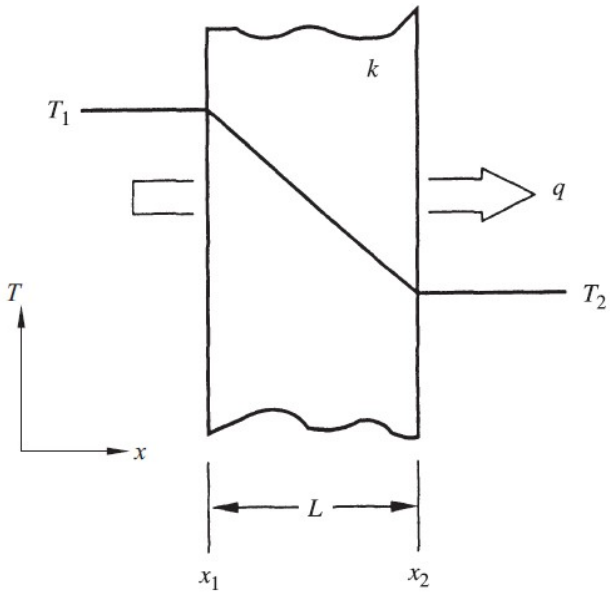

Figure 2.5. Heat transfer by conduction through a wall.
(Source: Bejan and Kraus 2003)

For transient conduction measurements (Hammerschmidt 2003), time-dependent temperature profiles, *T(t)*, are governed by Fourier's law.

$$q = -k \cdot gradT = \rho c \frac{\delta T}{\delta t} \tag{2.8}$$

Where q is the heat flux vector, $gradT$ the temperature gradient, k the thermal conductivity; ρ the density; c the specific heat and t the time. The transient measurement techniques are based on determining thermal performance depending on time.

Heat transfer in ceramics materials is a complex process and involves basic transport mechanisms such as:

(1) heat conduction in solid materials or a stationary fluid (air or water),

(2) convection heat transfer through pore fluid,

(3) thermal radiation from solid surfaces of pores (Bejan and Kraus 2003, Rice 1998).

Most ceramic materials are composed of mixtures of one or more solid phases together with inclusions or defects in the form of pores and micro-cracks. The thermal conductivity of the body depends on the amounts and arrangement of each phase present as well as their individual conductivity (Kingery, et al. 1976). In most ceramic materials an important constituent is the porosity in interconnecting or closed form. The presence of impurities or pores in the body leads to a decrease in the thermal conductivity. The heat flow is seriously disrupted, even though the total porosity is small. Pores or inclusions behave as a barrier or scattering centers for heat flow. In conclusion, they strongly reduce the heat flow path, and severely limit heat transfer mechanisms. Heat transfer is only possible through the fluid in the pore and there is a substantial reduction in the heat transferred (Abraitis, et al. 1999, Bhattacharjee and Krishnamoorthy 2004, Kingery, et al. 1976).

2.7.1. Conduction Heat Transfer Mechanism

Heat is transported by impact processes of the molecules constituting the material. This means that molecules, atoms or electrons of a higher energy level, hence at a higher temperature, collide with those at a lower energy level and hence a lower temperature. The heat flow is directed to pass from a higher to lower level. This is due to the motion of phonons over the crystal lattice. The mean free path of phonons depends on their scattering on other phonons, crystal boundaries and defects. The mean

free path decreases with these lattice imperfections, and affects thermal conductivity. This conduction will be decreased as the porosity increases (Kingery, et al. 1976).

In the solid phase the molecules vibrate in their lattice directions. Only at absolute zero temperature there are no more vibrations. If the vibration amplitudes in a material exist at different temperature, waves of molecules continues through the crystal lattice in the direction of the temperature gradient. Heat is transported in this way and a temperature equilibrium occurs. The heat transport mechanism in a pore-free solid lattice is provided by phonons conduction. If multi-phase structures or pores in the crystal lattice system are present, the phonon conduction is impeded and the thermal conductivity decreases (Kingery, et al. 1976).

The phonon thermal conductivity of perfect crystals can be expressed by following equations:

$$\text{at a low temperature, } k_{phonon} = \left(\frac{T}{\Theta}\right)^3 \exp\left(\frac{\Theta}{n_f T}\right) \tag{2.9}$$

$$\text{at a high temperature, } k_{phonon} \approx \frac{\Theta}{T} \tag{2.10}$$

Where k_{phonon} is the phonon thermal conductivity of material; Θ is the Debye temperature; T is the temperature and n_f is a certain empirical parameter. At higher temperatures the free path of phonons in the crystals remains constant and the change of heat conduction is determined by the temperature dependence between the heat capacity and the thermal radiation (Abraitis, et al. 1999).

Apart from the phonon conduction, heat transport also occurs due to the heat radiation emitted during vibration of the particles and by the convection of a fluid medium. Figure 2.6 shows the heat transport mechanisms in a heterogeneous porous material. The gas filled pores have a very small and the solid a relatively large thermal conductivity value.

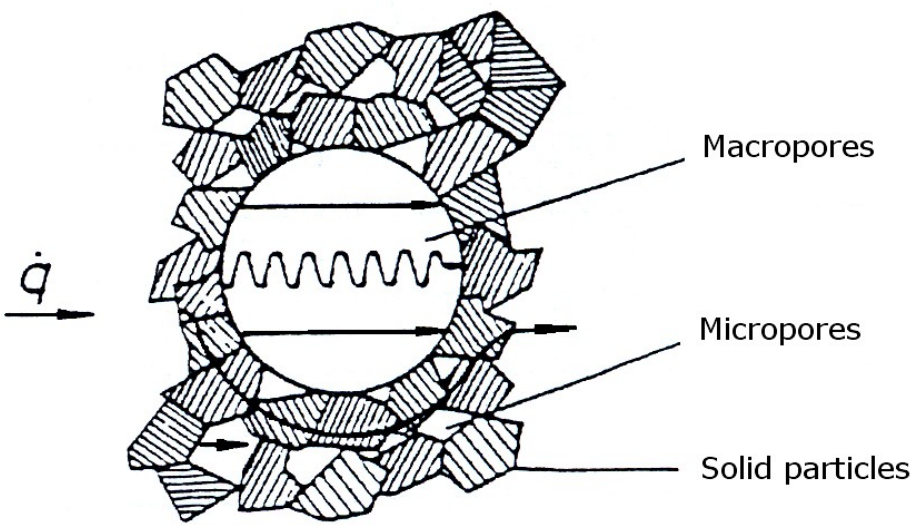

Figure 2.6. Model of heat transfer mechanisms.
(Source: Rimpel 1996)

The complex structure and the variety of mechanisms of heat transfer in ceramic materials explain the use of the term “effective thermal conductivity” (Kingery, et al. 1976). For this reason, the measured thermal conductivity includes some or all of the heat transfer mechanisms (Tsibin, et al. 1988). It reflects the phase composition and structure of the material. The structural changes affect the density and porosity of the material, which in turn affect the change of the effective thermal conductivity. The effective thermal conductivity of porous materials depends not only on the number of pores and microcracks but also on their orientation relative to the direction of the heat flow (Bhattacharjee and Krishnamoorthy 2004, Kingery, et al. 1976).

The porosity dependence of thermal conductivity can be predicted by using the models. The most useful predictions of the porosity dependence of thermal conductivity are Wiener (equation 2.12) and Hashin-Shtrikman upper bounds (Equation 2.13) relations. These relations can be written as

$$k_r = k/k_0 \tag{2.11}$$

$$k_r = 1-\phi \tag{2.12}$$

$$k_r = \frac{1-\phi}{1+\left(\frac{\phi}{2}\right)} \tag{2.13}$$

Where ϕ is the porosity, k_r is the relative thermal conductivity, k is the effective thermal conductivity of the porous material and k_0 is the thermal conductivity of solid phase. The non-linear Coble-Kingery approach (Equation 2.14) can be also used for small porosities;

$$k_r = 1 - \frac{3}{2}\phi \tag{2.14}$$

The modified exponential relation is

$$k_r = \exp\left(\frac{-(3/2)\phi}{1-\phi}\right) \tag{2.15}$$

Figure 2.7 shows the porosity dependence of relative thermal conductivity for these predicted models of some samples studied in literature (Tichá, et al. 2005). According to these models, the thermal conductivity exponentially decreases with increasing the porosity.

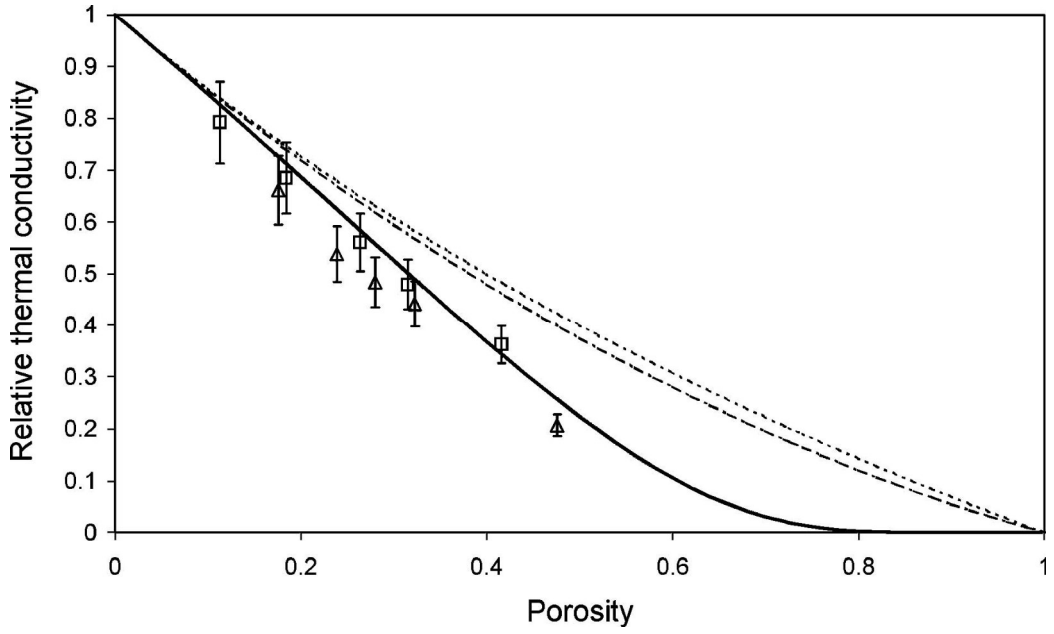

Figure 2.7. Porosity dependence of relative thermal conductivity; two sets of measured data (triangles: alumina, squares: zirconia) and three model predictions (dotted: Maxwell–Eucken/Hashin–Shtrikman upper bound, dashed: Coble–Kingery, solid: modified exponential) (Source: Tichá, et al. 2005)

2.7.2. Convection Heat Transfer Mechanism

Some of heat is transferred by convection in the pore, when the pores are filled with air or combustion gases. Convective transfer occurs due to the motion of a gas mass in the pores or macrocracks only in refractories with high gas permeability at a high pressure and temperature. Convection does not occur in such a material at normal pressure (even on heating from below with a temperature difference of 1000K) (Abraitis, et al. 1999, Tsibin, et al. 1988). Convective effects are dominated by the pore sizes, generally being considered to not become a factor until pore sizes of 1 to 4 mm are reached. This transfer is so small as to be negligible for the usual size of pores. However, the nature of the fluid in the pores is a factor (Rice 1998). The rate of convective heat transfer is given by

$$q = hA(T_s - T_b) \tag{2.16}$$

Where h is the constant heat transfer coefficient, A is the surface area of heat transfer, T_s is the surface temperature and T_b is the temperature of the fluid at bulk temperature.

2.7.3. Radiation Heat Transfer Mechanism

Radiative transfer is often dominant factor for ceramics at high temperatures (>1000°C) (Rice 1998). This transfer also depends on the material and pore character. Some radiative transfer can occur through the solid phase. Some of the heat flow at high temperatures may be due to direct radiation across the pores. For a given amount of porosity, the large pores will transfer more heat by radiation. This is due to the propagation of electromagnetic radiation energy at high temperatures. It is considered as a flow of photons that appear when the microparticles pass from one energy level to another and in radiation from external sources of radiant energy. When photons propagate through the material, they are absorbed and scattered on the walls of the pores, interfaces of two phases, defects of the crystal lattice and other imperfections (Kingery, et al. 1976). In practice, the photon conductivity of a refractory material is evaluated using following equation:

$$k_{photon} = \frac{16}{3} n^2 \sigma T^3 l_r \tag{2.17}$$

Where k_{photon} is the photon thermal conductivity of material; n is the refractive index; σ is the Stefan-Boltzmann constant; T is the temperature and l_r is the mean free path of the radiant energy (Kingery, et al. 1976).

In many cases, for a pore diameter smaller than 3 mm, the effect of convection and radiation in pores can be neglected at atmospheric conditions (Bhattacharjee and Krishnamoorthy 2004, Rice 1998).

2.8. Effect of Porosity and Perforations on Thermal Conductivity of Brick

When pores are introduced into bricks their thermal conductivities are reduced (Equation 2.15). This can be done by either micropores, like the closed pores introduced by pore-making additives before firing of the bricks, or by introducing perforations extending through the brick like in the case of vertically perforated brick. The latter is used extensively by the brick industry to save clay material, to decrease density of the product or to reduce thermal conductivity of the brick. In the case of insulating firebrick refractories, on the other hand, pores are created by addition of pore making substances like sawdust and the overall thermal conductivity of the refractory brick is reduced. In this thesis, both vertically perforated brick and insulating firebrick refractories are studied.

2.8.1. Vertically Perforated Brick

Vertically perforated bricks are manufactured extensively in both Turkey and in EU. These are excellent construction materials that are low-cost, environment friendly and energy saving materials. These properties are derived from their lightweight of 500–1000 kg/m^3 obtained by having continuous vertical perforations as shown in Figure 2.8.

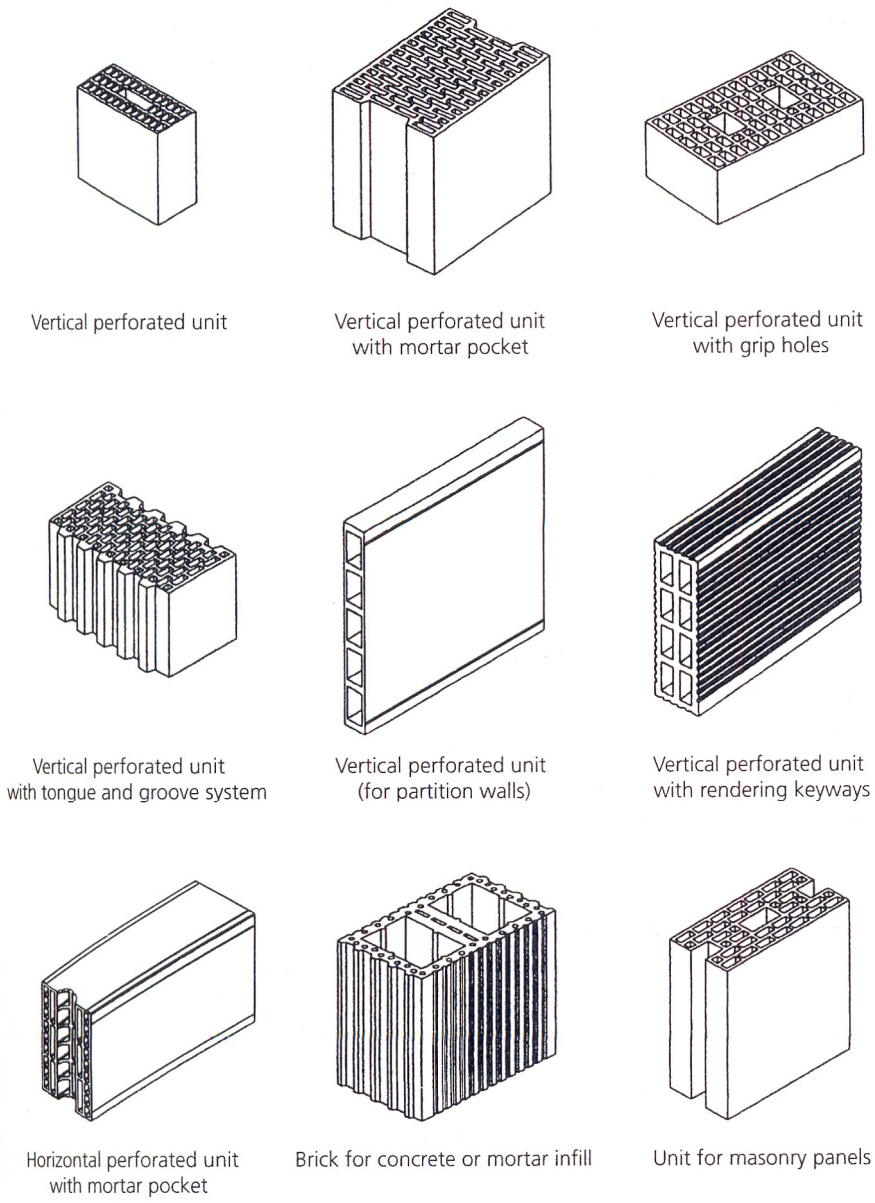

Figure 2.8. Vertically perforated bricks.
(Source: Kornmann 2007)

These perforations act as barriers to heat flow by conduction through the walls of the brick. A reduction in thermal conductivity from 0.8 to 0.2 W/mK is possible solely by introducing these perforations. Different perforation geometries are shown in Figure 2.9. If the path of heat loss is made to follow a zigzag pattern then the path is naturally longer and hence thermal conductivity is reduced. This technique is utilized in insulating brick which have significantly lower thermal conductivity values than their counterparts without zigzag patterns (Kornmann 2007). Notice in Figure 2.9 that the path is made longer by the zigzag placement of perforation for the heat to travel through the brick. Usually bricks are tested for thermal conductivities in a hot box test room

which is maintained at 20°C on one side and 0°C on the other side of the wall (Figure 2.10).

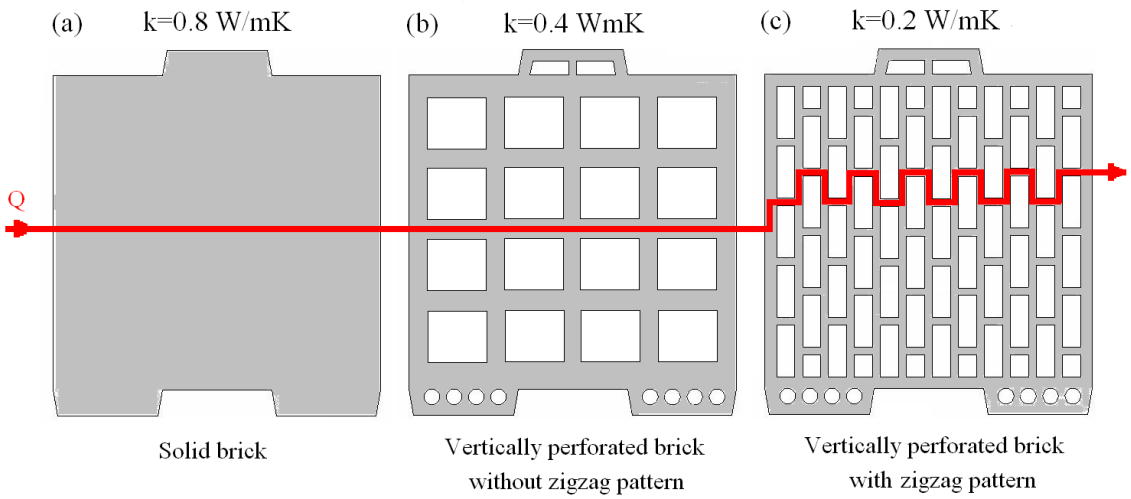

Figure 2.9. Different vertical perforation designs in brick lead to different thermal conductivities: (a) solid brick without perforation, (b) perforations in a regular array, and (c) perforations with a zigzag pattern that maximized the path traveled by heat. Direction of heat flow is shown with an arrow. Notice the benefit obtained from the zigzag pattern.

2.8.2. Insulating Firebrick Refractory

Insulating firebrick refractories are used as safety lining in most furnaces behind the refractory facing. These brick must have low thermal conductivity and low thermal load. Both requirements are met by porous brick geometry with pores ranging from micron scale to few millimeters. Solid ceramic part of these materials is usually of anorthite composition as discussed in section 2.6.2.

2.9. Methods for Thermal Conductivity Measurement

There are two methods for determining the thermal conductivity of ceramic material: (1) the steady-state methods and (2) transient methods. In practice they are realized by approaching the shape of the specimen and the heating regime as close as possible to the created mathematical model that describes a constant or variable temperature field (Bejan and Kraus 2003).

2.9.1. Steady-state Methods

The steady-state methods require a heat source, calorimeter and also additional guarded heaters to realize a static temperature field and to provide thermal equilibrium. The studies on heat conduction in ceramics by the steady-state method show that the measurements are effective only below 1500K (Abraitis, et al. 1999). At a higher temperature the efficiency of the measurements falls rapidly. The steady-state method for heat conduction based on measuring the longitudinal temperature profile is mainly practical for materials with high thermal conductivity. This method is not convenient for ceramic materials with low thermal conductivity (Bejan and Kraus 2003). Since, the accuracy of this measurement depends considerably on the accuracy of the determination of the derivative of the temperature profile. Difficulties on thermal conductivity measurement are often caused by convection and radiation at high temperature. Most commonly used steady-state apparatus for measurements are the hot-box, guarded hot-plate and heat-flow meter (Dondi 2004, Lacarriere 2006, Vivancos 2009). Usually bricks are tested for thermal conductivities in a hot box test room which is maintained at 20^{o}C on one side and 0^{o}C on the other side of the wall (Figure 2.10).

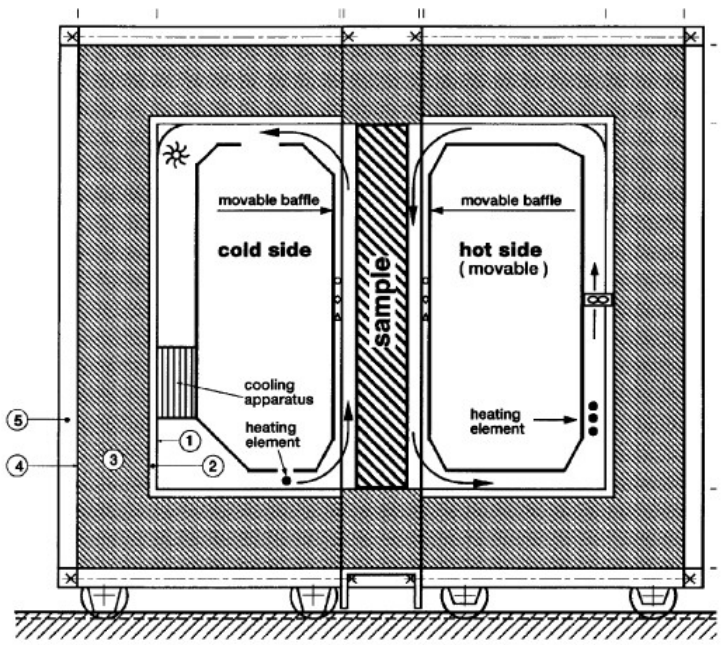

Figure 2.10. Hot-box test apparatus.
(Source: Ghazi Wakili and Tanner 2003)

Heat travels from the hot face to the cold face of the wall. Temperature measurements are made from several different positions on both sides of the wall as well as from the hot and cold chambers. Thermal conductivity measurement of industrial scale bricks are made after the hot box system reaches steady state of 20°C on one side and 0°C on the other side (Ghazi Wakili and Tanner 2003).

2.9.2. Transient Methods (Hot Wire Method)

The transient methods have a less complex structure, and are used to determine the rate of propagation of isotherms in the structure. They may be advantageous rather than stationary method due to shorter measurement periods. Since, one or two temperature-sensitive elements can provide experimental data in a wide temperature range. Common transient measurement apparatus for measurements are the line heat source (hot strip method, hot wire method, needle probe), plane heat source (pulse transient, step-wise transient, hot-plate transient) and the disc heat source (Kang and Morita 2006).

In this thesis, the transient line-source hot wire method was used to determine the thermal conductivity. Hot wire method is one of the transient measurement methods using a line heat source. Recently, the hot wire method is considered an effective and accurate way of determining the thermal conductivity of bricks and refractories (Abraitis, et al. 1999, Bhattacharjee and Krishnamoorthy 2004, Kang and Morita 2006). The hot wire technique is an absolute, non-steady state and direct method, and therefore, it makes the use of standards unnecessary (dos Santos 2008). In the mathematical formulation of the method, the hot wire is assumed to be an ideal infinitely thin and long heat source which is in an infinite surrounding material whose thermal conductivity is to be determined. Applying a constant electric current through the wire, a constant amount of heat per unit time and unit length is released by the wire and propagates throughout the material, generating a transient field of temperatures (Figure 2.11).

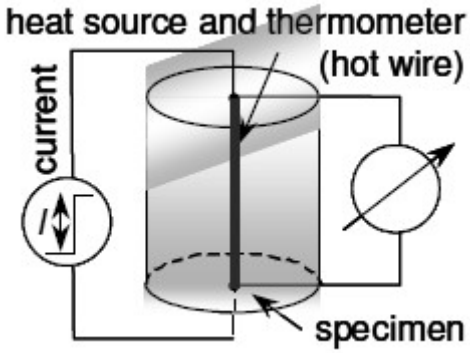

Figure 2.11. Schematic view of hot-wire method.
(Source: Hammerschmidt 2003)

In practice, the theoretical infinite linear source is approached by a thin electric resistance and the infinite solid is replaced by a finite sample. The probe consists of a single heater wire and thermocouple. If the distance from heat source to specimen is constant, thermal conductivity is directly measured by thermal change in the time interval. Probe is placed on the surface of the testing sample. When constant electric power is given to the heater, the temperature of the wire will rise in exponential progression. Temperature rising curve is plotted in linear line in below Figure 2.12 with time axis scaled in logarithm. The angle of this line increases if the sample has less thermal conductivity, and decreases if it has higher thermal conductivity. Therefore, thermal conductivity of a sample can be determined from the angle of the rising temperature line (Kyoto Electronics Manufacturing Co. Ltd. 2009).

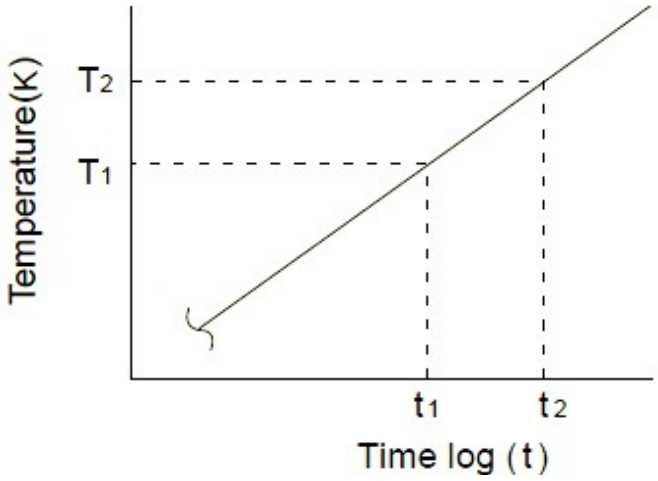

Figure 2.12. Log time and linearity temperature curve for thermal conductivity measurement. (Source: Kyoto Electronics Manufacturing Co. Ltd. 2009)

Hot-wire method determines thermal conductivity of sample by following equation:

$$k = \frac{q}{4\pi} \frac{\ln(t_2/t_1)}{(T_2 - T_1)} \tag{2.18}$$

Where k is the thermal conductivity of sample (W/mK), q is the generated heat per unit length and time of sample (W/m), t is the measured time length (sec), T is the temperature (K).

In this thesis, the thermal conductivity of the earthenware bricks and insulating firebricks was measured with the hot-wire technique. The thermal conductivity measurements were performed at ambient conditions using a Quick Thermal Conductivity Meter (QTM500, Kyoto Electronics) as shown in Figure 2.13a. This equipment is capable of measuring wide range of thermal conductivity from 0.02 to12 W/mK with good accuracy of different materials using hot wire method. It uses different types of sensor probe for different materials. In these studies, PD11 type probe was used to measure the thermal conductivity of the bricks. As can be seen from Figure 2.13b, the sensor probe consists of single heater wire and thermocouple.

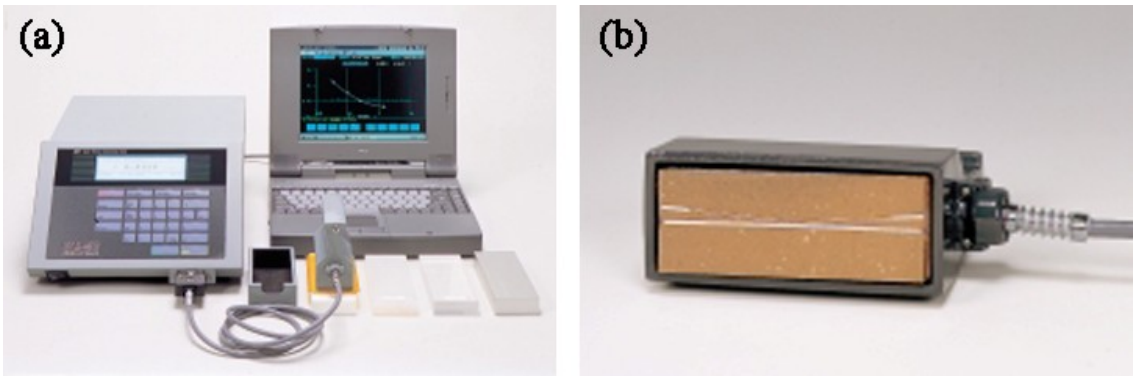

Figure 2.13. (a) A quick thermal conductivity meter (QTM-500, Kyoto Electronics), and (b) PD11 probe used in this thesis.

This method requires 10 to 200 seconds measuring time from start of loading heater current and during which time the temperature rises for only 20°C. This means this method is very effective for a sample of high temperature effect. Since measuring time is short, only the portion near surface is heated, where the obtained thermal

conductivity comes from, and the built-in processor QTM500 computes averaged value of obtained data of temperature curve (Kyoto Electronics Manufacturing Co. Ltd. 2009).

2.10. Effect of Porosity on Mechanical Strength of Bricks

Porosity is one of the main factors affecting the strength of ceramic materials. The presence of pores within the ceramic obviously decreases the cross-sectional area needed for load-bearing of the material. Many experimental studies showed that the strength of the porous ceramics is exponentially decreased with increasing porosity (Dorey 2002, Isobe 2007). Various analytical models have been suggested to represent the relationship between porosity (ϕ) and fracture strength (σ) or elastic modulus (E) (Kingery, et al. 1976, Rice 1998). The following general equations were proposed by Ryskewitsch and McKenzie, respectively:

$$\sigma = \sigma_0 \exp(-n\phi) \tag{2.19}$$

$$E = E_0\left(1 - \frac{\phi}{\phi_0}\right)^n \tag{2.20}$$

Where σ_0 and E_0 is the fracture strength and elastic modulus at P=0, respectively. n is an empirical constant in range 2 to 7, P is the volume fraction porosity (Kingery, et al. 1976). Figure 2.14 shows the relationship of elastic modulus versus porosity for alumina.

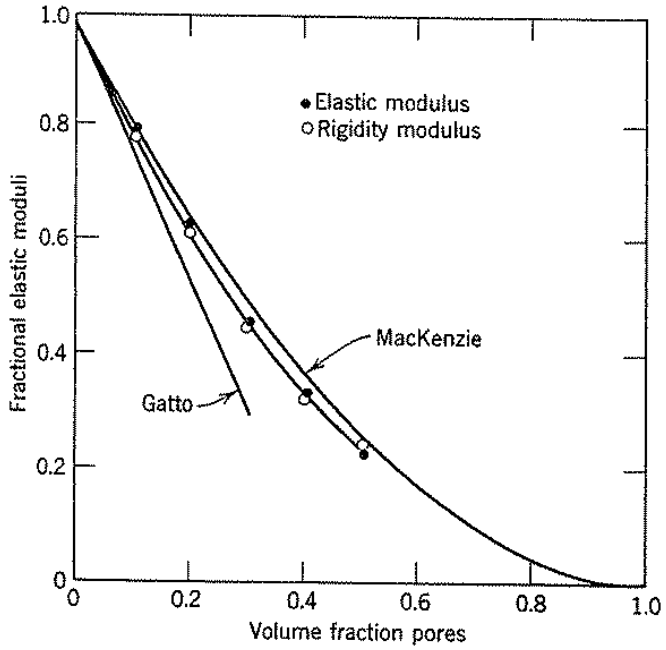

Figure 2.14. Relative elastic modulus of alumina versus porosity (Source: Kingery, et al. 1976).

The critical conditions for fracture are reached at defects such as porosity and inclusions in the sample and the material breaks in a brittle manner. The size of the largest flaw dictates the mechanical strength of material. For ceramics, an important criterion is often the stress intensity factor. As there is a distribution of defects of different sizes in the sample, the specimen breaks at the location of the largest defect under the maximum stress intensity (Kingery, et al. 1976, Rice 1998). The strength of the ceramics varies as a function of geometry, porosity and their orientation (Kornmann 2007).

CHAPTER 3

CHARACTERIZATION OF RECYCLED PAPER PROCESSING RESIDUES

In this chapter, results of characterization of recycled paper processing residue, which is extensively used throughout the thesis, are given. This material is added in various proportions to different types of clay to produce porous ceramic products as explained in Chapters 4, 5 and 6.

3.1. Introduction

In Turkey, there are 38 operational paper mills that produce over 2.0 million tons of varying grades of papers (Devlet Planlama Teşkilatı 2000). Some paper mills use raw wood as raw material feed while other take a semi-finished product of cellulose fibers as feed. Few other mills use a combination of recycled paper and imported cellulose fibers as raw material feed for paper production. Levent Kağıt A.Ş. is such a company located in Izmir, Turkey, the process flow of which is given in pictures in Figure 3.1.

The use of recycled waste paper in the pulp and paper industry generates paper production residues at significant amounts as a by-product from the process of recycling. Sludge generation rates can reach up to 30–40% depending on the processing and raw materials used. In Turkey, these residues are currently disposed of by methods such as landfill or land spread. In general, their moisture content is between 40 and 60%. Disposal of this sludge represents a significant problem.

In this thesis, recycled paper processing residues provided from a local paper producer (Levent Kağıt A.Ş., Izmir, Turkey) were used. Chemistry of these residues is different from that of primary paper mills. In the recycled paper production, process involves a number of filtration steps to maintain the cellulose fiber as much as possible. The fraction that passes the final filter is regarded by the paper producers as waste and is hence stockpiled. These residues contain about 40% organics (cellulose, lignin) and 60% inorganic components like calcite and other clayey materials. In the paper industry, considerably high amount of residue is produced as a result of different mechanical,

chemical and biological effluent treatment processes. Levent Kağıt Company has around 22,000 tons/year (in 2005) recycled paper production capacity. The quantity of residue generated corresponds to almost a half of the paper production. The residues are generally either deposited or burnt. Disposal of this residue is an important environmental and economical problem for the paper industry.

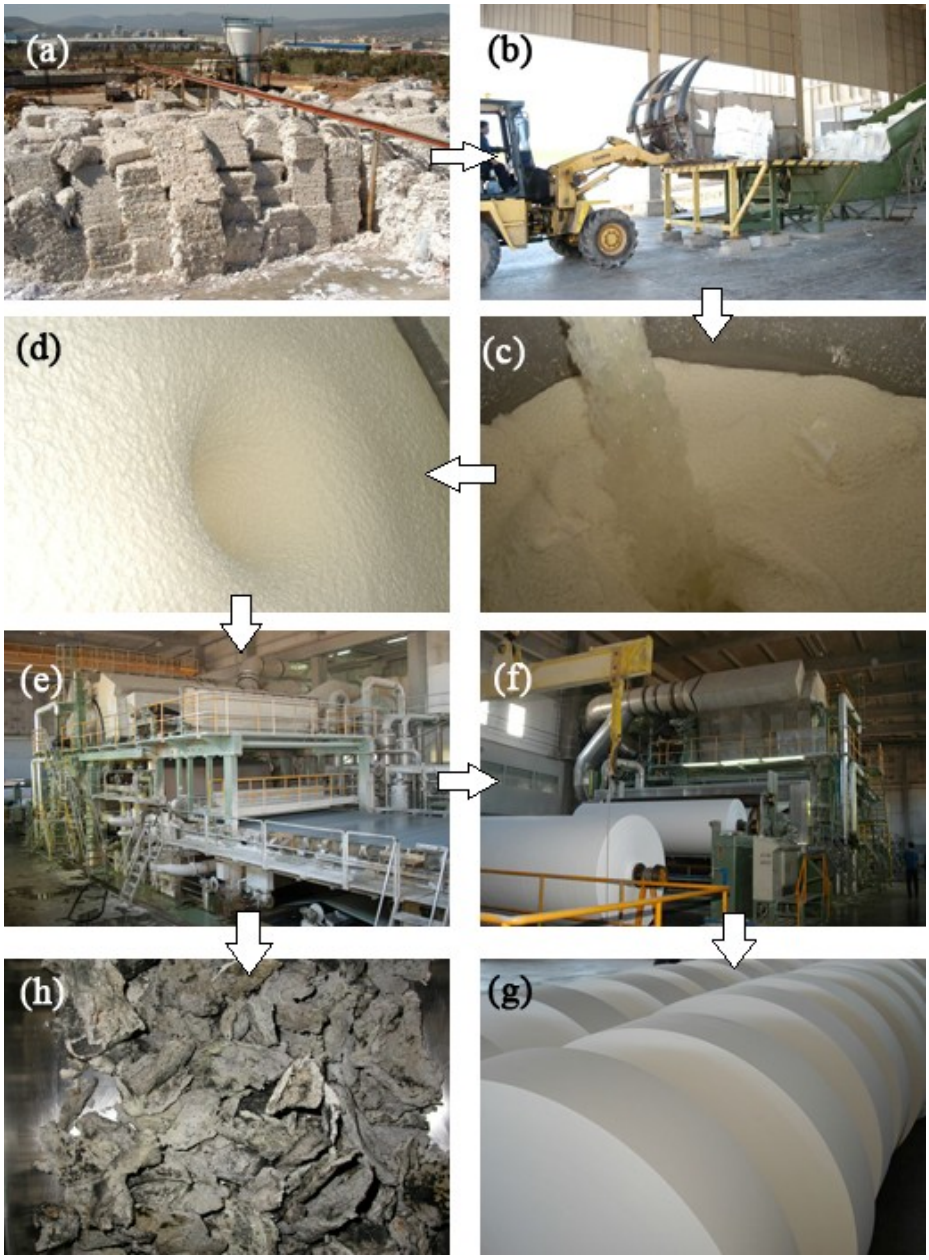

Figure 3.1. Recycled paper production: (a) cellulose and waste paper, (b) loading on the conveyor, (c) dissolution in water by mechanical pulp preparation machine, (d) pulp preparation with additives, (e) hot dispersion on the pulp pans, (f) paper milling, (g) the product and (h) paper processing residues in a sludge form. (Source: Levent Kağıt A.Ş. 2010)

The residues from Levent Kağıt Company have been stockpiled and the company was searching for possibilities to eliminate this residue in an environmentally safe way. In the literature, it has been proposed to convert these residues into an environmentally benign material by incorporating them into ceramic bodies (Dasgupta and Das 2002, Demir, et al. 2005, Dondi 1997, Ducman 2007, Liaw, et al. 1998). Use of these residues for various purposes like a pH-controlling substance (Boni, et al. 2004), synthesis of calcium aluminosilicates with multifunctional sorption ability (Jha, et al. 2006), pozzolanic addition in cement manufacturing (García, et al. 2008), glass-ceramics (Toya, et al. 2006), porous and high strength ceramics consisting of the different phases (Dasgupta and Das 2002) and as an organic pore-forming agent in bricks (Demir, et al. 2005) are also reported. Also, the recycling of paper processing residues into useful construction products such as softboard, hybrid MDF, cement bonded sludge board, tile, low density cement blocks and hardboard, is feasible (Goroyias 2004).

3.2. Material and Method

Paper processing residues that were randomly sampled from the production line were brought from the paper producer (Levent Kağıt, Turkey) into our laboratory in large 50 L plastic containers. The paper residues were initially dried in a laboratory oven at 100°C for 24 h to determine their water content. After drying, the residue turned into an agglomerated hard mass which was broken up in a disc mill (Pulverisette 13, Fritsch, Germany) to produce a workable powder with around 100 μm of average particle size. About 10 kg of a powdered paper residue stock was prepared for future experiments. Such powdered dry residue was the best for further mixing tests with clay. Characterization studies of the paper residues were performed to determine their chemical, mineralogical, physical and thermal properties. Microstructural observations of the paper residues were made by using Scanning Electron Microscope (SEM, Philips XL-30S FEG). Their chemical composition was determined by using energy dispersive X-ray fluorescence spectrometer (XRF, Spectro IQ II) and quantitative elemental analysis with energy dispersive X-ray spectroscopy detector (EDS) was also done on the paper residues. Their mineralogical content was identified by using X-ray diffractometer (XRD, Philips X'Pert Pro). Also, thermal properties of the paper residues

were determined with thermogravimetric analysis (TGA, Shimadzu TGA-51/51H) and differential thermal analysis (DTA).

3.3. Characterization Results of Paper Processing Residues

The paper residues were in the form of sludge which was dried in an oven at 100°C before breaking of agglomerates. As-received recycled paper processing residues obtained from the paper producer had about 65% moisture content.

3.3.1. Microstructural Characterization of the Paper Residues

In Figure 3.2, a general SEM micrograph of dried paper processing residues is shown. According to the SEM-EDS analysis, the paper residues essentially consisted of cellulose fibers and $CaCO_3$ along with some SiO_2, Al_2O_3 and MgO.

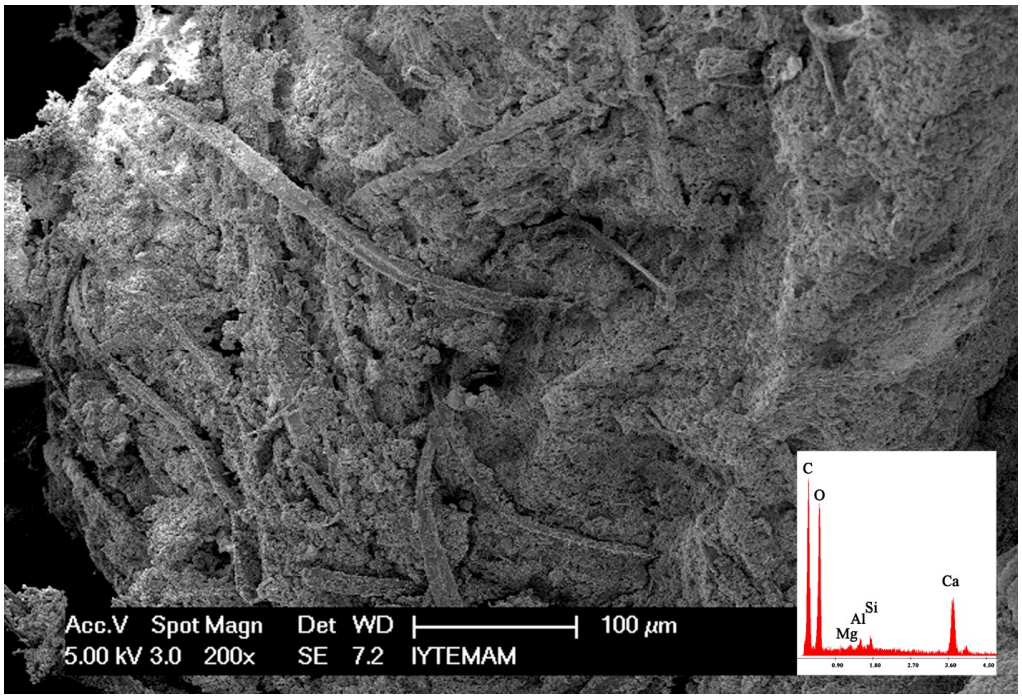

Figure 3.2. A general SEM micrograph of paper processing residues. Inset: EDS analysis.

In Figures 3.3(a) and (b), microstructures of short cellulose fibers and fine inorganic particles in the paper residues are shown, respectively. Thicknesses of the

cellulose fibers were between 5 μm and 20 μm. Microstructure of inorganic particles in the residues indicated that these particles were smaller than 5 μm.

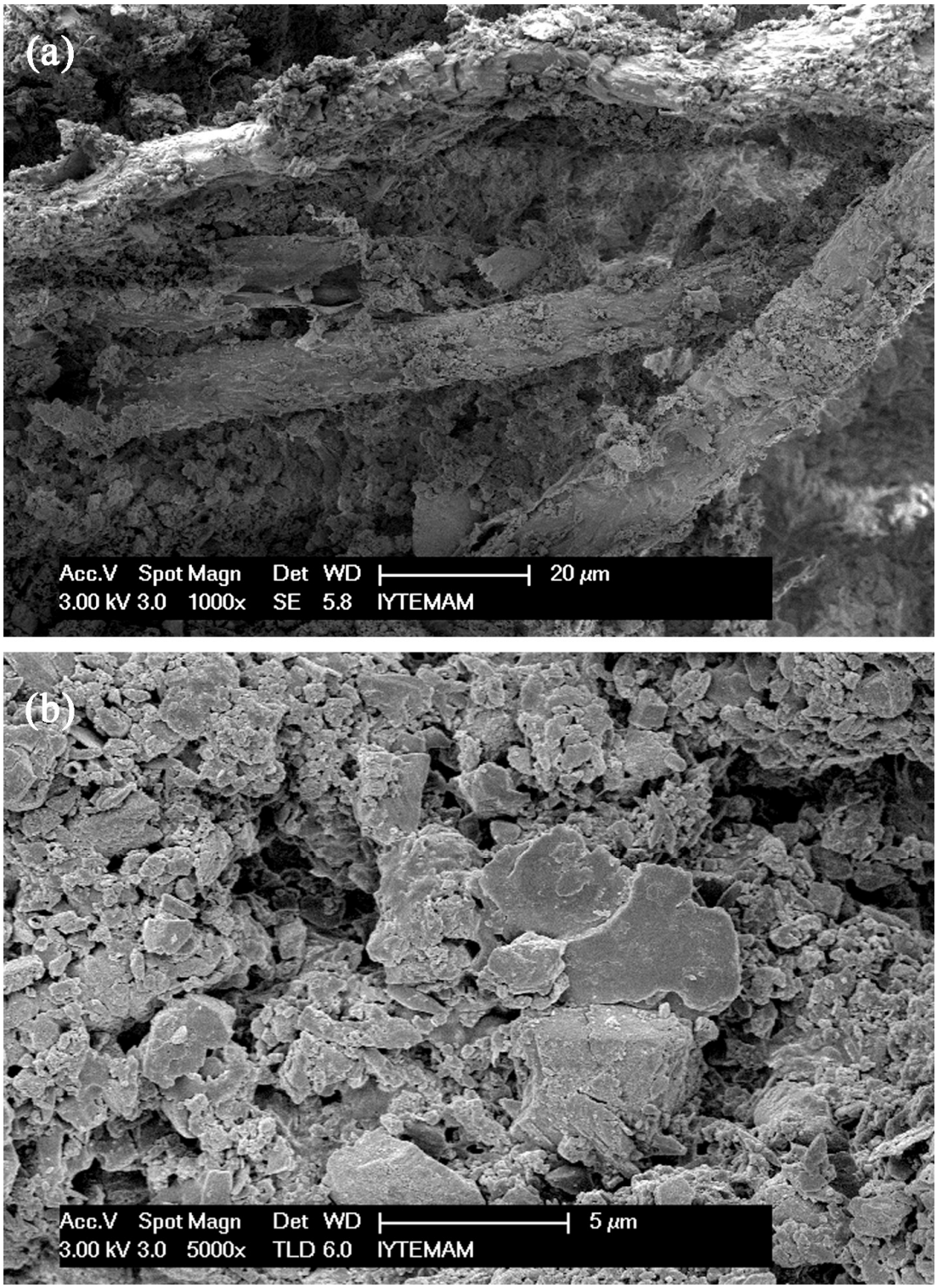

Figure 3.3. The recycled paper residue constituents: (a) cellulose fibers, and (b) inorganic particles (calcite, clay, etc.).

3.3.2. Chemical Analysis of the Paper Residues

Two different analysis methods such as X-ray fluorescence (XRF) and Energy dispersive X-ray spectroscopy (EDS) were applied to the paper residues to determine their chemical compositions. Chemical composition of the paper residues is given in Table 3.1 in oxide form. According to the XRF analysis, the paper residues included a large fraction of Ca in addition to Si, Al and Mg. This calcium most probably existed in the form of calcite ($CaCO_3$). Amount of the chlorine and sulfur (SO_3) was 0.17% and 0.09%, respectively. Loss on ignition (LOI) value of the residues upon heating at 1000^oC was around 54%. According to SEM-EDS analysis, the paper residues mainly consisted of calcium oxide and carbon dioxide (generated from burning of organics and decomposition of carbonates) along with some oxides of silicon, aluminum and magnesium.

Table 3.1. Chemical composition of the paper residues.

Constituents	XRF (wt.%)	EDS (wt.%)
CaO	32.91	21.6±1.3
Al_2O_3	4.14	2.5±0.3
SiO_2	6.42	5.1±0.6
MgO	1.54	1.3±0.1
K_2O	0.12	-
Fe_2O_3	0.28	-
TiO_2	0.09	-
CO_2	-	69.5±0.3
Loss on ignition (1000°C)	53.8	

3.3.3. Mineralogical Characterization

The mineral compounds of the paper processing residues were investigated by using XRD with CuK_α radiation (λ=1.542 Å) at 40 kV in the 2θ intervals of 5–70°. Figure 3.4 shows XRD patterns of as-received and heat-treated paper residues. XRD analysis showed that as-received paper residues contained calcite ($CaCO_3$, Ref. 47–

1743), cellulose (Ref. 50–2241) and some weak peaks for kaolinite-montmorillonite ($Na_{0.3}Al_4Si_6O_{15}(OH)_6 \cdot 4H_2O$, Ref. 29–1490). The paper residues that heat-treated at 1000°C consisted of calcium oxide (Ref. 48–1467) and minor calcium aluminates and silicates.

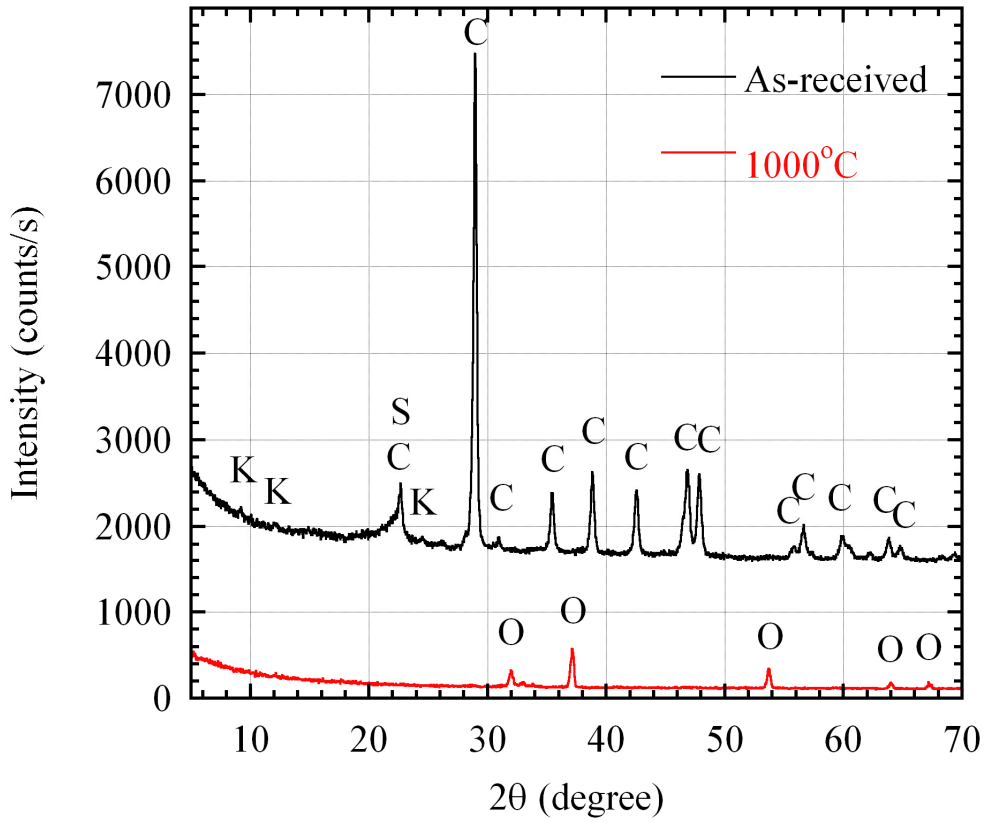

Figure 3.4. X-ray diffraction patterns of as-received and heat-treated paper processing residues (C: calcite, S: cellulose, K: kaolinite-montmorillonite, O: calcium oxide).

3.3.4. Thermal Analysis of the Paper Residues

Thermogravimetric analysis of the paper residues was carried out by using Shimadzu TGA–51/51H for TGA type of instrument. Approximately 11.5 mg sample was heated at 10°C/min under 40 ml/min nitrogen purge stream up to 1000°C. Figure 3.5 shows thermal analysis (TGA/dTGA and DTA) curves of paper processing residues. As can be seen from Figure 3.5a, total weight loss (loss on ignition) of about 54% was observed at 1000°C. The first 4% decrease in the mass occurred in between 25 and 250°C due to the evaporation of physical water. The second mass loss (28.5%) was

observed in the 250–500°C range which may be largely due to the burning of paper residues. The fast decomposition is most possible due to the removal of cellulose at 250–350°C. After rapid reaction, relatively slow pyrolysis reaction occurred between 350 and 500°C, and the slow reaction is most possible due to the lignin decomposition (Kalita 2009). The weight loss (21%) observed above 700°C may be due to the decomposition of carbonates.

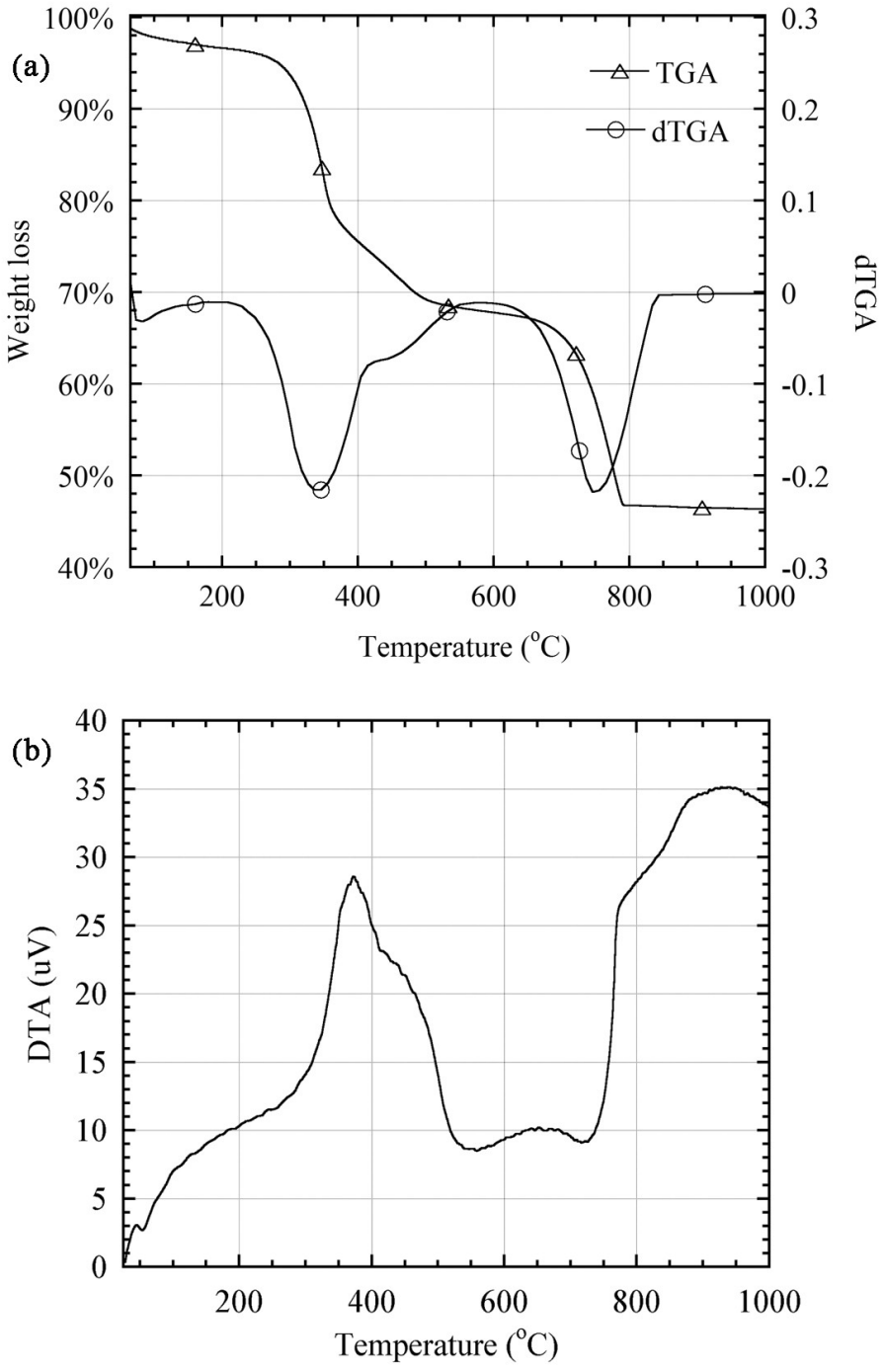

Figure 3.5. Thermal analysis of the paper residues: (a) TGA/dTGA and (b) DTA curves.

In DTA curve (Figure 3.5b), there is mainly one large exothermic reaction between 300 and 500°C corresponding to the burning of cellulose in paper residues. Another endothermic reaction was observed around 700°C which corresponds to the decomposition of calcium carbonate. The former exothermic peak can be considered useful as a contribution to ease the thermal load of the kiln on firing of the ceramic materials that contain the paper residue. The latter calcite decomposition peak is more a liability than asset for thermal load.

In another test, dried paper residues were also fired at 425 and 900°C to determine their organic and inorganic content. Solid part of these wastes contained about 30% organic and 70% inorganic components like calcite and other clayey materials. Figure 3.6 shows the solid contents of the paper residues.

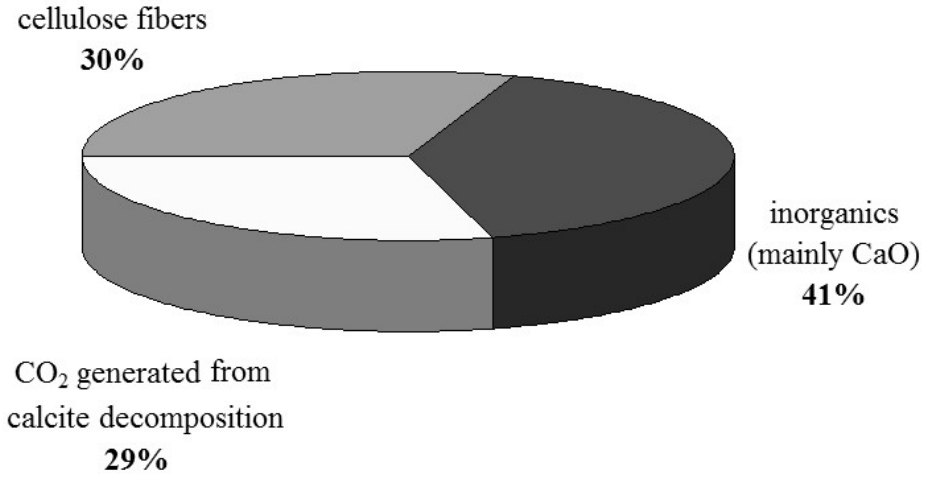

Figure 3.6. The solid content of the paper residues.

3.3.5. Eluate Analysis of the Paper Residues

Paper sludge mainly collected from wastewater treatment plants of the paper manufacturing factory were subjected to a toxicological characterization to provide a preliminary assessment of their suitability for brick and ceramic production. The leach ability and toxicity of organic compounds in the mentioned industrial waste was examined.

Eluate test analysis of the refining paper sludge was conducted according to Turkish Hazardous Wastes Regulation (TS EN 12457-4 (EK11A) 2005). In this test, liquid/solid waste ratio is 10 liters/kg. The eluate analysis results of the refining paper

sludge are given in Table 3.2. According to this analysis results, these paper residues do not represent a major threat for the environment in regard to heavy metal content, thus they could be classified as a non-hazardous waste (DEU 2006, Environmental Protection Agency 2006).

Table 3.2. Eluate test analysis of the paper sludge, (mg/L).
(Source: DEU 2006)

Parameters	Measured values	Standard values
As	<0.1	0.05–0.2
Ba	0.108	2–10
Cd	<0.01	0.004–0.1
Cr	<0.01	0.05–1
Cu	0.236	0.2–5
Hg	<0.01	0.001–0.02
Mo	<0.1	0.05–1
Ni	0.113	0.04–1
Pb	<0.025	0.05–1
Sb	<0.02	0.006–0.07
Se	<0.02	0.01–0.05
Zn	0.21	0.4–5
Cl	142	80–1500
F	1.94	1–15
SO_4	412	100–2000
DOC	74.3	50–80
TDS	4000	400–6000
TOC	48470 (mg/kg)	50000 (mg/kg)

DOC: Decomposed Organic Carbon
TDS: Total Decomposed Solid
TOC: Total Organic Carbon

3.4. Conclusions

The pulp and paper industry generates considerable amounts of waste. The waste is very diverse in composition and consists of different types of sludge and rejects.

Recycled paper processing residues constitute an important part of these paper processing wastes. These residues are generated in the production of recycled paper from waste printing paper. Paper residues are a combination of water, short cellulose fibers and minerals such as calcium carbonate and kaolin separated from the recovered paper feedstock.

Although paper sludge generation is continuously increasing, the studies about reuse of these wastes in agricultural applications or other industries are unfortunately not enough. In Turkey, these residues are currently disposed by methods such as landfill or land spread. The disposal of this sludge represents a significant disposal problem for wastes. Therefore, the utilization of these wastes either for energy recovery or conversion into useful products is much more convenient from both economical and ecological standpoints. This thesis study proposed to convert these residues into environmentally benign materials by incorporating into different types of the ceramic bodies such as brick clay, aluminum silicate, alkali clay and fireclay. They could be used as either pore former due to their organic and carbonate content or a new crystalline phase maker due to their inorganic content. Paper processing residues were used to produce porous and light-weight ceramic bodies. These porous ceramic bodies are expected to provide lower thermal conductivity in these studies.

The characterization studies of the recycled paper processing residues showed that the as-received paper residues had about 65% moisture content. Chemical, mineralogical, physical and thermal properties of these paper residues were determined. Solid part of these residues contained about 30% organics and 70% inorganic components like mainly calcite and other clayey materials. According to thermal analysis, total weight loss of dewatered residues was about 54% at 1000°C. Two main reactions occurred during heating of the residues. The first reaction occurred between 200 and 550°C was due to the burning of paper residues. The fast decomposition was due to the removal of cellulose at 250–350°C, and relatively the slow reaction was due to the lignin decomposition between 350 and 550°C. The second main reaction occurred between 600 and 850°C was due to the decomposition of carbonates. The firing regime of ceramics produced in following studies was planned according to the thermal behavior of the residues.

CHAPTER 4

THE USE OF RECYCLED PAPER PROCESSING RESIDUES IN MAKING POROUS BRICK WITH REDUCED THERMAL CONDUCTIVITY

4.1. Introduction

Energy savings is an important issue in the world because of both economic and environmental concerns. Consumption of energy from buildings constitutes about 33% of total consumption with about half of this lost through the walls (Wouter 2004). The European standard states that, depending on the location and climate, walls should be made of material with a heat transfer coefficient of 0.4 to 0.7 W/m^2K, the lower the better (EN ISO13790 2008). If the thermal conductivity is further reduced heat loss will be decreased and, hence many brick manufacturers are seeking to produce such materials (Wienerberger 2008). Earthenware clayey raw material is generally used with few pre-treatment steps for extruded perforated bricks. Firing temperature is generally of the order of 1000°C. The product consists of vertical perforations to reduce heat transfer through the brick (See section 2.8.1). There are two different thermal conductivity values of these bricks: first involves the bulk of the material constituting the walls while the second involves thermal conductivity of the entire product consisting of large vertical holes of rectangular cross-section. Bulk of the material has a thermal conductivity of roughly 0.8 W/mK. This value can be reduced by addition of pore-forming agents to the brick before firing (Demir 2008, Demir, et al. 2005, Dondi 1997, Ducman 2007, Junge 2000, Köhler 2002, Rimpel 1996, Swoda 1997). When this is made into an extruded product with vertical perforations its thermal conductivity will be much lower (e.g. as low as 0.08 W/mK) (Erker 1996, Rimpel 2001, Schlagmann Poroton 2009). Several different pore-forming agents like wood sawdust, polymers, leather residues, mineral additives, polystyrene, coal dust, organic residues, paper-making sludge, powder limestone have been used (Demir 2008, Demir, et al. 2005, Dondi 1997, Ducman 2007, Junge 2000, Köhler 2002, Russ, et al. 2005).

There are different sources of paper residues suitable for use in bricks. Some researchers used residues obtained from primary paper mills to be incorporated into a brick (Demir, et al. 2005). In this study, however, the residues from a recycled paper manufacturer are utilized in brick making. Chemistry of the residue is different from primary paper mills. In the recycled paper production, process involves a number of filtration steps to maintain the cellulose fiber as much as possible. The fraction that passes the final filter is regarded by the paper producers as waste and is hence stockpiled. This residue contains about 30–40% organic and 60–70% inorganic components like calcite and other clayey materials. In the paper industry, considerably high amount of residue is produced as a result of different mechanical, chemical and biological effluent treatment processes (for example; around 60 tons/day, in Levent Kağıt A.Ş., Turkey). The amount and chemical composition of residues depend on the paper manufacturing process, raw materials used and the wastewater treatments applied. The quantity of residue generated corresponds to almost a half of the paper production. The residues are generally either deposited or burnt. Disposal of this residue is an important environmental and economical problem for the paper industry. It has been proposed to convert this residue into an environmentally benign material by incorporating into a ceramic body (Dasgupta and Das 2002, Demir, et al. 2005, Dondi 1997, Ducman 2007). Use of this residue for different purposes like a pH-controlling substance (Boni, et al. 2004), synthesis of calcium aluminosilicates with multifunctional sorption ability (Jha, et al. 2006), pozzolanic addition in cement manufacturing (García, et al. 2008), glass ceramics (Toya, et al. 2006), lightweight, porous and high strength composite materials consisting of the mullite, cordierite and cristobalite phases (Dasgupta and Das 2002) and as an organic pore-forming agent in bricks (Demir, et al. 2005) are also reported.

The motivation behind this work which was inspired by the results of the above studies was the use of wastes in ceramic production where environmentally hazardous species would be used to produce a porous and lightweight ceramic body. Such a porous body can be used in making perforated bricks by extrusion to reduce thermal conductivity. Inorganic content of the residues used in this study was largely calcite with little more clay. This waste can form anorthite ($CaAl_2Si_2O_8$) or gehlenite ($Ca_2Al_2SiO_7$) upon thermal treatment at higher than 1000°C. Pores are expected to form when cellulose fibers are burnt at 300–500°C and also calcite decomposes above 700°C.

Below are given the procedure and results of tests to achieve a porous brick with improved thermal insulation properties.

4.2. Experimental

4.2.1. Raw Materials

In this study, brick raw material obtained from a brick manufacturer (Yüksel Tuğla in Turgutlu, Turkey) was used. Recycled paper processing residues (PPR) obtained from Levent Kağıt A.Ş. (in Izmir, Turkey) were used for pore making. Chemical, mineralogical, physical and thermal properties of the paper processing residues were presented in the Chapter 3.

4.2.2. Characterization of Raw Materials

Brick raw material and paper residues were initially subjected to pre-treatments such as drying and grinding. Particle size analysis of the brick raw material subjected to disc pulverizing was made on a Malvern Mastersizer-2000 Instrument to measure its particle size distribution.

Chemical analysis of brick raw material was made by using Energy dispersive X-ray fluorescence spectrometer (XRF, Spectro IQ II). Microstructural investigation of the brick raw material was performed by scanning electron microscopy (SEM, Philips XL-30S FEG). The brick raw material was characterized to determine its mineral composition by X-ray diffractometer (XRD-Philips X'Pert Pro). Its thermal properties were analyzed by thermo-gravimetric analysis (TGA) and differential thermal analysis (DTA). These tests were carried out to evaluate the behavior of clay during firing.

4.2.3. Procedure for Brick Production

Initially, brick raw material and paper processing residues (PPR) were dried at 110°C in oven. Then, they were powdered by a disc mill (Pulverisette 13, Fritsch, Germany). Dewatered paper residues were blended with industrially used brick clay raw

material in a Heidolph mixer at a mixing speed (650–800 rpm) for 30 min (Figure 4.1a). Solid powder mixture-water ratio of 1:1 was used in the blending process. The resulting mixtures contained up to 30% by weight of the paper residues. The mixtures were dried in an oven at 110°C for 16 hours. Dried powder mixtures were ground into mortar, and fine powder mixtures were spread out on a tray. Powder mixtures were granulated with sprayed cold water (average 10% moisture content) while shaken (Figure 4.1b).

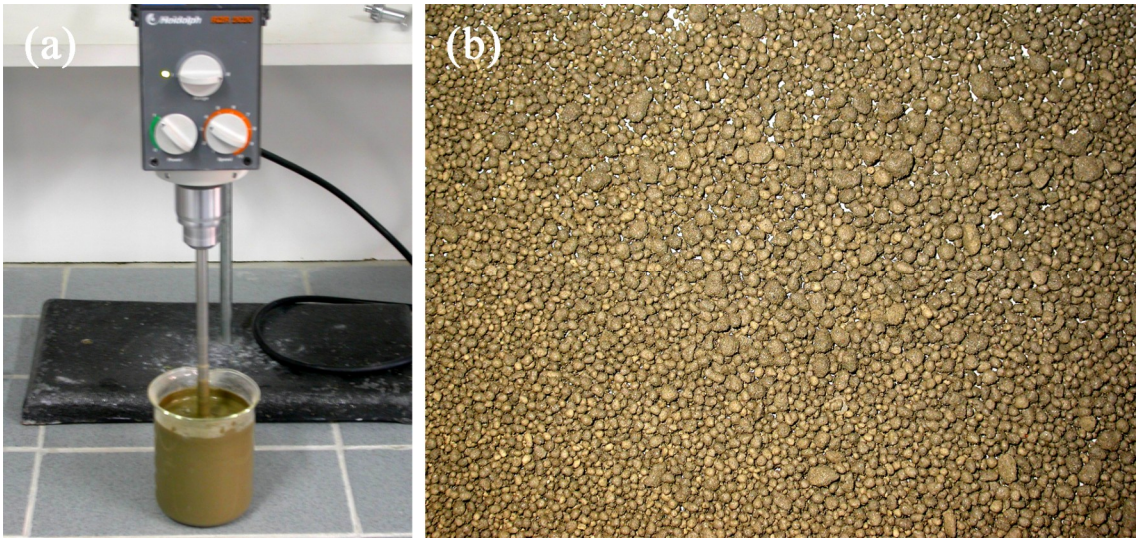

Figure 4.1. (a) Mixture blending process (solid mixture/water ratio: 1/1), (b) granule powders (around 10% moisture).

The granulated powder mixtures were uniaxially compacted in hydraulic press under a pressure of 10 MPa for the rectangular-shaped specimens (85 mm × 85 mm × 10 mm). Pressing method was adopted in this study because these tests are laboratory tests. More industrial scale field trials were done using vacuum press to extrude perforated bricks with similar paper residue contents. The pressed specimens were held overnight at room temperature followed by drying at 45°C for 1 hour in an oven. Dried specimens were fired in a laboratory-type electrical furnace at the rate of 2.5°C/min until 600°C, and then at the rate of 10°C/min until 1000 and 1100°C, for 1 hour. Figure 4.2 shows the experimental flowchart of the brick production process applied in this study.

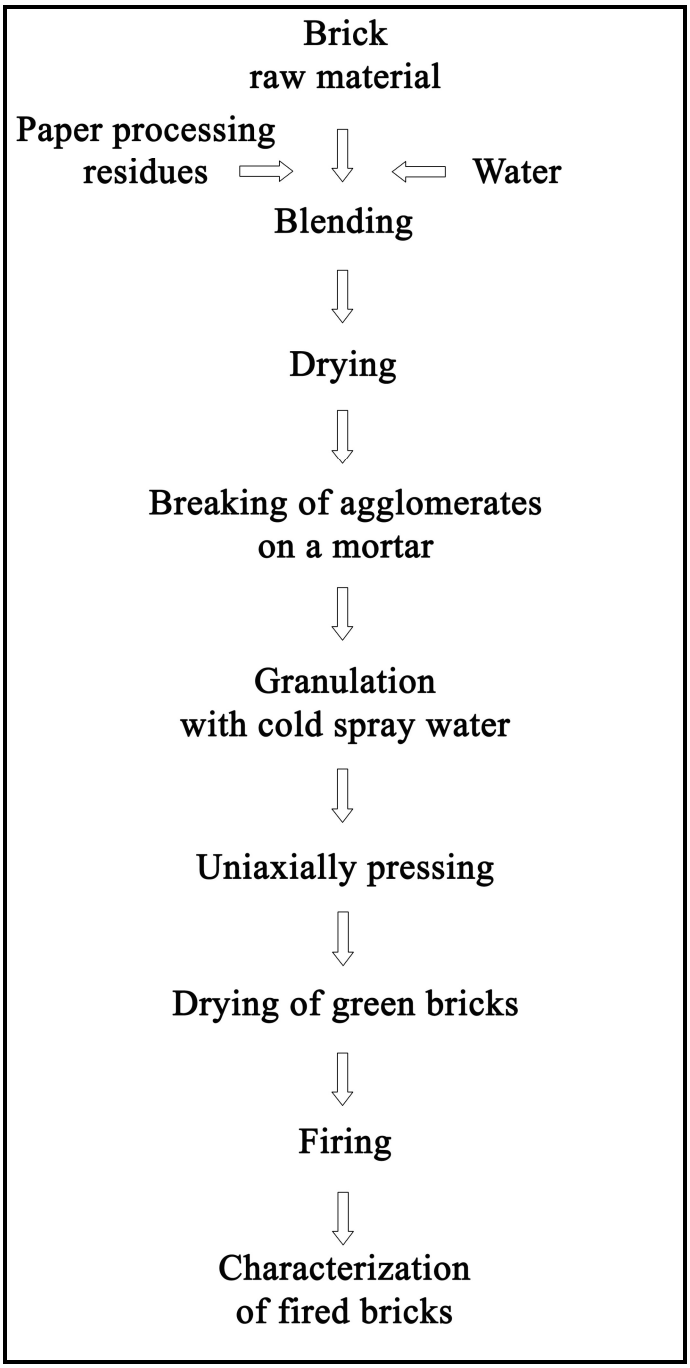

Figure 4.2. Experimental flowchart of brick production process applied in this study.

4.2.4. Characterization of the Fired Products

4.2.4.1. Thermal Dilatometric Test

Thermal dilatometric analysis provides information concerning product shrinkage during firing, the vitrification temperature, thermal expansion and the quartz

transformation temperature. Thermal dilatometric tests of the unfired samples without or with paper residues were performed using a horizontal dilatometer (Linseis, Germany). Small sized pellets (8 mm diameter and 8 mm length) were used for dilatometric analysis. The shrinkage behaviors of the samples were investigated using the same heating schedule as the other fired bricks. The expansions and contractions that will typically occur during firing of samples were precisely measured. Relative shrinkage and shrinkage rate was calculated by the following formulas:

$$Shrinkage(\%) = \left(\frac{\Delta L}{L_0}\right) \times 100 \tag{4.1}$$

$$Shrinkage\ rate = \left(\frac{d\left(\Delta L / L_0\right)}{dT}\right) \tag{4.2}$$

4.2.4.2. Physical Properties

Physical properties such as porosity, density, water absorption, and linear shrinkage of the fired brick samples were examined. Porosity is one of the main parameters which determine the properties of fired products. Porosity has a direct influence on thermal conductivity (Banhidi and Gomze 2008, Barea, et al. 2005). A more detailed discussion of this subject is presented in section 2.7.

After drying and firing the weights and dimensions of the samples were measured by a balance and caliper, and their green, dry and fired densities were calculated by the weight and volume of the bricks. Linear drying and firing shrinkages were also measured.

Also, Archimedes tests were applied to the fired samples, and their bulk density and apparent density, apparent porosity values and water absorption values were measured. The formulas for densities, absorption, and apparent porosity per ASTM C 20 are given below (ASTM Standard C20 2005):

$$\text{Bulk density} = \frac{d}{w - s},\ (\text{g/cm}^3) \tag{4.3}$$

$$\text{Apparent density} = \frac{d}{d-s}, \ (\text{g/cm}^3) \tag{4.4}$$

$$\text{Apparent porosity } (\%) = \frac{w-d}{w-s} \times 100 \tag{4.5}$$

$$\text{Water absorption } (\%) = \frac{w-d}{d} \times 100 \tag{4.6}$$

Where d is the dry weight, w is the wet weight (weight after boiling in water and then removing surface water with a wet cloth), s is the suspended weight.

4.2.4.3. Thermal Conductivity Measurements

Thermal conductivity of the bricks was measured with the hot-wire technique. This technique is considered to be an effective and accurate means of determining the thermal conductivity of ceramic materials (dos Santos 2008). The thermal conductivity measurements were performed at ambient conditions using a Quick Thermal Conductivity Meter (QTM500, Kyoto Electronics). A more detailed explanation of this technique is presented in section 2.9.2.

4.2.4.4. Microstructural and Phase Analysis

Microstructural analysis of the unfired and fired bricks was performed by scanning electron microscopy (SEM, Philips XL-30S FEG), and their elemental analysis was made by electron diffraction spectroscopy (EDS). X-ray diffraction (XRD, Philips X'Pert Pro) analysis was used to determine the phases or mineral compounds present in brick samples.

4.2.4.5. Mechanical Properties

There are several techniques used to assess the potential durability of brick. The first assessment is made using physical properties such as water absorption, C/B ratio and compressive strength. The compressive strengths of fired brick samples were examined as measured in different sample orientations such as pressing and transverse

directions. The compression test samples were prepared by cutting from the fired bricks (ASTM C67 2009). The compression tests were carried out at a cross head speed of 0.5mm/min in a Schimadzu AG-I 250kN universal testing machine. The compressive strength of each specimen was calculated as follows:

$$\sigma_C = \frac{F}{A} \tag{4.7}$$

Where, σ_c is the compressive strength, (kg/cm^2 or MPa), F is the maximum load, (kgf or N), A is the average of the gross areas of the upper and lower bearing surfaces of the specimen, (cm^2). Average compressive strength values of three specimens for each group brick were reported in this study.

For another performance based test, all bricks are subjected to a number of freezing and thawing cycles. According to ASTM C 67 standard, brick which are placed in water cycled once per day. For each cycle the whole brick is frozen and thawed. This test takes a number of 50 cycles to complete. In this study, the fired bricks were subjected to a non-standard freeze-thaw test for three cycles (ASTM C67 2009).

4.3. Results and Discussion

4.3.1. Characterization of Raw Materials

Chemical, mineralogical, physical and thermal properties of the paper processing residues were presented in Chapter 3. Chemical analysis of the brick raw material is given in Table 4.1 in oxide form. According to the XRF analysis, the brick raw material included a large fraction of Si in addition to Al, Fe, Ca, Mg and K. Loss on ignition of brick raw material upon heating at 1000°C was measured as 7.5%.

Table 4.1. Chemical analysis of brick raw material.

Constituents	Brick raw material (%)
Al_2O_3	15.71
SiO_2	61.65
CaO	2.16
MgO	2.30
K_2O	2.36
Fe_2O_3	6.77
TiO_2	0.82
CuO	0.26
Loss on ignition	7.5

Scanning electron microscope image of the brick raw material is shown in Figure 4.3. The SEM image indicated that it consisted of plate-like particles as well as agglomerated clay particles. The average grain size was below 20 μm. The brick raw material occasionally contained large chunks of rock (1–250 mm) that are removed during industrial brick manufacture at the beginning of the production process. The raw material used in this thesis was naturally cleaned from these large pieces of rock by sieving.

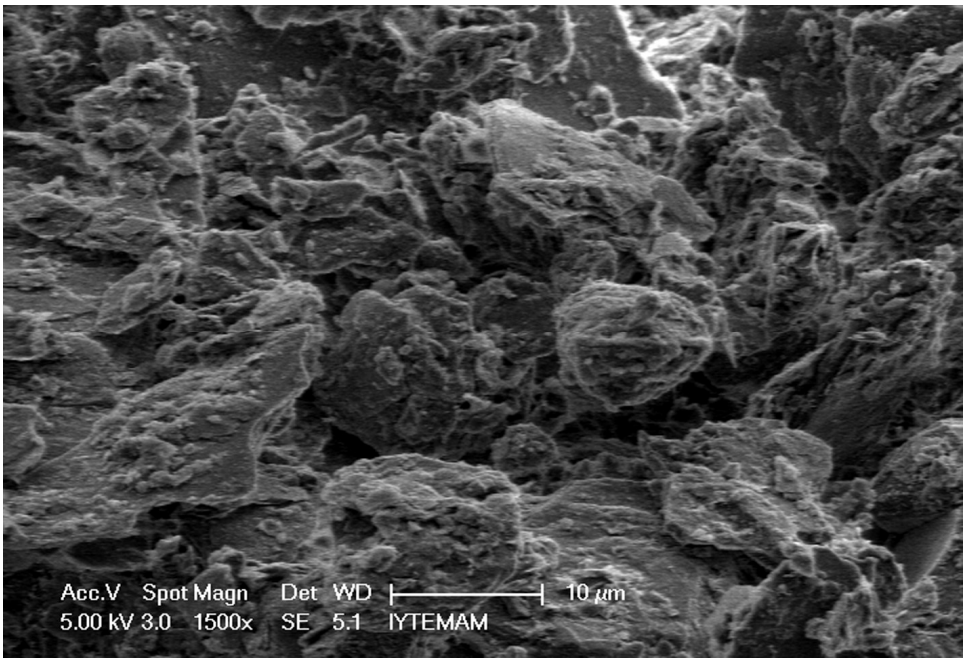

Figure 4.3. SEM image of the brick raw material.

The crystallinity and mineral compounds of brick raw material were investigated by using X-ray diffraction (XRD) with CuK_α radiation (λ=1.542 Å) at 40 kV in the 2θ intervals of 5–70°. Figure 4.4 shows XRD pattern of the brick raw material. Brick raw material includes mainly quartz (SiO_2), illite/muscovite ($KAl_2(AlSi_3O_{10})(OH)_2$), clinochlore ($(Mg,Al,Fe)_6(Si,Al)_4O_{10}(OH)_8$) and minor calcite ($CaCO_3$) constituents. The XRD patterns of the paper processing residues were given in Figure 3.4 (in Chapter 3). XRD analysis showed that the residues contained mainly calcium carbonate and a weak peak for cellulose was also observed.

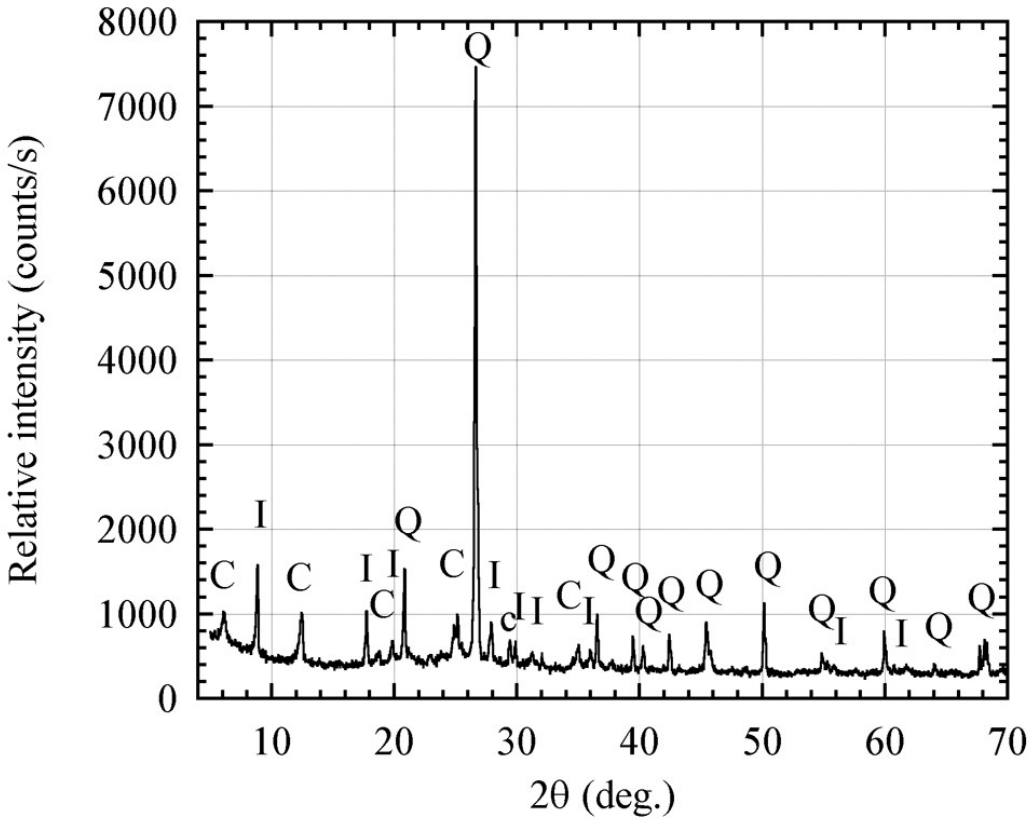

Figure 4.4. X-ray diffraction pattern of as-received brick raw material (Q: quartz [85–0796], I: illite/muscovite [02–0056] / [72–0496], C: clinochlore [79–1270], c: calcite [05–0586]).

Particle size distribution of brick raw material was measured by using a Malvern Mastersizer-2000 Instrument (Figure 4.5). Application of ultrasound to the sample was found to break up the agglomerates and to reduce the particle size. The median particle size (D_{50}) of brick raw material was about 16 and 24 μm according to the treatment type. There were some coarse particles larger than 200 μm as well as fine particles smaller than 1 μm.

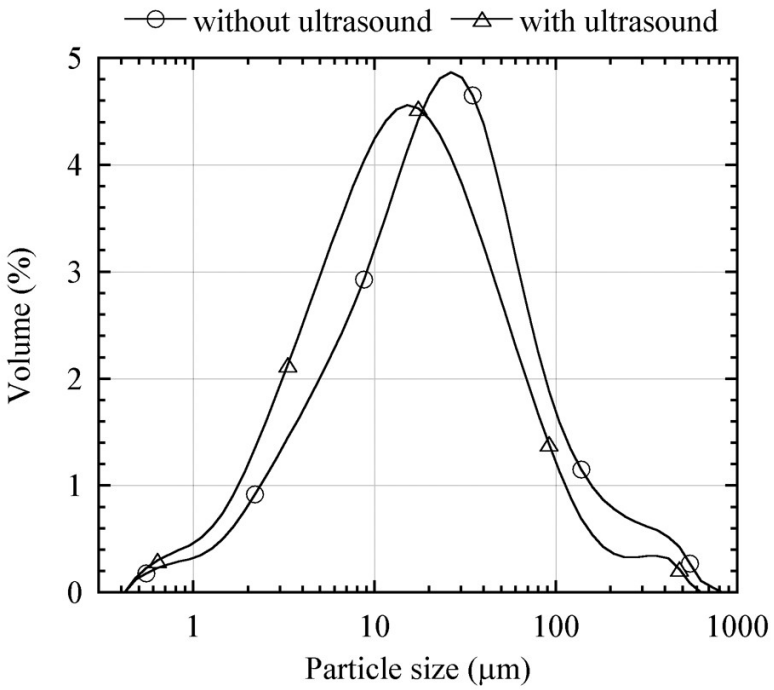

Figure 4.5. Particle size distribution of brick raw material.

Thermal analysis of paper processing residues was mentioned in the previous chapter (Figure 3.5). Thermo-gravimetric analysis (TGA) and differential thermal analysis (DTA) results of the paper residues were explained in detail. Their total weight losses of about 54% were observed at 1000°C. The weight losses were due to the burning of cellulose fibers (~25%) and the decomposition of carbonates (~20%).

Thermal analysis (TGA and DTA) of brick raw material was performed in nitrogen atmosphere. In Figure 4.6, the TGA and dTGA curves of brick raw material are given. Total weight loss of about 6% was observed at 950°C. The first 1.5% decrease in mass occurred between 20 and 200°C due to evaporation of physical water. The second (0.5%) and third (1.5%) weight losses were observed between 200–300°C and 300–525°C ranges which may be due to the burning of organic matter and the removal of chemical water (Vieira, et al. 2008). The larger weight loss (approximately 2%) was detected between 525–750°C range which is probably related with the dehydroxylation of clay minerals (Brosnan 2002b, Cultrone, et al. 2005). The DTA curve of the brick raw material shows two endothermic reactions around 100 and 650°C. The former is due to the evaporation of physical water, the latter is possibly due to the decomposition of the clay.

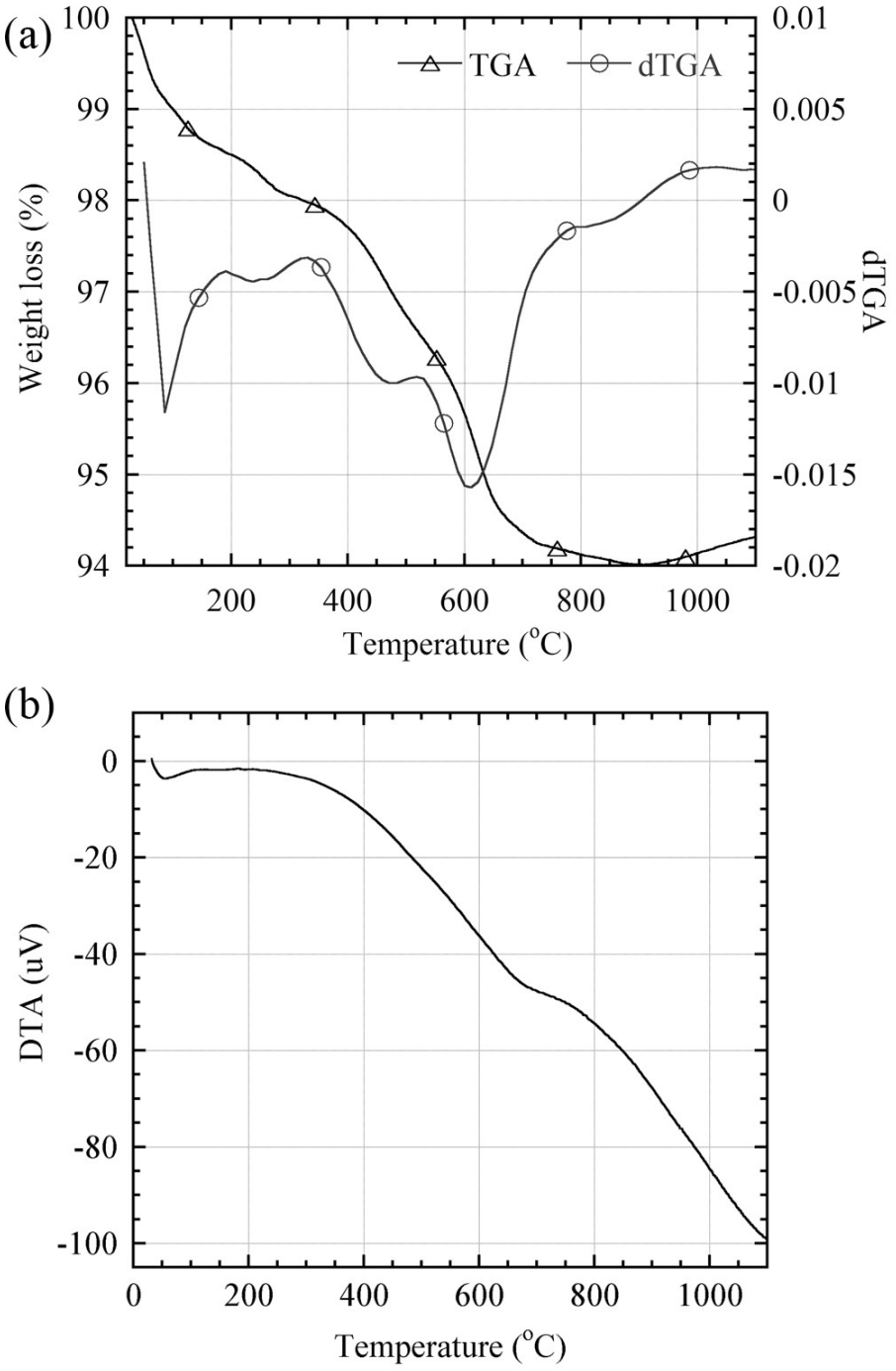

Figure 4.6. Thermal analysis curves of the brick raw material in nitrogen atmosphere: (a) TGA/dTGA and (b) DTA.

4.3.2. Dilatometric Analysis of the Brick Samples During Firing

Thermal dilatometric analysis was performed on unfired samples. Figure 4.7(a) and (b) shows linear shrinkage and shrinkage rate ($°C^{-1}$) curves during firing to 1100°C of the samples with or without additives.

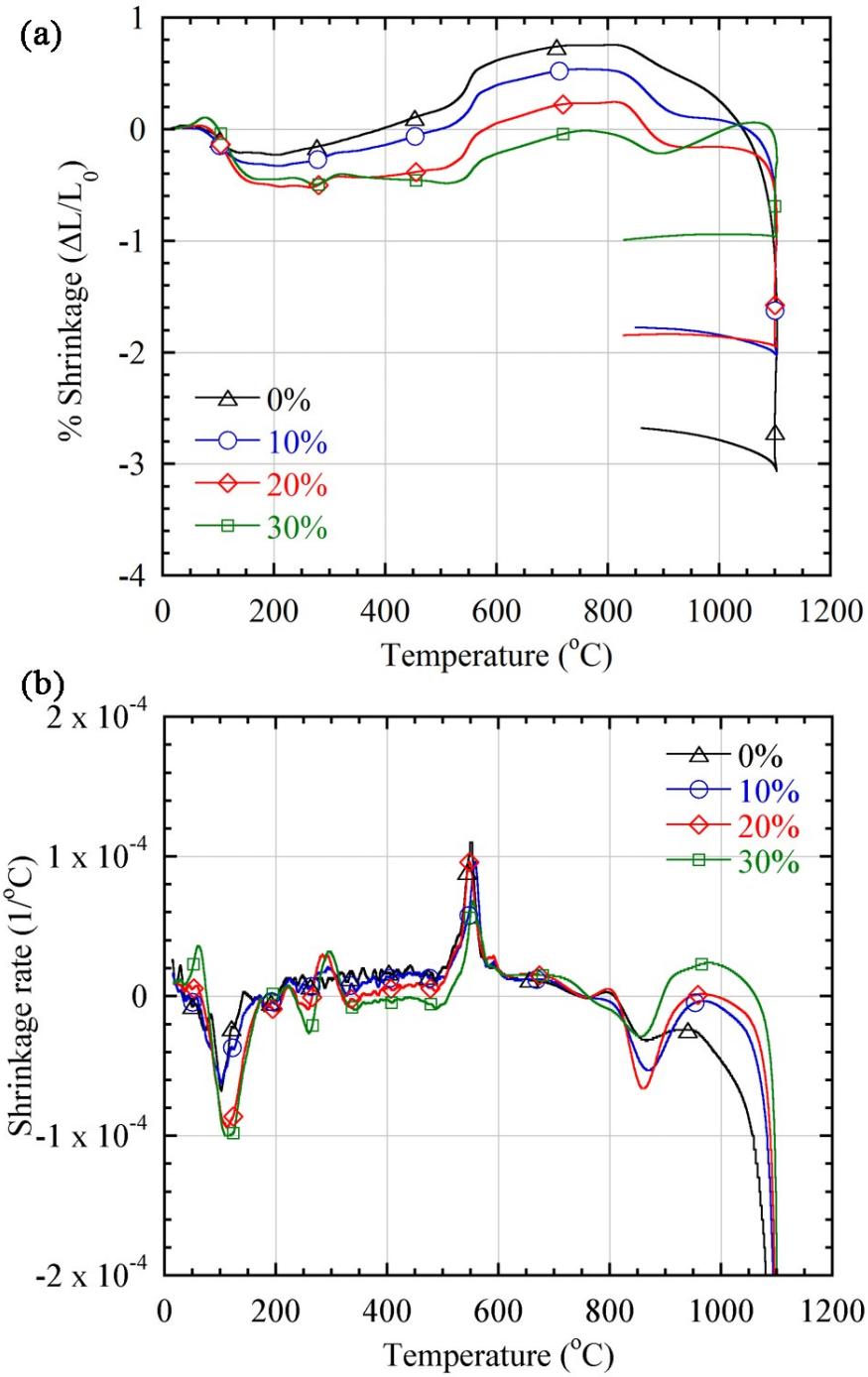

Figure 4.7. Dilatometric curves of the brick samples with paper residues during firing: (a) percent linear shrinkage, and (b) shrinkage rate.

Note that the irreversible trace goes through all of the expansions and contractions that will typically occur during first firing of samples. The only significant shrinkage occurs at about 100°C during drying, and this accounts for only about 0.2–0.5% of shrinkage for samples containing up to 30% waste. The expansion between 530°C and 585°C in all samples is observed to be about 0.4%. These reactions showed

that a quartz transformation (from α-quartz to β-quartz) is associated with a volume increase (Brosnan 2002b, Kingery, et al. 1976, Norton 1952). In all samples, shrinkage began at about 850°C, and in the curves of samples with paper residues a small plateau was formed at about 900°C as calcium aluminosilicate (anorthite and gehlenite) reactions occurred (Brosnan and Robinson 2003). In addition, after about 800°C, shrinkage of samples with residues is delayed compared to the sample without the residue due possibly to decomposition of calcite and its reaction to form calcium silicates. Finally, while the sample without residue shrinks about 3%, the samples with 10%, 20% and 30% residue shrink by 2%, 1.9% and 1%, respectively.

4.3.3. Physical Properties of the Brick Samples

Up to this point, paper residue additions of as much as 30wt% were done in making fired brick. In Figure 4.8, surface images of the paper processing residue-containing fired bricks are illustrated. It was observed that the color of the brick got lighter shades of red with increasing amount of residue additions due to the presence of higher amounts of calcium. This lightening of color can sometimes affect customer perception of brick products as being low-fired in Turkey. However, the same perception is not observed in EU (Kornmann 2007, Sahtas Terracotta 2010). Recently, there is increased demand for colored brick and roof tiles in EU, JP, US. Turkey will probably follow the trend.

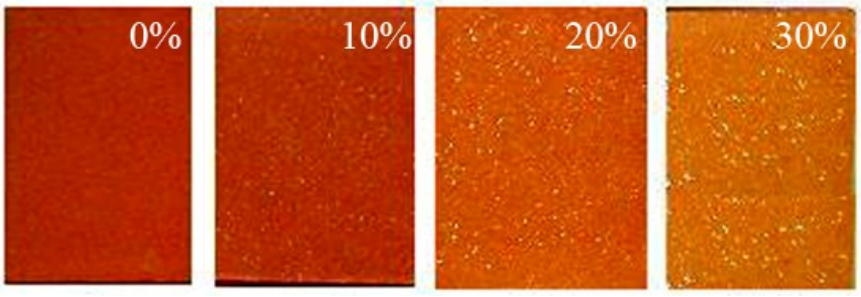

Figure 4.8. Paper processing residues-containing bricks fired at 1100°C.

Experimental results of the samples fired at 1000 and 1100°C are given in Table 4.2. Dimension and volume of the samples were measured by a caliper, and their green, dry and fired densities were calculated. Also, their bulk density, apparent density,

apparent porosity and water absorption values were measured by the Archimedes method using boiling water. The results obtained revealed that green, dry, fired and bulk densities decreased steadily with an increase in the amount of the residues. Firing temperature only moderately affected the properties of the samples. Drying shrinkage values of the bricks varied between 1 and 2%. These values are much smaller than bricks produced by extrusion which have about 6–10% shrinkage. This is due to the difference of their moisture content (Kornmann 2007).

Table 4.2. Density, porosity and water absorption results of the fired bricks.

Physical properties		Firing temp. (°C)	Percent paper residues additions by weight			
			0%	10%	20%	30%
by weight / volume	Green density (g/cm^3)	1000	2.15	1.97	1.96	1.90
		1100	2.16	2.03	1.96	1.83
	Dry density (g/cm^3)	1000	1.98	1.79	1.77	1.70
		1100	2.03	1.88	1.80	1.64
	Fired density (g/cm^3)	1000	1.85	1.57	1.46	1.32
		1100	1.92	1.65	1.49	1.28
Loss on ignition (%)		1000	7.5	13.0	17.4	22.3
		1100	7.5	12.3	17.0	22.0
by Archimedes method	Apparent porosity (%)	1000	31.7±0.8	40.7±0.9	46.7±0.5	50.7±0.7
		1100	30.8±0.9	38.9±0.3	46.2±1.2	52.0±0.8
	Water absorption (%)	1000	17.2±0.7	25.6±0.9	32.8±0.8	38.4±1.0
		1100	16.7±0.7	23.9±0.4	31.9±1.6	40.4±1.3
	Bulk density (g/cm^3)	1000	1.85±0.03	1.59±0.02	1.42±0.02	1.32±0.02
		1100	1.85±0.03	1.62±0.01	1.45±0.03	1.29±0.02
	Apparent density (g/cm^3)	1000	2.70±0.01	2.68±0.00	2.67±0.01	2.68±0.01
		1100	2.68±0.00	2.65±0.01	2.69±0.00	2.69±0.01

Figure 4.9a depicts the changes in density and loss on ignition values observed for bricks fired at 1100°C with respect to paper residue content. Fired density of the bricks decreased from 1.92 to 1.28 g/cm^3, which corresponds to a decrease by 33% compared to density of the brick without paper residues. Figure 4.9b also depicts the

Archimedes test results of the samples taken from bricks fired at 1100°C. The volumes of tested samples were about 1 cm^3. Apparent porosity and water absorption values increased with increase in waste addition while the bulk densities were significantly reduced. Lowest bulk density achieved so far was 1.29 g/cm^3.

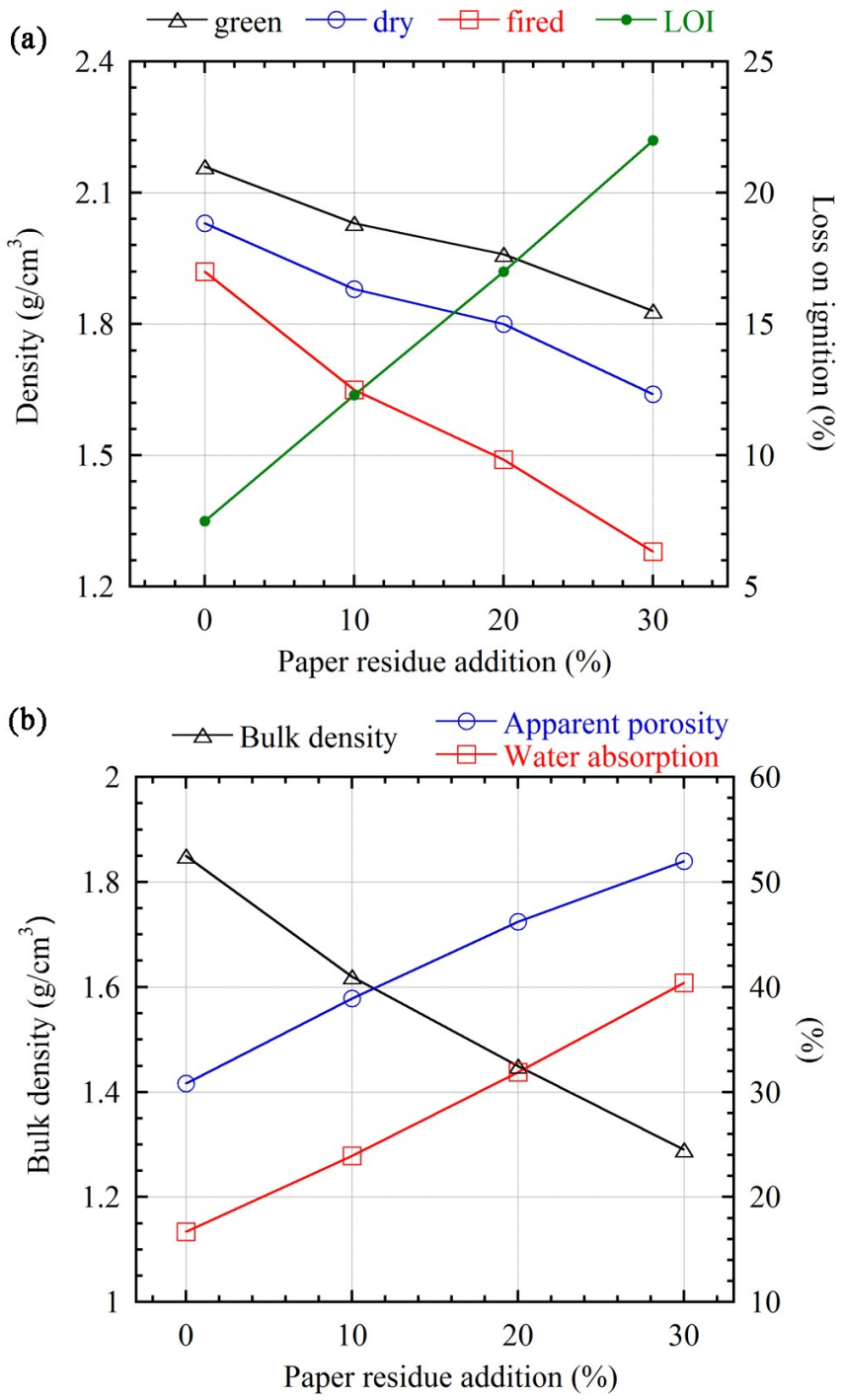

Figure 4.9. (a) Green, dry, fired densities and loss on ignition of the bricks as measured by weight/volume, and (b) Archimedes test results of the bricks fired at 1100°C.

4.3.4. Thermal Conductivity Measurements

Thermal conductivity measurement results of the bricks by hot-wire method at ambient conditions are given in Table 4.3. Thermal conductivity of the bricks considerably decreased with increasing paper residues contents. The paper residue addition into the bricks decreased the density of bricks after firing. Thermal conductivity of the bricks depends on the firing temperatures of bricks, the density and therefore porosity of the bricks. Thermal conductivity values of the bricks were increased with increasing of the firing temperatures of the bricks. Thermal conductivity of the porous brick with 30% paper residue produced as fired at 1100°C (0.42 W/mK) showed more than 50% reduction compared to the brick without paper residue (0.83 W/mK). The thermal conductivity of product with 30% paper residue fired at 1000°C showed a reduction of 43% according to the brick without paper residue. Reduction up to 50% of thermal conductivity is encouraging for higher energy saving potential in residential applications.

Table 4.3. Thermal conductivity values of the bricks.

Property	Firing temperature	Percent paper residues additions by weight			
		0%	10%	20%	30%
Thermal conductivity (W/mK)	1000°C	0.68±0.01	0.50±0.005	0.46±0.004	0.39±0.003
	1100°C	0.83±0.01	0.59±0.01	0.48±0.002	0.42±0.003

Figure 4.10 shows the relation between thermal conductivity and apparent porosity of the bricks fired at different temperatures. It can be clearly seen that thermal conductivities of the bricks are closely related with their porosities or densities and firing temperatures. Firing temperature of bricks is a factor affecting their thermal conductivity. Thermal conductivity of the bricks increased with increasing firing temperature. This case is most probable due to the increasing of crystallinity of the phases that formed in the brick, with increasing firing temperature (see Figure 4.12) (Kornmann 2007). It is evident that thermal conductivity strongly depends on the densities or porosities, and the structure or firing temperature of the bricks. Conversion

of this product to a perforated brick may reduce its thermal conductivity to very low values. It also is very sensitive to all defects such as inclusions and crystalline interfaces that scatter the thermal flow.

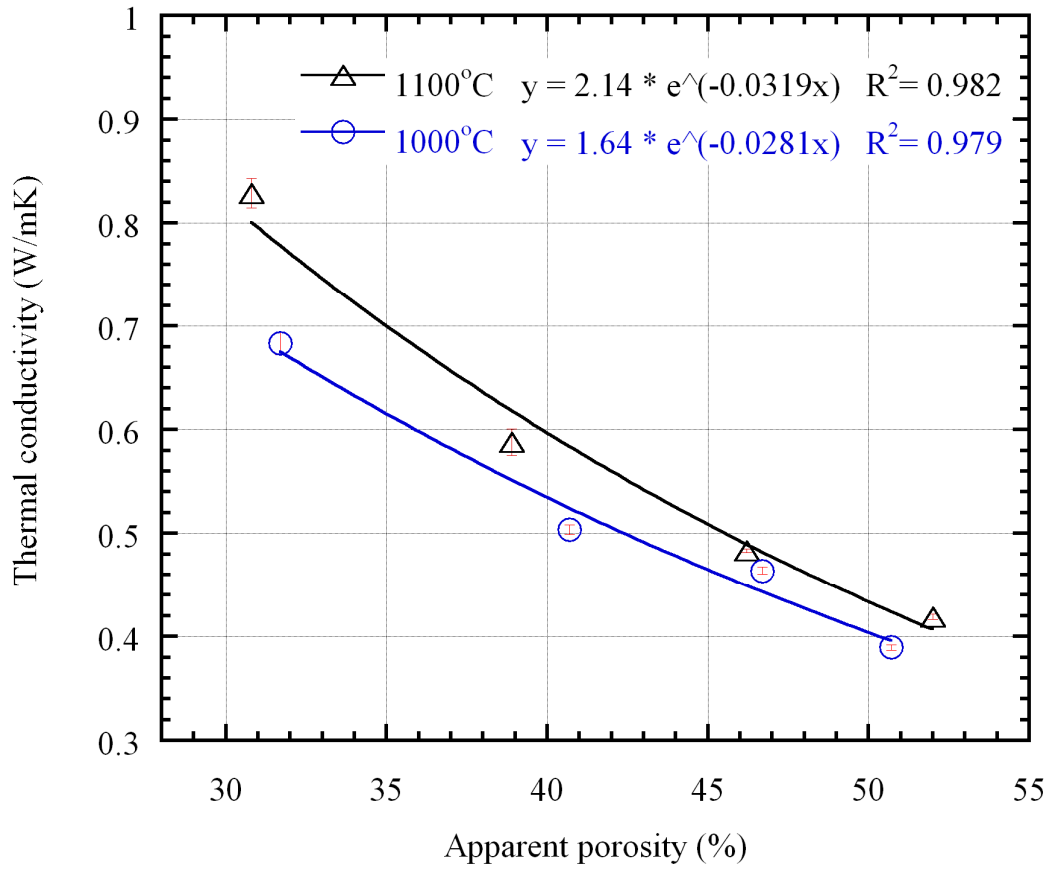

Figure 4.10. The relation between thermal conductivity and porosity of fired bricks.

4.3.5. Mineralogical Phase Analysis of the Bricks

The crystalline mineral phases in the fired brick bodies were identified using X-ray diffraction. X-ray patterns of the bricks fired at 1100°C are shown in Figure 4.11. XRD analysis obviously showed that non-additive brick consisted of quartz (SiO_2) on a large scale, and also hematite (Fe_2O_3) and sanidine ($KAlSi_3O_8$). Paper residue containing-bricks consisted mainly of quartz and hematite as well as anorthite ($CaAl_2Si_2O_8$) and gehlenite ($Ca_2Al_2SiO_7$). As addition of paper residues increased, amount of anorthite and gehlenite phases increased.

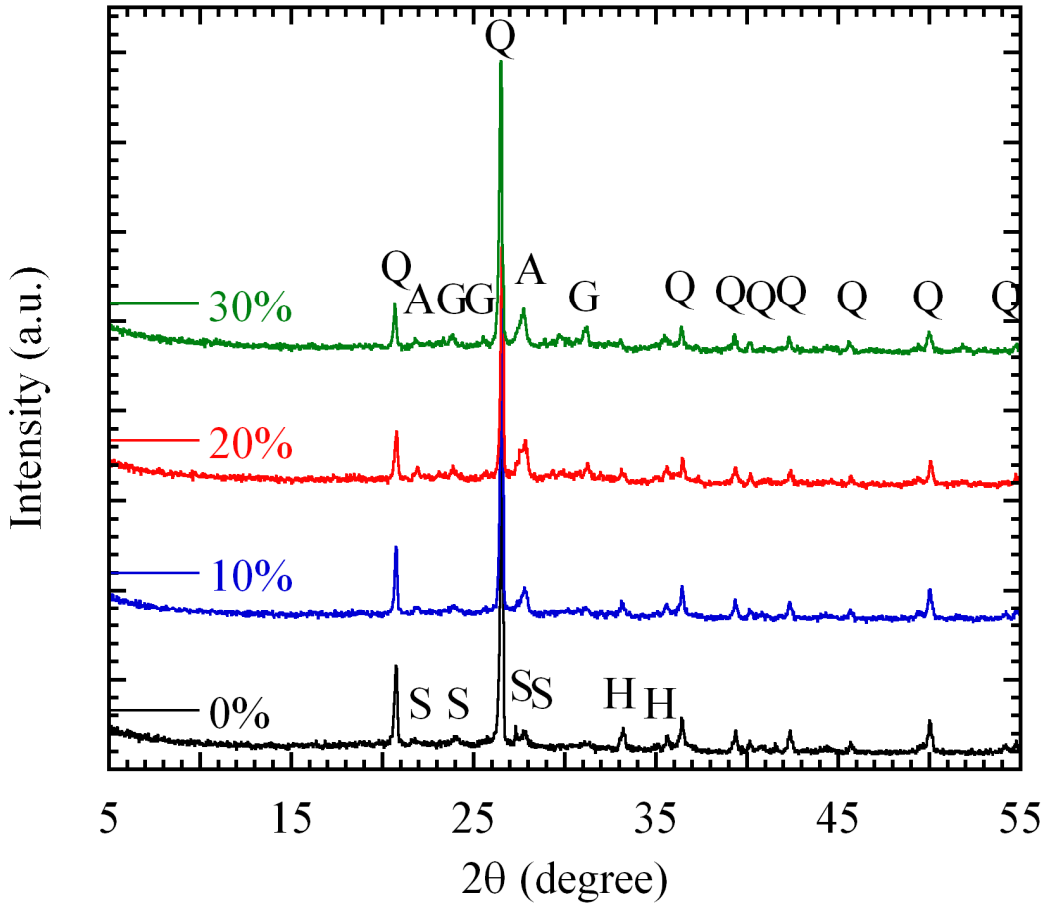

Figure 4.11. X-ray diffraction patterns of the bricks fired at 1100°C with 0, 10, 20 and 30% paper residue additives (Q: quartz, H: hematite, S: sanidine, A: anorthite, G: gehlenite).

When the clay and paper residue mixtures are heated to around 1000°C, $CaCO_3$ coming from the residues decomposes, and CaO forms inside the brick material. CaO reacts with aluminum silicates. At a temperature of 1100°C, the illite mineral in brick clay decomposes and transforms into a high-temperature K-feldspar (sanidine) or reacts with calcium oxide to form anorthite (Cultrone, et al. 2001, Jordán 1999, Jordán 2001, Montero 2009). In general, sanidine and anorthite formation is observed in the bricks fired at high temperature. In the brick composition without residue, illite mineral transformed into sanidine phase when fired at 1100°C. In the brick with paper residues, calcium oxide reacted with quartz and other minerals, and eventually minor calcium aluminum silicates such as anorthite and gehlenite phases as well as mainly quartz formed at 1100°C. Formation of gehlenite was observed possibly due to its ease of crystallization (Cultrone, et al. 2001).

Figure 4.12 shows a comparison of mineral phases of the bricks with 30% paper residues fired at 1000 and 1100°C. The XRD results indicated that the brick fired at 1100°C has higher crystallinity than brick fired at 1000°C. While the formation of gehlenite begins to occur at lower temperatures (800–900°C), and the anorthite phase begins to form at relatively higher temperatures (900–1000°C) (Cultrone, et al. 2001, Cultrone, et al. 2005, Cultrone, et al. 2004). Therefore, the formation of anorthite phase increased with increasing of firing temperature.

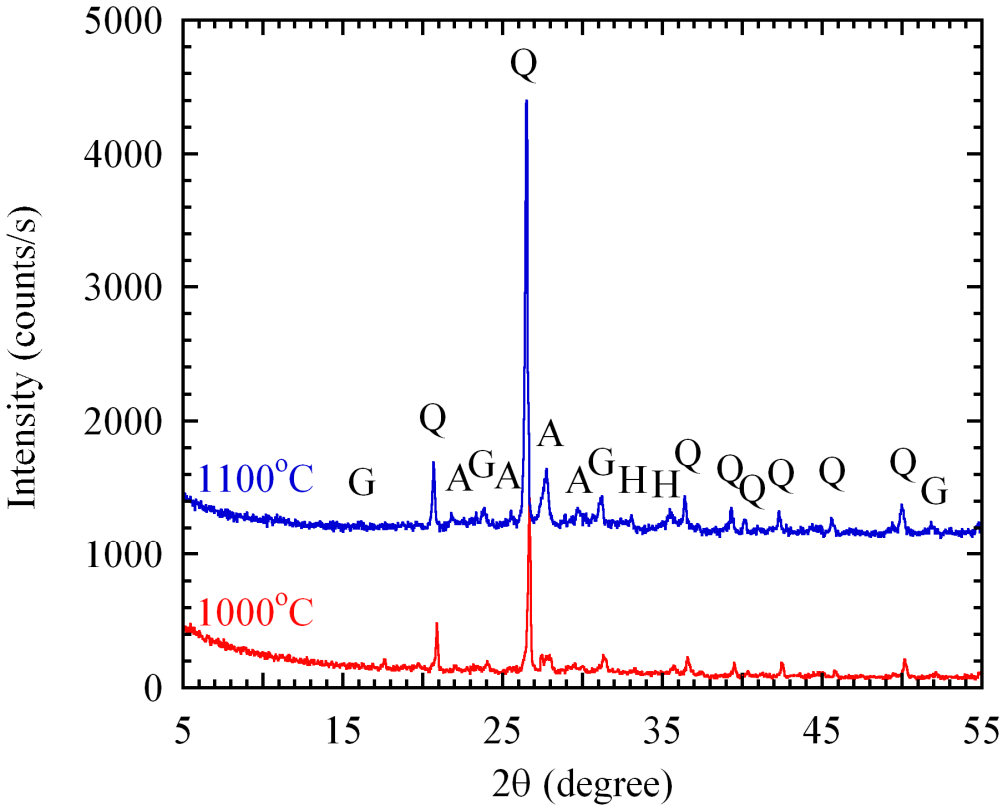

Figure 4.12. XRD graphs of the bricks with 30% paper residues fired at different temperatures (Q: quartz, H: hematite, A: anorthite, G: gehlenite).

Mineral phases that formed can be evaluated from the ternary equilibrium diagram of $CaO–Al_2O_3–SiO_2$. The compositions labeled inside the $CaO–Al_2O_3–SiO_2$ diagram are shown in Figure 4.13. In this diagram, the compatibility triangles are $SiO_2–CaO·Al_2O_3·2SiO_2–3Al_2O_3·2SiO_2$ (quartz–anorthite–mullite) for low percentages of the residue added, and $SiO_2–CaO·Al_2O_3·2SiO_2–CaO·SiO_2$ (quartz–anorthite–wollastonite) for high percentages of the residue. Mullite and wollastonite phases were not observed in the fired brick samples. Gehlenite phase is evaluated in the compatibility triangle of

$CaO \cdot SiO_2$–$CaO \cdot Al_2O_3 \cdot 2SiO_2$–$2CaO \cdot Al_2O_3 \cdot SiO_2$ (wollastonite–anorthite–gehlenite), which could locally form in locations with high CaO content in the brick body.

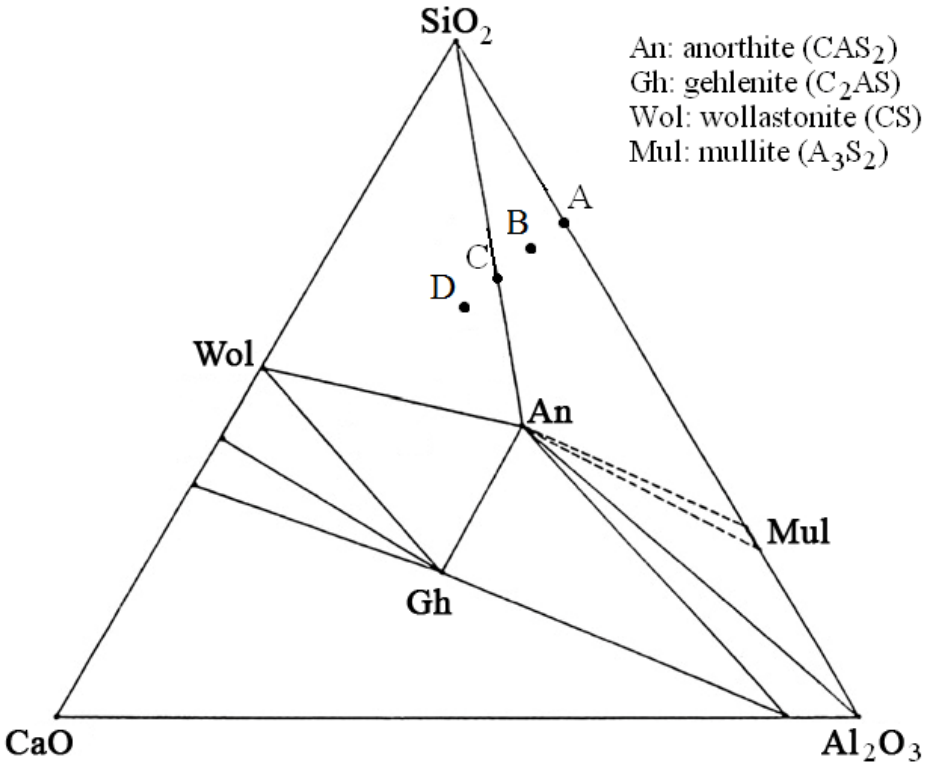

Figure 4.13. CaO–Al_2O_3–SiO_2 system. A(0%), B(10%), C(20%) and D(30%) compositions labeled inside this diagram according to the paper residues addition. An: anorthite ($CaO \cdot Al_2O_3 \cdot 2SiO_2$), Gh: gehlenite ($2CaO \cdot Al_2O_3 \cdot SiO_2$), Mul: mullite ($3Al_2O_3 \cdot 2SiO_2$), Wol: wollastonite ($CaO \cdot SiO_2$).

4.3.6. Microstructural Analysis

Microstructure of the bricks was investigated using scanning electron microscope (SEM). Figure 4.14 shows the SEM images in secondary electron (SE) mode of fired brick without residues at different temperatures (1000 and 1100°C) and magnifications. With increasing firing temperature of the bricks, the degree of vitrification increased. Pores were rounded as shown in Figure 4.14d. Also, Figure 4.15a illustrates a general micrograph in backscatter electron (BSE) mode of brick without paper residue fired at 1100°C. Coarse particles with dimensions of 100 μm are observed in the structure. They were identified as quartz (SiO_2) by SEM-EDS analysis.

Pores with sizes of 200 µm existed in the body. They could be a pull-out during polishing. Figure 4.15b shows local vitrification in the brick. At higher temperatures, the alkaline earth elements (especially potassium) in the feldspar minerals of brick clay raw material cause a small amount of liquid phase to form. As firing temperature is increased, quartz becomes more soluble in the liquid phase, and then forms a Si-rich final structure (Meyers 2003).

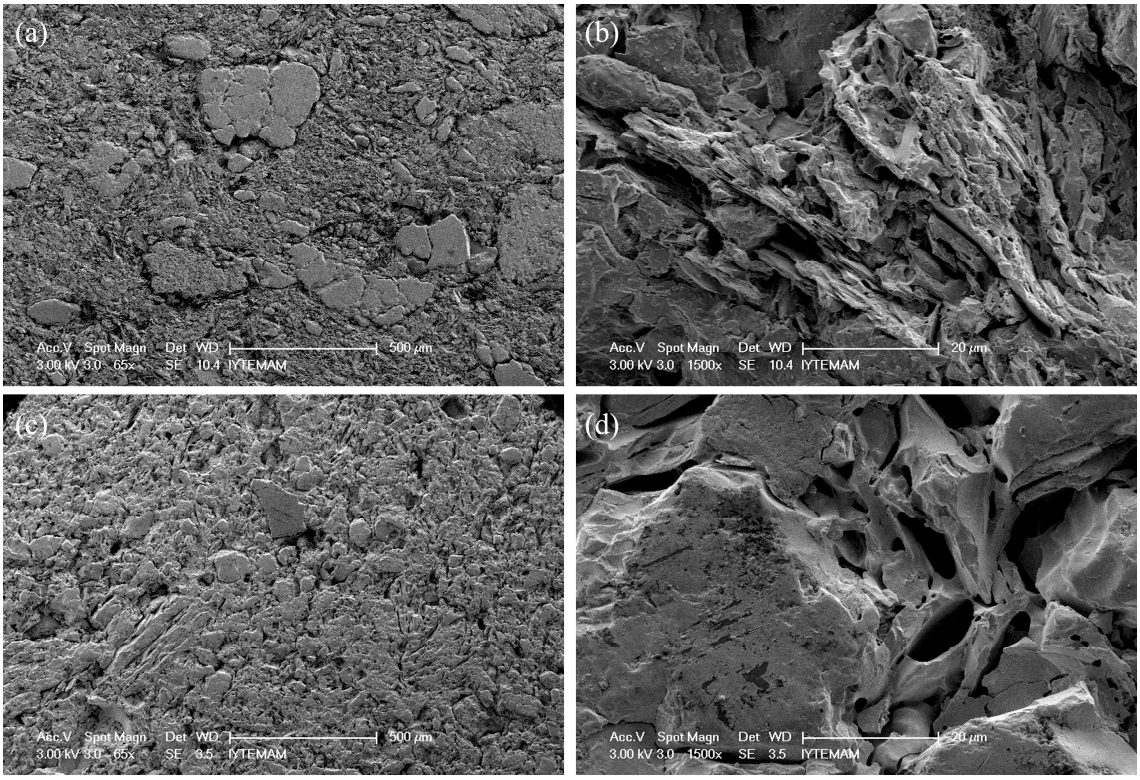

Figure 4.14. The SEM images in SE mode of fired brick without residues at different temperatures and magnifications: (a) 500x and (b) 1500x at 1000°C, (c) 500x and (d) 1500x at 1100°C.

Figure 4.15. The SEM images of brick without residue fired at 1100°C at backscatter electron (BSE) mode various magnifications: (a) 80x and (b) 2500x.

Figure 4.16 shows the SEM-EDS analysis of brick without residue fired at 1100°C. According to this analysis, the brick body contains (a) quartz particles, (b) potash-feldspar (sanidine) and (c, d) some layered chlorite minerals with substitution of Fe ion. It is most possible that these phases occurred from the illite and clinochlore minerals.

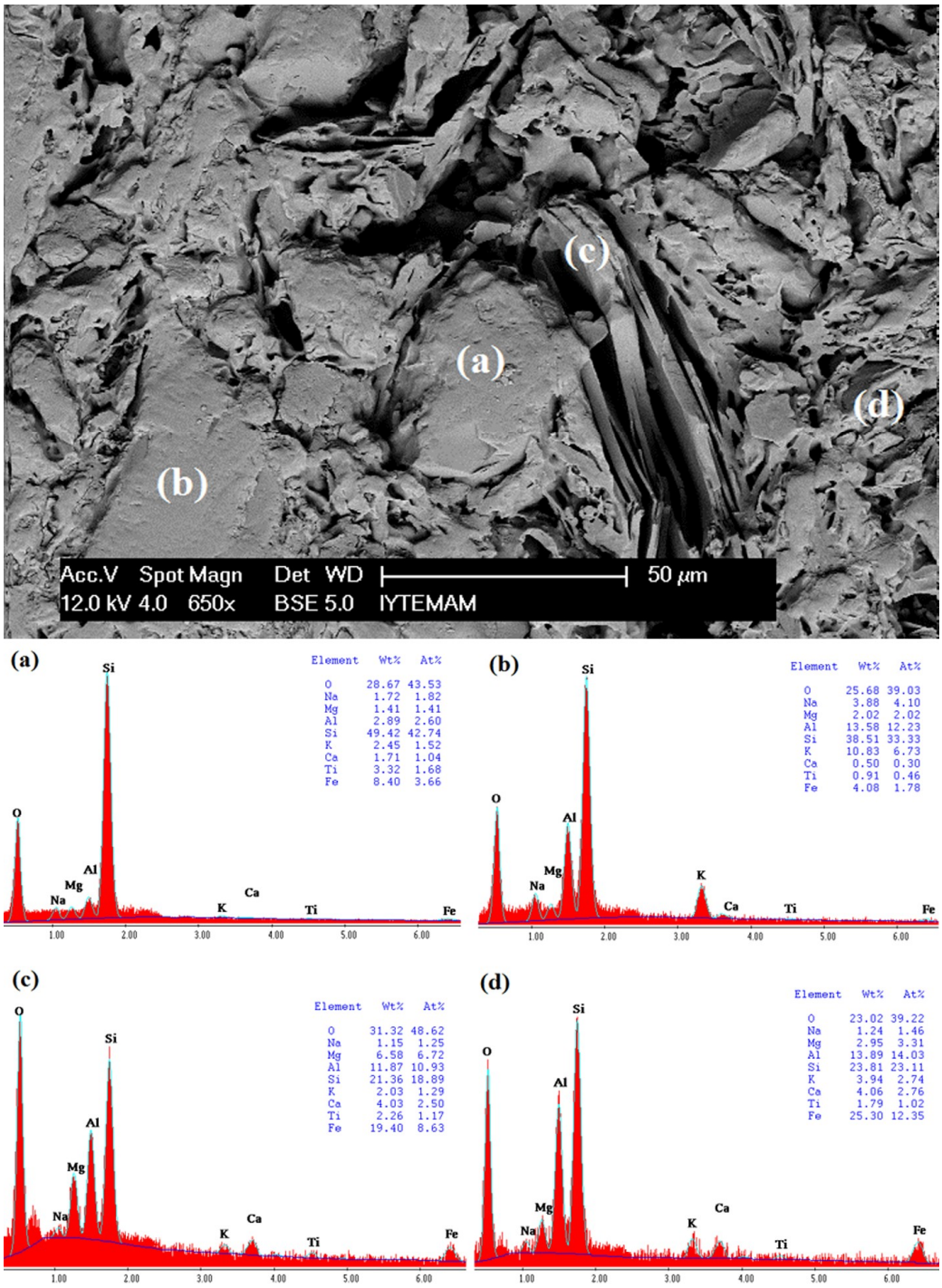

Figure 4.16. SEM-EDS analysis results of brick without paper residue fired at 1100°C: (a) quartz particles, (b) potash-feldspar (sanidine) and (c, d) some layered chlorite minerals.

Figure 4.17a shows the SEM image of unfired brick with 30wt% paper residues. This microstructure revealed that cellulose fibers were immersed in the green brick body. Thicknesses of the fibers varied from 5 to 20 µm. During firing, these cellulose fibers burned and vacant holes formed in their locations inside the brick body (Figure

4.17b). Also, micro-scale pores occurred due to the decomposition of calcium carbonate. In general, calcium carbonate is used as pore forming agent in the manufacture of porous materials. Calcium carbonate content of paper processing residues is an important feature for creating porosity in the material. Both the cellulose fibers and calcite helped to form the porosity in this study.

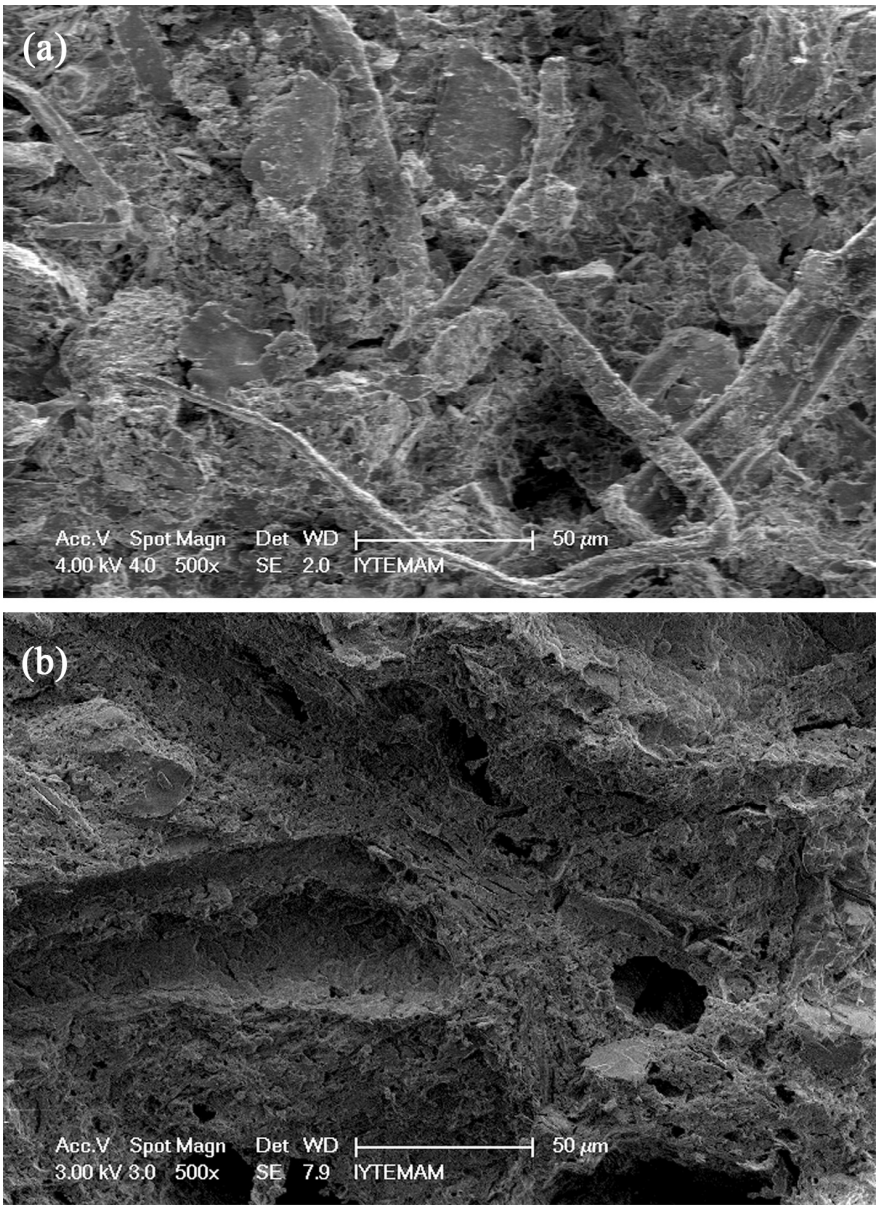

Figure 4.17. Microstructures of (a) unfired and (b) fired clay brick with 30% paper residues.

Figure 4.18 illustrates the SEM images of brick matrix with 30% residue fired at 1100°C. In Figure 4.18a, coarse silica particles with dimensions of 50 μm are observed.

Nevertheless, circular shape-closed pores with diameter of 10 μm are observed due to vitrification (Figure 4.18b). Fine crystals were also observed in the brick matrix, and EDS analysis was performed as shown in Figure 4.19. According to this analysis, these crystals were identified as calcium alumina silicates (anorthite or gehlenite phases). While the theoretical composition of anorthite is 20.2% CaO, 36.6% Al_2O_3 and 43.2% SiO_2 on a weight basis, the composition of gehlenite is 41% CaO, 34% Al_2O_3 and 25% SiO_2.

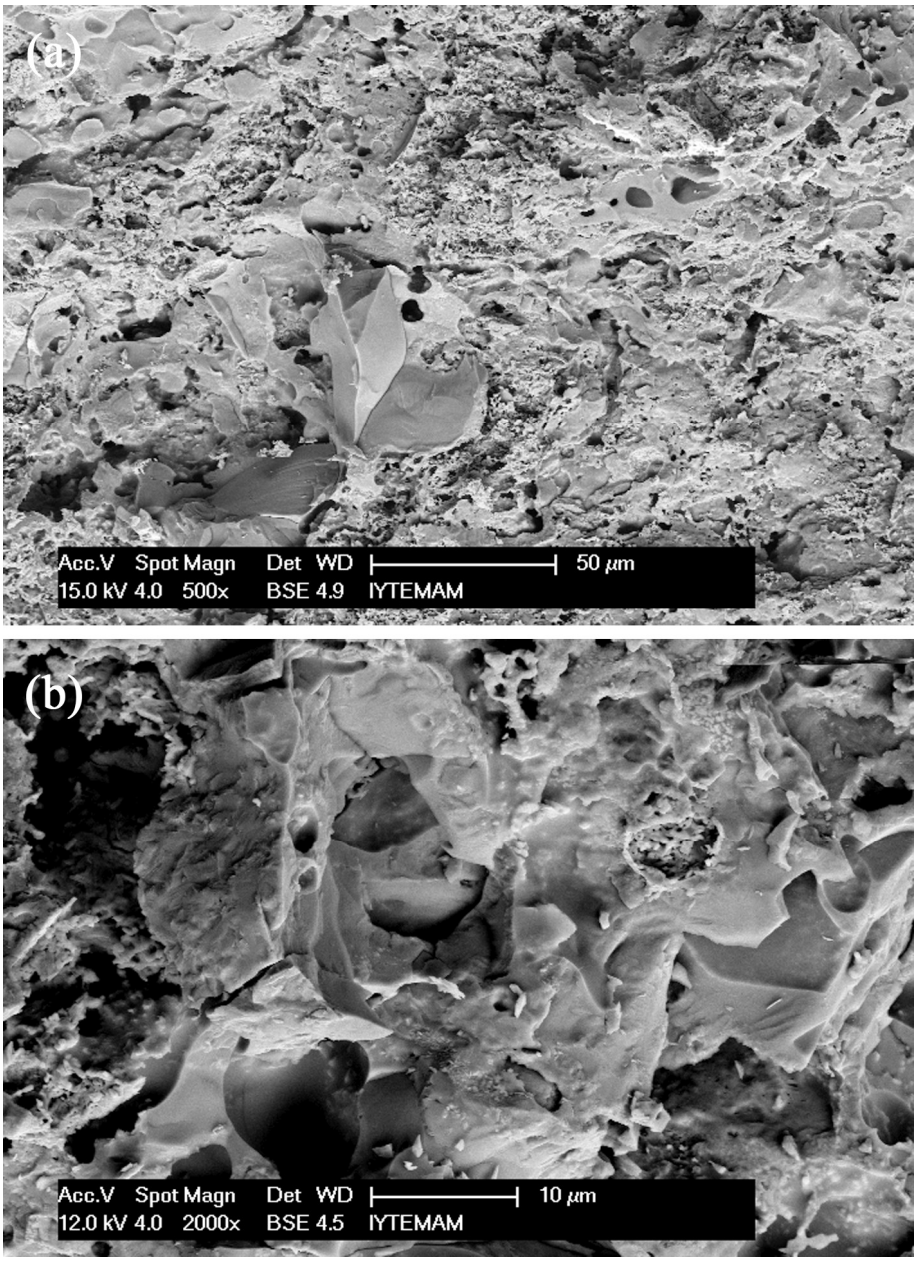

Figure 4.18. Micrographs at different magnifications of brick matrix with 30% residue fired at 1100°C.

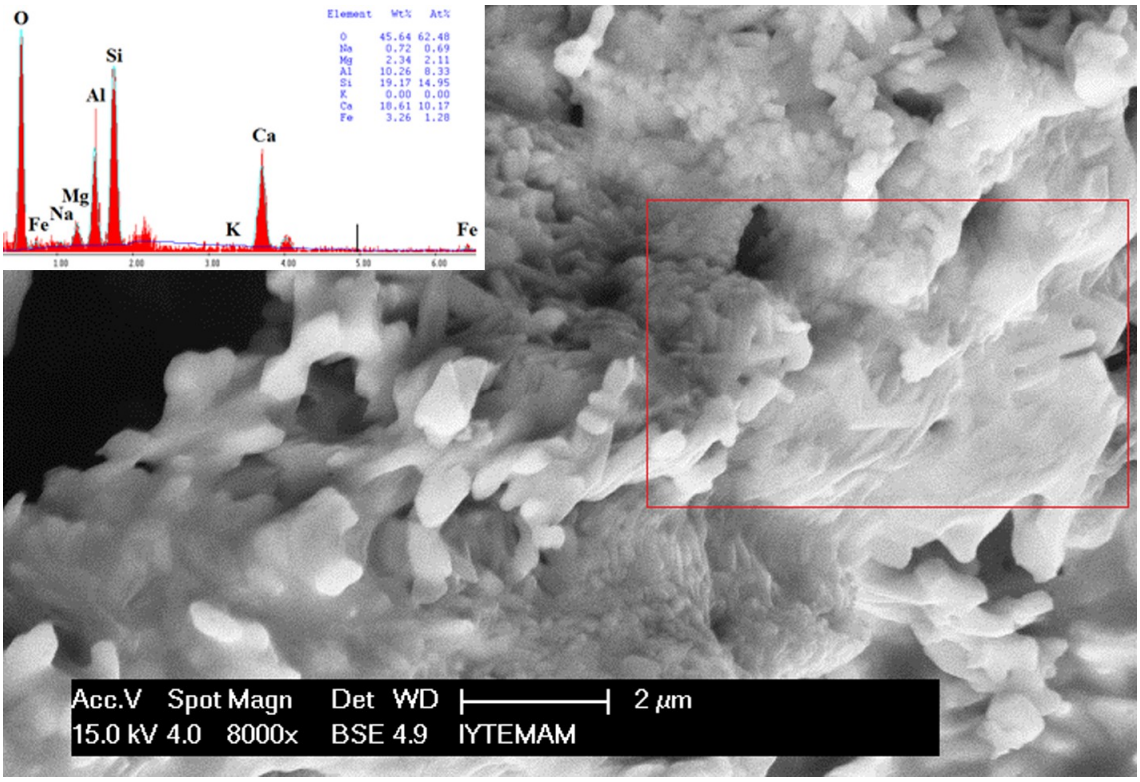

Figure 4.19. Fine calcium aluminosilicate crystallites the brick structure with 30% residue fired at 1100°C. Inset: EDS analysis of the marked region.

In the brick with 30% residue, the high amount of porosity existed due to the burning of organic matter and decomposition of calcite. In some regions of the bricks, calcite rich particles in the brick formed an extremely porous structure upon thermal treatment due to the loss of CO_2. These loosely bonded particles in brick probably contracted more than the bulk of the material during cooling leaving some space around them as shown in Figure 4.20(a) and (b). Figure 4.20b shows in closer view the fine network of highly porous structure which is extremely helpful in reducing thermal conductivity of the brick by resisting convective heat transport. Movement of air is restricted in this case as opposed to a completely vacant pore in which heat transfer would be freely carried out by air molecules. Heat conduction in air is low because its thermal conductivity is low. There is no significant convection in vacancies of limited size lower than 1 cm (Kornmann 2007).

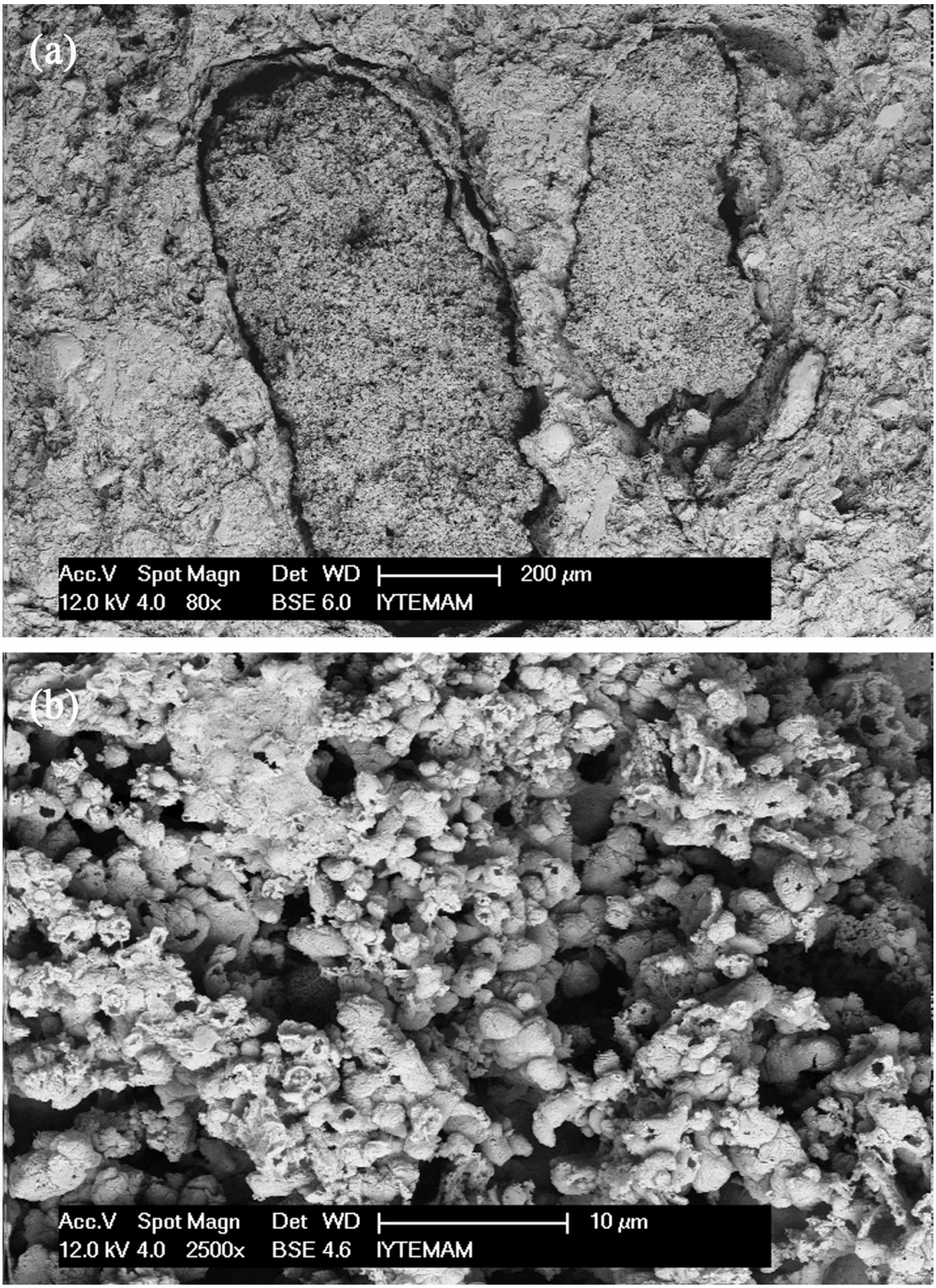

Figure 4.20. The SEM images of bricks with 30% residue fired at 1100°C, at various magnifications: (a) body with CaO-rich grains, (b) CaO-rich porous structure in brick with 30% residue.

The SEM-EDS line-scan analysis was performed on the large calcium-rich regions as shown in Figure 4.21. Chemistry of these particles of roughly 200–1000 μm

were largely calcium oxide with some oxides of Si, Al and Mg according to EDS line-scan analysis.

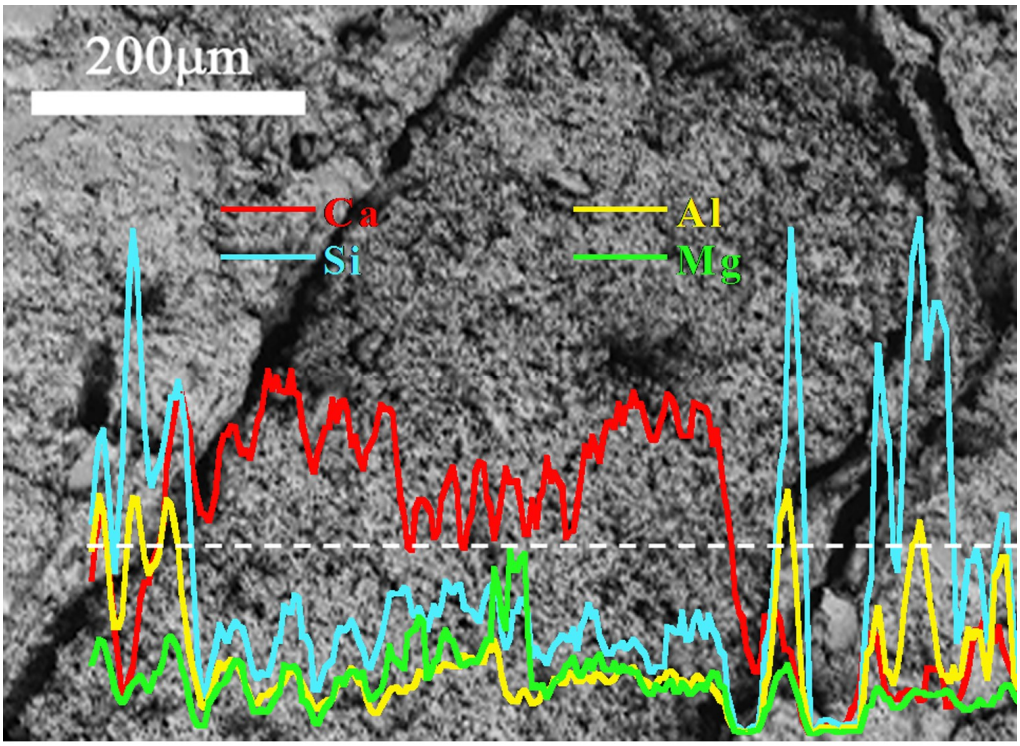

Figure 4.21. SEM-EDS line-scan elemental analysis of Ca-rich particle in the brick fired at 1100°C.

Calcite in the paper processing residues promoted the development of crystalline phases such as gehlenite and anorthite in the vitrified phase with increasing temperature. Ca-rich particles in the brick structure imply textural anisotropy in some regions which can result in lower mechanical durability (Cultrone, et al. 2005).

4.3.7. Mechanical Durability

4.3.7.1. Compressive Strength of the Bricks

The compressive strengths of fired brick samples were measured in their pressing and transverse directions at a cross head speed of 0.5 mm/min in a universal testing machine with a testing capacity of 250 kN. The results obtained are given in Table 4.4 for both application directions. The compressive strengths varied significantly

depending on the firing temperature and paper residue addition. With increasing of the firing temperature, the strength values of the bricks (especially for samples with 0% and 10% residues) partially increased. Figure 4.22 shows compressive strengths of the brick samples as measured in different sample orientations. Shaping (pressing) direction of the brick affected the mechanical strength of the bricks. Paper residue addition and the resulting porosity decreased the compressive strength of the samples which were still higher than the standard strength values. According to Turkish and corresponding European Standards (TS EN 771-1), the minimum strength for building bricks is about 7 MPa (TSE-EN771-1 2005). Compressive strength of the bricks shows a difference as depending on their porosity or density, and the firing temperature. The compressive strength for severe weathering solid brick is between 20 MPa (for 1,500 kg/m^3) and 40 MPa (for 2,000 kg/m^3) (Alleman 1983, Alleman and Berman 1984, Kornmann 2007). The compressive strength of vertical perforated bricks (40% of cavity) varies between 4 and 20 MPa depending on the density (<1,000 kg/m^3) (Kornmann 2007).

Table 4.4. Compressive strength values of the bricks.

Compressive strength (MPa)	Firing temperature	Percent paper residues additions by weight			
		0%	10%	20%	30%
in pressing direction	1000°C	37.1±2.2	12.4±0.7	8.8±0.1	8.7±0.4
at transverse direction		31.1±2.0	12.6±0.7	13.1±0.9	7.0±0.8
at pressing direction	1100°C	40.0±20	16.0±2.0	7.6±0.9	5.1±0.2
at transverse direction		45.0±15	23.5±1.5	15.0±1.0	7.4±0.1

Demir et.al (Demir, et al. 2005) found that compressive strength of the brick without kraft pulp residue produced with extrusion method as fired at 900°C decreased from 15.5 to 9.5 MPa with addition of 10% pulp residue into the brick. In our study, the strengths of samples without residue and with 10% residue were found as higher than that of their bricks. In our study, processing and firing temperatures of bricks, and also residue type used was different than that of their study.

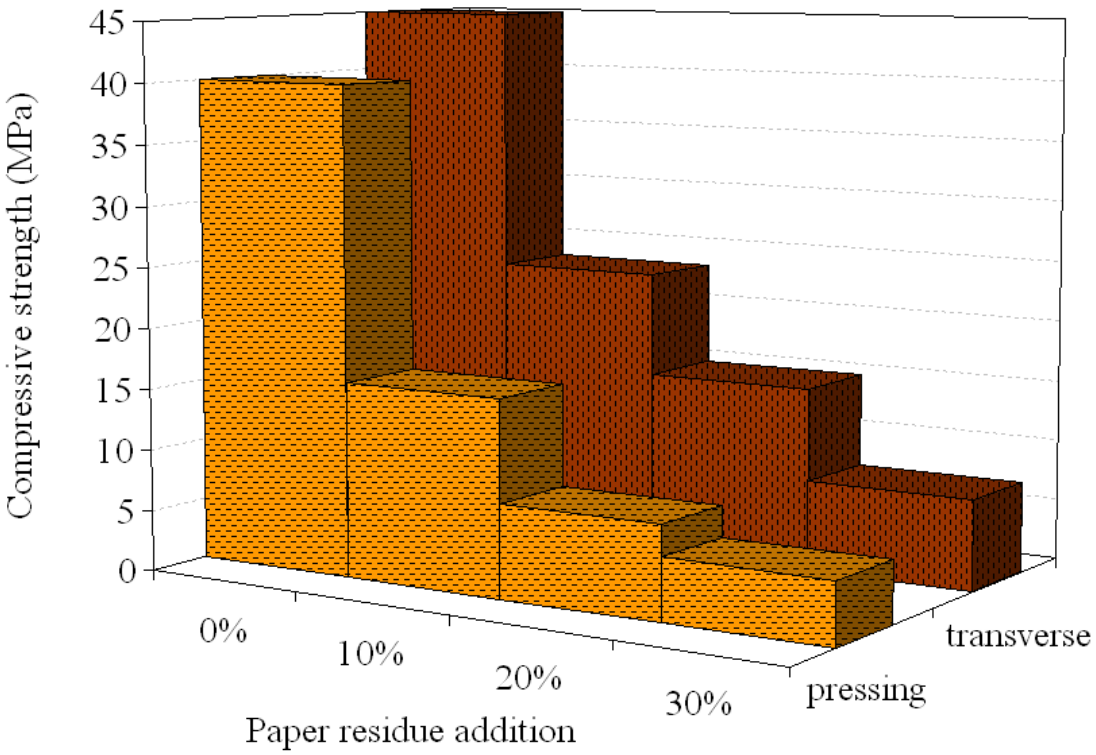

Figure 4.22. Compressive strengths of the samples produced at 1100°C according to loading direction.

Bricks exhibit a brittle fracture behavior. Under compression, they are initially deformed elastically. As the compression is not isotropic, shear forces are also generated. Then the critical conditions for fracture are reached at some locations such as defects (porosity, inclusions etc.) in the sample and the brick breaks in a brittle manner. Because the size of the largest flaw dictates the mechanical strength of the brick, the strength was compromised significantly when paper residue addition increased to 30%. For ceramics, an important criterion is often the stress intensity factor. As there is a distribution of defects of different sizes in the sample, the specimen breaks at the location of the largest defect under the maximum stress intensity (Kornmann 2007). The compressive strength of the fired bricks varies as a function of geometry, porosity and their orientation.

4.3.7.2. Frost Resistance

Like all porous building materials, bricks can be sensitive to freezing. After frozen in a saturated condition, a deformation in brick body such as gradual flaking can

be observed over time, leading to spalling, lamination and cracks. Fired porous clay bricks have mainly open porosity and a low level of closed porosity. The open pores can be partially filled with water. Upon solidification, water density decreases, resulting in a 9% increase in its volume. Internal pressure and stress increases in the saturated body, and the bricks can crack at certain locations due to this stress (Kornmann 2007). The pore size in brick body is an important factor on their frost resistance. Bricks with fine pores show increased hydraulic resistance, and are exposed to higher internal pressure. Some researchers indicated that the specimens containing a high proportion of pores with a diameter bigger than 3 μm provide good frost resistance (Maage 1984).

The bricks were subjected to freezing and thawing performance tests under saturated conditions to define their durability. Saturated bricks were placed in a pan of water. And then, they were placed in a freezer. The bricks were frozen at -15°C for 12 hours and then thawed and exposed to the sun (~25°C). Again they were allowed to refreeze two more cycles per day. Finally, deformations such as spalling and cracking on the bricks were not observed after three cycles. This non-standard test gave an indication of promising freeze-thaw resistance of the bricks.

4.3.8. An Industrial Scale Test

In this study, forming technique of bricks was pressing which gave good results in structural, thermal and mechanical properties of the products on small laboratory sized samples. An industrial partner (Yüksel Toprak Sanayii A.Ş., Turgutlu, Manisa) helped run industrial scale trials by extrusion technique which proved successful. In these runs paper residues of as much as 20% were added together with a total water content of 18% to produce vertical perforated bricks of improved thermal properties. An addition of 20% by volume of residue to brick raw material successfully produced a brick of 8% loss on ignition value with sufficient mechanical strength. Significant reductions in thermal conductivities are achieved in these products. A pattern of vertically perforated brick with 1500 kg/m^3 density, as shown in Figure 4.23 was tested on a Physibel software to estimate its thermal conductivity to be 0.158 W/mK. This value is much smaller than the 0.25 W/mK value of standard insulating bricks. A hot box test is necessary to verify the estimated thermal conductivity of the large sized brick. Industrial scale tests are in progress.

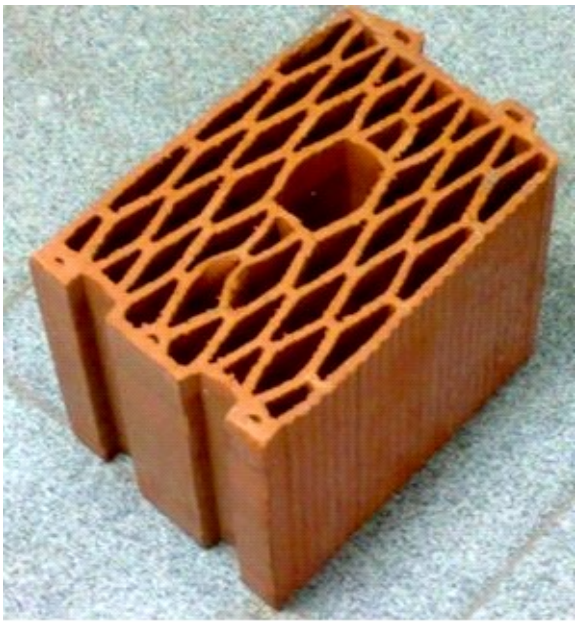

Figure 4.23. A new insulating brick design with 0.158 W/mK of thermal conductivity value.

4.4. Conclusions

In this chapter, incorporation of industrial paper production residues into a ceramic product and as a result, production of porous and lightweight bricks with reduced thermal conductivity and acceptable compressive strength is accomplished. Paper processing residues were used as an additive to an earthenware brick to produce the pores. Chemical, physical, mineral and thermal properties of the raw materials were performed. Mixtures containing brick raw materials and the paper waste were prepared at different proportions (up to 30% by weight). The granulated powder mixtures were compressed in a hydraulic press, and the green bodies were dried before firing at 1000 and 1100°C. The dilatometric behaviors, drying and firing shrinkages of the fired bricks were investigated as well as their loss on ignition, bulk density, apparent porosity and water absorption. Their mechanical and thermal conductivity measurements were performed. In addition, mineralogical and microstructural properties of the fired bricks were investigated.

Results indicated that little shrinkage (1–2%) occurred in the brick that contained residue while the brick without residue shrunk by about 3%. The results obtained showed that the use of paper processing residues decreased the fired density of

the bricks down to 1.28 g/cm^3. Their fired densities varied between 1.92 g/cm^3 and 1.28 g/cm^3, which correspond to a decrease of 33% compared to the density of the brick without residue. Apparent porosity and water absorption values were increased with increase in residue addition. Pressing direction of the bricks and shape of the pores in samples has a considerable effect on mechanical strength. Depending on the increase in the residue addition and porosity content, compressive strength of the samples decreased. Compressive strength of the samples was still higher than that required by the standards. Thermal conductivity of the porous brick produced in this study (<0.4 W/mK) showed more than 50% reduction compared to local brick of the same composition (0.8 W/mK). Although their thermal conductivities decreased by up to 50%, adequate mechanical strength could be maintained. Conversion of this product to a perforated brick showed that its thermal conductivity could be decreased down to 0.158 W/mK. Results indicated that the residues could be easily utilized as pore forming additives into brick bodies to facilitate production of vertically perforated insulation bricks.

CHAPTER 5

UTILIZATION OF RECYCLED PAPER PROCESSING RESIDUES AND CLAY OF DIFFERENT SOURCES FOR THE PRODUCTION OF POROUS ANORTHITE CERAMICS

5.1. Introduction

In the study in Chapter 4, it was noticed that the use of excessive amounts of paper residues can lead to the formation in the brick of new crystalline phases such as anorthite ($CaO \cdot Al_2O_3 \cdot 2SiO_2$) and gehlenite ($2CaO \cdot Al_2O_3 \cdot SiO_2$). These phases are also widely present in insulating refractories which have a porous structure (Brosnan 2004). Paper processing residues can be used to produce a porous and lightweight heat insulating ceramic material. These residues that contained calcium carbonate and cellulose fibers were used as a source of calcium oxide, and also for pore-making due to their organic and carbonate content. These residues together with clay minerals can easily form anorthite or gehlenite phases upon thermal treatment at higher than 1000°C. In order to obtain high refractoriness from such insulation brick the low-melting alkali content must be minimized. Therefore, the different sources of clay are initially studied to observe the influence of chemistry of clay on final product.

In this chapter, porous anorthite ceramics are developed with the addition of paper processing residues as a source of calcium oxide to different clay types in order to produce lightweight insulating refractory materials. This is a preliminarily study of anorthite lightweight insulating refractory production from paper processing residues. Below, brief information about mineralogy of anorthite is provided. Then a literature review about anorthite ceramics follows. Finally, experimental work and the results are presented.

5.1.1. Mineralogy of Anorthite

Anorthite ($CaAl_2Si_2O_8$) is one of the most important members of the plagioclase feldspar family. It is a rare constituent in magmatic and metamorphic rocks (Handbook of Mineralogy 2010). The plagioclase feldspars, also called the soda-lime feldspars, form a complete solid-solution series from pure albite, $NaAlSi_3O_8$, to pure anorthite, $CaAl_2Si_2O_8$. The plagioclase series is divided into six divisions, according to the relative amounts of albite and anorthite. These series by Dana's class are given in Table 5.1. Most of the properties of these species vary in a uniform manner with the change of their chemical compositions (Hurlbut 1959).

Table 5.1. Plagioclase feldspar series.
(Source: Hurlbut 1959)

Plagioclase feldspars		Percentage of albite	Percentage of anorthite
Albite	$NaAlSi_3O_8$	100–90	0–10
Oligoclase	$(Na,Ca)(Si,Al)_4O_8$	90–70	10–30
Andesine	$(Na,Ca)(Si,Al)_4O_8$	70–50	30–50
Labradorite	$(Na,Ca)(Si,Al)_4O_8$	50–30	50–70
Bytownite	$(Na,Ca)(Si,Al)_4O_8$	30–10	70–90
Anorthite	$CaAl_2Si_2O_8$	10–0	90–100

Anorthite has triclinic crystal structure. Figure 5.1 shows crystal structure of anorthite. Anorthite is chemically most nearly related to celsian ($BaAl_2Si_2O_8$), and crystallographically most similar to albite ($NaAlSi_3O_8$) and orthoclase ($KAlSi_3O_8$). Its unit cell is primitive, with a 14 Å c-axis; the c-axis is twice that of albite (Kempster, et al. 1962). Anorthite crystals may occur as euhedral (well-formed with sharp) and tabular crystals (Handbook of Mineralogy 2010, Palace 1935).

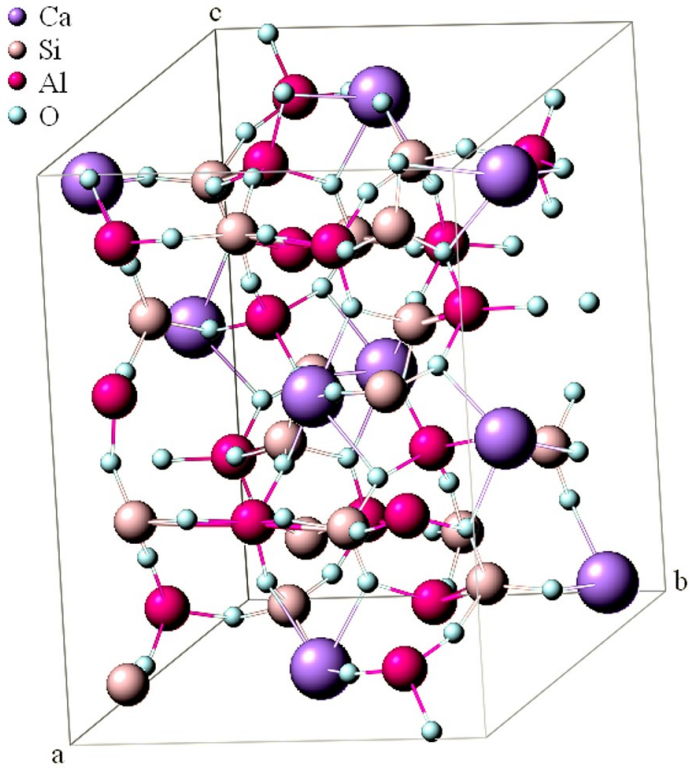

Figure 5.1. Crystal structure of anorthite.
(Source: Webmineral-Anorthite 2010)

Figure 5.2 shows crystal drawing of prismatic and tabular anorthite forms. Drawing is from Palache (1935) who provided crystallographic data (Franklin and Sterling Hill 2010). Combinations of anorthite crystals are formed as c(001), b(010), m(110), M(110), y(201), p(111), and o(111). Detailed mineral data of anorthite is given in Table 5.2 (Handbook of Mineralogy 2010).

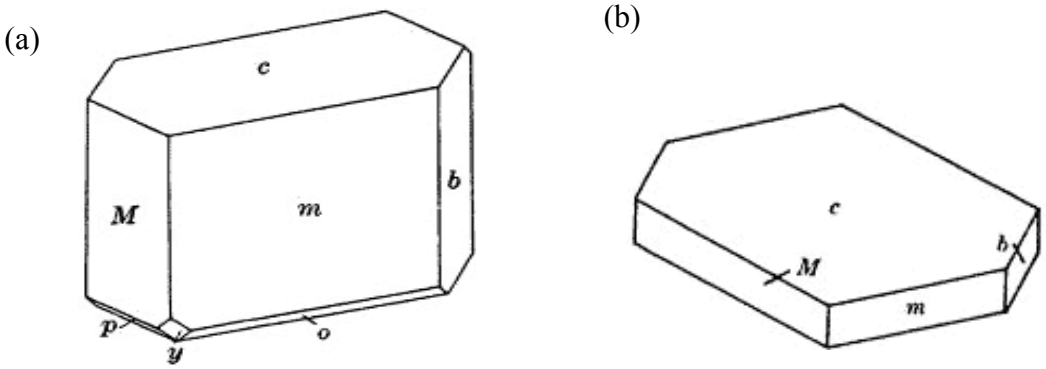

Figure 5.2. Crystal drawing of (a) prismatic and (b) tabular anorthite forms.
(Source: Franklin and Sterling Hill 2010)

Table 5.2. Anorthite mineral data.
(Source: Handbook of Mineralogy 2010)

Anorthite $Na_{0.1-0.0}Ca_{0.9-1.0}Al_{1.9-2.0}Si_{2.1-2.0}O_8$

Crystal Data: Triclinic. *Point Group*: $\bar{1}$. Crystals commonly short, prismatic on [001], rarely on [010], to 2 cm; lamellar, coarse granular, massive. *Twinning*: Commonly polysynthetic on the Albite law; also after the Pericline, Carlsbad, Manebach, and Baveno laws.

Physical Properties: *Cleavage*: Perfect on {001}, less so on {010}, imperfect on {110}. *Fracture*: Conchoidal to uneven. *Tenacity*: Brittle. Hardness = 6–6.5 D(meas.) = 2.74–2.76 D(calc.) = 2.760

Optical Properties: Transparent to translucent. *Color*: White, grayish, reddish; colorless in thin section. *Streak*: White. *Luster*: Vitreous.
Optical Class: Biaxial (–). *Dispersion*: $r < v$, weak. $\alpha = 1.573–1.577$ $\beta = 1.580–1.585$ $\gamma = 1.585–1.590$ 2V(meas.) = 78°–83°

Cell Data: *Space Group*: $P\bar{1}$ (low). $a = 8.1768$ $b = 12.8768$ $c = 14.1690$ $\alpha = 93.17°$ $\beta = 115.85°$ $\gamma = 92.22°$ $Z = 8$

X-ray Powder Pattern: Monte Somma, Italy (low).
3.19 (100), 3.18 (91), 3.21 (63), 3.26 (52), 4.04 (48), 3.12 (39), 3.62 (33)

Chemistry:

	(1)	(2)	(3)
SiO_2	45.88	45.62	43.19
TiO_2	0.04		
Al_2O_3	34.31	35.02	36.65
Fe_2O_3	0.83		
CaO	18.28	18.24	20.16
Na_2O	0.82	1.12	
K_2O	0.11		
H_2O^+	0.14		
Total	100.41	100.00	100.00

(1) Crookdene, Northumberland, England. (2) $Na_{0.10}Ca_{0.90}Al_{1.90}Si_{2.10}O_8$. (3) $CaAl_2Si_2O_8$.

Polymorphism & Series: Trimorphous with dmisteinbergite and svyatoslavite; low- and high-temperature structural modifications are recognized.

Mineral Group: Feldspar group, plagioclase series.

Occurrence: A rare constituent of mafic plutonic and volcanic rocks. In some granulite facies metamorphic rocks; in metamorphosed carbonate rocks; with corundum deposits. Known from meteorites.

Association: Olivine, pyroxene, corundum.

Distribution: A widely distributed rock-forming mineral. Classic occurrences include: from Monte Somma and Vesuvius, Campania; on Mt. Monzoni, Val di Fassa, Trentino-Alto Adige; and from the Cyclopean Islands, Italy. At Tunaberg, Södermanland, Sweden. From near Lojo, Finland. At Bogoslovsk and Barsowka, Ural Mountains, Russia. On Miyakejima Island, Tokyo Prefecture; at Toshinyama, Tochigi Prefecture; the Zao volcano, Yamagata Prefecture; Otaru, Hokkaido; and other places in Japan. In the USA, on Great Sitkin Island, Aleutian Islands, Alaska; from Grass Valley, Nevada Co., California. On Amitok Island, Labrador, Newfoundland, Canada.

Name: From the Greek for *oblique*, for its triclinicity.

5.1.2. Literature Review

The theoretical composition of anorthite is 20.2% CaO, 36.6% Al_2O_3 and 43.2% SiO_2 on a weight basis. Anorthite is a crystalline ceramic phase present in CaO-Al_2O_3-SiO_2 ternary phase system (see Figure 2.2). According to CaO–Al_2O_3–SiO_2 equilibrium phase diagram, pure anorthite exhibits a melting point of 1553°C (Levin 1975). Its theoretical density is 2.76 g/cm^3.

Dense anorthite ceramics are promising materials for substrate applications in electronics industry due to their good physical properties such as thermal expansion coefficient of 4.8x10^{-6}/°C and low dielectric constant of 6.2 at 1 MHz (Gdula 1971). Their thermal expansion coefficient is close to mullite (5.3x10^{-6}/°C). Anorthite based glass-ceramics may also be used in a wide range of applications such as supports of catalysts for the conversion of combustion gases from engines in industrial heat exchangers for gas turbines due to their low thermal expansion coefficient, high thermal shock resistance and low dielectric constant (Boudchicha, et al. 2001). The fluorapatite–anorthite binary system can be promising in biomedicine too, as material for joint prostheses or dental roots (Agathopoulos, et al. 2003). Because of these desirable properties, anorthite ceramics have attracted attention and several studies were carried out in order to decrease the firing and crystallization temperature below 1000°C (Kavalci, et al. 2008, Kobayashi and Kato 1994, Mergen and Aslanoglu 2003). For example, anorthite ceramics for substrate applications require co-firing with inexpensive conductive metals at low temperatures.

Synthesis of anorthite was extensively studied by using different methods such as sintering of mixtures of calcium carbonate, kaolinite, alumina, and aluminum hydroxide in addition to mechano-chemical treatments or employing different sintering aids (Kavalci, et al. 2008, Kobayashi and Kato 1994, Mergen and Aslanoglu 2003, Okada, et al. 2003, Traore, et al. 2003). Kobayashi and Kato have reported the fabrication of dense anorthite ceramics by sintering around 1000°C of kaolin and finely milled calcite mixtures (Kobayashi and Kato 1994). They concluded that reduction to 1.5 μm of the particle size of calcite led to the production of dense anorthite ceramics with a relative density of 94% at 950°C. Mergen and Arslanoglu have reported that single phase anorthite ceramic with 87% theoretical density could be obtained from sintering of raw materials with coarse particles at 950°C by using boron oxide addition

(Mergen and Aslanoglu 2003). Kavalcı et al. investigated the process variables such as temperature, soaking time, amount and type of additives and mechanochemical treatment on synthesis of anorthite ceramics (Kavalci, et al. 2008). They found that anorthite formation temperature decreased down to 900°C by the combined effect of additive usage and intensive grinding. In another study, a layered $CaAl_2Si_2O_8$ and anorthite formation by grinding effect in the samples fired at 900 and 1000°C, respectively was observed by the authors (Okada, et al. 2003). Also the effect of different sources of CaO such as $Ca(OH)_2$, $CaCO_3$, marble powder and gypsum mould waste was investigated in order to produce anorthite ceramics (Kurama and Ozel 2009). The authors showed that anorthite as could be produced as the main phase above 1200°C with a maximum density of 80% in samples with $Ca(OH)_2$. Above mentioned studies aimed to produce dense anorthite ceramics from different sources of calcia and aluminum silicates. Recently, paper processing residues are used as a new source of raw material in the production of porous brick and porous ceramic composite consisting of the cordierite, mullite and cristobalite phases (Dasgupta and Das 2002, Sutcu and Akkurt 2009). A recent study involved open cell anorthite foams (Hojamberdiev, et al. 2009). No study was found in the literature to target a porous anorthite structure from paper residues and from clay of different sources. In this study, porous anorthite ceramics are developed with the addition of paper processing residues as a source of calcium oxide to different clay types in order to produce lightweight insulating refractory materials. This is a preliminarily study of anorthite lightweight insulating refractory production from paper processing residues.

This study followed another study which dealt with the production of vertically perforated insulating earthenware brick for use in buildings the details of which are presented in Chapter 4 (Sutcu and Akkurt 2009). Paper processing residues composed of calcium carbonate and cellulose were used as an additive to clay raw material to make brick. In that study, different amount of paper residue additions were made to clayey material and it was found that excessive additions produced calcium aluminosilicate phases such as anorthite and gehlenite in the brick. So the idea of making anorthite brick with large amounts of porosity was inspired. Not only its calcium carbonate content but also its fine cellulose fibers helped in making porous anorthite based ceramics. Porous ceramics produced in this study could find applications up to 1200°C as refractories in backup insulation for industrial furnaces

and electrical kilns for industrial and lab use. Amount of porosity in these refractories can be up to 60%.

5.2. Materials and Method

Three different clay materials were used for anorthite production such as an enriched clay material of aluminum silicate ($Al_2Si_2O_7 \cdot 2H_2O$, Alfa Aesar Co., Germany), a commercial clay (K244, Kalemaden Co., Turkey) available in tonnage quantities and fireclay (chamotte-125, Eczacıbaşı Esan, Turkey) as alumina and silica source. The clay materials were characterized for chemical (XRF analysis), mineralogical (XRD analysis), microstructural (SEM) and thermal (TGA and DTA analysis) properties.

Recycled paper processing residues (PPR, Levent Kağıt, Turkey) that contained calcium carbonate and cellulose fibers were used as a source of calcium oxide. They were also used for pore-making due to their cellulose fiber and calcite contents. They were initially dried and broken of agglomerates in a mortar and pestle. Their chemical, mineral phase, microstructural and thermal properties are given in detail in Chapter 3 and in reference (Sutcu and Akkurt 2009).

Mixtures containing different sources of clay and paper residues (between 20 and 50% PPR by weight) were prepared to synthesize anorthite composition ($CaO \cdot Al_2O_3 \cdot 2SiO_2$). Powder mixtures were blended with ethanol in a mortar and pestle. Mixed cakes were dried in an oven at 110°C for 1 h and were powdered again before being uniaxially pressed into pellet form (Ø=15 mm) in a steel die at 100 MPa. Pellets were sintered at temperatures between 1100 and 1400°C for 1 h in a laboratory-type electrical kiln (Protherm, Turkey). The heating rate was 2.5°C/min until 600°C, and then 10°C/min up to the dwell temperatures.

Apparent specific gravity, bulk density and apparent porosity values were measured by using boiling water absorption via Archimedes method (ASTM Standard C20 2005). The crystalline phases of the samples were investigated by using XRD with CuK_α radiation (λ=1.542 Å) at 40 kV in the 2θ intervals of 5–70°. Sample surfaces were polished and thermally etched at 1100°C for 30 min. Microstructural analysis of the polished and thermally etched surfaces was performed by using SEM and SEM-EDS (Philips XL-30SFEG and EDAX). Compressive strength tests were done on some

of the samples that have the strongest anorthite composition using universal mechanical testing machine (Shimadzu AG250kN). Cylindrical samples of 15 mm diameter and 22–24 mm long were uniaxially dry pressed and fired in the laboratory type electrical kiln (Nabertherm, Germany).

5.3. Results and Discussion

In this study, anorthite was produced from mixtures of paper residues and clay of different sources in order to find out if and how the type of source of aluminum silicate affects the degree of anorthite synthesis. Hence, results are presented in this section for three different types of aluminum silicate sources.

5.3.1. Characterization of the Raw Materials

Chemical composition of the clay materials provided by producers and EDS analysis is given in Table 5.3. These clays have silica (SiO_2), alumina (Al_2O_3) as well as other species such as soda (Na_2O), potash (K_2O), lime (CaO), magnesia (MgO), iron oxide (Fe_2O_3) and titania (TiO_2). These species primarily exist in a combined form as clay crystals. The clays can contain free silica. It is noticeable that K244 clay has potassium oxide (K_2O) which acts a fluxing agent. Also, the fine particles of calcite ($CaCO_3$) come from paper residues that act as a flux as well (Brosnan 2002a, Brosnan 2002b). Calcite decomposes at about 800°C leaving a residue of calcium oxide (CaO) which will begin to react with clay at 1170°C. In the presence of K_2O flux, this reaction takes place at a lower temperature of 1070°C (Brosnan 2002a).

Figure 5.3 shows X-ray diffraction patterns of the clay raw materials. Enriched clay that was labeled as aluminum silicate included major kaolinite ($Al_2Si_2O_5(OH)_4$) as well as some illite or muscovite ($KAl_2(AlSi_3O_{10})(OH)_2$) and minor quartz ($SiO_2$) minerals. K244 clay contained mainly quartz and kaolinite with some illite or muscovite. Fireclay consists of quartz and mullite ($3Al_2O_3 \cdot 2SiO_2$) phases as well as some cristobalite (a high temperature form of SiO_2).

Table 5.3. Chemical analysis of clay raw materials (wt%).

Components	Enriched clay (Alfa Aesar)	K244 clay (Kalemaden)		Fireclay (Esan)	
	EDS analysis	*Published data*	*EDS analysis*	*Published data*	*EDS analysis*
SiO_2	48.5	59.12	56.0	59.0	49.5
Al_2O_3	43.8	26.87	33.9	38.5	43.5
TiO_2	–	0.80	–	1.1	–
Fe_2O_3	1.5	1.54	1.8	0.5	1.7
CaO	1.1	0.27	1.4	0.1	1.7
MgO	1.3	0.60	1.7	0.1	1.1
Na_2O	1.0	0.04	1.0	0.05	0.9
K_2O	2.7	2.17	4.2	0.4	1.6
Loss on ignition	–	8.5	–	0.1	–

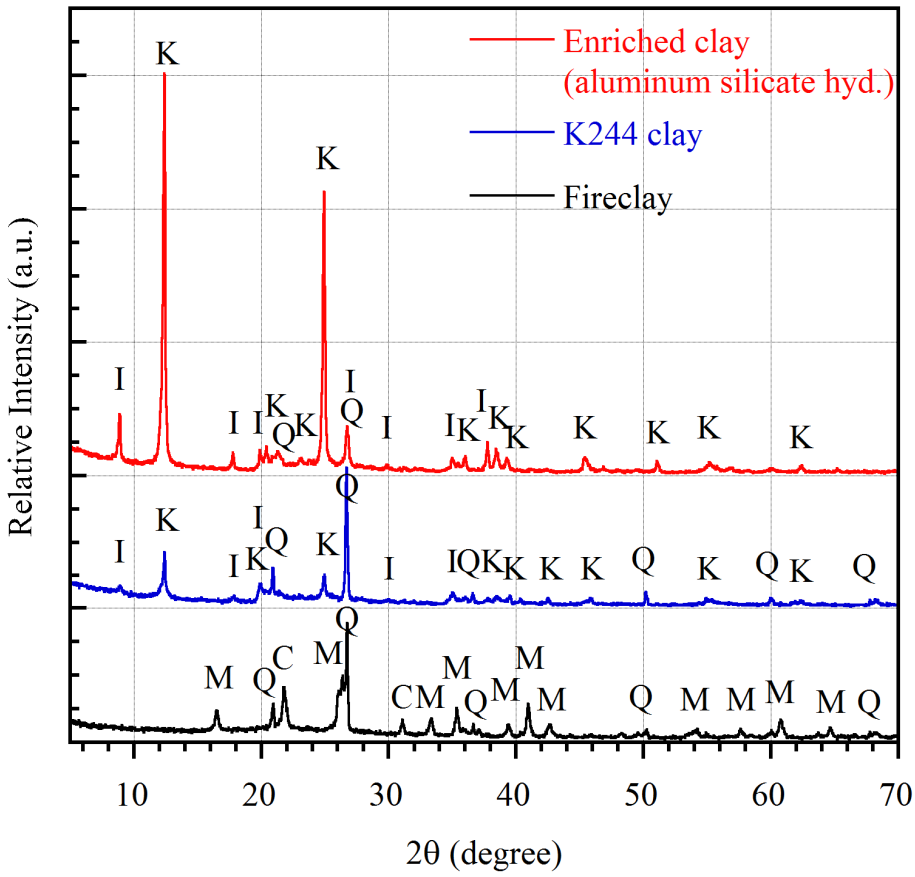

Figure 5.3. X-ray diffraction analysis of the clay raw materials (K: kaolinite, I: illite/muscovite, Q: quartz, M: mullite, C: cristobalite).

Figure 5.4 shows the microstructures of the enriched clay (a) and (b), K244 clay (c) and (d), and fireclay (e) and (f) at different magnifications, respectively. As can be seen from the micrographs, the enriched and K244 clays have agglomerates which consist of hexagonal plate-like crystallites with dimension of smaller than 2 μm. Agglomerates form because clay crystals attract each other due to their electrostatic forces (Brosnan 2002b). The fireclay raw material has coarse particles with size of 50 μm as well as finer particles below 45 μm. Its published data indicated that 75% of the particles were below 45 μm.

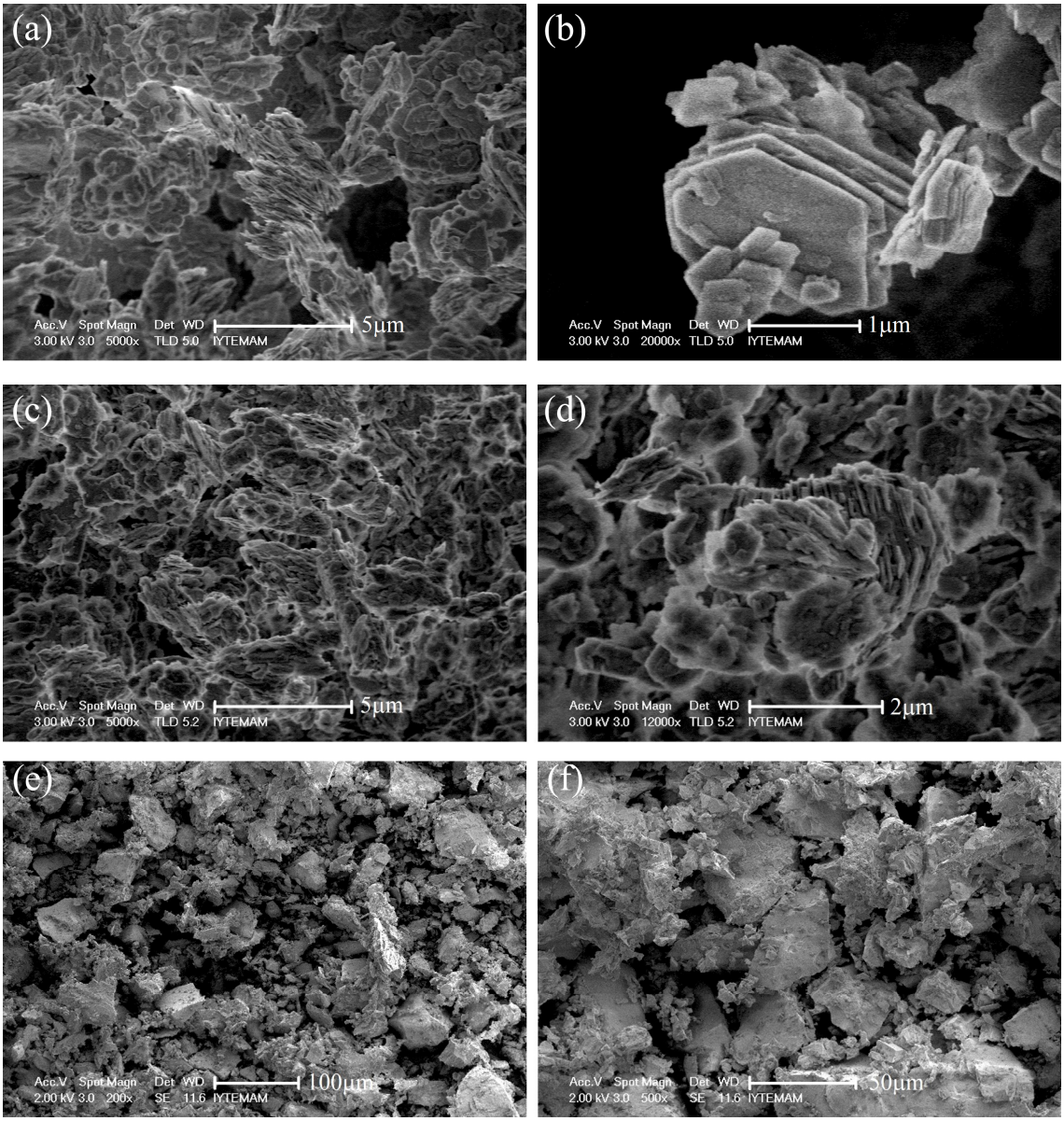

Figure 5.4. Scanning electron microscope images of the clay raw materials: (a) and (b) enriched clay, (c) and (d) K244 clay, (e) and (f) fireclay.

The thermal gravimetric analysis (TGA) curves of the clays are shown in Figure 5.5a. The loss on ignition values of the enriched clay (aluminum silicate hydrate), K244 clay and fireclay were measured as 12, 10 and 1%, respectively. The largest weight loss occurred between 500 and 650°C during heating of clays. It is attributed to dehydroxylation of kaolin to form metakaolin due to the disruption of structural hydroxyl groups in clays.

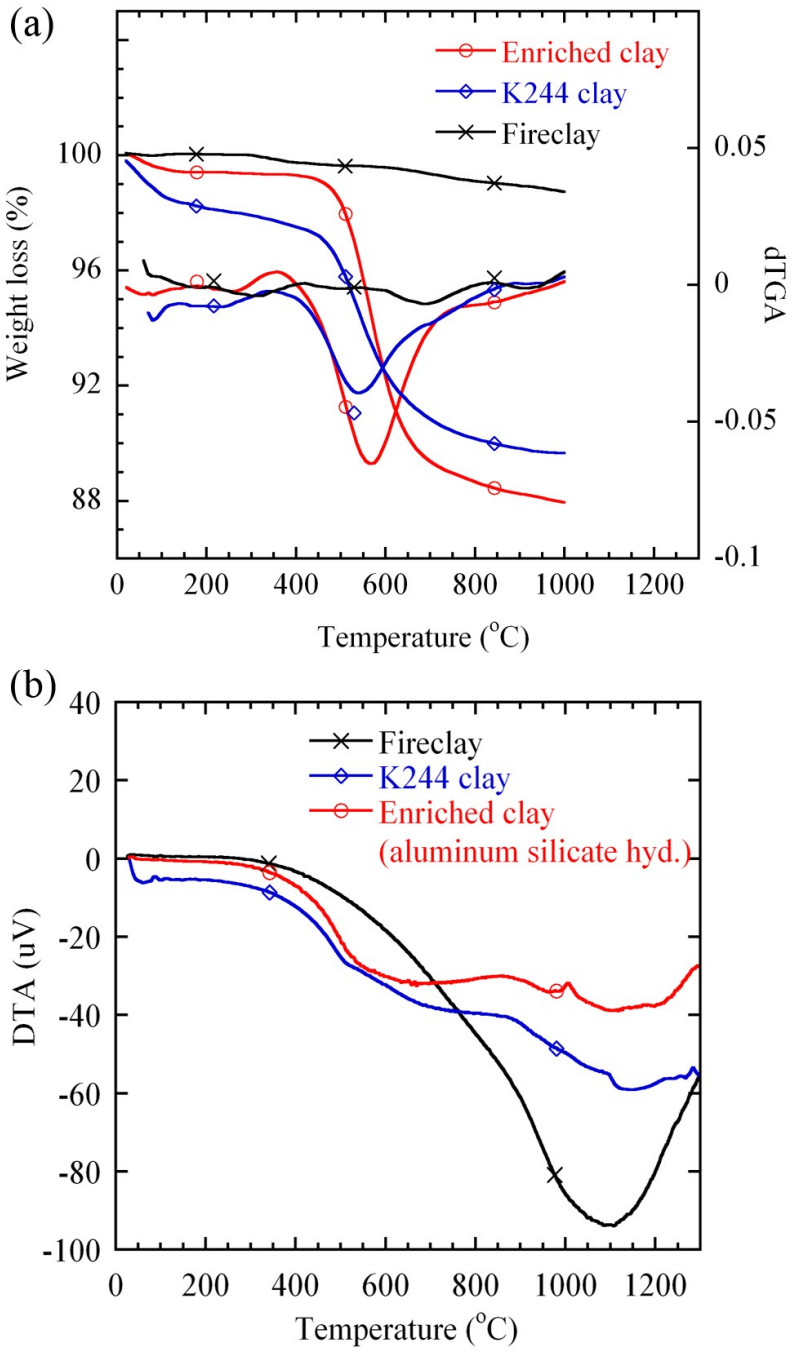

Figure 5.5. Thermal analysis (TGA and DTA) curves of the clays.

The differential thermal analysis (DTA) curves of the clays are shown in Figure 5.5b. A broad endothermic curve between 500 and 700°C, and the exothermic reactions at 1000°C and above 1200°C were observed for the enriched clay. The endothermic reaction corresponds to dehydroxylation of kaolin to form metakaolin and also dehydroxilation of illite. The exotherm at 1000°C corresponds to the onset of crystallization of mullite (Meyers 2003). The DTA curve of K244 clay represents an endotherm at 50–100°C, which corresponds to the adsorbed water. A broad endothermic curve between 500 and 700°C corresponds to dehydroxylation of kaolinite and illite (Budak 2003). Small exotherms at 1100°C and 1300°C represent the crystallization of mullite and the crystallization of glassy silica phase to form cristobalite, respectively (Meyers 2003). The DTA curve of fireclay indicated an exothermic increase above 1100°C. This is probably due to the continuation of the mullite formation with dissolving of quartz or a transition from quartz to cristobalite.

5.3.2. Mixtures Containing Enriched Clay (Aluminum Silicate) and Paper Processing Residue (PPR)

Mixtures containing enriched clay labeled as aluminum silicate (Alfa Aesar) and paper processing residue (PPR) were fired at different temperatures (1100-1300°C) and different PPR contents (20–50 wt%) in order to find the optimum conditions for anorthite synthesis. The aluminum silicate used in this study was obtained from Alfa Aesar and was used as received. It was an enriched clay treated to increase fraction of clay mineral but was still found to have some quartz. Experimental results of the samples (in the cylindrical pellet form) with aluminum silicate fired at different temperatures are given in Table 5.4. The results obtained revealed that loss on ignition values of the samples increased gradually with an increase in the amount of the residues. Bulk densities of the fired samples decreased with increasing paper residue content up to 50 wt%. However, samples fired at 1300°C resulted in increased density after 40% PPR additions possibly as a result of partial vitrification and pore closure. In addition to the experimental studies, compression test was performed to some samples in order to given an idea. Compressive strength of the samples fired at 1300°C ranged from 15 to 41 MPa depending on the amount of PPR addition.

XRD peak intensity results of the samples are given in Table 5.4. Observed crystalline phases are labeled as A: anorthite ($CaO{\cdot}Al_2O_3{\cdot}2SiO_2$), M: mullite

($3Al_2O_3 \cdot 2SiO_2$), G: gehlenite ($2CaO \cdot Al_2O_3 \cdot SiO_2$). According to XRD results, all samples contained anorthite as major phase and also minor amounts of mullite or gehlenite phases. Gehlenite occurred mostly at lower temperatures and in samples containing higher calcium (above 30wt% PPR). XRD patterns of all samples fired at 1300°C are also shown in Figure 5.6a. Samples with 20wt%, 30wt% and 40wt% PPR clearly indicated a predominant anorthite phase. Figure 5.6b shows XRD patterns of the samples with 30wt% paper residues fired at different temperatures. Gehlenite peaks appeared in the samples fired at 1100 and 1200°C which completely transformed to anorthite at 1300°C. These samples also contained less amount of mullite in addition to anorthite. The samples with 30wt% PPR that contained the most intensive anorthite peak had lower bulk densities (~1.5 g/cm^3).

Table 5.4. Experimental results of samples containing aluminum silicate and PPR (*s: strong, vs: very strong* for XRD peak intensity).

Temperature (°C)	PPR content (wt%)	XRD Peak Intensity*	Loss on ignition (%)	by Archimedes method (ASTM C20)			Compressive strength (MPa)
				Apparent Porosity (%)	Bulk density (g/cm^3)	Apparent specific gravity	
1100	30	A, M, G	25.2	41.0	1.46	2.48	-
	50	A, G (s)	33.7	54.7	1.33	2.95	-
1200	20	A, M	20.9	29.0	1.75	2.46	-
	30	A (s), M	25.2	35.5	1.49	2.31	-
	40	A (s), G	29.5	49.9	1.34	2.68	-
	50	A, G	33.7	48.1	1.29	2.48	-
1300	20	A, M	20.9	6.4	1.94	2.07	41.4±8.3
	30	A (vs), M	25.4	36.2	1.53	2.40	28.0±6.8
	40	A (vs), G	28.3	44.8	1.39	2.53	15.6±2.2
	50	-	34.2	30.4	1.71	2.47	-

* Decreasing dominance of phases from left to right

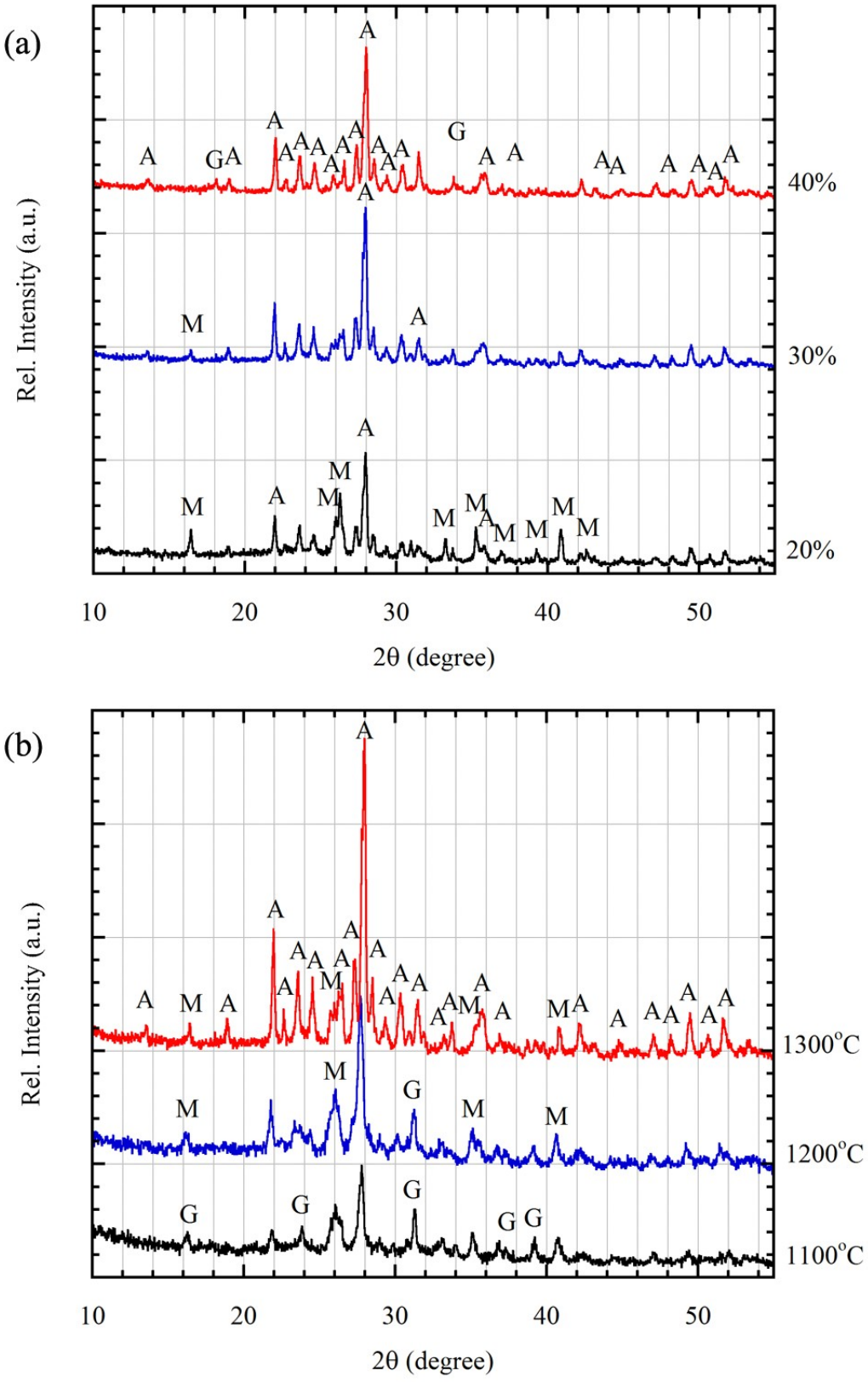

Figure 5.6. XRD patterns of: (a) samples with aluminum silicate and with 20, 30 and 40% PPR addition fired at 1300°C, (b) samples with aluminum silicate and 30wt% PPR fired at different temperatures (Reference numbers: (A) 86-1705, (G) 79-1726, (M) 83-1881).

The microstructures of samples were observed by back-scattered electron image (BSE) and secondary electron (SE) detector of an SEM. Microstructures (by BSE image) of polished and thermally etched surfaces of the sample containing aluminum silicate and 30wt% PPR fired at 1300°C are shown in Figure 5.7(a) and (b), respectively. As can be seen from Figure 5.7a, large sized pores were present in the matrix. These pores result largely from the removal of cellulose fibers and some minor contribution from calcium carbonate decomposition during firing. These local high calcium concentrations lead to anorthite formation (Traore, et al. 2003). Figure 5.7b exhibited the presence of anorthite crystals in a well-crystallized matrix in a porous structure. As can be seen from Figures 5.7(b) and 5.8(a), microstructure after thermal etching of the polished surfaces revealed that the crystalline grains are embedded in the matrix, randomly oriented. These grains that had a maximum thickness of 2 μm formed like an interconnected network (Figure 5.7b). This network supplied strength to the structure although pores are found in the matrix (Traore, et al. 2003). Well formed crystals of anorthite of about 10 micrometers of length were clearly identified by EDS analysis. As indicated in Figure 5.8, the SEM-EDS analysis were performed onto the crystalline grains that randomly oriented and embedded in the matrix, and also anorthite crystals in a porous structure of the thermally etched sample containing aluminum silicate and 30wt% PPR fired at 1300°C. Their oxides and elemental analysis results are presented in Table 5.5 and Figure 5.9, respectively. According to the results, the crystalline grains in the matrix and porous structure had strongly anorthite composition along with less amounts of impurities such as magnesium and potassium oxides. However, these impurities were insignificant in the anorthite composition.

Table 5.5. SEM-EDS results (oxide) of the sample containing aluminum silicate with added 30wt% PPR fired at 1300°C.

Oxides (wt%)	In Figure 5.8a			In Figure 5.8b	
	(1)	(2)	(3)	(4)	(5)
Al_2O_3	38.16	38.3	39.59	37.43	39.07
SiO_2	42.01	44.54	43.5	39.12	46.00
CaO	18.66	16.08	15.8	21.84	13.32
K_2O	0.41	0.46	0.00	0.30	0.92
MgO	0.75	0.63	1.12	1.31	0.69

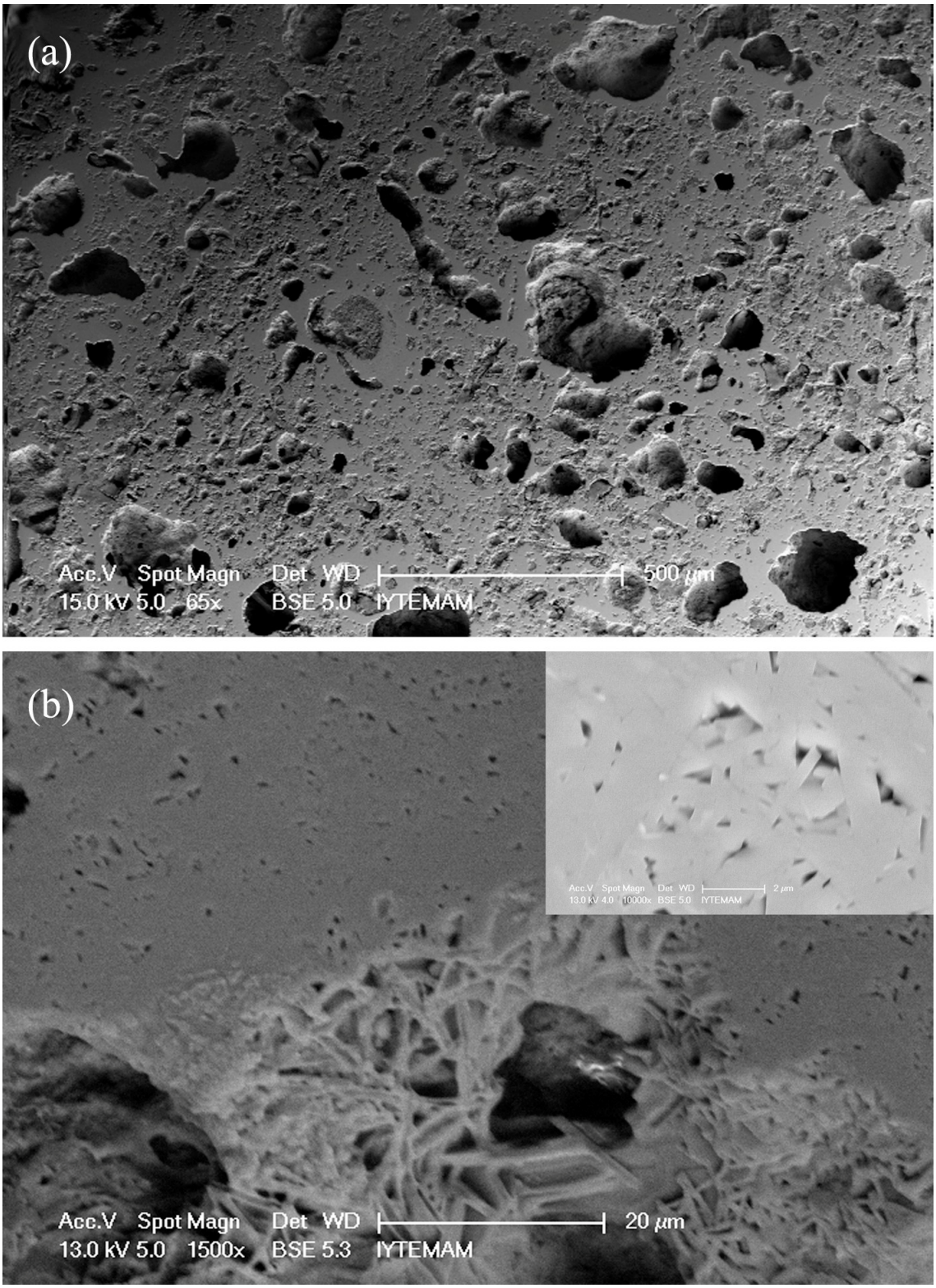

Figure 5.7. Microstructures of: (a) polished and (b) thermally etched surfaces of the sample containing aluminum silicate and 30wt% PPR fired at 1300°C. Inset: a close up view of the matrix in (b).

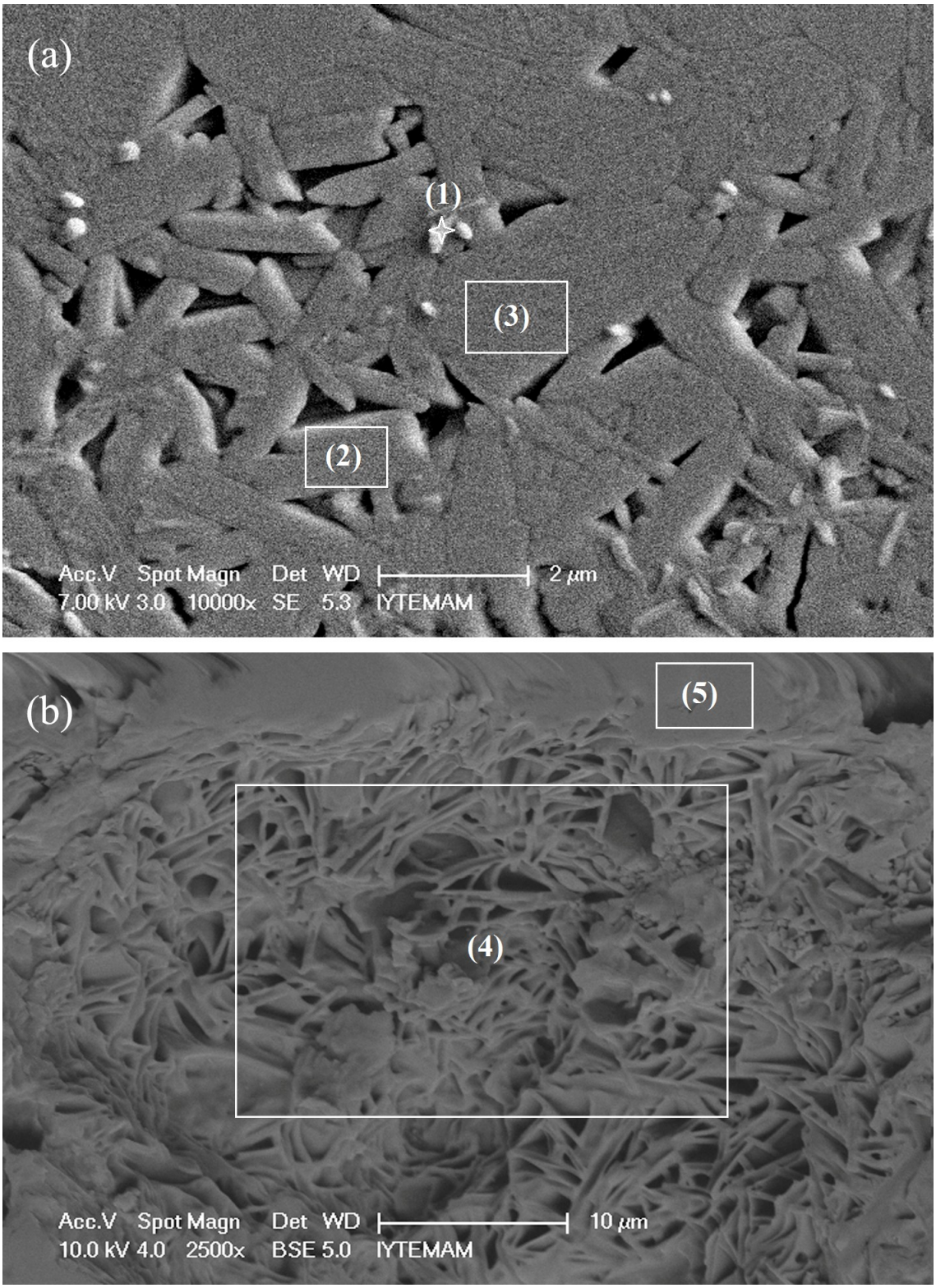

Figure 5.8. (a) Microstructure of thermally etched surface of the sample, and (b) anorthite crystals in a pore of the thermally etched sample containing aluminum silicate with added 30wt% PPR fired at 1300°C.

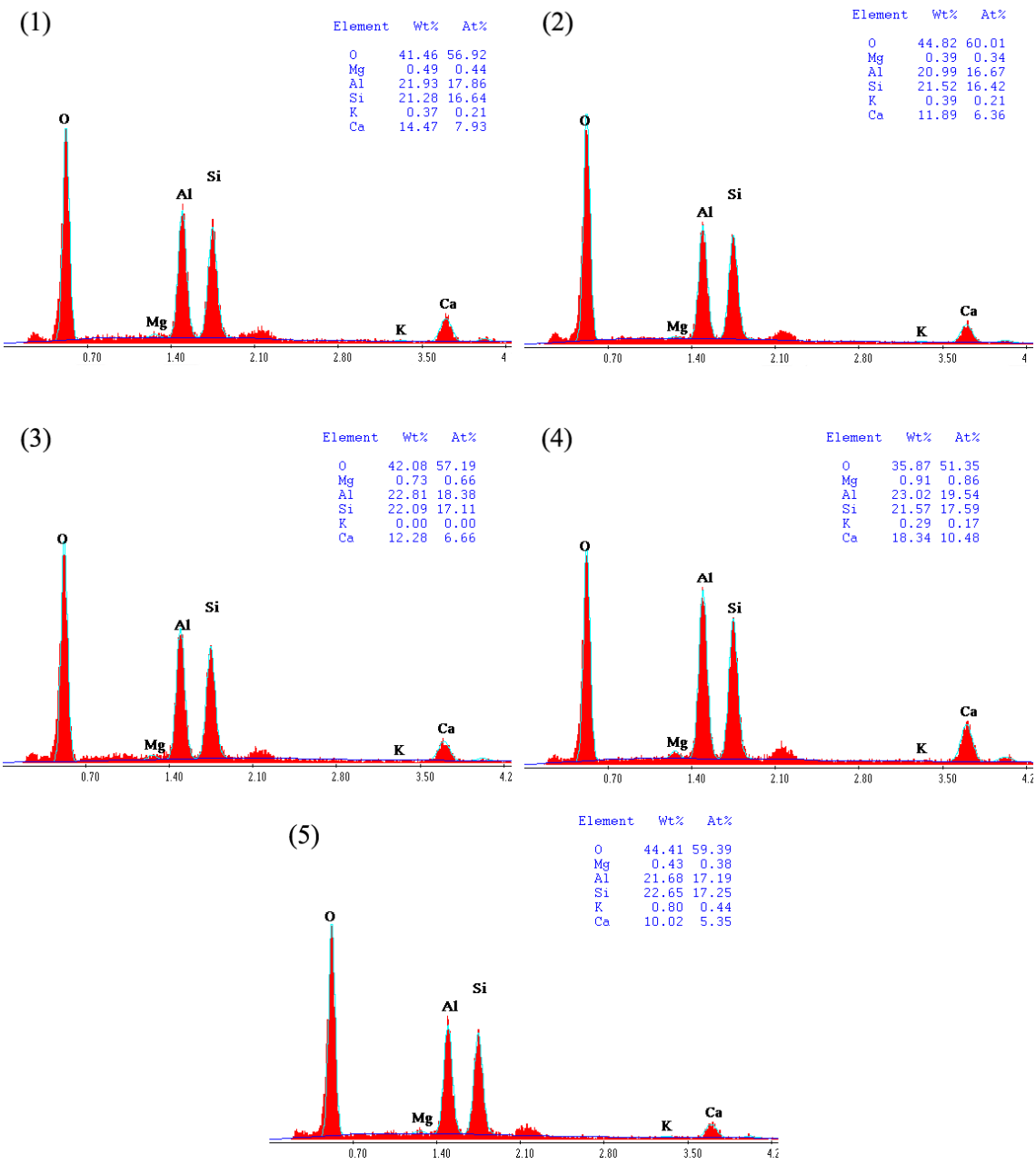

Figure 5.9. The EDS elemental analysis results of the regions indicated by the numbers in Figure 5.8.

5.3.3. Mixtures Containing Commercial Clay (K244) and Paper Processing Residue (PPR)

In this section, commercial clay (K244, Kalemaden, Turkey) together with the paper residues were used in order to produce porous anorthite ceramic bodies. Experiments were carried out at temperatures between 1100 and 1300°C. Paper residue contents of samples were varied from 20wt% to 50wt% in order to find optimum

conditions for formation of anorthite. Chemical composition of the K244 clay is given in Table 5.3. The clay has small amount of potassium oxide which acts a fluxing agent. The clay contained mainly quartz and kaolinite with some layered structures.

Experimental results of the samples containing K244 clay and PPR mixtures fired at different temperatures are given in Table 5.6. The results obtained revealed that loss on ignition values of the samples increased gradually with an increase in the amount of the residues. Their bulk densities generally decreased with increasing PPR content. Some increase in the densities of the samples with 30–50wt% PPR was observed probably due to vitrification at 1250 and 1300°C. In fact, the samples with 50wt% PPR melted at 1300°C. Apparent porosities of the samples began to decrease with increasing temperatures from 1200°C. The densities of anorthite based samples (with 30–40wt% PPR) varied from 1.51 to 1.98 g/cm^3. Compressive strength of the samples fired at 1250°C ranged from 22 to 33 MPa depending on the amount of PPR addition.

The main XRD peak intensities of the samples are given in Table 5.6. Observed crystalline phases are labeled as A: anorthite ($CaO{\cdot}Al_2O_3{\cdot}2SiO_2$), Q: quartz ($SiO_2$), M: mullite ($3Al_2O_3{\cdot}2SiO_2$), G: gehlenite ($2CaO{\cdot}Al_2O_3{\cdot}SiO_2$). Samples containing 30wt% and 40wt% PPR contained major anorthite phases at 1250°C and 1300°C of firing temperatures. When the firing temperature increased, anorthite and gehlenite formation became more stable. As expected, gehlenite occurred mostly in the sample containing 50wt% PPR. XRD patterns of all samples fired at 1250°C are shown in Figure 5.10a. XRD results of the samples with 20wt%, 30wt% and 40wt% PPR indicated strong anorthite formation at 1250°C. The bump in the XRD scan between 16 and 34° indicates the formation of a glass phase. Figure 5.10b shows XRD patterns of the samples with 30wt% PPR fired at different temperatures. Minor phases such as quartz and gehlenite appeared in the samples fired at 1100 and 1200°C that were completely transformed to anorthite at 1300°C.

Table 5.6. Experimental results of the samples containing K244 clay and PPR mixtures (*s: strong, vs: very strong* for XRD peak intensity).

Temperature (°C)	PPR content (wt%)	XRD Peak Intensity*	Loss on ignition (%)	by Archimedes method (ASTM C20)			Compressive strength (MPa)
				Apparent porosity (%)	Bulk density (g/cm^3)	Apparent specific gravity	
1100	30	Q (s), A, G	23.3	39.6	1.53	2.54	-
	50	G (s), Q, A	32.0	43.0	1.55	2.72	-
1200	20	Q, A, M	19.2	23.1	1.79	2.32	-
	30	A (s), Q	23.5	40.3	1.51	2.54	-
	40	A, Q, G	27.8	46.4	1.43	2.68	-
	50	A, G	33.8	50.1	1.32	2.65	-
1250	20	A (s), Q, M	19.0	16.0	1.81	2.16	32.3±8.4
	30	A (vs)	23.8	36.0	1.59	2.48	33.9±0.2
	40	A (vs)	28.0	9.9	1.98	2.20	22.8±6.1
1300	30	A (vs)	23.7	27.6	1.60	2.21	-
	50	-	Melted				

* Decreasing dominance of phases from left to right.

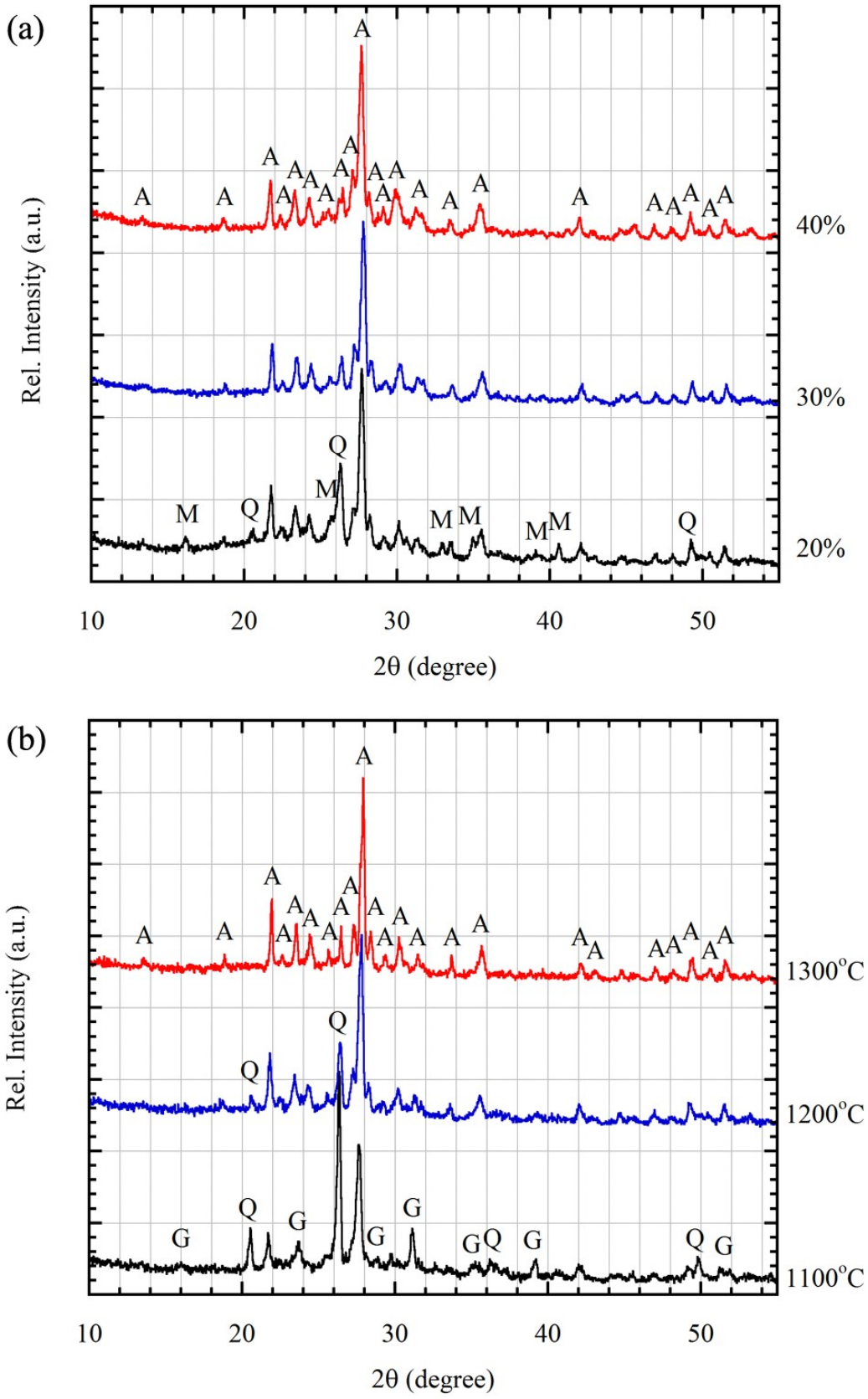

Figure 5.10. XRD patterns of: (a) K244 samples with 20, 30 and 40% PPR addition fired at 1250°C, (b) samples with 30wt% PPR fired at different temperatures.

The SEM images of polished and thermally etched surfaces of K244 samples with 30wt% PPR fired at 1300°C are shown in Figure 5.11(a) and (b), respectively. As can be seen from Figure 5.11a, pores of varying sizes (5 μm to 500 μm) were observed in the ceramic. Pores formed due to the removal of fine cellulose fibers in addition to decomposition of calcium carbonate during firing. Potassium oxide (K_2O) in the clay acts as a fluxing agent, therefore the fired body was easily vitrified at high temperatures. Fluxing agents cause a reduction in refractoriness properties of the samples. Therefore, this type clay may be unfavorable for production of insulating firebrick. Randomly oriented tabular and layered crystals with different geometric shapes appeared in the pores as shown in Figure 5.11b. They were identified from their crystal geometries based on literature (Palace 1935). SEM-EDS analysis of the sample with 30wt% PPR indicated that the tabular crystals in Figure 5.11b were anorthite with the following composition: Si (23.5wt%), Al (18.4wt%), Ca (16.5wt%) and also fluxing elements such as Mg (1.1wt%), Fe (0.9wt%) and K (0.8wt%).

The SEM images of thermal etched surface of the samples containing K244 clay and 30wt% PPR fired at 1250°C and 1300°C are shown in Figure 5.12(a) and (b), respectively. The thermal etching was quite helpful to observe the crystals in the microstructure. Figure 5.12a shows most probably a diffusion in the sample fired at 1250°C, which could be the dissolution of a quartz grain and the formation of fine anorthite crystals in the glassy matrix. In Figure 5.12a, the contraction of the quartz particle during cooling was observed. With increasing firing temperature to 1300°C, free quartz grains were not observed in the microstructure, and the crystalline phase formation in the glassy matrix was observed (Figure 5.12b). Figure 5.13(a) and (b) shows the microstructures of BSE and SE mode of anorthite crystals embedded in a pore of the thermal etched K244 sample with 30wt% PPR fired at 1300°C, respectively. The SEM-EDS analysis was performed onto the crystalline grains indicated by the numbers in Figure 5.13a. While the crystalline grains indicated by (1) and (3) is prismatic, grain indicated by (2) is tabular randomly oriented and embedded in the matrix. Secondary electron (SE) image of the grains indicated by (2) and (5) at 2500X magnification are shown in Figure 5.13b. As interesting, it was observed that the grain indicated by (2) and others had a layered structure. The region indicated by (5) had small crystallites around 1 μm. The SEM-EDS elemental and oxides analysis for each crystalline grain indicated by (1), (2), (3), (4) and (5) in Figure 5.13a was performed, and the elemental and oxide analysis results are presented in Figure 5.14 and Table 5.7,

respectively. According to the elemental analysis results, each grain indicated by (1), (2) and (3) had strongly anorthite composition. Al ratio decreased in the grain indicated by (4), on the other hand, Ca ratio increased in the grain indicated by (5). Grains indicated by (4) and (5) are small and fine crystallites in the matrix. Particularly, the grain indicated by (5) is smaller than the others, and it is a calcium silicate phase.

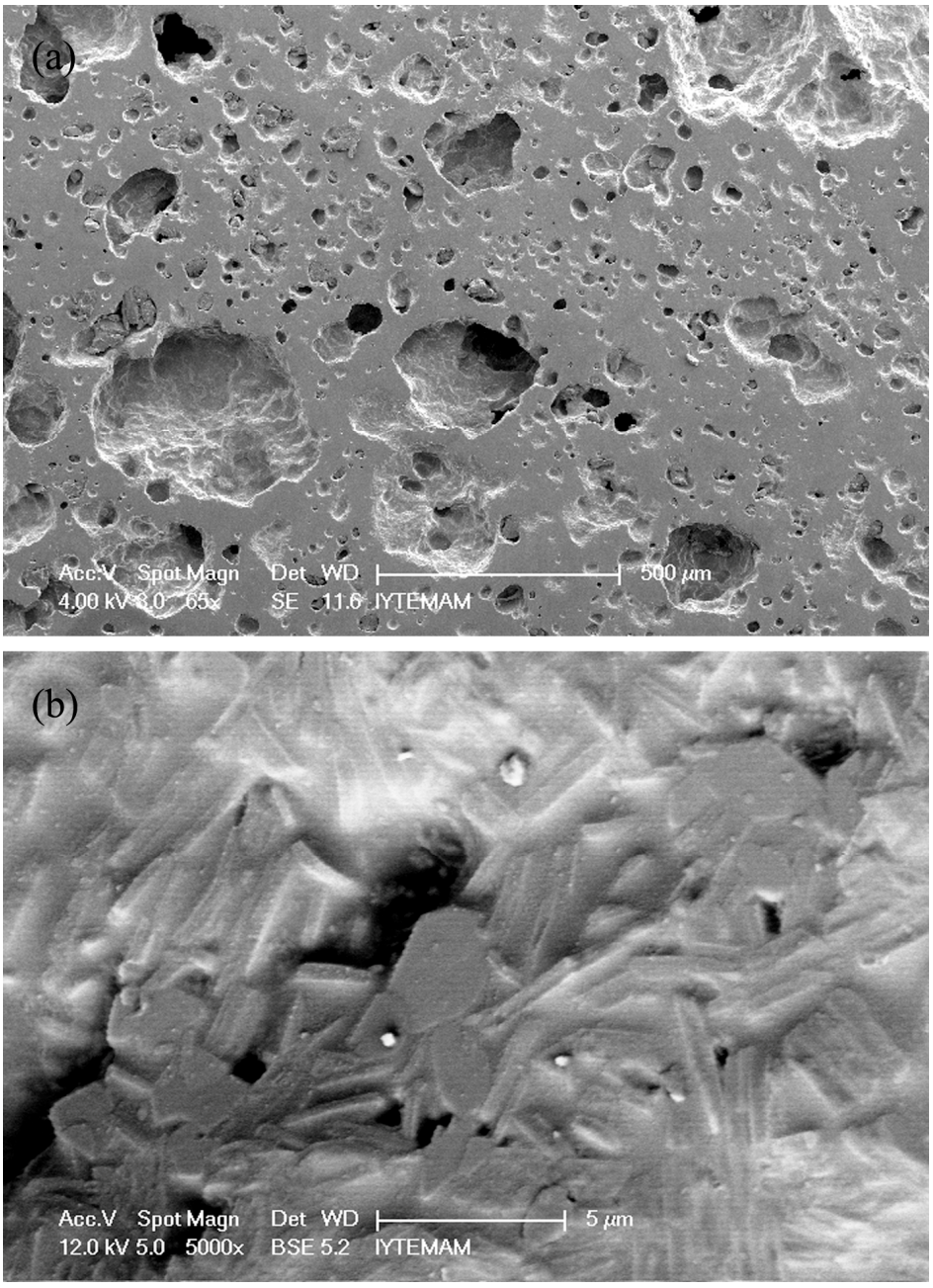

Figure 5.11. SEM images of the K244 sample with 30wt% PPR fired at 1300°C: (a) polished surface, (b) tabular anorthite crystals embedded in glassy matrix as observed in a pore. Both samples were thermally etched at 1100°C for 30 min.

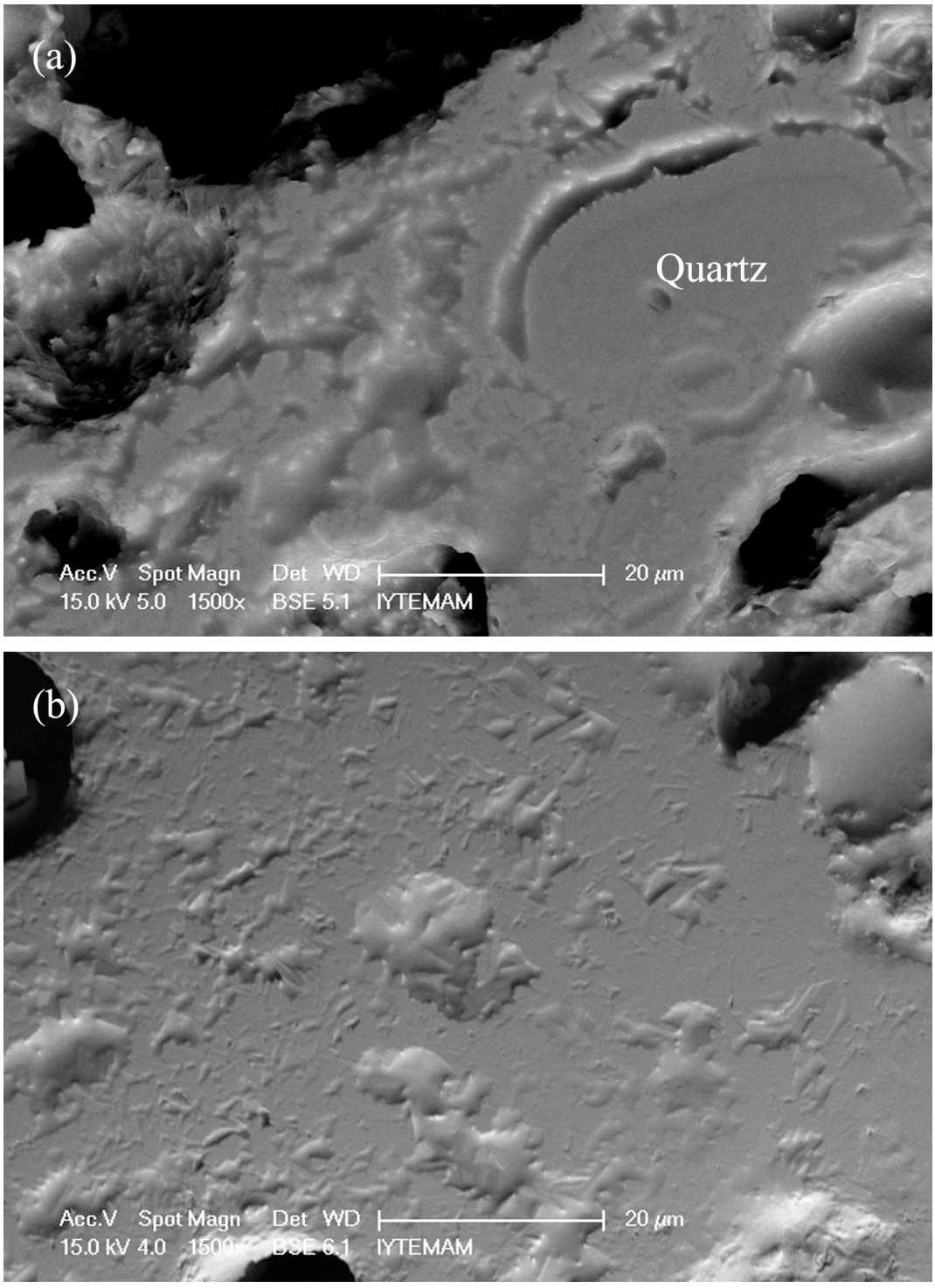

Figure 5.12. Microstructures of thermally etched surface of the K244 samples with 30wt% PPR fired at (a) 1250°C and (b) 1300°C.

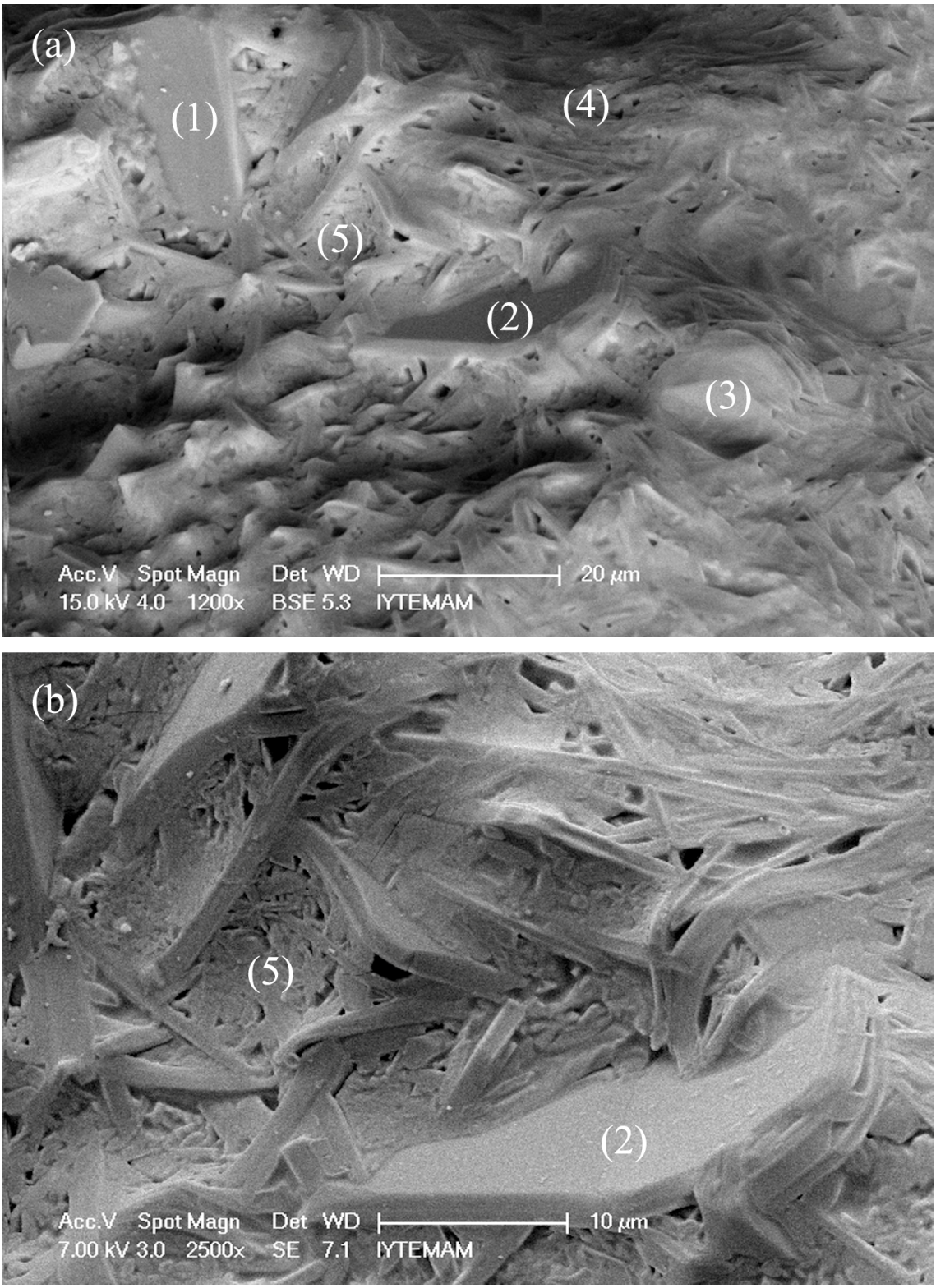

Figure 5.13. SEM images of different anorthite crystals embedded in a pore of thermally etched K244 sample with 30wt% PPR: (a) BSE mode at 1200x and (b) SE mode at 2500x.

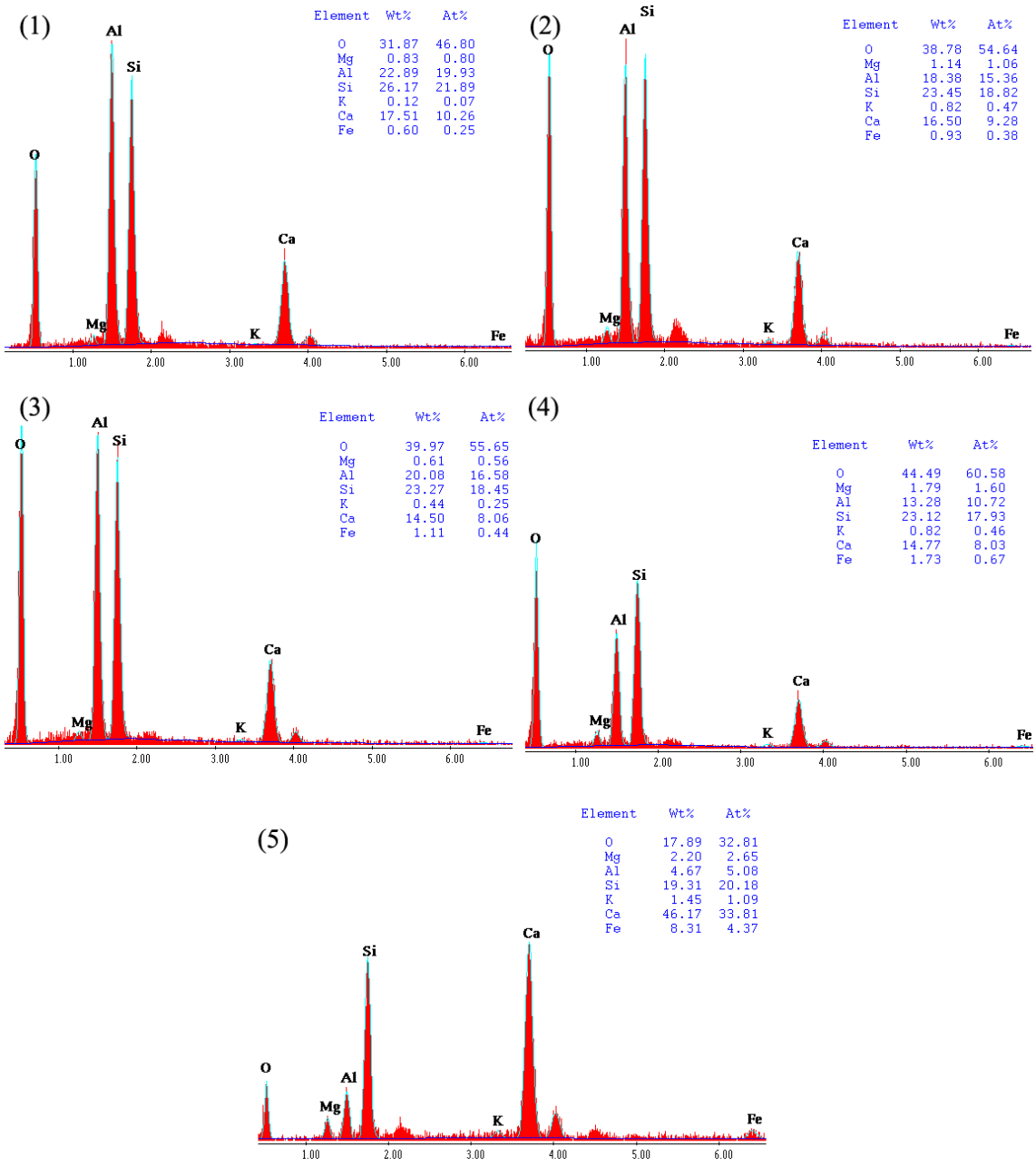

Figure 5.14. The EDS elemental analysis of the regions indicated by the numbers in Figure 5.13.

As can be clearly seen from Table 5.7, crystalline grains indicated by (1), (2), (3) and even (4) strongly had anorthite composition along with other impurities. Fine crystalline matrix structure between tabular anorthite crystals that randomly oriented was especially rich in calcium oxide (CaO) and iron oxide (Fe_2O_3). Potassium oxide (K_2O) and iron oxides in the clay act as a fluxing agent; therefore the fired body was easily vitrified at high temperatures. Experiments with commercial K244 clay indicated that alkalis along with other impurities were mainly responsible for premature

vitrification at lower than expected temperatures. Alkalis cause a reduction in refractoriness properties of the samples. Therefore, this type of clay may be unfavorable for production of thermally insulating ceramics. Maybe the K244 samples containing high amount of anorthite without free-quartz could be used for low temperature applications of 1100°C and below. Since, free-quartz causes the body to crack during cooling.

Table 5.7. SEM-EDS results of the sample containing K244 clay and 30wt% PPR fired at 1300°C.

Oxides (wt%)	In Figure 5.13				
	(1)	(2)	(3)	(4)	(5)
Al_2O_3	35.14	31.29	34.50	24.71	6.74
SiO_2	43.72	44.45	44.50	48.63	31.30
CaO	19.22	20.48	18.17	20.33	48.84
K_2O	0.11	0.88	0.48	0.97	1.33
MgO	1.13	1.72	0.93	2.92	2.79
Fe_2O_3	0.68	1.18	1.43	2.43	9.00

5.3.4. Mixtures Containing Fireclay (Chamotte) and Paper Processing Residue (PPR)

Experience with commercial K244 clay in the previous section indicated that alkalis along with other impurities were mainly responsible for premature vitrification at lower than expected temperatures. Therefore a decision was made to use a fireclay powder (chamotte) to increase refractoriness of the synthesized anorthite by reducing glassy material in the structure. In this section, ground fireclay (chamotte-125, obtained from Eczacıbaşı Esan, Turkey) was used as clay raw material for high refractoriness of the products. 75% of its particle size was below 45 μm. Its loss-on-ignition value was almost zero. Its chemical composition consisted of a high percentage of silica and alumina, and a low percentage of the oxides of sodium, potassium and calcium (Table 5.3). Mineral composition of the fireclay was found to consist of quartz, mullite and cristobalite (Figure 5.3). Since it is fired at a high temperature, kaolin mineral was

transformed to mullite and glass, besides a part of quartz was transformed to cristobalite.

In this study, 20, 30 and 40wt% PPR were added to fireclay in order to synthesize anorthite. Samples were fired at 1200 and 1400°C due to their higher refractoriness. Experimental results of the fireclay samples are given in Table 5.8. All of the samples that were fired at 1200°C, and the sample with 30wt% PPR fired at 1400°C showed dimensional stability. Whereas, the samples with 20wt% and 40wt% PPR sintered at 1400°C linearly shrank and expanded by around 6% and 7%, respectively. Bulk densities of samples with 20wt% and 30wt% PPR increased with increasing temperature. Interestingly, sample with 40wt% PPR was observed to have decreased bulk density with increasing firing temperature. This situation can be explained with higher firing temperature of 1400°C which is close to melting point of anorthite (1553°C), and also it may explain the increasing degree of anorthite crystallization and completion of anorthite formation with the dissolution of secondary phases such as quartz, mullite and gehlenite. In addition to the experimental studies, compression test was performed to some samples in order to obtain an idea about their mechanical properties. Compressive strength of the samples fired at 1400°C ranged from 8 to 43 MPa depending on the amount of PPR addition.

XRD patterns of the samples fired at 1200°C and 1400°C are shown in Figure 5.15(a) and (b), respectively. In the samples fired at 1200°C, the secondary phases such as gehlenite, mullite, cristobalite and quartz as well as anorthite were observed. In XRD pattern of the sample with 20% PPR fired at 1400°C, a broad hump peak was observed at 2θ interval of 18–32°, which corresponds to the formation of an amorphous (glassy) phase. However, this amorphous phase disappeared with increasing of paper residues addition. The degree of crystallinity of anorthite increased with increasing firing temperature (Figure 5.15b). In the samples with 30 and 40wt% additives, the secondary phases were transformed to anorthite as major phase with increasing temperature. Stoichiometric anorthite composition was apparently satisfied in the samples with 30 and 40wt% PPR by weight at 1400°C. In addition, less amount of mullite was observed in the sample with 30wt% PPR as there was enough calcium to produce anorthite.

Table 5.8. Experimental results of the fireclay samples with PPR (*s: strong, vs: very strong* for XRD peak intensity).

Temperature (°C)	PPR content (wt%)	XRD Peak Intensity*	Loss on ignition (%)	by Archimedes method (ASTM C20)			Compressive strength (MPa)
				Apparent porosity (%)	Bulk density (g/cm^3)	Apparent specific gravity	
1200	20	C, M, Q, A	11.6	43.8	1.50	2.67	-
	30	A, M, Q, C	16.5	47.5	1.42	2.70	-
	40	A, M, G, Q, C	22.1	51.9	1.33	2.76	-
1400	20	M (s), A	11.0	0.1	2.02	2.02	42.3±1.7
	30	A (vs), M	16.8	27.4	1.81	2.50	43.2±11.6
	40	A (vs)	22.0	54.3	1.21	2.65	8.9±2.3

* Decreasing dominance of phases from left to right.

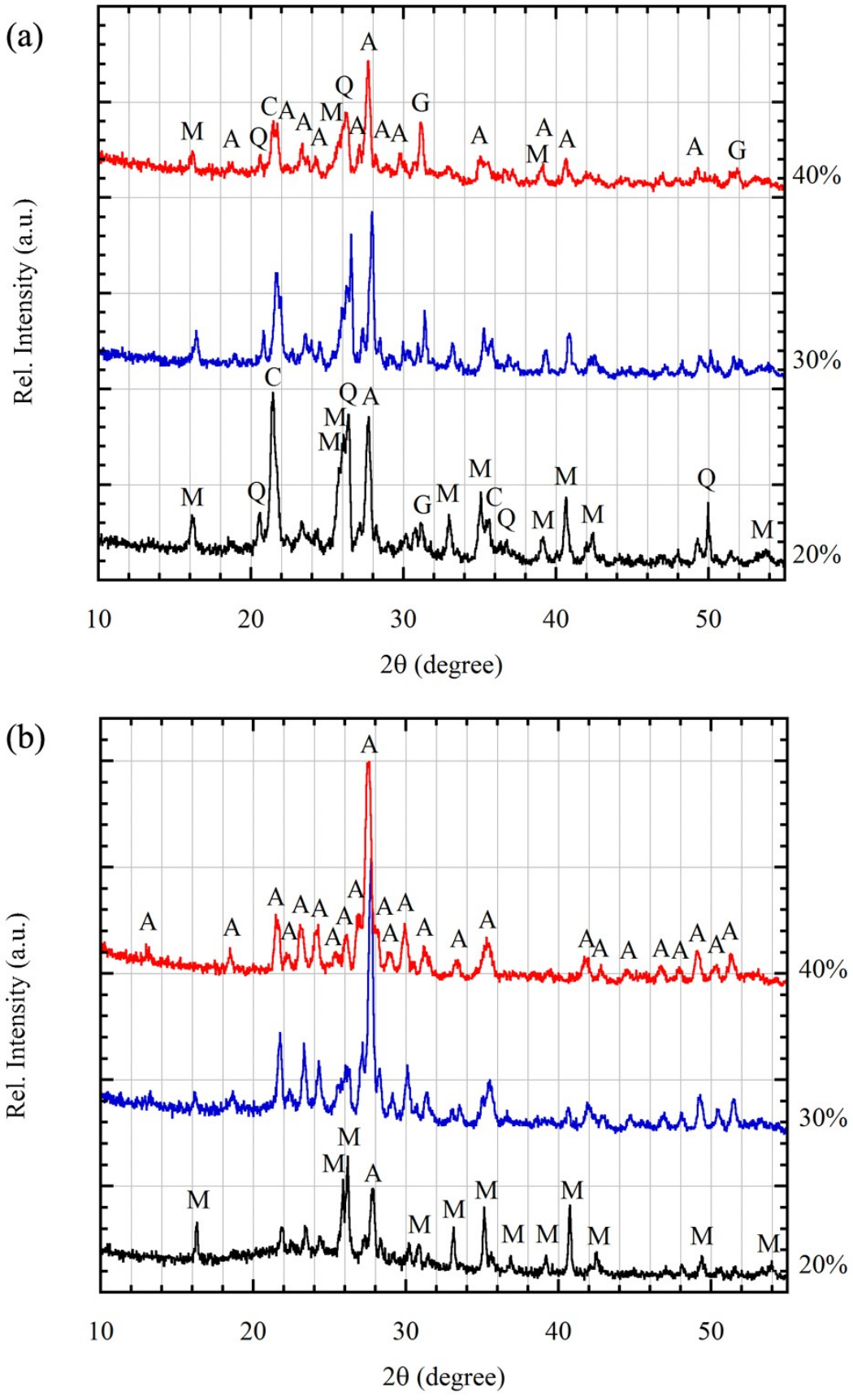

Figure 5.15. XRD patterns of the samples containing fireclay: (a) 1200°C, (b) 1400°C. Percentages indicate the amount of PPR addition to fireclay.

Microstructures of the samples having anorthite composition were investigated. As can be seen from SEM image of the sample with 30wt% PPR sintered at 1400°C in Figure 5.16a, large sized pores occurred in the body due to removal of fine cellulose fibers and calcium carbonate decomposition during firing. Randomly oriented tabular or plate-like crystals were observed in pores (Figure 5.16b), which are most possibly anorthite crystals.

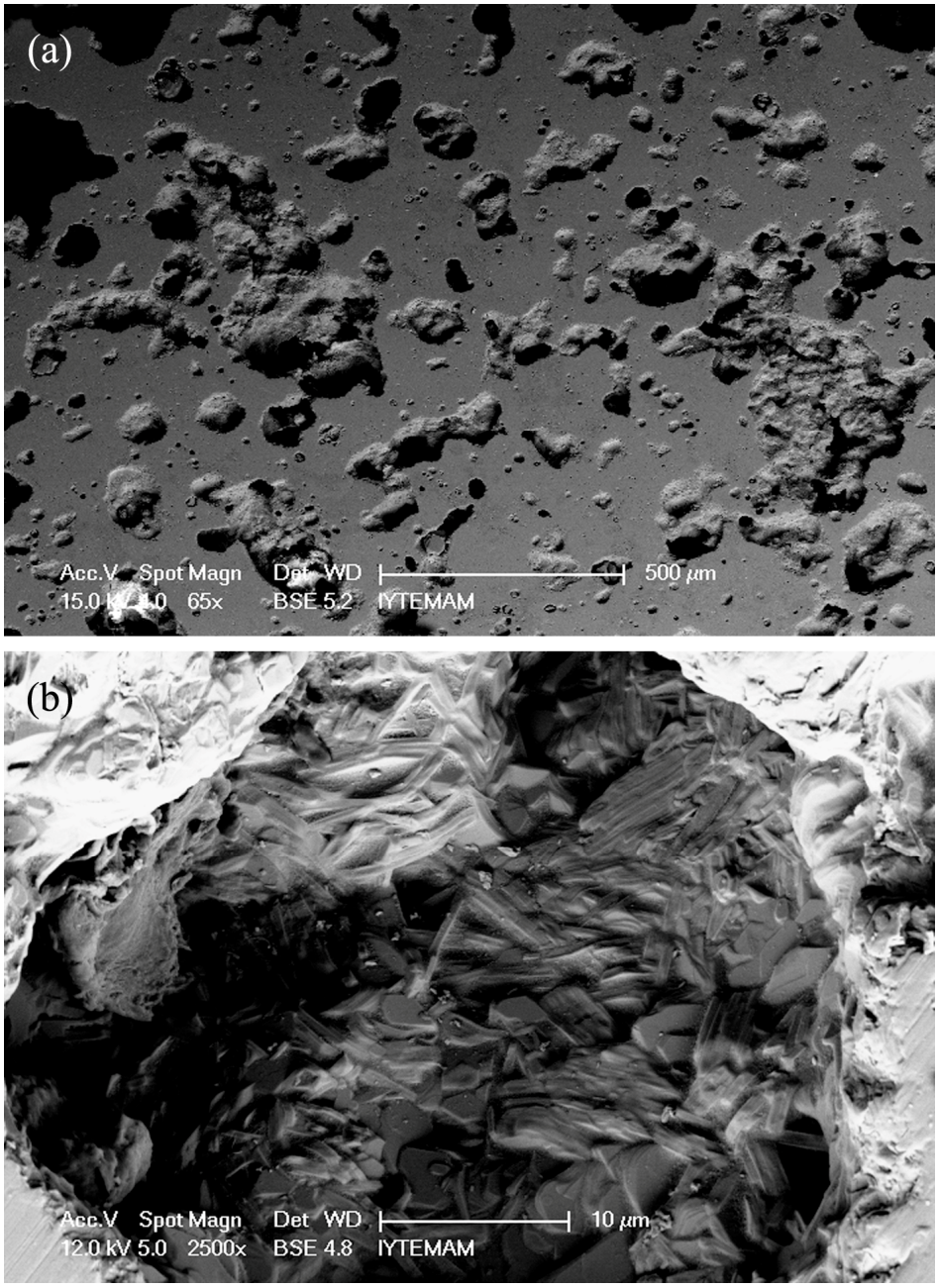

Figure 5.16. SEM images of the fireclay sample with 30wt% PPR fired at 1400°C: (a) thermal etched polished cross sectional surface, (b) tabular crystals in pores.

Because BSE (back scattered electron imaging mode) was used in imaging, brightness differences such as dark gray and lighter gray were observed in some regions of the specimen cross sectional surface (Figure 5.17). In Figure 5.17, SEM-EDS results of the sample with 30wt% PPR sintered at 1400°C indicated that light gray regions (Figure 5.17a) were anorthite and dark gray regions (Figure 5.17b) were mullite. While anorthite regions contained 28.9wt% Si, 19.6wt% Al and 12.4wt% Ca elements, mullite regions contained 27.6wt% Al and 27.3wt% Si. Since Si amount in both regions were partly higher, vitrification was observed. Their oxide analysis results were also given in Table 5.9. While mullite-rich regions have fine grained structure, anorthite-rich regions had coarse grained structure (Figure 5.18). SEM imaging after thermal etching of the polished surfaces revealed that the crystalline structures were embedded into the glassy matrix and were randomly oriented. Dimensions of anorthite grains were around 3×10 μm. Clusters of mullite grains were distributed throughout the polished cross section of sample with 30wt% PPR.

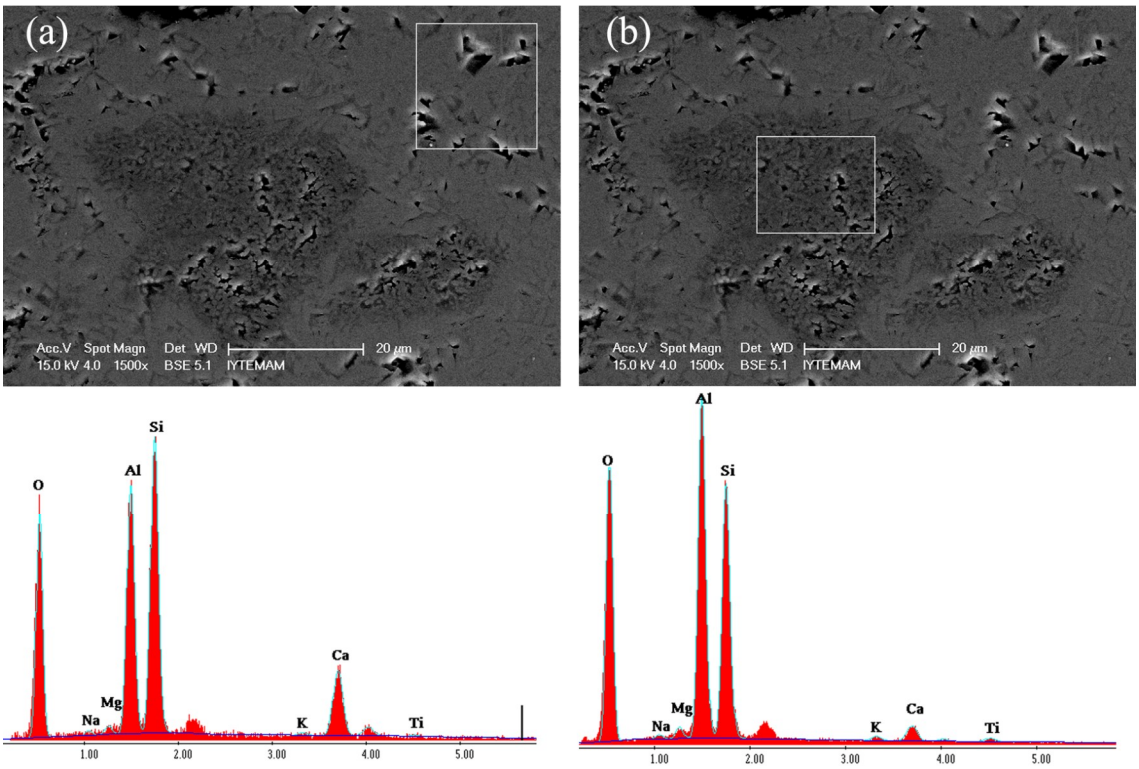

Figure 5.17. SEM-EDS results of the fireclay sample with 30wt% PPR fired at 1400°C: (a) light gray region, (b) dark gray region.

Table 5.9. The EDS oxide analysis results of the fireclay samples with different PPR additions fired 1400°C.

Oxides (wt%)	30wt% (in Figure 5.17)		40wt% (in Figure 5.19b)
	(a)	(b)	
Al_2O_3	31.02	43.12	33.92
SiO_2	51.86	48.29	45.59
CaO	14.58	3.58	17.36
K_2O	0.41	0.88	0.47
MgO	0.99	1.62	1.07
Na_2O	0.50	0.84	0.62
TiO_2	0.64	1.67	0.96

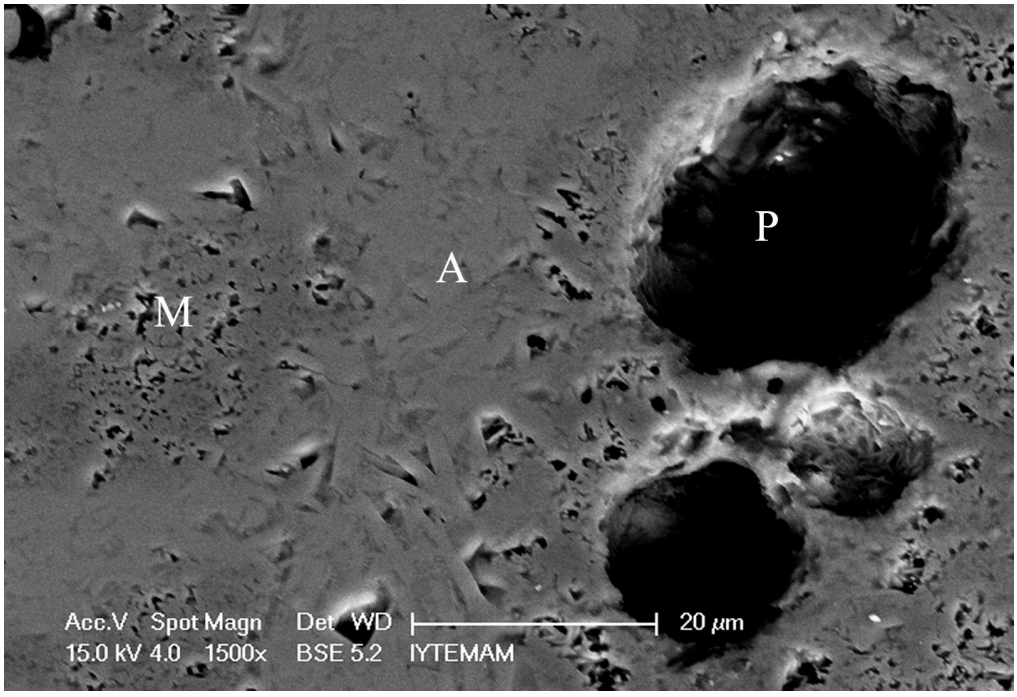

Figure 5.18. SEM image of polished, thermally etched surface of the fireclay sample with 30wt% PPR fired at 1400°C (A: anorthite region, M: mullite region, P: porosity).

Figure 5.19a shows the microstructure of thermally etched surface of the sample with 40wt% PPR sintered at 1400°C. Lengths of anorthite crystals (around 20 μm) were partially bigger in this sample with 40wt% PPR than that of samples with 30wt% PPR.

As can be observed from XRD results, this sample with 40wt% PPR included completely anorthite. Mullite was not observed. This was confirmed by SEM-EDS analysis (Figure 5.19b). According to the area that was analyzed, composition was an anorthite composition (23.4wt% Si, 19.7wt% Al, 13.7wt% Ca). The oxide analysis result is also given in Table 5.9. This result was almost similar with that of a commercial insulating firebrick (K23 type IFB, see Table 6.1) (Brosnan 2004).

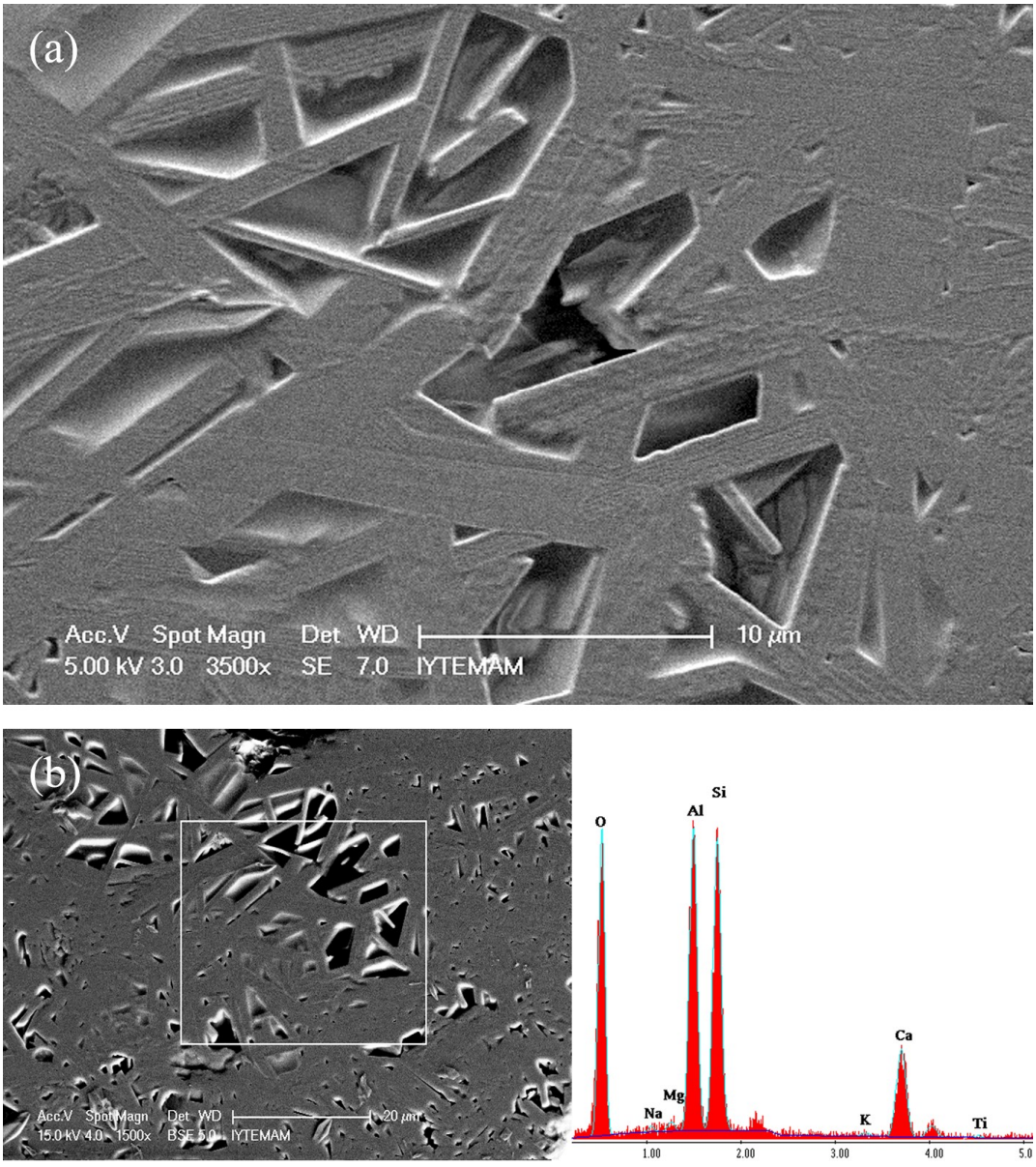

Figure 5.19. (a) Tabular anorthite crystals, and (b) SEM-EDS result of the sample with 40wt% PPR sintered at 1400°C.

Compressive strength measurements of the samples showed a large scatter due to a number of factors. Laminations may have occurred during dry pressing of the compacts. Different temperatures were used for firing these samples to obtain full anorthite composition, which may produce different state of densification, vitrification in samples. The sample with K244 clay (see Table 5.6) especially was partially vitrified after thermal treatment at 1250°C and was fully vitrified and deformed at 1300°C. The large K_2O content of this sample is a further factor to effect degree of vitrification and the mechanical behavior.

5.4. Conclusions

Production of porous anorthite ceramics from the mixtures of paper residue (PPR) with three different types of clays was successfully achieved. Suitability of three different clays such as aluminum silicate, clay with alkalis and fireclay in the manufacturing of anorthite based lightweight insulating firebricks was determined. Porous character to the ceramic was provided by addition of paper processing residues. All samples of mixtures with 30–40wt% PPR fired at 1200 to 1400°C contained anorthite as major phase and also minor secondary phases such as mullite or gehlenite phases in some mixtures. Laboratory grade enriched clay, when mixed with PPR, was able to produce anorthite at 1300°C in a porous ceramic form. Use of a commercial clay that is available in tonnage quantities produced anorthite at lower temperatures but with higher bulk densities. In these samples 1300°C was too high to produce a ceramic because of premature melting during firing. This was attributed to the presence of alkalis in the clay that fluxed the mixtures. Finally, a higher firing temperature of 1400°C was needed for the fireclay samples to produce anorthite in a porous ceramic form. Gehlenite phase formed mostly at lower temperatures and in samples containing higher calcium content (50wt% PPR). Compressive strengths of the samples ranged from 8 to 43 MPa. Upon completion of this study porous thermally insulating anorthite ceramics were successfully produced. More work needed to be done to further advance this study to produce larger and more porous ceramic pieces for thermal conductivity tests.

CHAPTER 6

PRODUCTION OF ANORTHITE INSULATING FIREBRICKS FROM MIXTURES OF CLAY AND RECYCLED PAPER WASTE WITH SAWDUST ADDITION

6.1. Introduction

Anorthite based insulating firebricks constitute one of the refractory groups which are the most frequently used for heat insulation in industrial applications today (Thermal Ceramics 2009). Insulating firebricks are porous and lightweight refractories having much lower thermal conductivity and heat capacity than other refractories. They are the most suitable materials used for lining of industrial furnaces with the aim of reducing heat losses. They are classified according to the bulk density and maximum service temperature (ASTM C155-97 2002). According to this, the ASTM 20 and 23 groups with high CaO content represent the anorthite ($CaO{\cdot}Al_2O_3{\cdot}2SiO_2$) based insulating firebricks with maximum temperature limits of 1093 and 1260°C, respectively.

Different types of insulating firebricks are produced by using the raw materials such as diatomite, perlite, expanded vermiculite, calcium silicate, fireclay, kaolin, quartz and hallow sphere alumina (Yurkov and Aksel'rod 2005). Insulating firebricks have high porosity between 45 and 90%. Their maximum pore diameters are smaller than 1 mm. High porosity causes low thermal conductivity and mechanical strength. The thermal conductivity not only depends on their total porosity, but also their pore size and shape, chemical and mineralogical composition. The porosity is normally formed by adding combustible material to the raw material mixture. Pore forming agents such as sawdust, foam polystyrene, fine coke, binders and organic foams, or granular materials such as hollow micro-spheres and bubble alumina are widely used to obtain decreased density or to create porosity in insulating firebricks (Dergaputskaya, et al. 1980, Horie 1981, Koronthalyova 2007, Kryuchkov, et al. 1999, Pirogov, et al. 1970,

Suvorov and Skurikhin 2003, Yurkov and Aksel'rod 2005). During firing, the sawdust burns out, and leaves a large fraction of interconnected pores within the fired body.

Anorthite lightweight insulating firebrick mixtures are generally made of kaolin clay, sawdust and gypsum ($CaSO_4 \cdot 2H_2O$) binder (Brosnan 2004, Dergaputskaya, et al. 1980). The mixture hardens after forming and is fired. A porous ceramic is produced with combustion of the sawdust. However, an important problem of this method is environmentally the release of sulfur compounds from gypsum, which is highly undesirable. Therefore, the use of recycled paper processing wastes as calcium oxide source and a pore forming material could be environmentally more convenient for production of anorthite based insulating firebricks.

In the early works, some researchers developed the anorthite lightweight refractories. Pirogov et al. (Pirogov, et al. 1970) reported the manufacture of anorthite insulating refractory with density of 0.4 g/cm^3 using kaolin, gypsum and perlite foam for service at 1100–1260°C. Authors (Pirogov, et al. 1972) also characterized the heat-insulating refractories produced by some foreign companies; they showed that the main constituent mineral of an insulating product is finely crystalline anorthite. Anorthite lightweight artifacts with density of 0.5–0.65 g/cm^3 were developed from kaolin and gypsum slurry mixtures with added sawdust and polystyrene for service up to 1300°C (Dergaputskaya, et al. 1980). The refractory mixtures containing perlite and finely pulverized porcelain scrap with added glue-colophony paste fired at 1400°C had apparent density between 0.35–0.7 g/cm^3 and exhibited the thermal conductivities between 0.20 and 0.32 W/mK and the strengths between 1 and 9 MPa (Kryuchkov, et al. 1999). Researchers (Kryuchkov, et al. 1999) found that the increase in the size of perlite grains leads to significantly increase the properties of products.

Recently, there has been considerable research on the use of wastes in the ceramic materials. Many industrial wastes are intensively used as a new source of raw material or pore-forming agents in the production of ceramic materials. Many silicate based wastes such as coal and fly ash, slag from steel production, hydrometallurgical mud, and different types of industrial sludge are proper materials for using in the ceramics due to their chemical and mineralogical contents (Aloisi, et al. 2004, Dondi 1997, Ducman 2007, Junge 2000, Montero 2009, Rawlings, et al. 2006). In the last decades, wastes from pulp and paper industry have been used in the ceramic materials, too (Ahmadi and Al-Khaja 2001, Brosnan 2003, Dasgupta and Das 2002, Demir, et al. 2005, Sutcu and Akkurt 2009, Sutcu and Akkurt 2010). Dasgupta and Das produced a

porous ceramic composite consisting of cordierite, mullite and cristobalite phases from mixtures of clay and paper pulp ash containing MgO by reaction sintering at 1400°C (Dasgupta and Das 2002, Sutcu and Akkurt 2009). The product with 50% porosity indicated a good mechanical (modulus of rupture, MOR of 4 MPa) and thermal resistance (up to 20 cycles). A patent was also reported on how to produce low density ceramics from paper recycling residuals (Brosnan 2003). This invention describes that produced ceramics can be used for high temperature applications as insulating materials and filtration devices between 1000 and 1600°C. However, in this invention, the intervals of parameters for producing ceramics are not sufficiently defined.

In this study, porous anorthite insulating firebricks were developed by adding the recycled paper processing wastes as a source of calcium oxide and pore-making agent to two different types of clay. The addition of recycled paper waste as source of CaO into a clay system closely located to anorthite composition in calcia–alumina–silica ternary system. Also, this waste supplied a finely micro-porous structure into the fired bodies due to their cellulose fibers and carbonates. In addition, the use of additional sawdust helped to increase the amount of porosity in the bricks.

6.2. Experimental Procedure

Initially, a commercial insulating firebrick (Thermal Ceramics, a division of the Morgan Crucible Company, UK) was investigated to define its mineral and microstructural properties before the experimental studies began. This commercial firebrick was found to have anorthite composition. When anorthite phase was observed in the earthenware bricks produced in Chapter 4, the processes in Chapters 5 and 6 were inspired.

In this study, production of anorthite based insulating firebrick was carried out from mixtures of two different clays, recycled paper processing waste and sawdust. Commercial K244 clay (Kalemaden, Turkey) and ground fireclay (chamotte-125, Esan, Turkey) were used as the alumina and silica source, while recycled paper waste (Levent Kağıt, Turkey) was used as a source of calcium oxide to achieve anorthite ($CaO \cdot Al_2O_3 \cdot 2SiO_2$) synthesis. This waste was also capable of producing porosity due to its cellulose fiber and calcium carbonate content. The waste was in sludge form and contained around 65% water. Chemical, mineralogical, thermal and microstructural

properties of the paper waste and the clays to be used in this study were previously reported (Chapters 3 and 5).

Rectangular samples (20 mm × 60 mm × 150 mm) were formed by a slurry casting method. In order to create additional porosity in the samples, wooden sawdust (<1–5 mm sizes) was used as burnout additive as well as the paper waste containing pore formers like cellulose fiber and calcium carbonate. The mixtures containing clay and 30wt% paper waste (on dry basis) that supplied the strongest anorthite composition (Sutcu and Akkurt 2009, Sutcu and Akkurt 2010) were prepared for production of the samples. The paper waste was dispersed into water and was mixed with the selected clay. Then, the sawdust (10%, 20% and 30% by weight) was added into these mixtures at certain ratios of the total mixtures. Water addition was made into the mixtures to decrease viscosity of the sludge to compensate for the reduction in flow after sawdust addition. Total water content of mixtures varied from 55 to 66% depending on amount of sawdust. The slurry mixtures for casting that had a consistency of a thick cream, were prepared in a mechanical mixer and were mixed for 30 minutes (Heidolph RZR-2020). Viscosities of the slurries were measured by a Brookfield Viscometer (DV II+Pro) to range from 0.7 to 2.5 Pa.s at 50 rpm of rotational speed of the spindle. The slurry mixtures were cast into hardboard molds (80 mm × 160 mm) placed onto plaster plates. The plaster suctioned excess water by capillary. In the meantime, top surface of the slurry was lightly compressed by hand in order to ensure complete filling of the mold. Green samples were removed from the mold after 1–2 h and were left to dry in ambient conditions for 24–72 h. Cellulose fibers in the paper sludge helped to improve the strength of the green samples. Samples were further dried in an oven maintained at 50°C for 12 h and then at 100°C for 24 h. Figure 6.1 shows a dried and unfired sample containing fireclay and paper waste with 30wt% sawdust.

Figure 6.1. A dried and unfired sample containing fireclay and paper waste with 30wt% sawdust addition.

According to the type of clay used, dry samples were fired either at 1200°C (for K244 clay) or at 1300°C (for fireclay) for 1 h in a laboratory-type electrical kiln. The heating rate was 2.5°C/min until 600°C, and 10°C/min until the dwell temperatures. Firing temperatures used in this study (1200 and 1300°C) were 100°C lower than those predicted in a previous study (Chapter 5). This was because the sawdust addition was expected to supply additional heat to the sample during firing and hence samples may warp due to premature melting. Pure anorthite melts congruently at 1553°C, according to the $CaO–Al_2O_3–SiO_2$ phase system although this may be lowered due to impurities present in the raw materials.

The crystalline phases in the fired samples were investigated by using X-ray diffraction (XRD) with CuK_α radiation (λ=1.542 Å) at 40 kV in the 2θ intervals of 10–55°. Microstructural analysis of the polished surfaces was performed by using scanning electron microscope (SEM) and energy dispersive X-ray analysis (EDS) (Philips XL-30SFEG and EDAX).

Dimensions of the samples after firing were measured by a caliper, and their bulk densities were calculated by according to ASTM C134 (ASTM Standard C134-95 2005). Samples taken from firebricks were also measured by ASTM C20 test method. Bulk density, apparent specific gravity and apparent porosity measurements of the samples were performed by boiling water immersion for 2 hours and soaking in water for 24 hours.

Small sized samples (8 mm × 8 mm × 16 mm) were cut from the larger fired samples to be used for dilatometric test. Coefficient of thermal expansion (CTE) and percent linear change of the samples were measured by a horizontal dilatometer (Linseis, Germany). Also, the CTE values of the samples were linearly calculated from slope of shrinkage ($\Delta L/L_0$) versus temperature (T).

Thermal conductivity measurements were employed on 20 mm × 60 mm × 150 mm sized samples at room temperature by hot wire method using Quick Thermal Conductivity Meter (QTM500 Kyoto Electronics). The measuring principles are given in section 2.9.2.

A mechanical test was applied to determine the cold modulus of rupture (cold MOR) of the fired samples, which is a method for determining the room temperature flexural strength in three-point bending. According to ASTM C133-97 standard, the preferred test specimens should be 228 mm × 114 mm × 64 mm or 76 mm bricks or specimens of equivalent size ground or cut from refractory shapes (ASTM C133-97 2003). In this study, these brick sizes were impossible in the laboratory so alternative specimen sizes of 45 mm × 22.5 mm × 15mm were prepared by cutting 5 times smaller samples from the larger fired samples. For testing, a mechanical test machine (Shimadzu AGS-J 5kN) with three-point bending apparatus was used. Span (L) interval is 35 mm. Strain rate was selected as 1 mm/min. The modulus of rupture was calculated using equation following:

$$MOR = 3PL/2bd^2 \tag{6.1}$$

Where:

MOR is the modulus of rupture (MPa),

P is the maximum applied at rupture (N),

L is the span between supports (mm),

b is the breadth or width of specimen (mm),

d is the depth of specimen (mm).

Thermal shock tests were performed on samples to find out their resistance to repeated heating and cooling cycles by heating to 1200°C and cooling to room temperature in five cycles (ASTM C1171-96 2003).

6.3. Results and Discussion

Initially, the properties of a commercial insulating firebrick (Thermal Ceramics, a division of the Morgan Crucible Company, UK) were investigated by SEM and XRD. Then, the production of anorthite based insulating firebricks was carried out from mixtures of two different clays, recycled paper processing waste and sawdust. The results are given below.

6.3.1. Characterization of A Commercial Insulating Firebrick

A commercial insulating firebrick (Thermal Ceramics, a division of the Morgan Crucible Company, UK) was firstly analyzed using XRD, SEM and SEM-EDS for its mineralogical and microstructural properties.

Information on some commercial insulating firebricks is given in Table 6.1. Anorthite lightweight products are generally used for service at 1260°C and 1371°C. K25 product (1371°C) resists to a high temperature due to its high alumina content. Their densities are around 0.5–0.7 g/cm^3. As can be seen from the $CaO–Al_2O_3–SiO_2$ system (see Figure 2.2), these products had anorthite ($CaO·Al_2O_3·2SiO_2$) phase composition.

While their thermal conductivities vary between 0.13 and 0.17 W/mK at room temperature, increase up to 0.3 W/mK at high temperatures. The highest thermal conductivity is exhibited by products made on the basis of the higher densities or large pores. While the large pores in the firebricks increase the convective heat transfer at low temperatures, the increased size of the pores leads to increased radiation heat transfer at high temperatures. Both factors decrease the heat insulating efficiency (Kryuchkov, et al. 1999).

Table 6.1. Properties of some commercial insulating firebricks.
(Source: Brosnan 2004, Thermal Ceramics 2009)

Physical properties	TC23	TC23HS	K23	IFB 23	K25
Use limit (°C)	1260	1260	1260	1260	1371
Density (g/cm^3)	0.6-0.7	0.64	0.5-0.53	0.59	0.6-0.64
Melting temp. (°C)	1510	1510	1510	1510	1538
Modulus of rupture (MPa)	0.7-1.0	1.0	0.79	0.72	0.83
Cold crushing strength (MPa)	0.97-1.52	1.4	0.9	0.86	1.21
Permanent linear change (%) @1230°C	-0.1 to -0.4	0.0	0.0	0.0	-
Coefficient of thermal expansion	$5.4x10^{-6}$	-	$5.4x10^{-6}$	-	$5.6x10^{-6}$
Chemical analysis (%)					
Al_2O_3	39-43	38.8	38.3	38.8	45
SiO_2	43-45	47.8	44.3	47.8	38
CaO	10-12	10.9	15	10.9	14.5
Fe_2O_3	0.5	0.4	0.3	0.4	0.2
TiO_2	1.5-1.9	1.6	1.6	1.6	1.6
MgO	0.2	0.2	0.1	0.2	0.2
Alkalis (Na_2O, K_2O)	0.4-0.7	0.3	0.4	0.3	0.5
Thermal conductivity (W/mK)					
@260°C	0.17	0.17	0.13	0.14	0.16
@538°C	0.20	0.22	0.17	0.18	0.18
@815°C	0.25	0.25	0.21	0.23	0.21
@1093°C	0.27	0.29	0.25	0.25	0.24

X-ray diffraction (XRD) analysis of the commercial insulating firebrick is given in Figure 6.2. XRD analysis of ground powder sample indicated that this product had extensively anorthite ($CaO{\cdot}Al_2O_3{\cdot}2SiO_2$) phase and minor mullite ($3Al_2O_3{\cdot}2SiO_2$) phase with the ratio of peak intensities ~8:1.

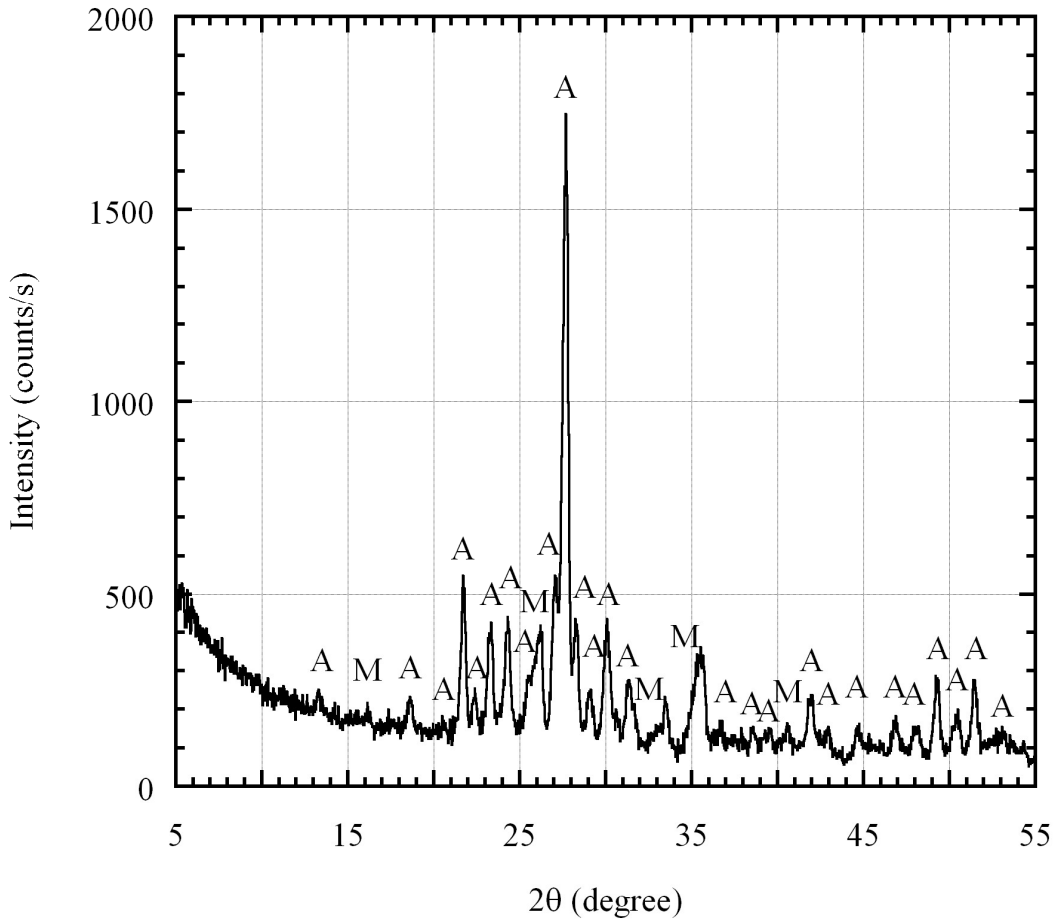

Figure 6.2. X-ray diffraction pattern of the commercial insulating firebrick (A: anorthite (86-1705), M: mullite (83-1881)).

The SEM images of the commercial insulating firebrick are shown in Figure 6.3(a) and (b). It has large sized pores with size of 500 μm along with a micro-porous structure. Microstructures indicated that large pores originating most likely from the removal of burnout additives. Some larger pores had a spherical form. Probably, it could be due to using spherical shaped pore-former such as polystyrene or by gas entrapment method. Fine crystallites embedded in the matrix structure were clearly observed.

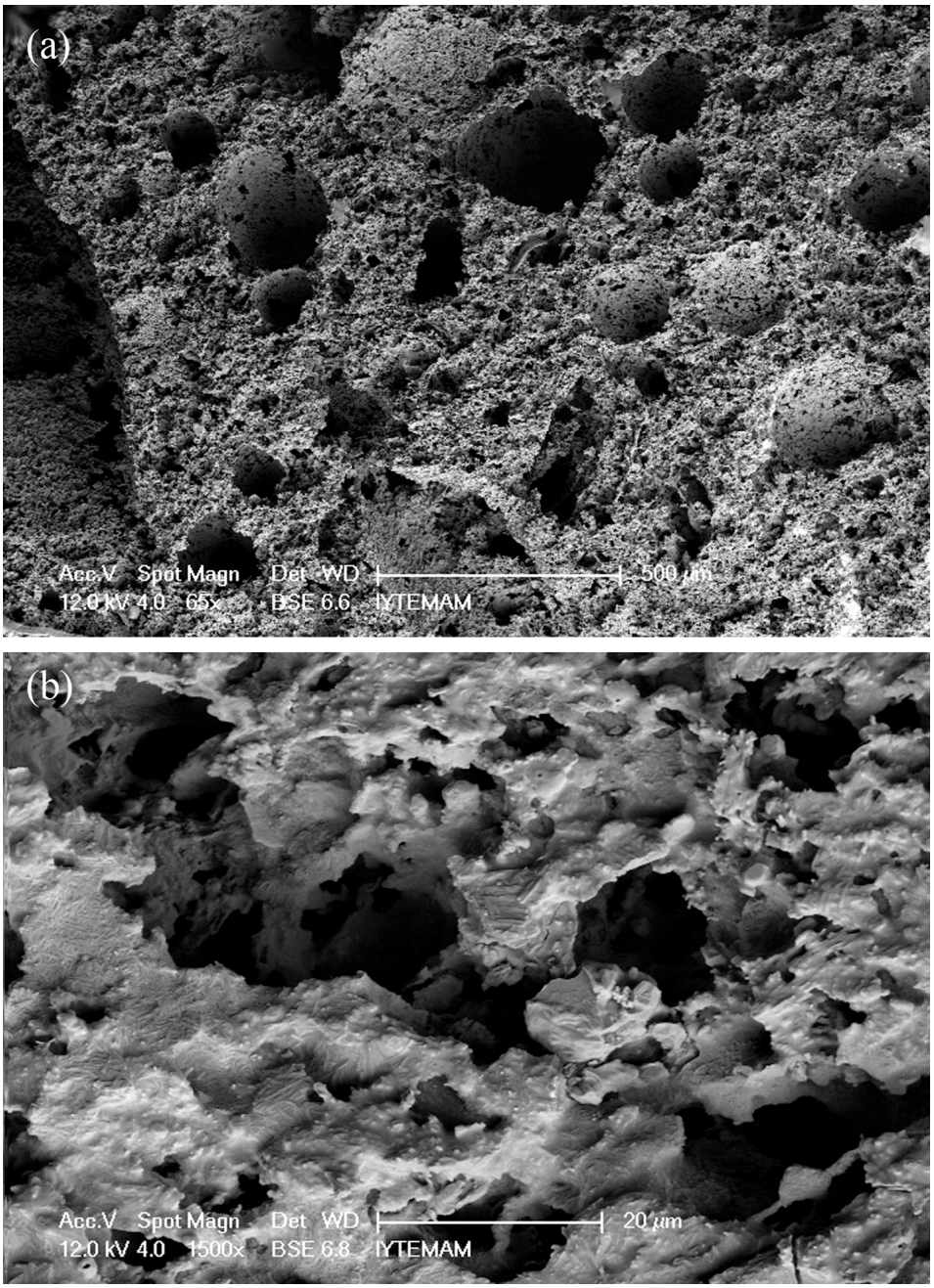

Figure 6.3. (a) General aspect of the commercial insulating firebrick with porous structure, and (b) microstructure of fine crystallites in the matrix of the insulating firebrick.

SEM-EDS elemental analysis of the insulating firebrick was performed on a wide area as seen from Figure 6.4. The oxide analysis results in 35.6% Al_2O_3, 47.8% SiO_2 and 16.5% CaO. This result obviously revealed that the material has anorthite composition.

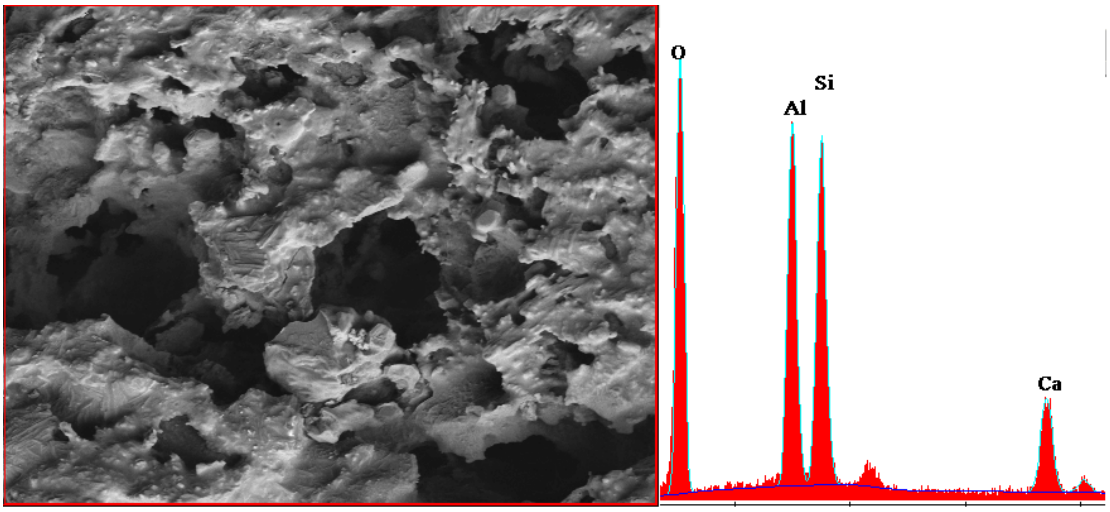

Figure 6.4. SEM-EDS analysis result of the commercial insulating firebrick.

6.3.2. Characterization of Raw Materials and Slurry Mixtures

The recycled paper waste was obtained from a local paper manufacturer (Levent Kağıt A.Ş.) that produced paper from recycled paper. The waste had about 65% moisture content. Solid part of this waste contains about 40% organic matter (cellulose fiber) and 60% inorganic components like calcite and other clayey materials. Thermal properties of the clays and paper residues were investigated in previous chapters (Chapters 3 and 5).

Fireclay was selected as the clay raw material for high refractoriness of the products. Its chemical composition consisted of 59% SiO_2, 38.5% Al_2O_3, 1.1% TiO_2, 0.5% Fe_2O_3, 0.4% K_2O, 0.1% CaO, 0.1% MgO and 0.05% Na_2O. Its mineralogical composition showed the presence of quartz (SiO_2), mullite ($3Al_2O_3 \cdot 2SiO_2$) and cristobalite (high-temperature form of SiO_2) phases. K244 clay included 59.1% SiO_2, 26.9% Al_2O_3, 0.8% TiO_2, 1.5% Fe_2O_3, 2.2% K_2O, 0.3% CaO, 0.6% MgO and 0.04% Na_2O. Mineral content of K244 clay was mainly quartz and kaolinite ($Al_2Si_2O_5(OH)_4$) with some illite ($2K_2O \cdot 3MgO \cdot Al_2O_3 \cdot 24SiO_2 \cdot 12H_2O$). Microstructural analysis of paper waste and clays (K244 and chamotte) were determined in Chapter 3 and 5, respectively. The SEM images at different magnifications of wood sawdust additive are shown in Figure 6.5. Sizes of the sawdust were between 0.5 and 1 mm.

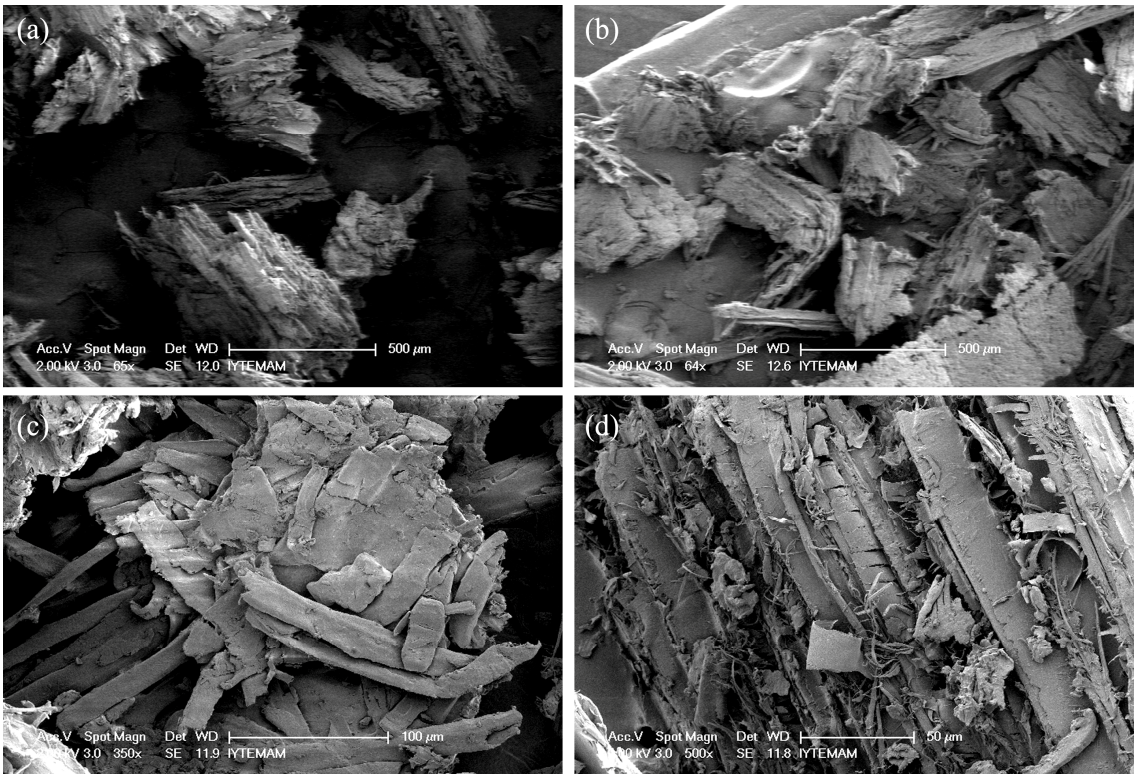

Figure 6.5. The SEM images of wood sawdust additives.

The main components of wood sawdust are hemicellulose, cellulose, and lignin, and these components are decomposed at different temperature ranges; hemicellulose, cellulose, and lignin are decomposed at 150–300°C, 275–300°C, and 250–500°C, respectively (Kalita 2009). Thermo-gravimetric (TGA and differential TGA) analysis curves of the sawdust at a heating rate of 10°C/min are shown in Figure 6.6. From this figure it is observed that the maximum moisture removal takes place at about 85°C. The moisture loss (about 5%) took place up to 150°C followed by pyrolysis. Then the major weight loss (about 65%) is due to the fast decomposition of hemicellulose and cellulose at 180–350°C. After rapid pyrolysis, relatively slow pyrolysis occurred over 350°C, and the second weight loss (about 30%) caused by the lignin decomposition.

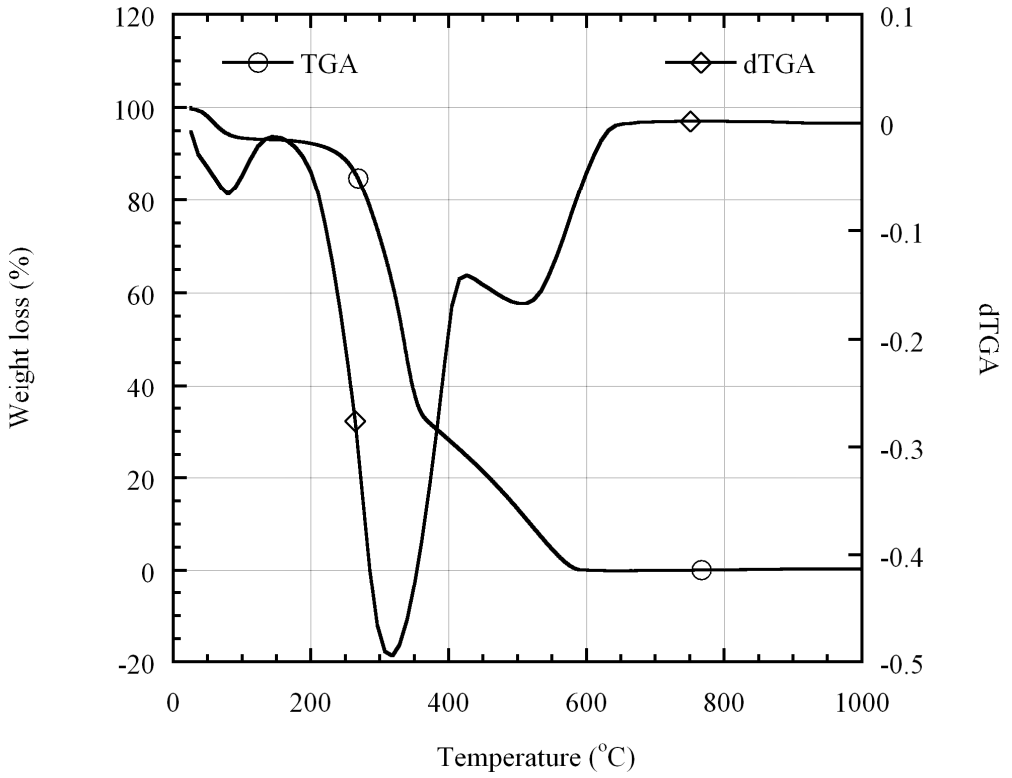

Figure 6.6. Thermo-gravimetric analysis of sawdust.

Figure 6.7(a) and (b) shows the viscosity as a function of rotational speed of the spindle for the slurries containing fireclay and K244 clay with paper waste at different sawdust additions, respectively. As it can be seen in the figures, shear thinning behavior was observed for the slurries containing either fireclay or K244 clay, such that viscosity is reducing with the increase of rotational speed of the spindle. The viscosity of the slurries containing K244 clay is relatively higher than that of the slurries containing fireclay. This is related with their particle size and surface area, and also type of the clays. The particle size of K244 clay (<5 μm) is lower than that of the fireclay (<45 μm).

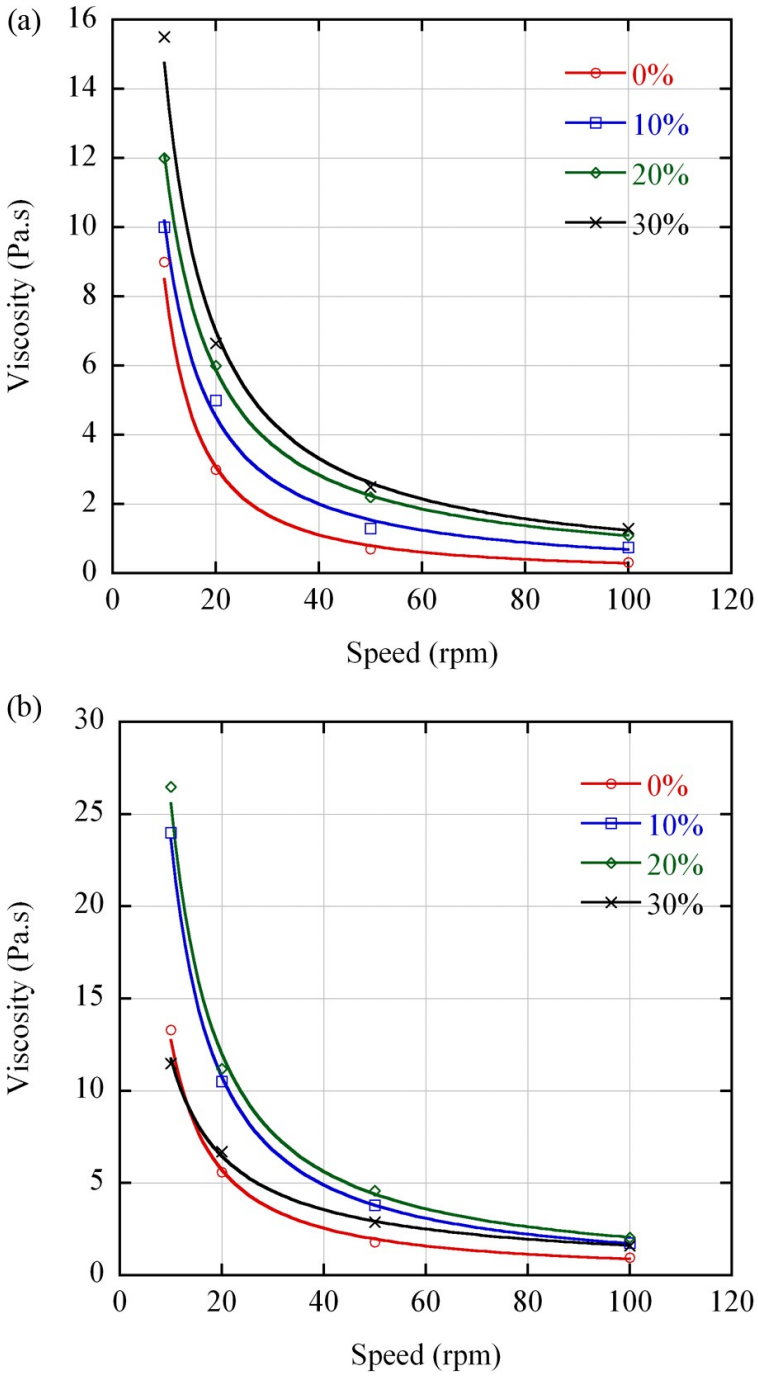

Figure 6.7. Viscosity of the slurry mixtures containing (a) fireclay and (b) K244 clay with sawdust addition as a function of rotational speed of the spindle.

6.3.3. Fired Samples Containing K244 Clay and Paper Waste Mixture with Sawdust Addition

In the previous study (Chapter 5), detailed XRD analysis of the samples were given for samples containing K244 clay and 30wt% paper waste mixture that were fired

at different temperatures. Mainly anorthite phase and a minor amount of quartz were observed in the samples fired at 1200°C. Quartz was completely dissolved with increasing temperature to 1250 and 1300°C, and the final composition was fully anorthite. However, the K244 samples showed higher vitrification behavior (premature melting) due to the alkali content of the clay. Therefore, in the current study, the samples with sawdust addition were only fired at 1200°C, since they showed vitrification at temperatures above 1200°C. Sawdust addition provides extra heat to the kiln due to the burning of the wood at temperatures between 200 and 600°C. Alkali content (especially potassium oxide) caused warping in the samples with increasing firing temperatures. Therefore, ideal firing temperature for samples with K244 clay was defined as 1200°C. The samples prepared from mixtures containing K244 clay and paper waste with sawdust addition (up to 30% by weight) fired at 1200°C are shown in Figure 6.8.

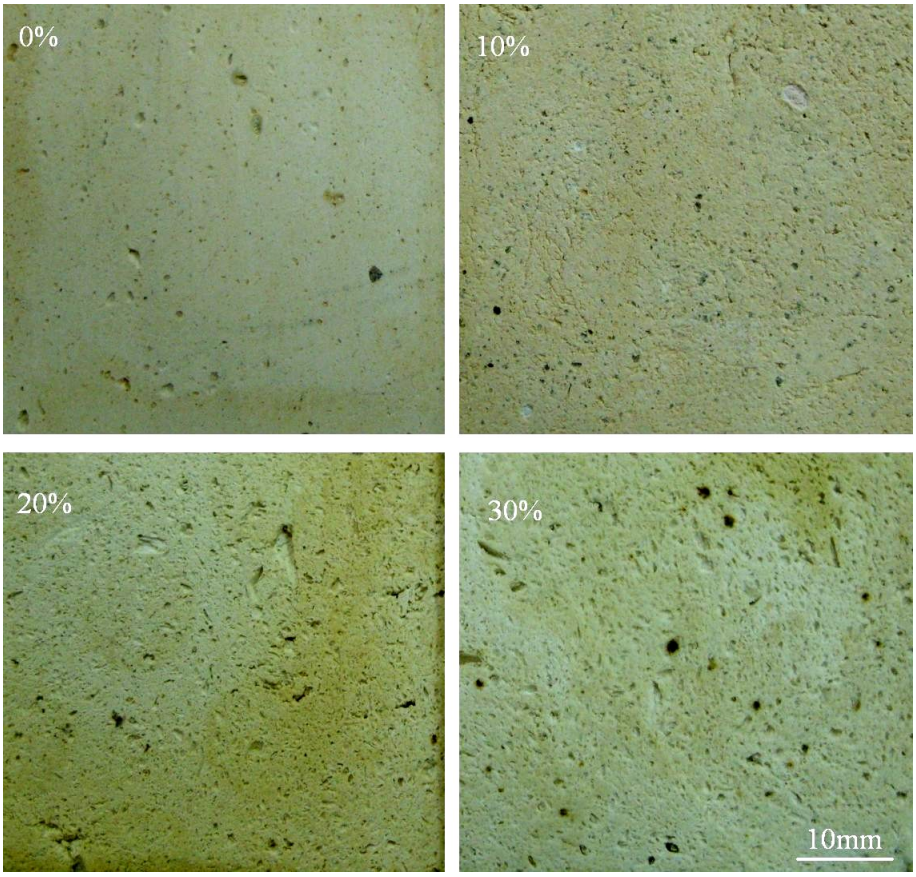

Figure 6.8. Anorthite samples containing K244 clay and paper waste according to the percentage of sawdust additive.

In this study, X-ray diffraction analyses of the samples fired at 1200°C were performed for determining the phases present. XRD results of the fired samples containing the mixture of K244 clay, 30wt% paper waste and 0–30% sawdust additions showed that anorthite could be successfully produced with some quartz-alpha phase (Figure 6.9). Observed crystalline phases are labeled as A: anorthite (reference number: 86–1705) and Q: quartz (reference number: 85–0335). These samples may not be suitable for use in the kilns for insulation due to their quartz content which can cause cracks upon heating and cooling cycles.

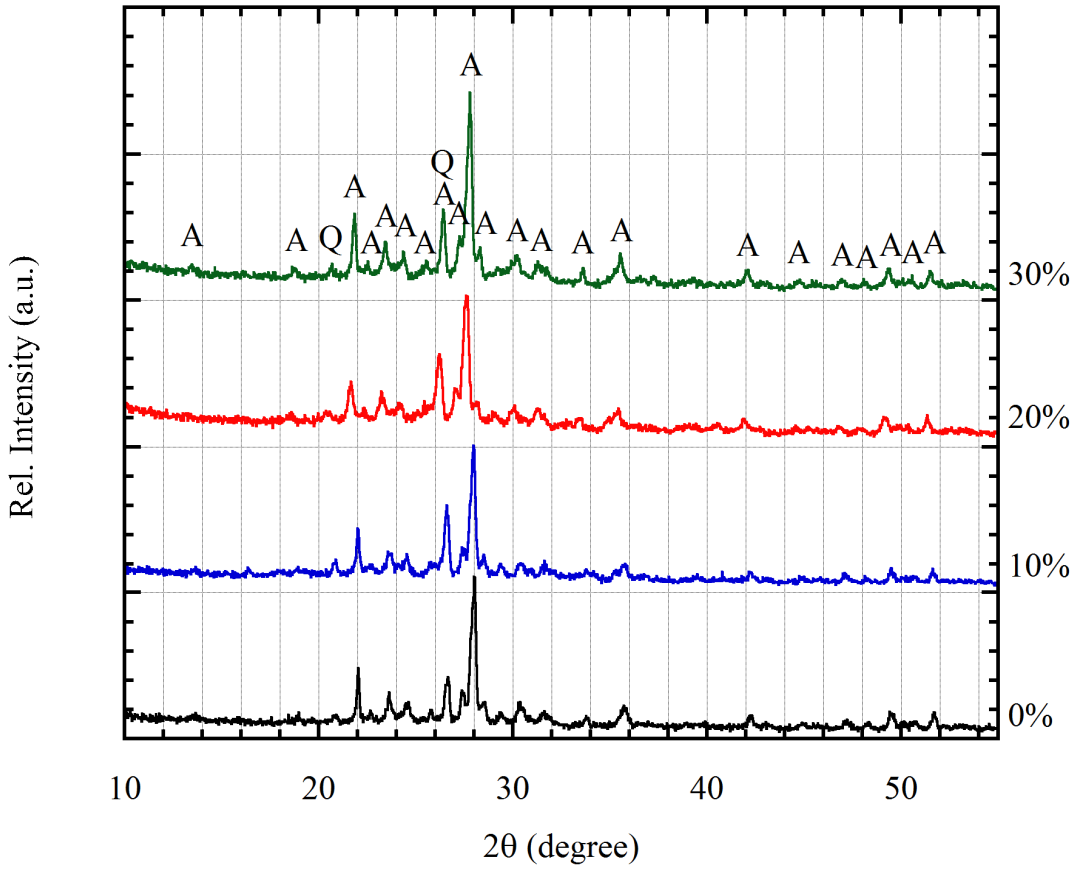

Figure 6.9. XRD patterns of the fired samples containing mixtures of K244 clay and paper waste with sawdust additive.

Experimental results of the samples containing K244 clay and 30wt% paper waste mixture with sawdust additive are given in Table 6.2. Their thermal conductivity and bulk densities values were reduced with increasing sawdust addition. Thermal conductivity and bulk density of the product with 0% and 30% sawdust showed a reduction of 49% and 33%, respectively, after firing at 1200°C. In other words, thermal

conductivities of the samples were reduced with decreasing bulk densities. The lowest bulk density and thermal conductivity values of 0.87 g/cm^3 and 0.20 W/mK, respectively, were achieved in samples with 30wt% sawdust that were fired at 1200°C. Their density values were lower than that of samples without sawdust addition (Sutcu and Akkurt 2010). The apparent porosity values of fired samples ranged from 48 to 58% with sawdust addition.

Table 6.2. Test results of the anorthite samples containing K244 clay and paper waste with sawdust addition fired at 1200°C.

Physical properties	Mass ratio of sawdust addition			
	0%	10%	20%	30%
Bulk density (g/cm^3) ASTM C134	1.30±0.02	1.09±0.02	0.93±0.03	0.87±0.06
Apparent porosity (%) ASTM C20	48.2±0.5	55.5±0.5	57.0±1.0	57.5±0.5
Thermal conductivity (W/mK) at room temperature	0.39±0.01	0.30±0.01	0.23±0.01	0.20±0.01
Cold modulus of rupture (MPa)	15.3±1.2	7.04±0.8	4.97±0.5	4.49±0.5

The linear and volumetric firing shrinkages were about 4.5 and 12.5%, respectively. The samples without sawdust addition fired at 1250 and 1300°C had a warped shape due to vitrification. Their test results are given in Figure 6.10. Their densities and thermal conductivities increased with rising of firing temperature. Experience with K244 clay indicated that alkalis (especially K_2O content) along with other impurities were mainly responsible for premature vitrification at lower than expected temperatures. The impurities originated from K244 clay. In general, insulating firebricks are susceptible to alkali attack by surface glazing or expansion reaction (Brosnan 2004). Maximum operation temperature for materials containing K244 clay should not exceed 1200°C.

Modulus of rupture (MOR) results of the samples with sawdust addition is given in Table 6.2. Depending on the increase in the sawdust addition and porosity content, cold modulus of rupture of the samples progressively decreased from 15.3 to 4.49 MPa, since the bridges between the pores become thinner (Kryuchkov, et al. 1999). In

literature, the MOR values measured for commercial anorthite based insulating firebricks (<1.60 g/cm^3 or >45% porosity) are between 0.72 and 1.0 MPa (Thermal Ceramics 2009). The MOR values of samples were quite higher than that of the ASTM 20 and 23 groups-insulating firebricks. This case is possibly due to their vitrified structures. The kaolin content in clay raw material improves the strength of the products, however causes to increase shrinkage of the material, leading to product deformation.

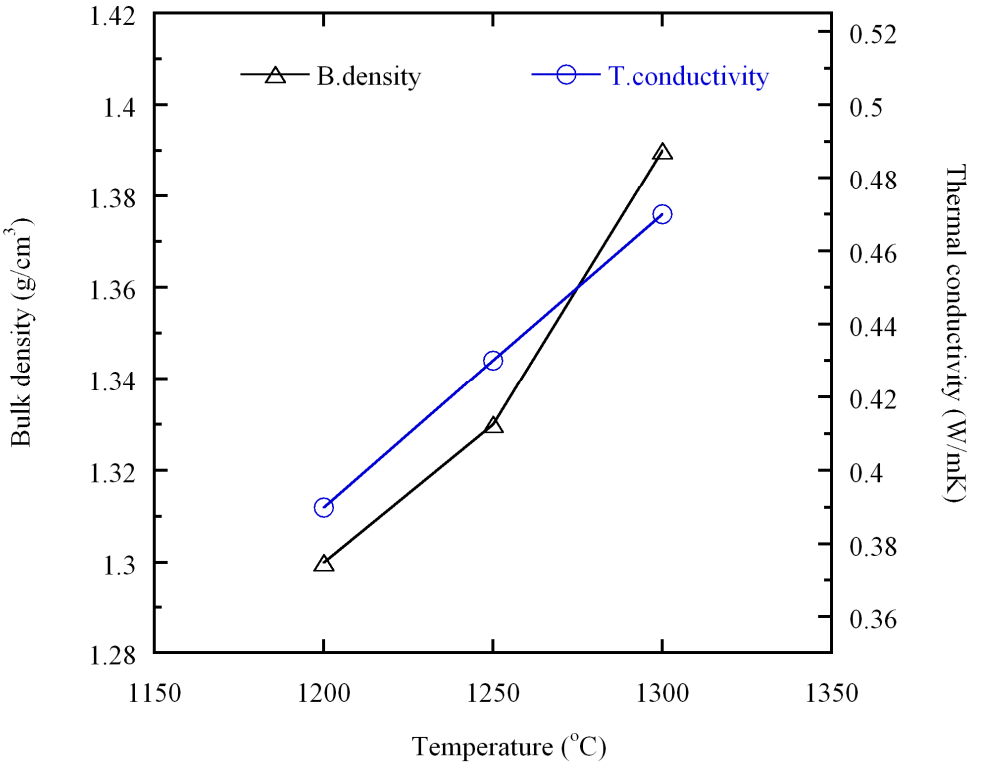

Figure 6.10. The test results of fired samples containing K244 clay and paper waste without sawdust at different temperatures.

Thermal dilatometer analysis was performed on the fired samples containing K244 clay to measure the coefficients of thermal expansion. Percent linear changes of the fired porous samples are shown in Figure 6.11. Sample without sawdust began to shrink after about 1125°C, while other samples shrank sooner (1000–1100°C) depending on the amount of sawdust addition. Total thermal expansion of the samples up to 1100°C was around 0.6%. Final reheat shrinkages for the samples were below a standard limiting value of 2% reheating shrinkage for insulating firebricks. All samples were chemically, thermally and dimensionally stable at temperatures up to 1100°C. The

coefficient of thermal expansion of the samples were measured around 6.0×10^{-6} (1/°C) in the temperature range 200 to 900°C.

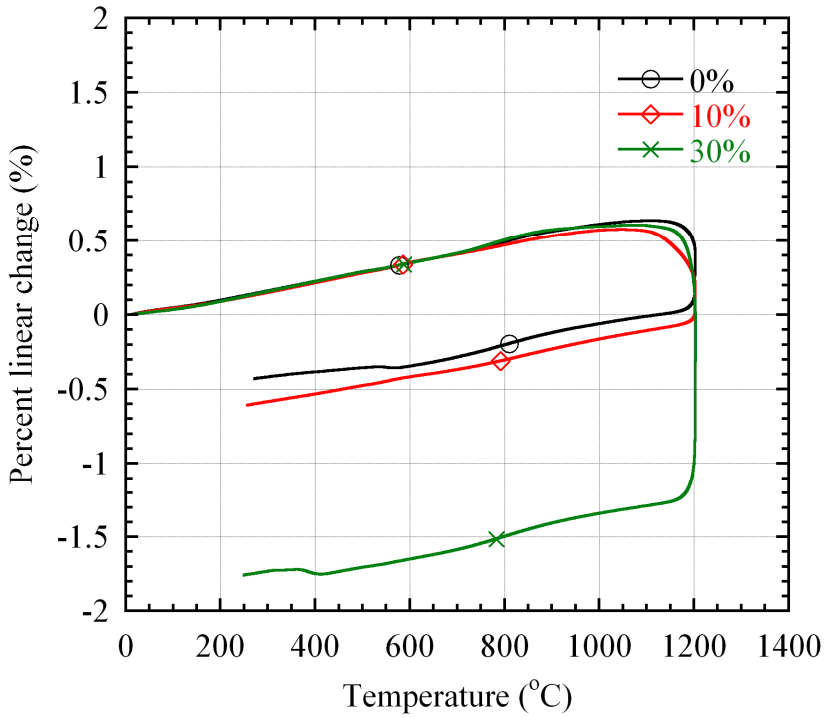

Figure 6.11. Percent linear changes of the fired samples containing K244 clay and paper waste with sawdust addition.

As can be seen from the microstructures of the fired samples with different amount of sawdust additive in Figure 6.12, the large sized porosities of 500 μm as well as small sized porosities formed in the structures. Micro-pores less than 20 μm existed in the fired structures. Figure 6.12a shows microstructure of the fired sample without sawdust addition, Figures 6.12(b), (c) and (d) show microstructures of the samples with 10, 20 and 30% sawdust addition, respectively. Effect of sawdust addition was obviously observed from the microstructures. Macro-scale pores formed probably from removal of sawdust additives while micro-scale pores occurred most likely from removal of cellulose fibers and decomposition of calcium carbonate during firing. Formation of a highly porous structure provides low thermal conductivity. Figure 6.13 shows at higher magnification the microstructure of the fired sample with sawdust addition of 20wt%. Fine micro-porosities can be clearly observed.

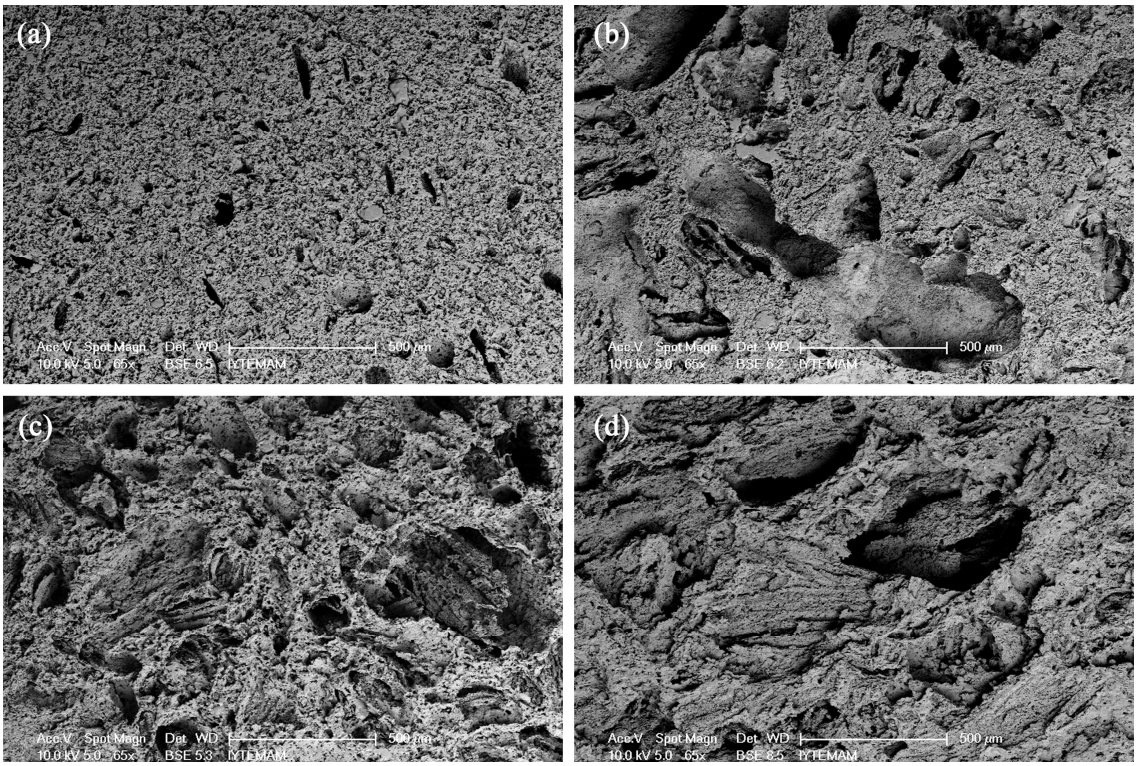

Figure 6.12. The SEM images of the fired samples containing K244 clay and paper waste according to sawdust addition of (a) 0%, (b) 10%, (c) 20% and (d) 30%.

EDS analysis taken from three different regions of the fired samples (Table 6.3) confirmed the composition to be in the anorthite region of $CaO–Al_2O_3–SiO_2$ ternary phase diagram (Levin 1975). Fired samples were rich in silica with impurities such as iron, potassium, magnesium and sodium. In EDS analysis of the product with alkali, the concentration of iron oxide of the products was high, which means the products can be unfavorable to be used in protective carbon containing atmospheres (Dergaputskaya, et al. 1980, Pirogov, et al. 1972).

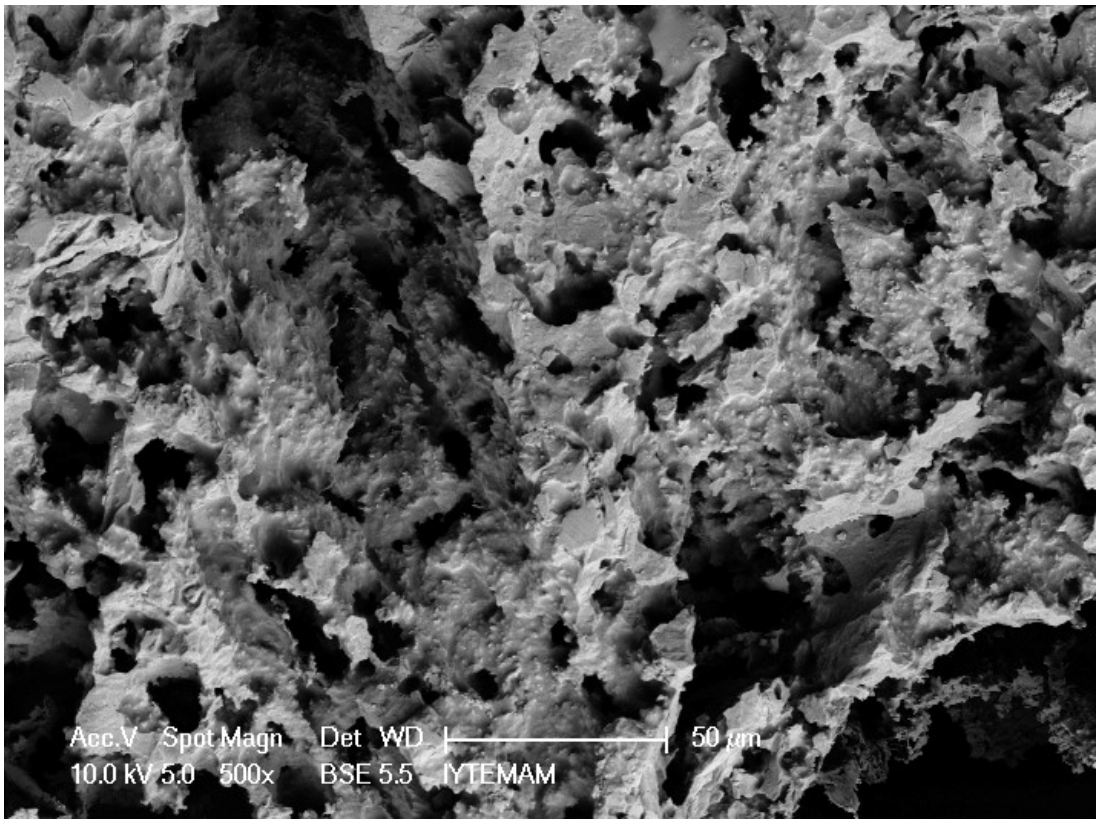

Figure 6.13. The SEM image of the fired sample containing K244 clay and paper waste with sawdust addition of 20%.

Table 6.3. The EDS analysis results of fired samples containing K244 clay and paper waste with sawdust addition.

Sawdust addition	CaO	Al_2O_3	SiO_2	MgO	K_2O	Fe_2O_3	Na_2O
0%	18.6±0.3	22.3±0.5	49.7±0.4	1.4±0.1	3.0±0.1	3.9±0.1	1.0±0.1
10%	16.6±0.3	23.6±0.4	49.2±1.8	1.7±0.1	2.6±0.1	5.5±0.5	1.4±0.1
20%	18.2±2.0	22.4±0.9	47.0±1.0	2.1±0.1	2.3±0.7	6.9±0.7	1.3±0.1
30%	20.1±0.9	22.1±0.1	48.6±0.6	1.4±0.3	2.3±0.2	4.3±0.7	1.2±0.1

6.3.4. Fired Samples Containing Fireclay and Paper Waste Mixture with Sawdust Addition

Fireclay (chamotte) was used to increase the refractoriness of the product by reducing the amount of glassy phase in the structure. Sawdust addition was made to help create porosity. In the previous study (Chapter 5) (Sutcu and Akkurt 2010), detailed XRD analysis of the samples containing fireclay and 30wt% paper waste (without sawdust) was presented. Samples fired at two different temperatures (1200–1400°C) showed that a firing temperature of 1200°C for this clay type was too low to produce anorthite ceramic. A firing temperature in excess of 1400°C effectively formed anorthite. Mainly anorthite crystals and some minor mullite phase were observed in the fireclay-containing samples with 30 and 40% paper waste. However, a firing temperature of 1400°C is very close to the melting point of anorthite (1553°C). Also, during firing additional heat is expected to be supplied by sawdust addition. For this reason, in this current study, samples containing fireclay and 30wt% paper waste with sawdust additive were fired at 1300°C. Figure 6.14 shows anorthite bricks produced by using fireclay and paper waste with sawdust addition. The products may be easily cut by a hacksaw.

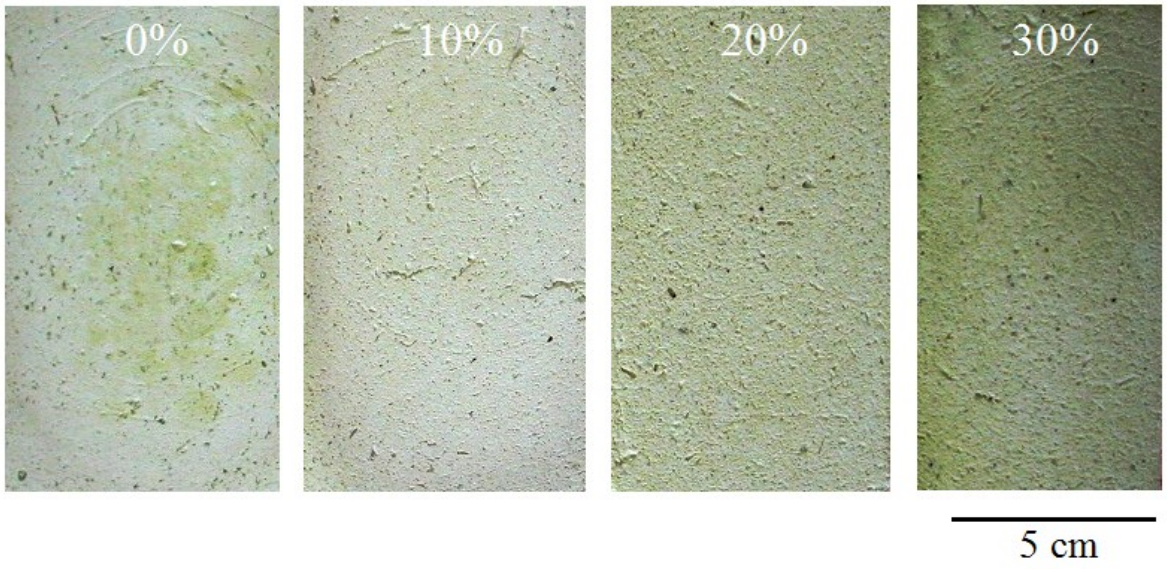

Figure 6.14. Anorthite samples containing fireclay and paper waste with different amounts of sawdust addition fired at 1300°C.

X-ray diffraction patterns of all samples containing fireclay and paper waste mixture fired at 1300°C are shown in Figure 6.15. Observed crystalline phases are labeled as A: anorthite ($CaO \cdot Al_2O_3 \cdot 2SiO_2$), M: mullite ($3Al_2O_3 \cdot 2SiO_2$), C: cristobalite ($SiO_2$). XRD analysis of all samples showed strong anorthite peaks with minor amount of mullite but there was no difference between samples containing different amounts of sawdust. Their mineral contents resembled that of an ASTM 23 grade insulating firebrick sample (Brosnan 2004).

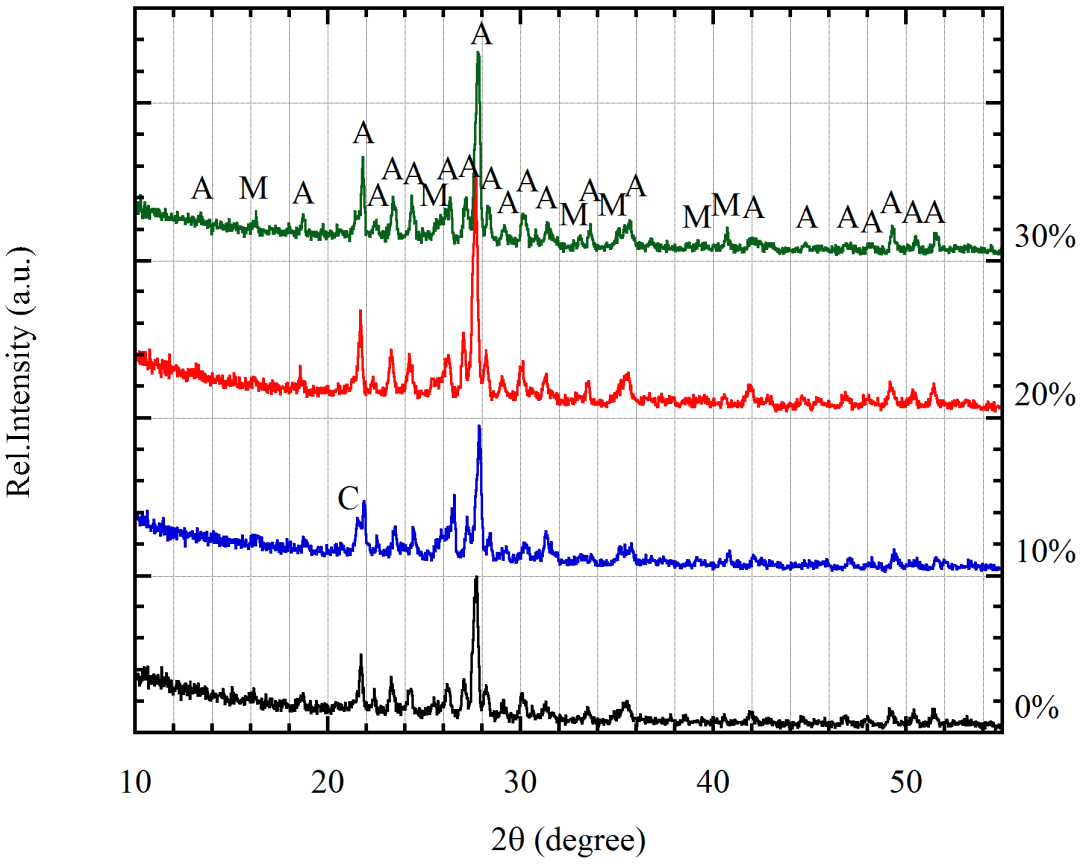

Figure 6.15. XRD patterns of the fired samples containing fireclay and paper waste with sawdust addition (A: anorthite, M: mullite, C: cristobalite).

An illustration of the variation of the pore size in the fired samples as a function of sawdust addition is shown in Figure 6.16. As can be seen from Figure 6.16, pore sizes of the samples are generally less than 2 mm, but there are occasionally some larger pores in the structure.

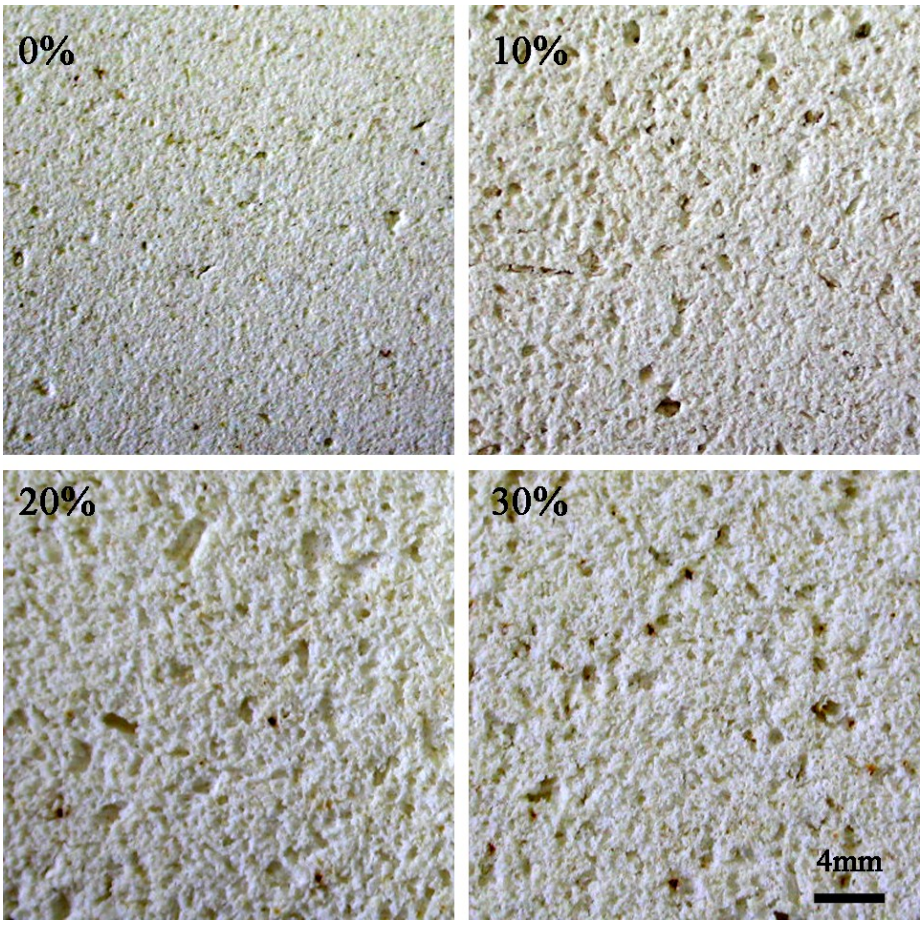

Figure 6.16. Illustration of the variation of pore size of fired samples according to the percentage of sawdust addition.

Pore size distribution of the fired sample containing fireclay and paper waste mixture without sawdust addition as measured by mercury intrusion porosimetry (Figure 6.17) showed a bi-modal distribution at about 17 μm and 100 μm of average pore size. Pores larger than 213 μm were not measured. This result was also confirmed by SEM analysis. Pore size distribution of the fired samples with sawdust addition was not measured due to their larger porosities (>200 μm) beyond the detection limit of the device.

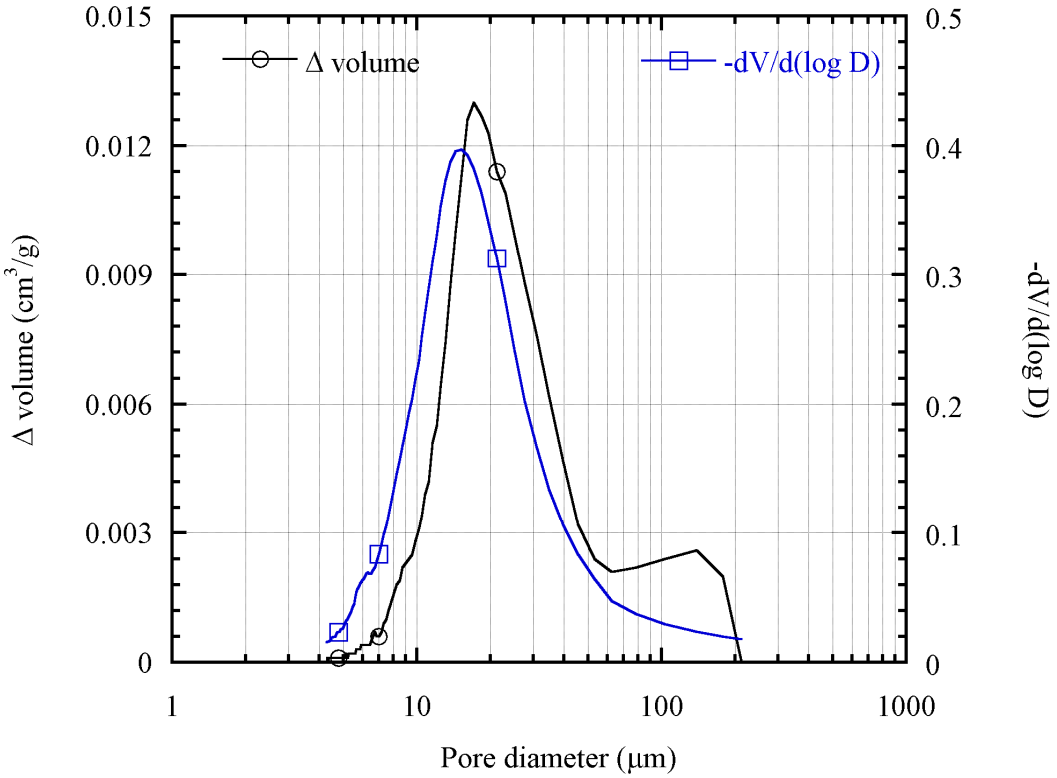

Figure 6.17. Pore size distribution measured by mercury intrusion method of the fired sample without sawdust addition

Figure 6.18 shows the SEM image of the fired sample containing a mixture of fireclay and paper waste without sawdust addition. The SEM image of this sample indicated that pore sizes were approximately about 20 μm, besides there were some larger pores with dimensions of 100 μm (Figure 6.19a).

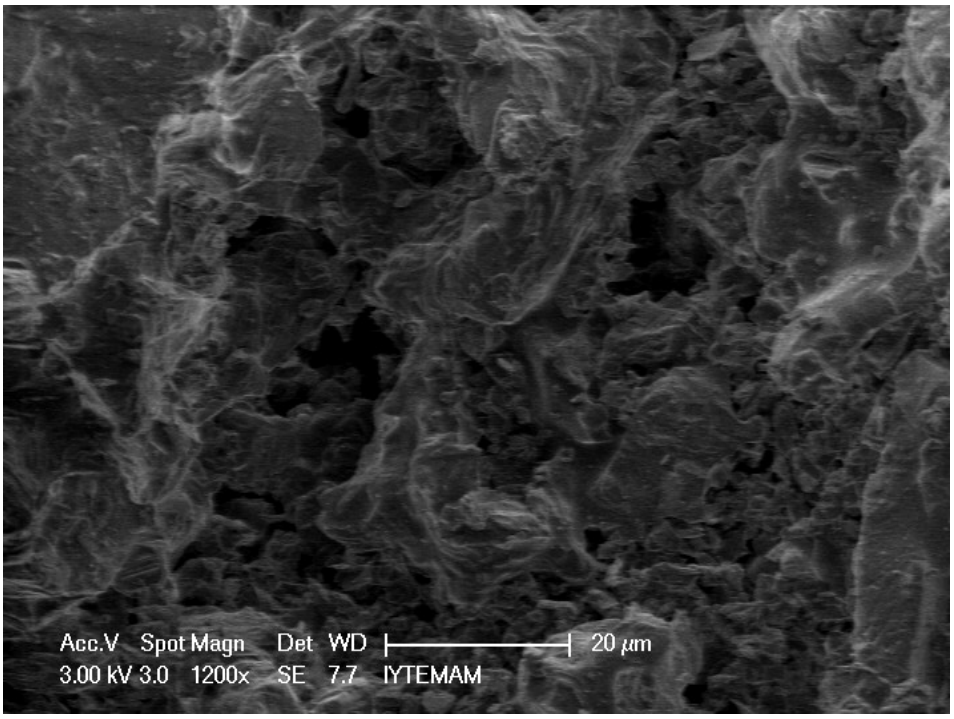

Figure 6.18. The SEM image of the fired sample without sawdust addition.

Figure 6.19 shows the SEM images of the fired samples according to the mass ratio of sawdust addition. Porous structures result from the burning of sawdust and organic matters in the paper waste, and also from the decomposition of calcium carbonate in the waste. The SEM images indicated that the amount and size of pores increased with increasing mass ratios of sawdust addition. Also, the EDS analyses were performed to find out that there was no change in chemical composition of the fired samples as a result of the addition of sawdust and that the composition was matching anorthite. The oxide analysis results taken from three different regions are given in Table 6.4.

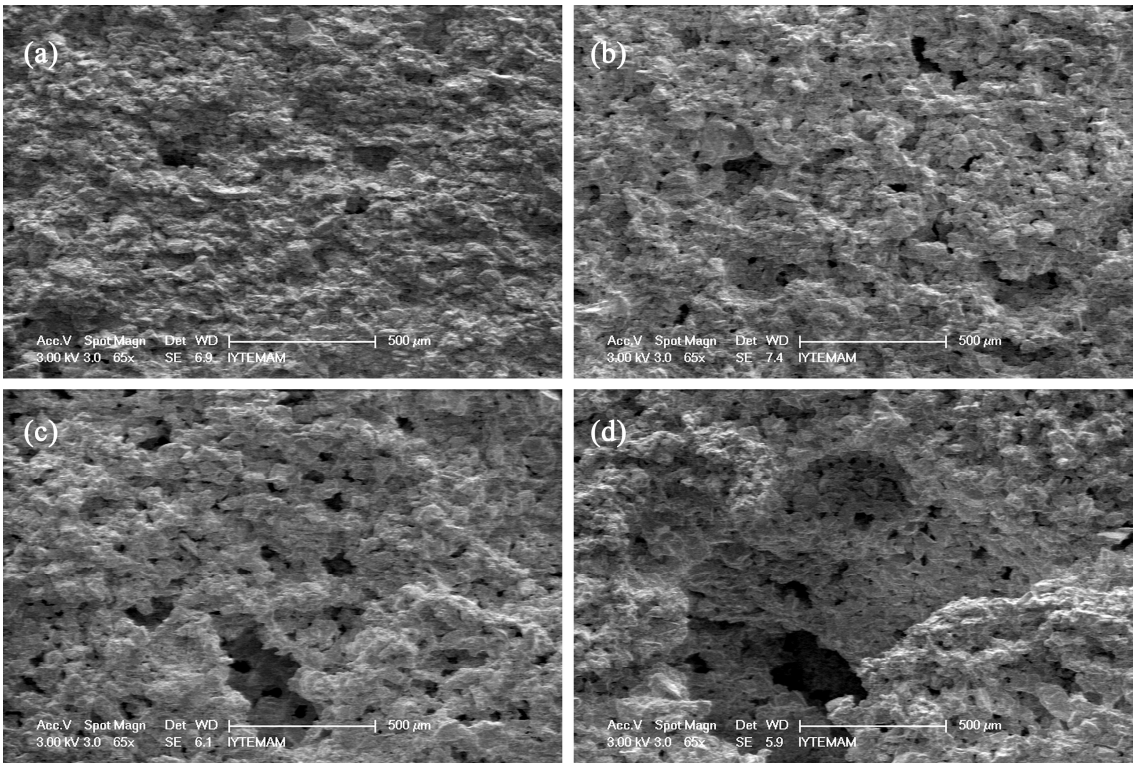

Figure 6.19. The SEM images of the fired samples according to the mass ratio of sawdust addition: (a) 0%, (b) 10%, (c) 20% and (d) 30%.

Table 6.4. The EDS analysis results of fired samples containing fireclay and paper waste with sawdust addition.

Sawdust addition (by weight)	CaO	Al_2O_3	SiO_2	MgO	K_2O	Na_2O
0%	19.5±0.0	31.1±0.8	46.6±0.1	1.3±0.1	0.8±0.2	0.7±0.1
10%	21.0±0.6	30.4±0.4	45.5±0.5	1.1±0.1	1.1±0.1	0.9±0.0
20%	21.5±0.3	29.2±0.2	46.2±0.5	1.2±0.2	1.1±0.3	0.8±0.1
30%	20.1±0.5	30.6±0.3	46.0±0.1	1.3±0.0	1.1±0.2	0.8±0.1

The physical properties such as bulk density, apparent specific gravity, and apparent porosity, coefficient of thermal expansion, linear reheat shrinkage, thermal conductivity, modulus of rupture and thermal shock resistance of the firebricks produced in this study were measured. ASTM C134 standard test method was used for measuring the weight, dimensional measurements and bulk density of the produced bricks. Test results of the refractory bricks produced in this study are given in Table 6.5. Bulk density values of the firebricks ranged from 1.12 to 0.64 g/cm^3 depending on the

mass ratio of sawdust addition. Their bulk densities decreased with increasing sawdust addition (Figure 6.20). Samples taken from firebricks were also measured by ASTM C20 test method. Bulk density, apparent specific gravity and apparent porosity measurements of the samples were performed by boiling water immersion for 2 h and soaking in water for 24 h. According to Archimedean test results given in Table 6.5, their bulk densities varied from 1.16 to 0.68 g/cm^3 with sawdust addition. The bulk density results measured by this method were compatible with that of measured by the other method. Apparent porosity values of the samples measured between 57% and 74% with increasing sawdust addition. Apparent specific gravity ranged between 2.63 and 2.70 g/cm^3.

Table 6.5. Results of the samples containing fireclay and paper waste with sawdust addition fired at 1300°C.

Physical properties		Mass ratio of sawdust addition			
		0%	10%	20%	30%
Bulk density (g/cm^3) ASTM C134		1.12±0.04	0.92±0.02	0.75±0.01	0.64±0.00
Archimedes method (ASTM C20)	Bulk density (gr/cm^3)	1.16±0.01	0.94±0.01	0.76±0.00	0.68±0.00
	Apparent specific gravity	2.68±0.01	2.65±0.01	2.70±0.02	2.63±0.00
	Apparent porosity (%)	56.9±0.5	64.7±0.4	71.8±0.2	74.1±0.1
Thermal conductivity (W/mK)		0.25±0.00	0.19±0.01	0.15±0.01	0.13±0.00

Their thermal conductivity values measured at ambient temperature ranged from 0.25 to 0.13 W/mK depending on the mass ratio of sawdust addition (Figure 6.20). The fired brick with added 30% sawdust is well-matched with the ASTM 23 grade insulating firebrick (Brosnan 2004).

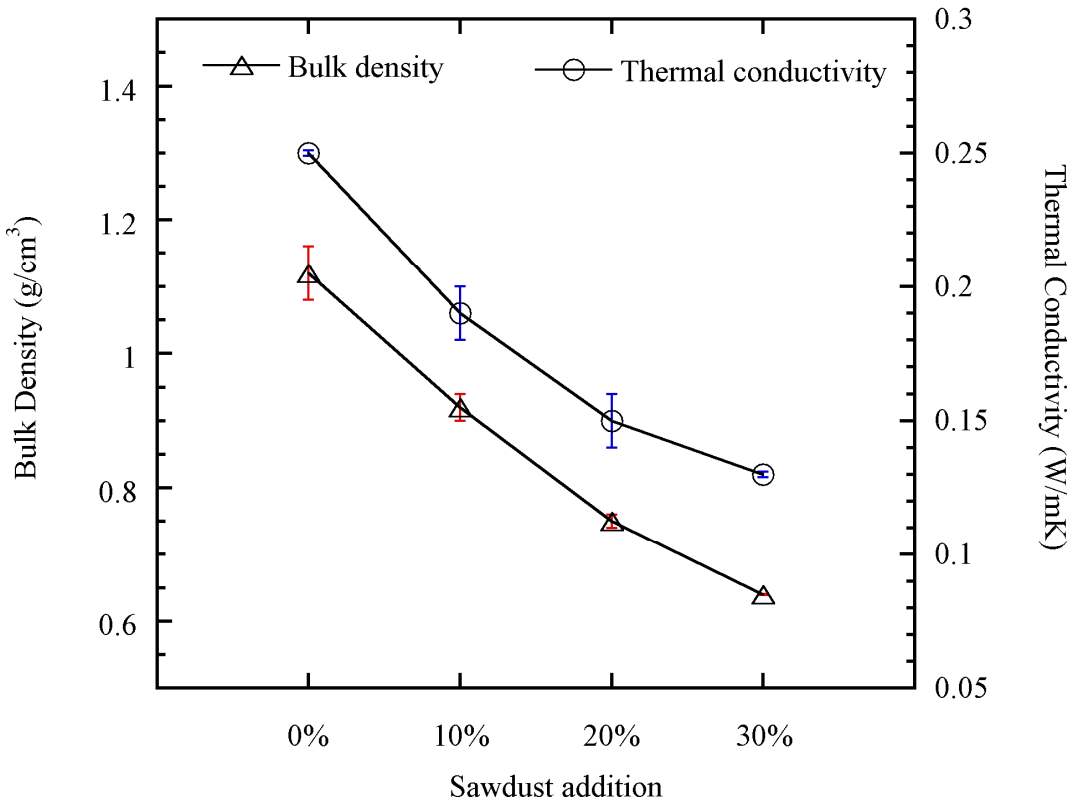

Figure 6.20. Bulk density and thermal conductivity results of the samples.

Thermal dilatometer analysis was performed on the fired samples containing fireclay and paper waste with sawdust addition to measure the coefficients of thermal expansion. Expansion (+) and shrinkage (–) behaviors of the fired porous samples are shown in Figure 6.21. Sample without sawdust began to shrink after about 1150°C, while other samples shrank sooner (1100–1150°C) depending on the amount of sawdust addition. Total thermal expansion of the samples up to 1100°C varied from 0.6 to 0.7%. Final reheat shrinkages for the samples with 0, 10, 20 and 30% sawdust was around 0.2, 0.7, 1.5 and 0.6%, respectively. The shrinkage values were below a standard limiting value of 2% reheating shrinkage for insulating firebricks. All samples were chemically, thermally and dimensionally stable at temperatures up to 1100°C. The safe operating temperature may be established by the softening onset point on the dilatometric curve. The bricks produced in this study may be safely used up to 1100°C. In addition, the reheat change test was performed at 1230°C for 8 h. All samples were dimensionally stable after the test. Considerable linear and volumetric changes were not observed as measured by caliper.

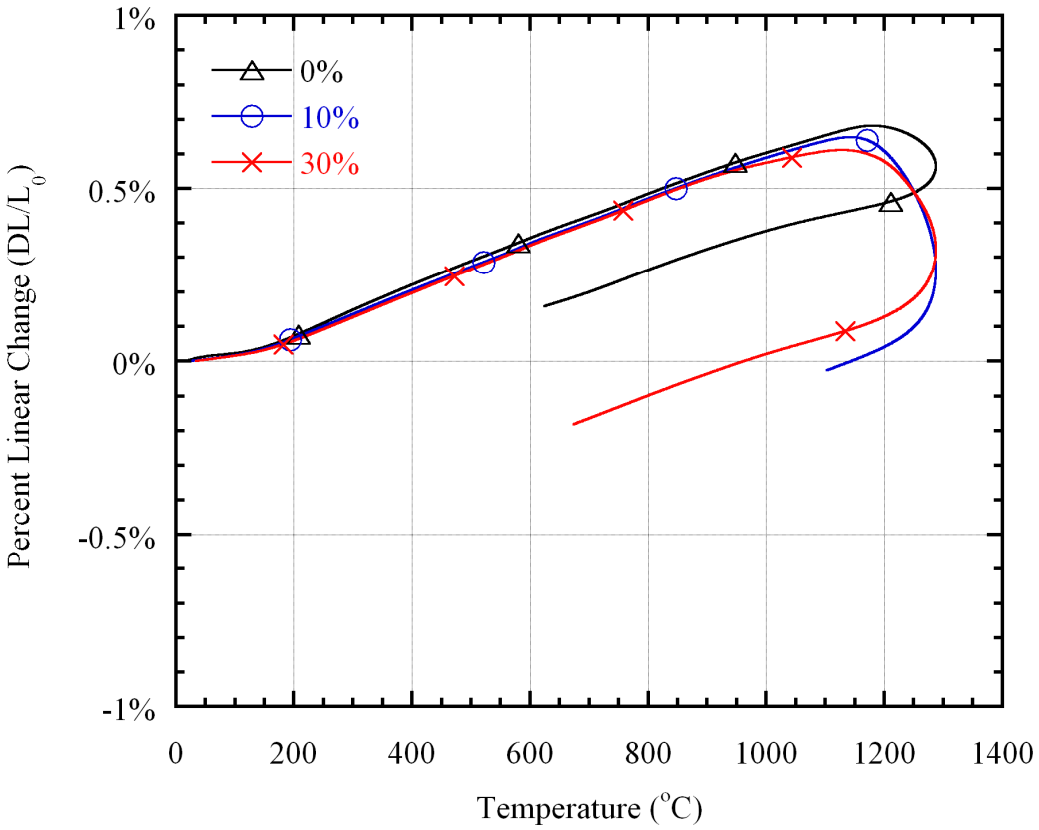

Figure 6.21. Percent linear changes of the fired samples containing fireclay and paper waste according to the ratio of sawdust additives.

Measured coefficients of thermal expansion (CTE) curves of the samples (200-900°C) are shown in Figure 6.22. Their CTEs ranged between 6×10^{-6} and 8×10^{-6} (1/°C). In addition, CTE values of the samples were linearly calculated from slope of shrinkage (ΔL/Lo) versus temperature (T) between 200 and 900°C. The coefficient of thermal expansion of the samples were measured around 6.7×10^{-6} (1/°C) in the temperature range 200 to 900°C.

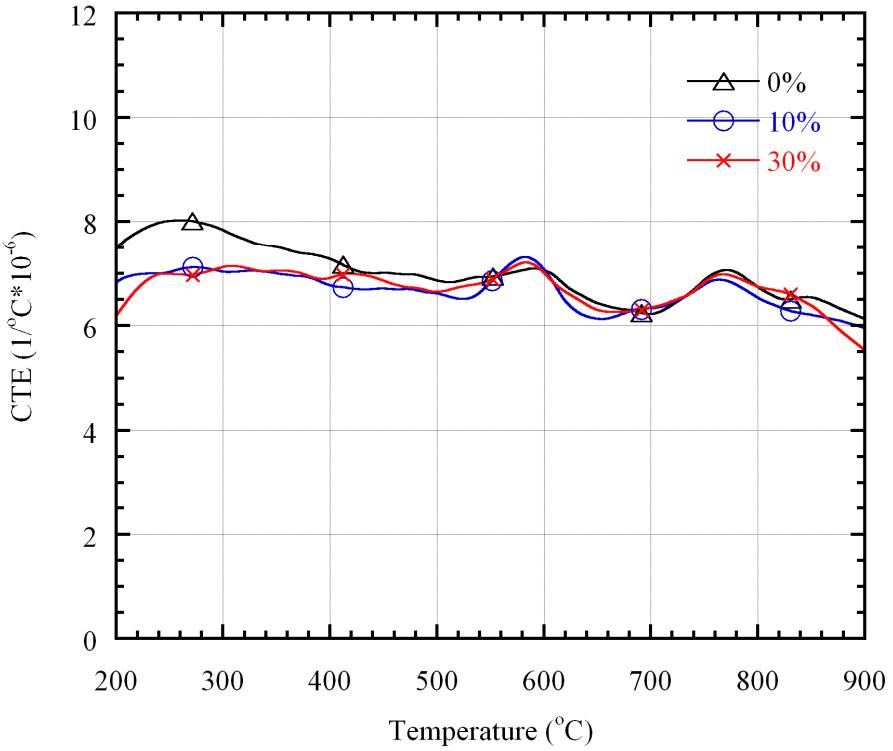

Figure 6.22. Thermal expansion coefficients of the samples containing fireclay and paper waste according to the ratio of sawdust additives.

A mechanical test was applied for determination of the cold modulus of rupture (MOR) of the fired samples. The cold strength of a refractory material is an indication of its suitability for use in refractory construction. It is not a measure of performance at elevated temperatures. This test is a method for determining the room temperature flexural strength in the three-point bending. The three-point bending test apparatus is shown in Figure 6.23. After loading applied to the samples, a crack occurred in the middle of samples and began to propagate, and then the samples were broken. The modulus of rupture results of the samples with sawdust addition is graphically given in Figure 6.24. Depending on the increase in the sawdust addition and porosity content, cold modulus of rupture of the samples progressively decreased from 2.73 to 0.61 MPa, since the bridges between the pores became thinner (Kryuchkov, et al. 1999). In the literature, MOR values measured for commercial insulating firebricks (<1.60 g/cm^3 or >45% porosity) are between 0.72 and 1.0 MPa (Ruh and McDowell 1962, Thermal Ceramics 2009). The MOR value of firebrick with 30% sawdust was slightly lower than that of commercial insulating firebricks.

Figure 6.23. The MOR testing apparatus for firebrick sample.

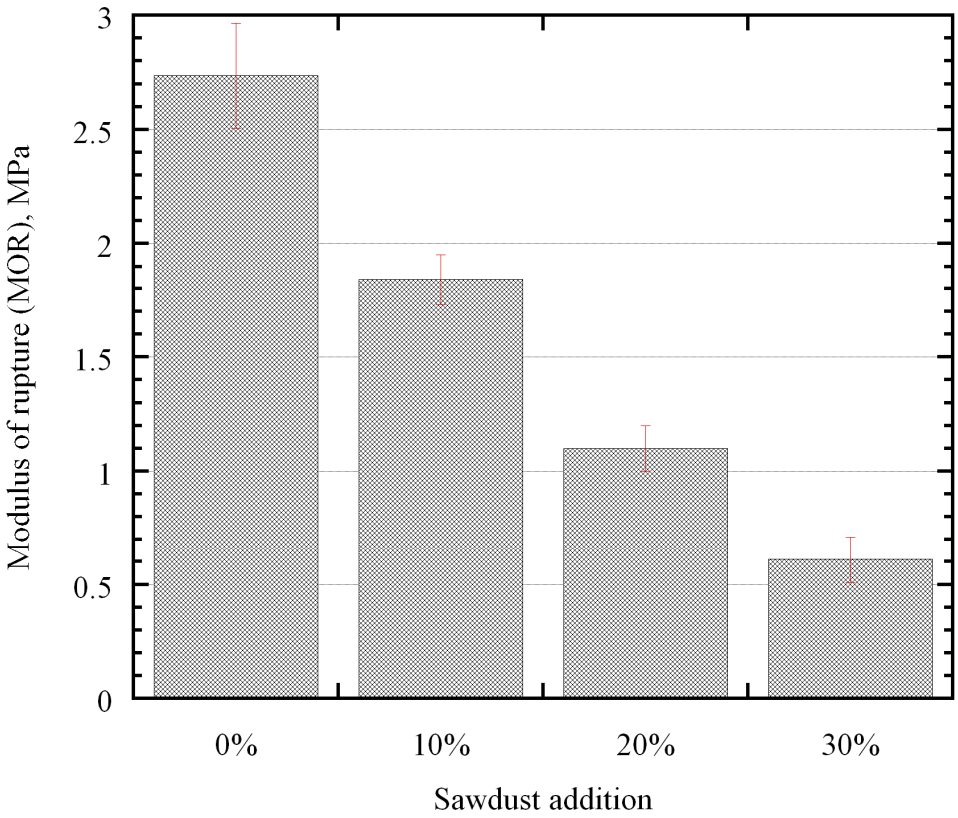

Figure 6.24. Cold modulus of rupture (MOR) values of the samples containing fireclay and paper waste with sawdust addition.

Finally, thermal shock tests were performed on samples to find out their

resistance to repeated heating (15 minutes) and cooling (15 minutes) cycles by heating to 1200°C and cooling to room temperature in five cycles. Samples were found to be intact after the test.

6.4. Conclusions

In this study, the production of porous and lightweight anorthite based insulating ceramics from mixtures of different types of clay (K244 clay and fireclay), recycled paper processing waste and pore-making sawdust addition was investigated. It was concluded that the recycled paper processing wastes could be used as a suitable alternative raw material source for production of porous anorthite ceramics due to their organic and inorganic content. Suitability of K244 clay with alkalis and fireclay in the manufacturing of anorthite based lightweight insulating ceramics was also evaluated. Sawdust addition into the mixtures with anorthite composition contributed to increase porosity of the samples.

Mineralogical phase analysis of all samples revealed that the reaction between calcium oxide from paper residues and aluminum silicate from clays resulted in the formation of anorthite ($CaO{\cdot}Al_2O_3{\cdot}2SiO_2$). Observed secondary phases in the samples with alkaline clay and fireclay were minor quartz and mullite, respectively.

In the samples with K244 clay and paper waste mixtures temperatures above 1200°C were too high to produce a porous anorthite ceramic because of premature melting during firing. This was attributed to the presence of alkalis in the clay that fluxed the mixtures. For this reason, a firing temperature of 1200°C was enough for production of anorthite ceramics. Their bulk densities ranged from 1.30 to 0.87 g/cm^3, thermal conductivities varied from 0.40 to 0.20 W/mK.

Porous and lightweight anorthite ceramics from the mixtures of fireclay and paper waste with sawdust addition were successfully produced. It was concluded that their bulk densities and thermal conductivities decreased with increasing sawdust addition. While their densities ranged from 1.12 to 0.64 g/cm^3, their thermal conductivities varied from 0.25 to 0.13 W/mK with increasing of apparent porosity from 57 to 74%. The shrinkage values were below a standard limiting value of 2% reheating shrinkage. The products were stable at high temperatures up to 1100°C. Depending on the increase in the sawdust addition and porosity content, their cold

modulus of rupture varied from 2.8 to 0.6 MPa. These results are usable values for insulating firebricks. Physical properties of samples with 20 and 30% sawdust are compatible with that of the commercial product (ASTM 23 group insulating firebricks).

CHAPTER 7

CONCLUSIONS

7.1. Summary and Conclusions

Residues from recycled paper production containing calcite, little clay and cellulose were successfully incorporated into brick and insulating firebrick. Four different types of clay were used in the thesis. First was a clayey material obtained from Turgutlu area which is still commercially used to produce extruded earthenware brick and tile. The other clay types used were an enriched aluminum silicate hydrate, a commercially used clay (K244) and a fireclay. The paper residues were used as not only pore former due to their organic and carbonate content but also a new crystalline phase maker due to their mineral content to produce porous and light-weight ceramic bodies, and to provide lower thermal conductivity. Two different products were successfully produced using the above materials; a construction brick and a refractory firebrick.

As received paper residues were composed of 65% water. Solid part of these residues contained about 30% organics (cellulose fibers) and 70% inorganic components like mainly calcite and other clayey materials. According to thermal analysis, total weight loss of dewatered residues was about 54% at 1000°C. Two main reactions occurred during heating of the residues. The first reaction occurred between 200 and 550°C due to the burning of paper residues. The fast decomposition was due to the removal of cellulose at 250–350°C, and relatively slow reaction was due to the lignin decomposition between 350 and 550°C. The second main reaction that occurred above 700°C was due to the decomposition of carbonates. The firing regime of ceramics produced in following studies was planned according to the thermal behavior of the residues. When this residue is used in a brick the thermal burned on the furnace will be less due to the burning of cellulose.

Firstly, the use of these recycled paper processing residues in making porous brick with reduced thermal conductivity and acceptable mechanical strength was studied. The paper residues were used as an additive into an earthenware brick to produce the pores. Chemical, physical, mineral and thermal properties of the brick raw

material were determined. The bricks containing the paper residues up to 30wt% produced by semi-dry pressing method were fired at 1000 and 1100°C. The dilatometric behaviors of the fired bricks were investigated as well as their loss on ignition, bulk density, apparent porosity and water absorption. The dilatometric results indicated that little shrinkage (1-2%) occurred in the brick that contained residue while the brick without residue shrunk by about 3%. The test results showed that the use of paper processing residues decreased the fired density of the bricks down to 1.28 g/cm^3. Their fired densities varied between 1.92 g/cm^3 and 1.28 g/cm^3, which correspond to a decrease of 33% compared to the density of the brick without residue. Apparent porosity and water absorption values were increased with increase in residue addition. Their mechanical and thermal conductivity measurements were performed. Pressing direction of the bricks and shape of the pores in samples has a considerable effect on mechanical strength. It was found that compressive strengths of the samples decreased depending on the increase in the residue addition and porosity content. However, their strength values were still acceptable up to 20% paper residue addition. Thermal conductivity of the porous brick produced in this study (<0.4 W/mK) showed more than 50% reduction compared to local brick of the same composition (0.8 W/mK). Although their thermal conductivities decreased by up to 50%, adequate mechanical strength could be maintained. Conversion of this product to a perforated brick showed that its thermal conductivity could be decreased down to 0.158 W/mK. Results indicated that the residues could be easily utilized as pore forming additives into brick bodies to facilitate production of vertically perforated insulation bricks. Mainly quartz and minor amount of calcium aluminosilicate phases such as anorthite and gehlenite were observed in the brick. The proportion of anorthite was found to be significantly higher when the firing temperature and residue addition was increased. This observation inspired the work done in the next phase of the thesis; insulating anorthite refractories.

Secondly, the production of porous anorthite ceramics from the mixtures of paper residues with three different types of clays was successfully achieved. Suitability of three different clays such as aluminum silicate, K244 clay with alkalis and fireclay in the manufacturing of anorthite based lightweight insulating firebricks was determined. Porous character to the ceramic was provided by addition of paper processing residues. All samples of mixtures with 30–40wt% PPR fired at 1200 to 1400°C contained anorthite as major phase and also minor secondary phases such as mullite or gehlenite phases in some mixtures. Laboratory grade enriched clay, when mixed with paper

residues, was able to produce anorthite at 1300°C in a porous ceramic form. Use of K244 clay with alkali that is commercially available in tonnage quantities produced anorthite at lower temperatures but with higher bulk densities. In these samples 1300°C was too high to produce a ceramic because of premature melting during firing. This was attributed to the presence of alkalis in the clay that fluxed the mixtures. Finally, a higher firing temperature of 1400°C was needed for the fireclay samples to produce anorthite in a porous ceramic form. Gehlenite phase formed mostly at lower temperatures and in samples containing higher calcium content (50wt% PPR). Compressive strengths of the samples ranged from 8 to 43 MPa. Upon completion of this study porous thermally insulating anorthite ceramics were successfully produced.

Moreover, in Chapter 6, the production of porous and lightweight anorthite based insulating ceramics from mixtures of different types of clay (K244 clay and fireclay), recycled paper processing waste and pore-making sawdust addition was investigated. Suitability of clay 244 with alkalis and fireclay in the manufacturing of anorthite based lightweight insulating ceramics was also evaluated. It was concluded that the recycled paper processing wastes could be used as a suitable alternative raw material source for production of porous anorthite ceramics due to their organic and inorganic content. Sawdust addition into the mixtures with anorthite composition contributed to increase porosity of the samples. Mineralogical phase analysis of all samples revealed that the reaction between calcium oxide from paper residues and aluminum silicate from clays resulted in the formation of anorthite ($CaO{\cdot}Al_2O_3{\cdot}2SiO_2$). Observed secondary phases in the samples with alkaline clay and fireclay were minor quartz and mullite, respectively. In the samples with K244 clay and paper waste mixtures temperatures above 1200°C were too high to produce a porous anorthite ceramic because of premature melting during firing. This was attributed to the presence of alkalis in the clay that fluxed the mixtures. For this reason, a firing temperature of 1200°C was enough for production of anorthite ceramics. Their bulk densities ranged from 1.30 to 0.87 g/cm^3, thermal conductivities varied from 0.40 to 0.20 W/mK. Porous and lightweight anorthite ceramics from the mixtures of fireclay and paper waste with sawdust addition were successfully produced. It was concluded that their bulk densities and thermal conductivities decreased with increasing sawdust addition. While their densities ranged from 1.12 to 0.64 g/cm^3, their thermal conductivities varied from 0.25 to 0.13 W/mK with increasing of apparent porosity from 57 to 74%. The shrinkage values were below a standard limiting value of 2% reheating shrinkage. The products

were stable at high temperatures up to 1100°C. Depending on the increase in the sawdust addition and porosity content, their cold modulus of rupture varied from 2.8 to 0.6 MPa. These results are usable values for insulating firebricks. Physical properties of samples with 20 and 30% sawdust are compatible with that of the commercial product (ASTM 23 group insulating firebricks).

To sum up two different commercially usable products were produced by the use of an otherwise useless paper residue.

7.2. Recommendations for Future Works

Software can be used to predict the thermal conductivity of different perforation designs of vertically perforated bricks. Extruder dies should be produced accordingly. Insulation bricks can be produced with as low as 0.10 W/mK of thermal conductivity.

As far as the insulation firebrick are concerned pores with a smaller and more narrow size distribution can be produced by using smaller pore formers to reduce thermal conductivity further. Different forming techniques can be tested. For example, vacuum forming would be tested. More work needs to be done to further advance this study to produce larger and more porous ceramic pieces.

REFERENCES

Abraitis, R. J., Dargis, A. K., Rusyatskas, A. A. and Sakalauskas, E. J., 1999, A study of thermal conductivity of structural ceramic materials. Part I. State of research of thermal conductivity of structural materials. *Refractories and Industrial Ceramics*. 40(7-8): p. 351-358.

Agathopoulos, S., Tulyaganov, D. U., Marques, Paap, Ferro, M. C., Fernandes, M. H. V. and Correia, R. N., 2003, The fluorapatite-anorthite system in biomedicine. *Biomaterials*. 24(7): p. 1317-1331.

Ahmadi, B. and Al-Khaja, W., 2001, Utilization of paper waste sludge in the building construction industry. *Resources, Conservation and Recycling*. 32(2): p. 105-113.

Alleman, J.E., 1983, Beneficial Use of Sludge in Building Components. (Grant No. ISP-8021357).

Alleman, James E. and Berman, Neil A., 1984, Constructive Sludge Management: Biobrick. *Journal of Environmental Engineering*. 110(2): p. 301-311.

Aloisi, M., Karamanov, A. and Pelino, M., 2004, Sintered glass-ceramic from municipal solid waste incinerator ashes. *Journal of Non-Crystalline Solids*. 345: p. 192-196.

ASTM C67, 2009, Standard Test Methods for Sampling and Testing Brick and Structural Clay Tile,ASTM International, West Conshohocken, PA, www.astm.org.

ASTM C133-97, 2003, Standard Test Methods for Cold Crushing Strength and Modulus of Rupture of Refractories,ASTM International, West Conshohocken, PA, www.astm.org.

ASTM C155-97, 2002, Standard Classification of Insulating Firebrick,ASTM International, West Conshohocken, PA, www.astm.org.

ASTM C1171-96, 2003, Standard Test Method for Quantitatively Measuring the Effect of Thermal Shock and Thermal Cycling on Refractories,ASTM International, West Conshohocken, PA, www.astm.org.

ASTM Standard C20, 2005, Standard Test Methods for Apparent Porosity, Water Absorption, Apparent Specific Gravity, and Bulk Density of Burned Refractory Brick and Shapes by Boiling Water,ASTM International, West Conshohocken, PA, www.astm.org.

ASTM Standard C134-95, 2005, Standard Test Methods for Size, Dimensional Measurements, and Bulk Density of Refractory Brick and Insulating Firebrick,ASTM International, West Conshohocken, PA, www.astm.org.

Banhidi, V. and Gomze, L. A., 2008, Improvement of insulation properties of conventional brick products, Materials Science, Testing and Informatics IV, ed. P. J. Szabo, T. Reti and T. Czigany, 1-6, Trans Tech Publications Ltd.

Barea, R., Osendi, M. I., Ferreira, J. M. F. and Miranzo, P., 2005, Thermal conductivity of highly porous mullite material. *Acta Materialia*. 53(11): p. 3313-3318.

Bejan, A. and Kraus, A.D., 2003, Heat Transfer Handbook, John Wiley & Sons, Inc.

Bhattacharjee, B. and Krishnamoorthy, S., 2004, Permeable porosity and thermal conductivity of construction materials. *Journal of Materials in Civil Engineering*. 16(4): p. 322-330.

Bingham, P. A. and Hand, R. J., 2006, Vitrification of toxic wastes: a brief review. *Advances in Applied Ceramics*. 105(1): p. 21-31.

Boni, Maria Rosaria, D'Aprile, Laura and De Casa, Giancarlo, 2004, Environmental quality of primary paper sludge. *Journal of Hazardous Materials*. 108(1-2): p. 125-128.

Boudchicha, M. R., Achour, S. and Harabi, A., 2001, Crystallization and sintering of cordierite and anorthite based binary ceramics. *Journal of Materials Science Letters*. 20(3): p. 215-217.

Brosnan, D. A., 2003, Low density ceramics produced from paper recycling residuals, US Patent 6,569,797 B1.

Brosnan, D. A. and Robinson, G.C., 2003, Introduction to Drying of Ceramics with Laboratory Exercises, The American Ceramic Society.

Brosnan, D.A., 2002a, Chemical and physical changes in the soak zone of the kiln. *Brickyard Road*. April: p. 24-29.

Brosnan, D.A., 2002b, What's Happening During Preheat?-Part II: Decomposition of clay crystals and quartz inversions. *Brickyard Road*. January: p. 21-24.

Brosnan, D.A., 2004, Alumina-silica brick, Refractories Handbook ed. C. A. Schacht, 79-107, Marcel Dekker Inc.

Budak, M., Sütçü, M., Akkurt, S., Böke, H., 2003, Koruma amaçlı Horasan harcı hazırlanmasında kullanılacak ticari killerin kullanım koşullarının araştırılması. *11. Ulusal Kil Sempozyumu*. 11. Ulusal Kil Sempozyumu Bildiriler Kitabı: p. 381-389.İzmir.

Carniglia, S.C. and Barna, G.L., 1992, Handbook of Industrial Refractories Technology - Principles, Types, Properties and Applications, Noyes Publications.

CEMBUREAU-The European Cement Association, 1997, Alternative fuels in cement manufacture:Technical and environmental review.

Cernec, F., Zule, J., Moze, A. and Ivanus, A., 2005, Chemical and microbiological stability of waste sludge from paper industry intended for brick production. *Waste Management & Research*. 23(2): p. 106-112.

Confederation of European Paper Industries, *Discovering the high potential of pulp and paper production residues*, http://www.cepi.org, (accessed March 15, 2010).

Confederation of European Paper Industries, *Special Recycling 2005 Statistics*, www.cepi.org, (accessed March 15, 2010).

Cultrone, G., Rodriguez-Navarro, C., Sebastian, E., Cazalla, O. and De La Torre, M. J., 2001, Carbonate and silicate phase reactions during ceramic firing. *European Journal of Mineralogy*. 13(3): p. 621-634.

Cultrone, G., Sebastian, E. and de la Torre, M. J., 2005, Mineralogical and physical behaviour of solid bricks with additives. *Construction and Building Materials*. 19(1): p. 39-48.

Cultrone, G., Sebastian, E., Elert, K., de la Torre, M. J., Cazalla, O. and Rodriguez-Navarro, C., 2004, Influence of mineralogy and firing temperature on the porosity of bricks. *Journal of the European Ceramic Society*. 24(3): p. 547-564.

Dasgupta, S. and Das, S. K., 2002, Paper pulp waste - A new source of raw material for the synthesis of a porous ceramic composite. *Bulletin of Materials Science*. 25(5): p. 381-385.

Demir, Ismail, 2008, Effect of organic residues addition on the technological properties of clay bricks. *Waste Management*. 28(3): p. 622-627.

Demir, Ismail, Serhat BaspInar, M. and Orhan, Mehmet, 2005, Utilization of kraft pulp production residues in clay brick production. *Building and Environment*. 40(11): p. 1533-1537.

Dergaputskaya, L. A., Gaodu, A. N. and Litvin, L. G., 1980, Anorthite lightweight refractories for service in carbon-containing media. *Refractories and Industrial Ceramics*. 21(7): p. 366-368.

DEU, 2006, Dokuz Eylul University-Laboratory of Environmental Engineering Department, Eluate analysis report of the refining paper sludge, Izmir, Turkey.

Devlet Planlama Teşkilatı, *VIII. Kalkınma Planı Kağıt Sanayii Özel İhtisas Komisyonu Raporu*, http://ekutup.dpt.gov.tr/imalatsa/kagit/oik541.pdf, (accessed 2010).

Dondi, M., Marsigli, M. and Fabbri, B., 1997, Recycling of industrial and urban wastes in brick production. *Tile and Brick International*. 13(3): p. 218–225.

Dondi, M., Mazzanti, F., Principi, P., Raimondo, M., Zanarini, G., 2004, Thermal conductivity of clay bricks. *Journal of Materials in Civil Engineering*. 16(1): p. 8-14.

Dorey, R.A., Yeomans, J.A., Smith, P.A., 2002, Effect of pore clustering on the mechanical properties of ceramics. *Journal of European Ceramic Society*. 22: p. 403-409.

dos Santos, W. N., 2008, Advances on the hot wire technique. *Journal of the European Ceramic Society*. 28(1): p. 15-20.

Ducman, V., Kopar, T., 2007, The influence of different waste additions to clay-product mixtures. *Materiali in Tehnologije*. 41(6): p. 289-293.

EN ISO13790, 2008, Energy performance of buildings-Calculation of energy use for space heating and cooling, Switzerland.

Environmental Protection Agency, 2006, Hazardous Waste: Interpretation of the definition and classification of hazardous waste, Appendix A.,www.environment-agency.gov.uk.

Erker, A., Heyder, F., 1996, The influence of the cross sectional design of vertically perforated clay masonry units on thermal insulating requirements. *Ziegelindustrie International*. 49(2): p. 123-131.

Franklin and Sterling Hill, http://franklin-sterlinghill.com/dunn/ch19/anorthite.stm, (accessed 01.01.2010).

García, R., Vigil de la Villa, R., Vegas, I., Frías, M. and Sánchez de Rojas, M. I., 2008, The pozzolanic properties of paper sludge waste. *Construction and Building Materials*. 22(7): p. 1484-1490.

Gdula, R.A., 1971, Anorthite ceramic dielectrics. *American Ceramic Society Bulletin*. 50: p. 555–557.

Ghazi Wakili, K. and Tanner, Ch, 2003, U-value of a dried wall made of perforated porous clay bricks: Hot box measurement versus numerical analysis. *Energy and Buildings*. 35(7): p. 675-680.

Goroyias, G., Elias, R., Fan, M., 2004, The Waste & Resources Action Programme (WRAP), Research into using recycled waste paper residues in construction products,

Hammerschmidt, U., 2003, A Quasi-Steady State Technique to Measure the Thermal Conductivity. *International Journal of Thermophysics*. 24(5): p. 1291-1312.

Handbook of Mineralogy, www.handbookofminerology.org/pdfs/anorthite.pdf, (accessed 01.01.2010).

Harbison-Walker Refractories, 2005, Handbook of Refractory Practice, Harbison-Walker Refractories Company.

Hojamberdiev, M., Torrey, J. D., Beltrao, M. S. D. and Wondraczek, L., 2009, Cellular Anorthite Glass-Ceramics: Synthesis, Microstructure and Properties. *Journal of the American Ceramic Society*. 92(11): p. 2598-2604.

Horie, E., Saeki, T., Oosawa, S., Hisaka, H., Tanetani, N., 1981, Process for making heat insulating firebricks, US Patent 4,307,199.

Hurlbut, C.S., 1959, Dana's Manual of Mineralogy, John Wiley&Sons, Inc.

Isobe, T., Kameshima, Y., Nakajima, A., Okada, K., Hotta, Y., 2007, Gas permeability and mechanical properties of porous alumina ceramics with unidirectionally aligned pores. *Journal of European Ceramic Society*. 27(53-59).

Jha, Vinay Kumar, Kameshima, Yoshikazu, Nakajima, Akira, Okada, Kiyoshi and Mackenzie, Kenneth J. D., 2006, Multi Functional Uptake Behaviour of Materials Prepared by Calcining Waste Paper Sludge. *Journal of Environmental Science and Health, Part A: Toxic/Hazardous Substances and Environmental Engineering*. 41(4): p. 703 - 719.

Jordán, M.M., Boix, A., Sanfeliu, T., De la Fuente, C., 1999, Firing transformations of cretaceous clays used in the manufacturing of ceramic tiles. *Applied Clay Science*. 14: p. 225–234.

Jordán, M.M., Sanfeliu, T., De la Fuente, C., 2001, Firing transformations of tertiary clays used in the manufacturing of ceramic tiles. *Applied Clay Science*. 20: p. 87-95.

Junge, K., 2000, Additives in the brick and tile industry. *Zi Brick and Tile Industry International* 53(12): p. 25-39.

Kalita, P., Mohan, G., Pradeep Kumar, G. and Mahanta, P., 2009, Determination and comparison of kinetic parameters of low density biomass fuels. *Journal of Renewable and Sustainable Energy*. 1 (023109): p. 1-12.

Kang, Y. and Morita, K., 2006, Thermal conductivity of the CaO-Al2O3-SiO2 system. *Isij International*. 46(3): p. 420-426.

Kavalci, S., Yalamac, E. and Akkurt, S., 2008, Effects of boron addition and intensive grinding on synthesis of anorthite ceramics. *Ceramics International*. 34(7): p. 1629-1635.

Kempster, C. J. E., 12, Megaw, H. D., 18 and Radoslovich, E. W., 15, 1962, The structure of anorthite, CaAl2Si2O8. I. Structure analysis 18. *Acta Crystallographica*. 15 2a(10): p. 1005-1017.

Kingery, W.D., Bowen, H.K. and Uhlmann, D.R., 1976, Introduction to Ceramics, John Wiley & Sons Inc.

Kobayashi, Y. and Kato, E., 1994, Low-temperature fabrication of anorthite ceramics. *Journal of the American Ceramic Society*. 77(3): p. 833-834.

Kornmann, M. and CTTB, 2007, Clay Bricks and Roof Tiles, Manufacturing and Properties, Technical Centre for Roof Tiles and Bricks (CTTB).

Koronthalyova, O., Matiasovsky, P., 2007, Pore structure and thermal conductivity of burnt clay bricks. *Thermophysics 2007*: p. 100-106

Köhler, R., 2002, Use of leather residues as pore-forming agents for masonry bricks. *Ziegelindustrie International* 58(3): p. 30-38.

Kryuchkov, Y. N., Mineev, V. P., Troyanskaya, S. V. and Tkach, V. V., 1999, A heat-insulating lightweight material. *Glass and Ceramics*. 56(5-6): p. 158-159.

Kurama, S. and Ozel, E., 2009, The influence of different CaO source in the production of anorthite ceramics. *Ceramics International*. 35(2): p. 827-830.

Kyoto Electronics Manufacturing Co. Ltd., *QTM500 Quick Thermal Conductivity Meter*, http://www.kyoto-kem.com, (accessed 2009).

Lacarriere, B., Trombe, A., Monchoux, F., 2006, Experimental unsteady characterization of heat transfer in a multi-layer wall including air layers-Application to vertically perforated bricks. *Energy and Buildings*. 38: p. 232-237.

Lee, W. E., Souza, G. P., McConville, C. J., Tarvornpanich, T. and Iqbal, Y., 2008, Mullite formation in clays and clay-derived vitreous ceramics. *Journal of the European Ceramic Society*. 28(2): p. 465-471.

Leigh, H.D., 1982, Refractories: Reprinted from Kirk-Othmer: Encyclopedia of Chemical Technology, John Wiley & Sons. Inc.

Levent Kağıt A.Ş., http://www.leventkagit.com.tr, (accessed March 10, 2010).

Levin, E.M., Robbins, C.R. and McMurdie, H.F., 1975, Phase Diagrams for Ceramists, The American Ceramic Society.

Liaw, Chin-Tson, Chang, Hui-Lan, Hsu, Wen-Ching and Huang, Chi-Ru, 1998, A novel method to reuse paper sludge and co-generation ashes from paper mill. *Journal of Hazardous Materials*. 58(1-3): p. 93-102.

Maage, M., 1984, Frost resistance and pore size distribution in bricks. *Materials and Structures*. 17(5): p. 345-350.

Marra, J.C. and Jantzen, C.M., 2004, Glass-An Environmental Protector. *American Ceramic Society Bulletin*. 83(11): p. 13-17.

Mergen, A. and Aslanoglu, V. Z., 2003, Low-temperature fabrication of anorthite ceramics from kaolinite and calcium carbonate with boron oxide addition. *Ceramics International*. 29(6): p. 667-670.

Meyers, K.S., and Speyer, R.F., 2003, Thermal analysis of clays, Handbook of Thermal Analysis and Calorimetry, Vol. 2: Applications to Inorganic and Miscellaneous Materials ed. M. E. Brown, and Gallagher, P.K., 261-306, Elsevier.

Monte, M. C., Fuente, E., Blanco, A. and Negro, C., 2009, Waste management from pulp and paper production in the European Union. *Waste Management*. 29(1): p. 293-308.

Montero, M. A., Jordan, M. M., Almendro-Candel, M. B., Sanfeliu, T. and Hernandez-Crespo, M. S., 2009, The use of a calcium carbonate residue from the stone industry in manufacturing of ceramic tile bodies. *Applied Clay Science*. 43(2): p. 186-189.

Montero, M.A., Jordán, M.M., Almendro-Candel, M.B., Sanfeliu, T., Hernández-Crespo, M.S., 2009, The use of a calcium carbonate residue from the stone industry in manufacturing of ceramic tile bodies. *Applied Clay Science*. 43: p. 186-189.

Murray, A., Price, L., 2008, Lawrence Berkeley National Laboratory Report, Use of alternative fuels in cement manufacture: Analysis of fuel characteristics and feasibility for use in the Chinese cement sector, Berkeley, California, USA.

Norton, F.H., 1949, Refractories, McGraw-Hill Company Inc.

Norton, F.H., 1952, Elements of Ceramics, Addison-Wesley Publishing Co.Inc.

Okada, K., Watanabe, N., Jha, K. V., Kameshima, Y., Yasumori, A. and MacKenzie, K. J. D., 2003, Effects of grinding and firing conditions on CaAl2Si2O8 phase formation by solid-state reaction of kaolinite with CaCO3. *Applied Clay Science*. 23(5-6): p. 329-336.

Palace, C., 1935, U.S. Geological Survey Professional Paper 180, The Minerals of Franklin and Sterling Hill.

Pereira, F.R., Hotza, D., Segadaes, A.M., Labrincha, J.A., 2006, Ceramic formulations prepared with industrial wastes and natural sub-products. *Ceramics International*. 32: p. 173-179.

Pirogov, A. A., Rakina, V. P., Mirak'yan, M. M. and Volkov, N. V., 1970, Anorthite insulating refractory. *Refractories and Industrial Ceramics*. 11(5): p. 303-307.

Pirogov, A. A., Yutina, A. S., Rakina, V. P. and Drizheruk, M. E., 1972, Characteristics of heat-insulating refractories produced by some foreign companies. *Refractories and Industrial Ceramics*. 13(7): p. 545-547.

Rawlings, R. D., Wu, J. P. and Boccaccini, A. R., 2006, Glass-ceramics: Their production from wastes-a review. *Journal of Materials Science*. 41(3): p. 733-761.

Rice, R.W., 1998, Porosity of Ceramics, Marcel Dekker Inc.

Rimpel, E., 1996, Industrial production of high-porosity brick materials. *Ziegelindustrie International Annual* p. 174-207.

Rimpel, E., Rehme, F., 2001, Development of extruded, high thermal insulating bricks. *Ziegelindustrie International*. 57(12): p. 36-41.

Ruh, E. and McDowell, J.S., 1962, Thermal conductivity of refractory brick. *Journal of The American Ceramic Society*. 45(4): p. 189-195.

Russ, Winfried, Mörtel, Heinrich and Meyer-Pittroff, Roland, 2005, Application of spent grains to increase porosity in bricks. *Construction and Building Materials*. 19(2): p. 117-126.

Sahtas Terracotta, http://www.sahtas.com, (accessed 15.04.2010).

Sarkar, R. and Das, S. K., 2003, Porous ceramic tiles from industrial solid wastes. *Tile & Brick International*. 19(1): p. 24-27.

Schlagmann Poroton, *Poroton T8*, www.schlagmann.de, (accessed 15.12.2009).

Segadaes, A. M., 2006, Use of phase diagrams to guide ceramic production from wastes. *Advances in Applied Ceramics*. 105(1): p. 46-54.

Stefanov, S., 2003, Additives in brickmaking. *Tile & Brick International*. 19(3): p. 162-166.

Sutcu, M. and Akkurt, S., 2009, The use of recycled paper processing residues in making porous brick with reduced thermal conductivity. *Ceramics International*. 35(7): p. 2625-2631.

Sutcu, M. and Akkurt, S., 2010, Utilization of recycled paper processing residues and clay of different sources for the production of porous anorthite ceramics. *Journal of the European Ceramic Society*. 30(8): p. 1785-1793.

Suvorov, S. A. and Skurikhin, V. V., 2003, Vermiculite - A promising material for high-temperature heat insulators. *Refractories and Industrial Ceramics*. 44(3): p. 186-193.

Swoda, M., 1997, Improvement of Production and Product Characteristics with Vupper. *Ziegelindustrie International*,(March): p. 100-106.

The Brick Industry Association, *Manufacturing of brick- Technical notes on brick construction (TN9)*, www.gobrick.com, (accessed 9 December 2006).

Thermal Ceramics, http://www.thermalceramics.com/pdfs-uploaded/datasheets/americas/114-3.pdf, (accessed 06 May 2009).

Tichá, G., Pabst, W. and Smith, D., 2005, Predictive model for the thermal conductivity of porous materials with matrix-inclusion type microstructure. *Journal of Materials Science*. 40(18): p. 5045-5047.

Toya, T., Nakamura, A., Kameshima, Y., Nakajima, A. and Okada, K., 2007, Glass-ceramics prepared from sludge generated by a water purification plant. *Ceramics International*. 33(4): p. 573-577.

Toya, Tomohiro, Kameshima, Yoshikazu, Nakajima, Akira and Okada, Kiyoshi, 2006, Preparation and properties of glass-ceramics from kaolin clay refining waste (Kira) and paper sludge ash. *Ceramics International*. 32(7): p. 789-796.

Traore, K., Kabre, T. S. and Blanchart, P., 2003, Gehlenite and anorthite crystallisation from kaolinite and calcite mix. *Ceramics International*. 29(4): p. 377-383.

TS EN 12457-4 (EK11A), 2005, Tehlikeli Atıkların Kontrolü Yönetmeliği,T.C. Çevre ve Orman Bakanlığı, Turkey.

TSE-EN771-1, 2005, TSE, Specification for masonry units-Part 1: Clay masonry units.

Tsibin, I. P., Litovskii, E. Ya and Fedina, I. G., 1988, Effective thermal conductivity of a refractory concrete. *Refractories and Industrial Ceramics*. 29(3): p. 174-177.

Uslu, T., Arol, A.I., 2004, Use of boron waste as an additive in red bricks. *Waste Management*. 24: p. 217-220.

Vieira, C. M. F., Sánchez, R. and Monteiro, S. N., 2008, Characteristics of clays and properties of building ceramics in the state of Rio de Janeiro, Brazil. *Construction and Building Materials*. 22(5): p. 781-787.

Vivancos, J., Soto, J., Perez, I., Ros-Lis, J.V., Martinez-Manez, R., 2009, A new model based on experimental results for the thermal characterization of bricks. *Building and Environment*. 44: p. 1047-1052.

Webmineral-Anorthite, http://webmineral.com/data/Anorthite.shtml, (accessed 15 March 2010).

Wienerberger, *Poroton*, http://www.wienerberger.de, (accessed 01.04.2008).

Wouter, P., 2004, ENPER-TEBUC, Energy Performance of Building: Assessment of Innovative Technologies.

WRAP, 2007, A New Approach to Paper Mill Sludge. *The Waste & Resources Action Programme*. MSP002.

Yurkov, A. L. and Aksel'rod, L. M., 2005, Properties of heat-insulating materials (a review). *Refractories and Industrial Ceramics*. 46(3): p. 170-174.

Zivcova, Z., Gregorova, E., Pabst, W., Smith, D.S., Michot, A., Poiler, C., 2009, Thermal conductivity of porous alumina ceramics prepared using starch as a pore-forming agent. *Journal of European Ceramic Society*. 29: p. 347-353.

VITA

Mücahit SÜTÇÜ
1979 Gördes

EDUCATION

- B.Sc: (2000) Department of Metallurgical and Materials Engineering, Yıldız Technical University, Turkey.
- M.Sc: (2004) Materials Science and Engineering Programme, Izmir Institute of Technology, Turkey (in English).
- PhD: (2010) Department of Mechanical Engineering, Izmir Institute of Technology, Turkey (in English).

SELECTED PUBLICATIONS

- Sutcu M., Akkurt S., Utilization of recycled paper processing residues and clay of different sources for the production of porous anorthite ceramics, *Journal of European Ceramic Society*, Vol.30, Issue:8 (2010) 1785–1793.
- Sutcu M., Akkurt S., The use of recycled paper processing residues in making porous brick with reduced thermal conductivity, *Ceramics International*, Vol.35, Issue:7 (2009) 2625–2631.
- Sutcu M., Akkurt S., Okur S., A microstructural study of surface hydration on a magnesia refractory, *Ceramics International*, Vol.36, Issue:5 (2010) 1731–1735.
- Sutcu M., Akkurt S., ANN Model for prediction of powder packing, *Journal of the European Ceramic Society*, Vol.27, Issue:2–3 (2007) 641–644.

AWARD

- Second Award, *VII. Ne Üretelim? Etkinlikleri ve Proje Yarışması*, IYTE, Department of Chemical Engineering, Izmir (27 November 2008) (with undergraduate students Bayram A.and Uluca U.).